



Deactivation of SCR Catalysts by Additives

Castellino, Francesco

Publication date:
2008

Document Version
Publisher's PDF, also known as Version of record

[Link back to DTU Orbit](#)

Citation (APA):
Castellino, F. (2008). *Deactivation of SCR Catalysts by Additives*.

General rights

Copyright and moral rights for the publications made accessible in the public portal are retained by the authors and/or other copyright owners and it is a condition of accessing publications that users recognise and abide by the legal requirements associated with these rights.

- Users may download and print one copy of any publication from the public portal for the purpose of private study or research.
- You may not further distribute the material or use it for any profit-making activity or commercial gain
- You may freely distribute the URL identifying the publication in the public portal

If you believe that this document breaches copyright please contact us providing details, and we will remove access to the work immediately and investigate your claim.

Deactivation of SCR Catalysts by Additives

Ph.D. Thesis

Francesco Castellino

*Department of Chemical and Biochemical Engineering
Technical University of Denmark*

2008

Copyright © Francesco Castellino, 2008

ISBN 978-87-91435-81-1

Printed by Frydenberg a/s, Copenhagen, Denmark

Preface

The present dissertation is written in accordance with the partial requirements of the Ph.D. degree. The Ph.D. project was carried out at the Department of Chemical and Biochemical Engineering (KT), Technical University of Denmark (DTU), within the CHEC (Combustion and Harmful Emission Control) research centre. Professors Anker Degn Jensen and Jan Erik Johnsson from KT, and Associate Professor Rasmus Fehrmann from the Department of Chemistry, DTU, were supervisors.

Funding by the PSO system and catalyst supply by Haldor Topsøe A/S are gratefully acknowledged.

I would like to thank my supervisors for their guidance and interest in my work. A special thank goes to Anker Degn Jensen for giving me the opportunity to work on this project, and for having been determinant, through his excellent supervision, in my professional development.

I owe special thanks to Søren Birk Rasmussen for carrying out the EPR measurements and for many valuable discussions. I am grateful to the technical staff of the CHEC group, in particular Carsten Nørby, for having always been very helpful.

The Summary was translated in Danish by Michael Lykke Heiredal, who is gratefully acknowledged.

Finally, I would like to thank my girlfriend Dorte for her patience, support, and in particular for having taken special care of our splendid daughter Sophia during my work-related absence.

Francesco Castellino

Lyngby, Denmark
December 2008

Summary

Biomass (co)-combustion has for more than a decade been practised in countries like Denmark and Sweden, and is regulated by the governments in order to limit the net emissions of CO₂. The use of biomass at central power stations presents however different issues, which reduce the efficiency of the process and make its operation rather complicated. In particular, fouling and corrosion of the superheater exchangers by KCl and K₂SO₄ are the main problems encountered during straw combustion.

In order to overcome these problems, the addition of P/Ca compounds to the biomass has been proposed. During combustion, the reaction conditions at which the potassium released to the gas phase is bound in a solid phase consisting of K₂O-CaO-P₂O₅ are formed, thereby favouring (i) the release of Cl in the gas phase; and (ii) the formation of ashes melting at temperatures higher than e.g. 1000°C, thus minimising sticking on the superheater exchangers.

While preliminary combustion tests of straw with the additives have shown their potential for solving the above mentioned fouling and corrosion problems in the boiler, little is known about their effects on the lifetime of the catalysts employed at the SCR process. Both P and Ca are known as deactivating compounds for the vanadia-based catalysts normally used. Therefore, some concerns about their utilisation at full scale have risen. The main objective of this work has been to study the potential effects of the P and Ca additives on vanadia-based commercial SCR catalysts by clarifying their mechanism of deactivation under well defined and *realistic* conditions.

In the first part of this work, commercial vanadia-based SCR monoliths have been exposed to flue gases in a pilot scale setup into which phosphoric acid has been added and the deactivation has been followed during the exposure time. Separate measurements by SMPS showed that the phosphoric acid formed polyphosphoric acid aerosols, which were characterized by particle number concentrations in the order of $1 \cdot 10^{14} \text{ \#/m}^3$ at 350 °C and diameters $< 0.1 \text{ \mu m}$. Three full-length monoliths have been exposed to flue gases doped with 10, 100 and 1000 ppmv H₃PO₄ for 819, 38 and 24 hours respectively. At the end of the exposure the relative activities were equal to 65, 42 and 0% respectively. Af-

Summary

ter exposure, samples of the spent monoliths have been characterized by ICP-OES, Hg-porosimetry, SEM-EDX and in-situ EPR. The results showed that the polyphosphoric acids chemically deactivate the vanadia-based catalysts by decreasing the redox properties of the catalyst surface and by titrating the number of V(V) active species. When plate-shaped commercial catalysts have been wet impregnated with different aqueous solutions of H_3PO_4 obtaining P/V ratios in the range 1.5-5, the relative activity for the doped catalysts in the whole P/V range was 0.85-0.90 at 350 °C. These results show that the presence of phosphor compounds in the flue gas may be much more harmful than indicated by simple wet chemical impregnation by phosphoric acid. The reason has been found in the nature of the polyphosphoric acid aerosol formed in the combustion process, which cannot be reproduced by the wet impregnation process.

In the second part of this work, the commercial vanadia-based full-length monoliths have been exposed to aerosols formed by injection of K_3PO_4 (dissolved in water) in a hot flue gas ($T > 850$ °C) from a natural gas burner. Such aerosols may form when burning fuels with high K- and P-content, or when P-compounds are mixed with biomass as a K-getter additive. The formed aerosols have been characterized by using both a SMPS system and a low pressure cascade impactor, showing a dual-mode volume-based size distribution with a first peak at around 30 nm and a second one at diameters > 1 μm . The different peaks have been associated with different species. In particular, the particles related to the 30 nm peak are associated to condensed phosphates, whereas the larger particles are associated to potassium phosphates. Two monoliths have been exposed during addition of 100 and 200 mg/Nm^3 K_3PO_4 for 720 and 189 hours respectively. Overall, deactivation rates up to 3 %/day have been measured. The spent catalysts have been characterized by bulk chemical analysis, Hg-porosimetry and SEM-EDX. NH_3 -chemisorption tests on the spent elements and activity tests on catalyst powders obtained by crushing the monoliths have also been carried out. The catalyst characterization has shown that poisoning by K is the main deactivation mechanism. This result was further confirmed by the poisoning tests carried out in the laboratory with catalyst plates wet impregnated with different K_3PO_4 solutions. The results show that binding K in K-P salts will not reduce the rate of catalyst deactivation. Regeneration may, however, be possible by washing the spent catalysts with 0.5 M H_2SO_4 aqueous solutions, as indicated by the regeneration tests made in the laboratory with catalyst plates.

Finally, a commercial V_2O_5 - WO_3 - TiO_2 SCR corrugated monolith has been exposed for 1000 hours in a pilot-scale setup to a flue gas doped with KCl, $\text{Ca}(\text{OH})_2$, H_3PO_4 and H_2SO_4 by spraying a water solution of the components into the hot flue gas. The mixture composition has been adjusted in order to have P/K and P/Ca ratios equal to 2 and 0.8 respectively. At these conditions,

it is suggested that all the K released during biomass combustion gets captured in P-K-Ca particles and the Cl is released in the gas phase as HCl, thus limiting deposition and corrosion problems at the superheater exchangers during biomass combustion. Aerosol measurements carried out by using a SMPS and a low pressure cascade impactor have shown two distinct particle populations with volume-based mean diameters equal to 12 and 300 nm, respectively. The small particles have been associated to polyphosphoric acids formed by condensation of H_3PO_4 , whereas the larger particles are due to P-K-Ca salts formed during evaporation of the water solution. No Cl has been found in the collected particles. During the initial 240 h of exposure, the catalyst element lost about 20% of its original activity. The deactivation then proceeded at slower rates, and after 1000 h the relative activity loss had increased to 25%. Different samples of the spent catalyst have been characterized after 453 h and at the end of the experiment by bulk chemical analysis, Hg-porosimetry and SEM-EDX. NH_3 chemisorption tests on the spent elements and activity tests on catalyst powders obtained by crushing the monolith have also been carried out. From the characterization, it was found that neither K nor Ca were able to penetrate the catalyst walls, but only accumulated on the outer surface. Poisoning by K has then been limited to the most outer catalyst surface and did not proceed at the fast rates known for KCl. This fact indicates that binding K in P-K-Ca compounds is an effective way to reduce the negative influence of alkali metals on the lifetime of the vanadia-based SCR catalysts. On the other hand, P-deposition was favoured by the formation of the polyphosphoric acids, and up to 1.8 %wt P was accumulated in the catalyst walls. Deactivation by polyphosphoric acids proceeded at about 0.2 %/day. About 6-7 % of the initial activity was lost due to the accumulation of these species. However, the measured relative activity reached a steady-state level during the last 240 h of exposure indicating that the P-concentration in the bulk reached a steady-state level due to the simultaneous hydrolysis of the polyphosphoric acids.

Based on the results obtained in this work, deactivation of vanadia-based SCR catalysts during utilisation of the P/Ca-based additives will be mainly controlled by (i) the amount of vaporised P, and (ii) by the amount of K which will still be present at the SCR reactor inlet in water soluble fine particles. Overall, it is believed that, if the optimal operating P/K and P/Ca molar ratios, at which all the K and P are captured in relatively high melting point Ca-K-P-compounds having low water solubility, are found, it is possible to avoid deactivation of SCR catalysts by K and by P.

Resumé på Dansk

Biomasseforbrænding har været anvendt i mere end en dekade i lande som Danmark og Sverige og bliver reguleret af myndighederne med henblik på at begrænse nettoemissionen af CO_2 . Anvendelsen af biomasse på kraftværkerne skaber dog forskellige problemer, som reducerer effektiviteten af processen og vanskeliggør driften. Specielt i forbindelse med halmforbrænding optræder der problemer med askebelægninger og korrosion på overhederen på grund af KCl og K_2SO_4 .

Med henblik på at imødegå disse problemer er det blevet foreslået at tilsætte P- og Ca-forbindelser til biomassen. I forbindelse med biomasseforbrænding forårsager reaktionsbetingelserne, at kalium frigives til gasfasen og herefter i dannelse af en faststoffase bestående af $\text{K}_2\text{O}-\text{CaO}-\text{P}_2\text{O}_5$. Resultatet heraf er (i) frigivelse af Cl til gasfasen som HCl og (ii) dannelse af aske med et smeltepunkt over f.eks. 1000°C , som minimerer vedhæftning og korrosion på overhederen.

Selvom foreløbige undersøgelser af halmforbrænding med disse additiver har vist deres potentiale som løsning på ovennævnte problemer med askebelægninger og korrosion på overhederen i kedlen, eksisterer der ikke megen viden om deres indvirkning på levetiden af disse katalysatorerne, som anvendes på kraftværkerne i forbindelse med SCR processen. Både P og Ca er kendt som komponenter, der deaktiverer disse vanadium baserede katalysatorer, der normalt anvendes i SCR anlæg, og det har derfor ført til bekymring i forbindelse med deres anvendelse i fuldskalaanlæg. Hovedformålet med dette studie har været at undersøge deaktiveringspotentiale og -mekanismer af P and Ca additiver overfor kommercielle vanadium baserede SCR katalysatorer under veldefinerede realistiske driftsbetingelser.

I den første del af studiet blev kommercielle vanadium baserede SCR katalysatorer eksponeret for røggas tilsat fosforsyre i en pilotopstilling, og deaktiveringen af katalysatorerne blev fulgt under eksponeringen. Målinger med SMPS udstyr viste, at fosforsyren dannede polyfosforsyreaerosoler som blev karakteriseret til en partikelantalskoncentration i størrelsesordenen $1 \cdot 10^{14} \text{ \#/m}^3$ og med partikeldiametre mindre end $0.1 \mu\text{m}$. Tre katalysatorer i fuld længde blev eksponeret for røggas tilsat 10, 100 og 1000 ppmv H_3PO_4 , i henholdsvis 819,

38 og 24 timer. Efter endt test var de relative aktiviteter henholdsvis 65, 42 og 0 %. Dele af monolitterne blev efterfølgende karakteriseret ved hjælp af ICP-OES, Hg- porøsitet, SEM-EDX og in-situ EPR. Resultatet viste, at polyfosforsyren kemisk deaktiverede disse vanadium baserede katalysatorer ved at hæmme redox egenskaberne af katalysatorernes aktive sites samt titrere antallet af aktive V(V) komponenter. Når kommercielle katalysatorer med pladeformet geometri blev vådimprægneret med forskellige vandige opløsninger af H_3PO_4 , hvorved der blev opnået et P/V forhold i størrelsesordenen 1.5-5, var den relative aktivitet for de eksponerede katalysatorer i hele P/V området 0.85-0.90 ved 350 °C. Resultaterne fra dette studie viste, at tilstedeværelsen af fosforforbindelser i røggassen kan være meget mere skadelig end det tydede på ud fra simple vådkemiske imprægneringer med fosforsyre. Årsagen blev fundet til at være den måde disse polyfosforsyreaerosoler blev dannet i forbrændingsprocessen, som ikke kan reproducere ved en vådkemisk imprægneringsproces.

I anden del af studiet blev kommercielle vanadium baserede SCR katalysatorer i fuld længde eksponeret for aerosoler dannet ved injektion af en vandig opløsning af K_3PO_4 i den varme røggas ($T > 850$ °C) fra naturgasbrænderen. Disse aerosoler kan dannes, når der anvendes brændstoffer med højt indhold af K- og P-forbindelser eller når P-forbindelser blandes med biomasse som et K-getter additiv. De dannede aerosoler blev karakteriseret ved både SMPS udstyr og lavtrykskaskade impactor. Dette viste en bidispers volumenbaseret størrelsesfordeling med den første top omkring 30 nm og en anden top ved diameter større end 1 μm . De forskellige toppe blev associeret med forskellige komponenter. Specielt blev partiklerne relateret til toppen omkring de 30 nm forbundet med kondenseret fosfor (polyfosforsyre), hvorimod de større partikler blev relateret til kaliumfosfater. To monolitter blev eksponeret i henholdsvis 720 og 180 timer med tilsætning af 100 og 200 mg/Nm^3 af K_3PO_4 , hvorved der blev målt deaktiveringshastigheder på op til 3 %/dag. De eksponerede katalysatorer blev karakteriseret ved hjælp af bulk kemiske analyser, Hg-porøsitet og SEM-EDX. NH_3 kemisorptionstest på de eksponerede elementer samt aktivitetstest på katalysatorpulver, dannet ved at knuse monolitterne, blev også udført.

Katalysatorkarakteriseringen viste, at forgiftning med K er hoveddeaktiveringsmekanismen i disse forsøg. Dette resultat blev yderligere bekræftet i laboratoriet ved forgiftningstest udført på forskellige katalysatorplader, der blev vådimprægneret med forskellige opløsninger af K_3PO_4 . Resultaterne viste, at hvis K bindes i K-P saltforbindelser ville dette ikke reducere hastigheden af katalysatorens deaktivering. Regenereringstest udført i laboratoriet på katalysatorplader viste, at regenerering af de eksponerede katalysatorer var muligt ved at vaske dem med 0.5 M vandig opløsning af H_2SO_4 .

Som det sidste blev en kommerciel V_2O_5 - WO_3 - TiO_2 SCR monolit eksponer-

et i 1000 timer for røggas tilsat en vandig opløsning af KCl, $\text{Ca}(\text{OH})_2$, H_3PO_4 og H_2SO_4 i en pilotopstilling. Blandingens sammensætning blev justeret med henblik på at have et P/K og P/Ca forhold på henholdsvis 2 og 0.8. Ved disse betingelser er det foreslået, at al K frigivet under forbrænding af biomasse bliver optaget i P-K-Ca partikler og at Cl bliver frigivet i gasfasen som HCl og dermed begrænser problemerne med belægninger og korrosion på overhederen. Aerosolmålinger udført ved anvendelse af SMPS udstyr og lavtrykskaskade impactor viste to klart adskilte partikelpopulationer med volumenbaseret middeldiameter på henholdsvis 12 og 300 nm. De små partikler blev forbundet med polyfosforsyre dannet ved kondensation af H_3PO_4 , hvorimod de større partikler skyldtes P-K-Ca salte dannet under fordampning af vandopløsningen. Ingen Cl blev fundet i de opsamlede partikler. Under de første 240 timers eksponering mistede katalysatorerne omkring 20 % af deres oprindelige aktivitet. Deaktivering fortsatte derefter ved lavere hastigheder, og efter 1000 timer var deres relative aktivitetstab steget til 25 %. Forskellige prøver af eksponerede katalysatorer blev karakteriseret efter 453 timer og ved afslutningen af eksperimentet ved bulk kemiske analyser, Hg- porøsitet og SEM-EDX. NH_3 kemisorptionstest på de eksponerede elementer samt aktivitetstest på katalysatorpulver, dannet ved at knuse monolitterne, blev også udført. Baseret på karakteriseringen blev det fastslået, at hverken K eller Ca var i stand til at trænge ind i katalysatorvæggene, men blev akkumuleret på de ydre overflader. Forgiftning pga. K var derfor begrænset til de yderste katalysatoroverflader og foregik ikke med de hastigheder, der blev observeret for KCl eller K_3PO_4 . Dette faktum indikerer at kemisk binding af K i P-K-Ca-forbindelser er en effektiv måde at reducere den negative indflydelse på levetiden af vanadium baserede SCR katalysatorer hidrørende fra alkalimetaller. På den anden side blev fosforafsætning og -belægningsdannelse favoriseret ved dannelsen af polyfosforsyre og op til 1.8 %wt P blev akkumuleret på katalysatorvæggene. Deaktivering forårsaget af polyfosforsyre foregik ved omkring 0.2 %/dag. Omkring 6-7 % af den oprindelige aktivitet blev tabt pga. akkumulering af disse komponenter. Imidlertid nåede den målte relative aktivitet et stationært niveau under de sidste 240 timers eksponering, som indikerede at P-koncentrationen i bulk nåede et stationært niveau på grund af samtidig hydrolyse af polyfosforsyre.

Baseret på resultaterne opnået i nærværende studie, vil deaktivering af vanadium SCR katalysatorer ved anvendelse af P og Ca baserede additiver hovedsageligt blive kontrolleret af (i) mængden af fordampet P og (ii) mængden af K, som stadig vil være tilstede i indløbet af SCR reaktoren som fine vandopløselige partikler. Overordnet menes det, at hvis det optimale molære forhold af P/K og P/Ca under drift findes, hvor alle K og P er bundet i Ca-K-P-forbindelser med relativt højt smeltepunkt og vandopløselighed, vil det sandsynligvis være muligt at undgå deaktivering af SCR katalysatorer pga. K og P.

Contents

| | |
|------------------------|-----------|
| List of Figures | xx |
|------------------------|-----------|

| | |
|-----------------------|------------|
| List of Tables | xxi |
|-----------------------|------------|

| | |
|---|----------|
| 1 Introduction | 1 |
| 1.1 Background | 1 |
| 1.2 Objectives | 3 |
| 2 Literature Study | 5 |
| 2.1 Introduction | 5 |
| 2.2 NO _x Control Technologies | 6 |
| 2.2.1 Sources of Nitrogen Oxides | 6 |
| 2.2.2 Primary Measures | 8 |
| 2.2.3 Secondary Measures | 10 |
| 2.3 The SCR Process | 12 |
| 2.3.1 The Reactions | 12 |
| 2.3.2 Process Design and Optimization | 13 |
| 2.4 Supported-Vanadia Catalysts in the SCR of NO by NH ₃ | 16 |
| 2.4.1 Catalyst Characterization | 16 |
| 2.4.2 Adsorption and Surface Reaction Studies | 21 |
| 2.4.3 Reaction Mechanism | 24 |
| 2.4.4 Kinetics of the SCR Reaction | 30 |
| 2.4.5 Catalyst Design and Reactor Modelling | 40 |
| 2.5 Deactivation of SCR Vanadia-based Catalysts | 43 |
| 2.5.1 General Aspects | 43 |
| 2.5.2 Poisoning | 44 |
| 2.5.3 Fouling and Channel Blocking | 45 |
| 2.5.4 Sintering and Solid-state Transformation | 46 |
| 2.5.5 Performed Investigations on Deactivating Compounds | 48 |
| 2.6 Conclusions | 62 |

Contents

| | | |
|----------|--|------------|
| 3 | Experimental | 65 |
| 3.1 | The Catalyst | 65 |
| 3.2 | SCR Pilot Plant | 65 |
| 3.3 | Laboratory Gas Flow Setup | 67 |
| 3.4 | Activity Measurements | 67 |
| 3.5 | Ammonia Chemisorption Tests | 70 |
| 3.6 | Catalyst Characterization | 70 |
| 3.7 | Aerosol Measurements | 71 |
| 4 | Deactivation by Polyphosphoric Acids | 73 |
| 4.1 | Introduction | 73 |
| 4.2 | Experimental | 74 |
| 4.3 | Results | 75 |
| 4.3.1 | Aerosol Measurements at the Pilot-scale Setup | 75 |
| 4.3.2 | Activity Tests at the Pilot-scale Setup | 76 |
| 4.3.3 | Lab-scale Investigations | 81 |
| 4.3.4 | In-situ EPR Spectroscopy | 82 |
| 4.3.5 | Catalyst Characterization | 84 |
| 4.4 | Discussion | 86 |
| 4.4.1 | Polyphosphoric Acids Formation and Deposition | 87 |
| 4.4.2 | Deactivation Mechanism | 91 |
| 4.5 | Conclusions | 93 |
| 5 | Deactivation by Potassium Phosphates | 95 |
| 5.1 | Introduction | 95 |
| 5.2 | Experimental | 96 |
| 5.3 | Results | 97 |
| 5.3.1 | Aerosol Measurements at the Pilot-scale Setup | 97 |
| 5.3.2 | Catalyst Characterization | 99 |
| 5.3.3 | Deactivation at the Pilot-scale Setup | 101 |
| 5.3.4 | Deactivation at the Lab-scale Setup | 105 |
| 5.4 | Discussion | 108 |
| 5.4.1 | K- and P-accumulation and Penetration Mechanisms | 108 |
| 5.4.2 | Deactivation Mechanism | 113 |
| 5.5 | Conclusions | 114 |
| 6 | Deactivation by Additives Mixture | 117 |
| 6.1 | Introduction | 117 |
| 6.2 | Experimental | 118 |
| 6.3 | Results | 118 |
| 6.3.1 | Aerosol Measurements at the Pilot-scale Setup | 118 |

| | | |
|----------|---|------------|
| 6.3.2 | Catalyst Characterization | 121 |
| 6.3.3 | Deactivation at the Pilot-scale Setup | 125 |
| 6.3.4 | Laboratory Activity and Hg-porosimetry Tests | 129 |
| 6.4 | Discussion | 130 |
| 6.4.1 | Polyphosphoric Acids Formation | 130 |
| 6.4.2 | Particle Deposition and Penetration | 131 |
| 6.4.3 | Deactivation Mechanism | 133 |
| 6.5 | Conclusion | 134 |
| 7 | Further Discussion of the Results | 137 |
| 7.1 | Deactivation by P | 137 |
| 7.2 | Deactivation by K | 139 |
| 7.3 | Deactivation by Additives | 140 |
| 8 | Summary, Conclusions and Suggestions to Further Work | 143 |
| 8.1 | Deactivation by Polyphosphoric Acids | 143 |
| 8.2 | Deactivation by Potassium Phosphates | 144 |
| 8.3 | Deactivation by Additives Mixture | 145 |
| 8.4 | Suggestions to Further Work | 146 |
| | Bibliography | 149 |
| A | | 163 |
| B | | 179 |
| C | | 191 |

List of Figures

| | | |
|------|--|----|
| 2.1 | Temperature influence on the amount of NO_x produced from the three NO_x formation mechanism in the case of coal combustion. Data from [1]. | 8 |
| 2.2 | The three combustion zones in a reburning process [1]. | 9 |
| 2.3 | NO_x reduction (circles) and ammonia slip (squares) as a function of reagent normalized stoichiometric ratio. NO_x inlet: 425 ppm; temperature: 368 °C. Data from [2]. | 14 |
| 2.4 | SCR process arrangements. SCR: selective catalytic reduction; AH: air preheater; ESP: electrostatic precipitator; H-ESP: high temperature ESP; GGH: gas-gas heater; FGD: flue gas desulphurisation. From [3]. | 15 |
| 2.5 | Structure of SCR reactors [4]. | 16 |
| 2.6 | Possible molecular configurations for supported vanadium oxides (with S the support cation): (a) isolated vanadium oxide species; (b) dimeric vanadium oxide species; (c) two-dimensional vanadium oxide chains; (d) V_2O_5 crystals. From [5]. | 18 |
| 2.7 | Distribution of monomeric, polymeric and crystalline vanadia species as a function of the vanadia surface density. Data from [6]. . . | 19 |
| 2.8 | NO conversion versus temperature: (a) 9 %wt WO_3 - TiO_2 ; (b) 0.78 %wt V_2O_5 - TiO_2 ; (c) 1.4 %wt V_2O_5 - TiO_2 ; (d) 0.78 %wt V_2O_5 -9 %wt WO_3 - TiO_2 ; (e) 1.4 %wt V_2O_5 -9 %wt WO_3 - TiO_2 . Feed: He, 800 ppmv NH_3 , 800 ppmv NO, 1 %v O_2 . Data from Ref. [7]. | 20 |
| 2.9 | Proposed structures for NH_3 adsorbed on V_2O_5 - TiO_2 : (a) Lewis-bonded NH_3 at Ti sites; (b) H-bonded NH_3 on oxide sites; (c) Lewis-bonded NH_3 at vanadyl sites; (d) ammonium ions bonded at V Brønsted acid sites. From [7]. | 22 |
| 2.10 | Mechanism of the NO- NH_3 reaction on vanadium oxide in the presence of oxygen. Miyamoto et al. [8]. | 25 |
| 2.11 | Mechanism of the NO- NH_3 reaction on vanadium oxide in the presence of oxygen. Ramis et al. [9]. | 26 |

List of Figures

| | |
|--|----|
| 2.12 Mechanism of the NO-NH ₃ reaction on vanadium oxide in the presence of oxygen. Topsøe et al. [10]. | 27 |
| 2.13 Scheme illustrating the cycle of the SCR reaction over V ₂ O ₅ /TiO ₂ catalyst [11]. | 29 |
| 2.14 A: Effect of NO _x concentration on NO _x conversion; B: effect of NH ₃ /NO _x ratio, NO _x =500 ppm, on NO _x conversion; C: effect of O ₂ concentration on NO _x conversion; D: effect of water concentration on NO _x conversion. From [12]. | 30 |
| 2.15 Experimental values of θ_{NH_3} , NO: 100 ppmv. From [13]. | 35 |
| 2.16 Dynamics of the NH ₃ + NO reaction. (A) Step changes of the NH ₃ inlet concentration (0 → 700 → 0 ppm) in He + NO + O ₂ at 493 K over model V ₂ O ₅ -WO ₃ /TiO ₂ catalyst. (B) Linear changes of the NH ₃ inlet concentration (0 → 840 → 0 ppm) in He + NO + O ₂ at 573 K over model V ₂ O ₅ -WO ₃ /TiO ₂ catalyst. From [14]. | 36 |
| 2.17 Conversion of NO versus oxygen concentration. Feed: 0-11.5%v O ₂ , 1000 ppmv NO, 1000 ppmv NH ₃ , 5%v H ₂ O, balance N ₂ . From [15]. | 37 |
| 2.18 Influence of water on reaction rate, O ₂ =10%, T=250 °C. From [13]. | 38 |
| 2.19 Conversion of NO versus temperature, LH-SCR and ER-SCR paths. Feed: 10% O ₂ , 5% H ₂ O, 1000 ppm NO, 1000 ppm NH ₃ , balance N ₂ . Catalyst weight: 4.41 g; particle size: 250 μm; flow 260 L/h (NTP). From [16]. | 39 |
| 2.20 Calculated NO conversion vs. micropore void fraction for different values of micropore radius r_{mi} ; macropore radius = 200 nm. From [4]. | 42 |
| 2.21 Effect of vanadia-loading on the relative BET surface area of model V ₂ O ₅ -WO ₃ -TiO ₂ (circles) [17] and model V ₂ O ₅ -TiO ₂ (squares) [18] calcined at 500 and 600 °C respectively. | 47 |
| 2.22 Activities of 5% V ₂ O ₅ /TiO ₂ doped with different amounts of metal oxide poisons. Operating conditions: NO=NH ₃ =1000 ppm, O ₂ =2%, T=300 °C, space velocity=15000 h ⁻¹ [19]. | 49 |
| 2.23 IR spectra in the OH region of the 1 %wt V ₂ O ₅ -WO ₃ -TiO ₂ fresh catalyst and doped one with K/V=1 after activity measurement [20]. | 50 |
| 2.24 Model of alkali deactivation [21]. | 51 |
| 2.25 Accumulation of alkali on the SCR catalyst samples as function of the corresponding catalytic deNO _x activity (measured at a temperature of 300 °C). P, peat; FR, forest residues; B, bark; DW, demolition wood; S, sulphur. From [22]. | 53 |
| 2.26 Relative activity vs. concentration of sulphuric acid at different temperatures. From [23]. | 54 |

List of Figures

| | |
|---|----|
| 2.27 Effects of washing by 0.5 M H_2SO_4 and 1 M NH_4Cl on the activity of K-poisoned 1 wt% $\text{V}_2\text{O}_5(\text{WO}_3)/\text{TiO}_2$ catalysts. From [20]. | 55 |
| 2.28 Model of gaseous arsenic deactivation [21]. | 56 |
| 2.29 Effects of P_2O_5 doped on 5% $\text{V}_2\text{O}_5/\text{TiO}_2$ catalyst in the SCR reaction at 150 (triangles), 200 (diamonds), 250 (squares) and 300 °C (circles). Data from [19]. | 58 |
| 2.30 Proposed reactions of calcium phosphates along the flue gas path. From [24]. | 59 |
| 2.31 Relation of surface P, alkali and Ca concentration compared to k/k_0 of honeycomb and plate catalysts exposed to sewage sludge and MBM co-combustion. From [24]. | 60 |
| 3.1 The pilot-scale SCR setup. | 66 |
| 3.2 The laboratory gas flow setup. | 68 |
| 3.3 Sketch of the laboratory reactor. All shown measures are in millimetres. (1) Bottom gas inlet. (2) Top gas inlet. (3) Thermocouple. (4) Gas outlet. | 69 |
| 4.1 Particle size distribution of polyphosphoric acids measured at the SCR reactor inlet at different H_3PO_4 addition by SMPS. $T = 350\text{ }^\circ\text{C}$ | 76 |
| 4.2 Relative activity of the P1000 element during the first 2 hours of exposure. $T = 350\text{ }^\circ\text{C}$. Total flow: $40\text{ Nm}^3/\text{h}$. Gas composition on dry basis: $\text{NO} = 496\text{ ppmv}$, $\text{NH}_3 = 735\text{ ppmv}$, $\text{O}_2 = 10\%\text{v}$, $\text{CO}_2 = 6\%\text{v}$, N_2 balance. $10\%\text{v H}_2\text{O}$ | 77 |
| 4.3 Relative activity of P10 at $350\text{ }^\circ\text{C}$ as a function of exposure time. Total flow: $40\text{ Nm}^3/\text{h}$. Average gas composition: $\text{NO} = 500\text{ ppmv}$, $\text{NH}_3 = 735\text{ ppmv}$, $\text{O}_2 = 10\%\text{v}$, $\text{CO}_2 = 6\%\text{v}$, and $10\%\text{v H}_2\text{O}$ in N_2 | 78 |
| 4.4 Activity measurement for P100 at $350\text{ }^\circ\text{C}$ and $50\text{ Nm}^3/\text{h}$ after 134 hours of operating time. Gas composition on dry basis: $\text{NO} = 515\text{ ppmv}$, $\text{NH}_3 = 600 - 1200\text{ ppmv}$, $\text{O}_2 = 11\%\text{v}$, $\text{CO}_2 = 5.6\%\text{v}$, N_2 balance. $10\%\text{v H}_2\text{O}$ | 80 |
| 4.5 Activity test on powdered samples. Total flow: 2.8 NL/min . $\text{NO} = 521\text{ ppmv}$, $\text{NH}_3 = 622\text{ ppmv}$, $\text{O}_2 = 5.2\%\text{v}$, $\text{H}_2\text{O} = 1.47\%\text{v}$, N_2 balance. Catalyst mass $W = 0.072\text{ g}$ | 81 |
| 4.6 NH_3 chemisorption test on fresh and P100plate samples at $350\text{ }^\circ\text{C}$. Total flow: 2.75 NL/min . $\text{NO} = 501\text{ ppmv}$, $\text{NH}_3 = 601\text{ ppmv}$, $\text{O}_2 = 5\%\text{v}$, N_2 balance. Catalyst mass $W = 0.45\text{ g}$ | 82 |

List of Figures

| | | |
|------|---|-----|
| 4.7 | In situ EPR spectra acquired at 350 °C of catalyst samples taken from pilot plant tests fresh, P10 and P100, exposed to various simulated flue gas compositions. Gas composition: 1000 ppmv NO (—), 1000 ppmv NO + 1000 ppmv NH ₃ (· · ·), 1000 ppmv NH ₃ (---) and 3.5%v O ₂ , 3%v H ₂ O in N ₂ | 83 |
| 4.8 | Pore size distribution and cumulative intrusion volume measured by Hg porosimetry with different monolithic samples. | 86 |
| 4.9 | Total intrusion volume measured by Hg-porosimetry as a function of P-content measured in the bulk of the different spent monoliths. | 87 |
| 4.10 | SEM analysis of fresh and spent catalyst: (a) fresh surface; (b) P10T surface; (c) P100T surface; (d) P10B wall cross section; (e) P100B wall cross section; (f) P1000B wall cross section. | 88 |
| 4.11 | P-content measured by EDX across some catalyst walls showed in Figure 4.10. | 89 |
| 4.12 | Vapour pressure of polyphosphoric acids as a function of temperature at different P ₂ O ₅ weight content. The lines are calculated by extrapolating at lower pressures the equation fitting the experimental data found at higher partial pressures [25]. | 90 |
| 5.1 | Number-based (a) and volume-based (b) particle size distributions measured by SMPS at the reactor inlet during addition of 100 mg/Nm ³ K ₃ PO ₄ . T = 350 °C. | 97 |
| 5.2 | K- and P-content and K:V and P:V molar ratios along the KP100B and KP200T walls as measured by SEM-EDX. | 102 |
| 5.3 | Pore size distribution for fresh and spent samples measured by Hg-porosimetry. | 103 |
| 5.4 | Relative activity as a function of exposure time. Total flow: 40 Nm ³ /h. Gas composition: NO = 500 ppmv, NH ₃ = 600 ppmv, O ₂ = 10%v, CO ₂ = 6%v, and 10%v H ₂ O in N ₂ | 104 |
| 5.5 | NH ₃ chemisorption test for the element exposed to 100 mg/Nm ³ K ₃ PO ₄ at different times during the exposure. | 105 |
| 5.6 | Activity measurements on powder samples. Total flow: 2.8 NL/min. NO = 521 ppmv, NH ₃ = 622 ppmv, O ₂ = 5.2%v, H ₂ O = 1.47%v, N ₂ balance. Catalyst mass W = 0.072 g. | 106 |
| 5.7 | K/V and P/V molar ratios measured on catalyst plates doped by wet impregnation with K ₃ PO ₄ aqueous solutions. | 107 |
| 5.8 | Relative activity measured as a function of K/V molar ratios with catalyst plates doped in the laboratory with K ₃ PO ₄ . Total flow: 2.8 NL/min. Gas composition: 500 ppmv NO, 600 ppmv NH ₃ , 5% O ₂ in N ₂ . Catalyst mass: 0.17 g. | 108 |

List of Figures

| | | |
|------|--|-----|
| 5.9 | Relative chemisorbed NH_3 measured as a function of K/V molar ratios with catalyst plates doped in the laboratory with K_3PO_4 . Total flow: 2.8 NL/min. Temperature: 250 °C. Gas composition: 500 ppmv NO, 600 ppmv NH_3 , 5% O_2 in N_2 . Catalyst mass: 0.17 g. . . . | 109 |
| 5.10 | Activity vs. temperature for different catalyst plates relative to a fresh sample wet impregnated with water. Total flow: 2.8 NL/min. Gas composition: 500 ppmv NO, 600 ppmv NH_3 , 5% O_2 in N_2 . Catalyst mass: 0.17 g. | 110 |
| 5.11 | Possible reactions during heating of K_3PO_4 solution droplets. The compounds in bold boxes are the ones most likely found at the SCR reactor inlet. | 111 |
| 6.1 | Number-based (a) and volume-based (b) particle size distributions measured by SMPS at the reactor inlet during addition of KCl (10 mg/ Nm^3), $\text{Ca}(\text{OH})_2$ (13 mg/ Nm^3), H_3PO_4 (26 mg/ Nm^3) and H_2SO_4 (20 mg/ Nm^3). T = 350 °C. | 119 |
| 6.2 | Particle size distribution measured by a LPI at the reactor inlet during simultaneous addition of KCl (10 mg/ Nm^3), $\text{Ca}(\text{OH})_2$ (13 mg/ Nm^3), H_3PO_4 (26 mg/ Nm^3) and H_2SO_4 (20 mg/ Nm^3). T = 90 °C. The curves for each single element have been obtained knowing their concentration on each single stage from EDX analysis. . | 120 |
| 6.3 | SEM images of catalyst samples taken after 453 h of exposure: a) ADD1T; b) ADD1B; c) ADD1B. | 124 |
| 6.4 | SEM images of: a,b) catalyst sample taken after 1000 h of exposure (ADD2B); c,d) fresh sample. Magnification: a,c) 2 kX; b,d) 20 kX. . | 125 |
| 6.5 | P-concentration profile inside the spent catalyst walls. | 126 |
| 6.6 | Activity measurement made on fresh and spent monolith at 350 °C. Gas dry composition: NO = 500 ppmv, NH_3 = 600 ppmv, O_2 = 10 %v, CO_2 = 6 %v. H_2O = 10 %v. Flow: 40 Nm^3/h | 127 |
| 6.7 | Relative activity as a function of exposure time. The activity measurement were made at 350 °C. Gas dry composition: NO = 500 ppmv, NH_3 = 600 ppmv, O_2 = 10 %v, CO_2 = 6 %v. H_2O = 10 %v. Flow: 40 Nm^3/h | 128 |
| 6.8 | PO_x deactivation effect as a function of exposure time. The data points represent the difference between “Max X” and “Steady-state X” curves in Figure 6.7. | 129 |
| 6.9 | Activity measurement on spent catalyst exposed for 1000 hours to the doped flue gas and 96 additional hours to a clean flue gas. T = 350°C. Gas dry composition: NO = 500 ppmv, NH_3 = 600 ppmv, O_2 = 10 %v, CO_2 = 6 %v. H_2O = 10 %v. Flow: 40 Nm^3/h | 131 |

List of Figures

| | |
|--|-----|
| 6.10 Activity test on powder samples. Catalyst mass, $W = 0.07$ g. Total flow $F = 2.8$ Nlitre/min. Gas composition: $\text{NO} = 500$ ppmv, $\text{NH}_3 = 600$ ppmv, $\text{O}_2 = 5\%$, $\text{H}_2\text{O} = 1.4\%$ in N_2 | 132 |
| 6.11 Pore size distribution measured by Hg-porosimetry. | 133 |

List of Tables

| | | |
|-----|--|-----|
| 1.1 | Theoretical products of biomass combustion in the presence of additives | 2 |
| 2.1 | Global inventory of NO _x sources [26]. | 7 |
| 2.2 | Primary measure reduction capabilities in coal-fired boilers [1]. . | 10 |
| 2.3 | Simultaneous removal of SO _x and NO _x processes [1]. | 11 |
| 2.4 | Proposed rate expressions for the SCR of NO by NH ₃ | 32 |
| 2.5 | Correlations for estimating the external mass transfer in monolith catalysts. | 41 |
| 2.6 | Ash analysis: MBM and sewage sludge. Data from CATDEACT final report. | 57 |
| 4.1 | Performed SMPS experiments. | 75 |
| 4.2 | Results of the activity measurements performed with the P100 element. | 79 |
| 4.3 | Results of the bulk and surface chemical analysis, and of the Hg-porosimetry for the fresh and spent monoliths. | 85 |
| 5.1 | K- and P-content measured on the impactor stages by EDX. The particles were collected during addition of 100 mg/Nm ³ K ₃ PO ₄ . . | 98 |
| 5.2 | Bulk, surface and Hg-porosimetry analysis for the fresh and spent monoliths. | 101 |
| 5.3 | Solubility and melting temperature for different K-species. | 112 |
| 6.1 | EDX analysis performed on the foils of the impactor stages. | 121 |
| 6.2 | Bulk and surface analysis for the fresh and spent monoliths. . . . | 122 |
| 6.3 | Relative chemisorbed NH ₃ and relative activity as a function of exposure time. | 130 |

Chapter 1

Introduction

1.1 Background

Biomass (co)-combustion has for more than a decade been practised in countries like Denmark and Sweden, and is regulated by the government in order to limit the net emissions of CO₂. For instance, straw and wood chips are partially replacing coal in the Danish heat and power production. Owing to government demand, since the year 2000, 1.2 million tones of straw and 200000 tones of wood chips are to be used annually in the power plants, providing approximately 6% of the annual energy consumption in the Danish power stations. In the long term, the Danish government is planning to increase even more the use of biomass at central power stations.

Despite the above mentioned positive effect, biomass combustion presents different issues, which may reduce the efficiency of the process and make its operation rather complicated. For instance, fouling and corrosion of the superheater exchangers are the main problems encountered during straw combustion. Both these two effects are due to the composition of the fly ash produced, which is particularly rich in potassium chloride, KCl. This salt has a relatively low melting point temperature (i.e. 776 °C) and is therefore found in a liquid phase at the temperature of the superheater exchangers. This fact makes the fly ash particularly sticky and deposition on the metal surfaces of the heat exchangers causing the formation of a fouling layer is then favoured. Heat transfer through the heat exchanger is consequently decreased, and so is the overall efficiency in energy production. Furthermore, due to the presence of chlorine in the deposits, these are particularly corrosive and may irreversibly damage the heat exchangers.

In order to overcome these problems, the use of different additives to the biomass has been proposed [27–29]. The objective of the addition process is

Introduction

Table 1.1: Theoretical products of biomass combustion in the presence of additives

| | $T_m, ^\circ\text{C}$ | P/K | P/Ca |
|--------------------------------------|-----------------------|------|------|
| $\text{K}_4\text{P}_2\text{O}_7$ | 1105 | 0.5 | - |
| $\text{K}_2\text{CaP}_2\text{O}_7$ | 1143 | 1.0 | 2 |
| K_3PO_4 | 1340 | 0.33 | - |
| KCaPO_4 | 1560 | 1.0 | 1 |
| $\text{K}_4\text{Ca}(\text{PO}_4)_2$ | 1645 | 0.5 | 2 |
| $\text{Ca}_3(\text{PO}_4)_2$ | 1670 | - | 0.66 |

to change the fly ash composition produced during combustion and thereby favour (i) the release of Cl in the gas phase; (ii) the formation of ashes melting at temperatures higher than e.g. 1000°C , thus minimising sticking on the superheater exchangers. In particular, Danish power companies have seen as promising additives those involving P and Ca compounds proposed in the international patent by Sørensen et al. [27]. According to the invention, the addition process creates the reacting conditions at which all the potassium released during biomass combustion is bound in a phase consisting of $\text{K}_2\text{O}-\text{CaO}-\text{P}_2\text{O}_5$, that have melting points above 1000°C , and eventually K_3PO_4 , that have a melting point of 1340°C , while releasing the Cl in the gas phase. In order to meet these conditions, a fuel analysis is required and the amount of P and Ca to be added is calculated according to the following formulas:

$$P_{added} = q_1(31/39K_w + 31/23Na_w - P_w - 31/35.4Cl_w) \quad (1.1)$$

$$Ca_{added} = q_2(40/31(P_{added} + P_w) - Ca_w) \quad (1.2)$$

where E_w indicates the amount of the element E in parts by weight per 100 parts by weight of the non-combustible inorganic portion of fuel material before addition of additives. According to the invention, the two parameters q_1 and q_2 are ranging between 0.33 and 5 and 0 and 3 respectively. Based on the adopted values, the ash resulting from the combustion of the biomass-containing fuel will be dominated by the compositions showed in Table 1.1.

Tests using a macro-TGA (thermo-gravimetric analysis) and a bench scale atmospheric fluidized bed, involving wheat samples impregnated by aqueous solutions of H_3PO_4 and/or $\text{Ca}(\text{H}_2\text{PO}_4)_2 \cdot \text{H}_2\text{O}$, have been giving good results in terms of decreased ash sintering, indicating higher melting temperatures [27]. The ash produced by heating up the pretreated fuel was in the worse case only partially sintered, containing few fused ash particles at temperature around

1000 °C. In these tests the major products measured using X-ray diffraction were the ones showed in Table 1.1. Addition of monocalcium phosphate monohydrate as crushed dry particles showed also good results.

Different types of biomass pretreated with Ca and P additives have been tested at the CHEC research centre solid fuel flow reactor modified in order to make deposition tests [30]. Here, a very high reduction (98%) of Cl deposit contents was observed when the obtained ratios in the prepared fuel and additive mixture were approximately: $P/(Na+K) = 2$ and $P/Ca = 0.8$. These results pointed out the great potential of this technique in solving the problems encountered at the superheater section during biomass combustion.

While these preliminary combustion tests of biomass with the additives have shown their potential for solving the above mentioned fouling and corrosion problems in the boiler, little is known about their effects on the lifetime of the catalysts employed at the Selective Catalytic Reduction (SCR) process. This process is, among the various technologies available nowadays for removing NO_x from stationary sources, the best-developed and worldwide applied technology during fossil fuel combustion. In this process, the NO_x present in the flue gas is reduced to nitrogen by ammonia on a catalyst surface. Moreover its application to biomass and secondary fuel combustion is increasing due always stricter regulations. As it will be shown in Chapter 2 of this work, both P and Ca are known as deactivating compounds and therefore some concerns about their utilisation at full scale have risen.

1.2 Objectives

The main objective of this work has been to study the potential effects of the P and Ca additives on vanadia-based commercial SCR catalysts by clarifying their mechanism of deactivation under well defined and *realistic* conditions. For this purpose, besides standard poisoning tests carried out in the laboratory, deactivation tests have been performed in a pilot-scale SCR reactor by exposing commercial SCR monoliths to a flue gas doped with P, K and Ca, both independently and as a mixture.

The experimental work has been divided into the following three parts:

1. *Deactivation by Phosphorus*
2. *Deactivation by Potassium phosphates*
3. *Simultaneous deactivation by K, P and Ca*

In the first part, the deactivating effects due to P have been studied both in the laboratory, by doping the catalyst according to the conventional wet im-

Introduction

pregnation methods, and in the pilot plant. Here P, injected in the flue gas as a H_3PO_4 water solution, was exposed to more realistic combustion temperatures and underwent important both chemical and physical changes, which revealed its real deactivation strength. The work carried out in this part can be considered the first reference of deactivation by P under combustion conditions and have improved the understanding of various deactivation mechanisms experienced at full scale during combustion of P-rich fuels. The results of this investigation are reported in Chapter 4. The work has been published in the international peer-reviewed journal *Applied Catalysis B: Environmental*.

The second part of the work dealt with deactivation by potassium phosphate. This was carried out both at the laboratories and at the SCR pilot plant. The work at the laboratory was carried out by Sonia Pueyo Sin in partial fulfilment of her 40 ECTS points M.Sc. project¹. In the project, poisoning by K_3PO_4 was measured by doping the catalyst according to the conventional wet impregnation methods. Moreover, regeneration of the spent catalysts by washing with H_2SO_4 aqueous solutions was also studied. At the pilot plant, instead, K_3PO_4 was added by spraying a aqueous solution of this salt directly into a hot flue gas, thus allowing the formation of aerosols similar to those that may be present at full-scale applications. The results of these investigations are reported in Chapter 5. The work has been submitted for publication in the international peer-reviewed journal *Applied Catalysis B: Environmental*.

The investigation about deactivation by K_3PO_4 has mainly served the following two purposes. According to the invention by Sørensen et al. [27], K_3PO_4 may be one of the most desired products of the addition process, since it has a relatively high melting point temperature (i.e. 1340 °C) and would require the release of Cl in the gas phase during its formation. Therefore, the first purpose of the tests was to verify the poisoning strength of this compound. Moreover, since in previous works the strong K-deactivation has been related to the melting point of the compounds in which K is included, this test has also served the purpose to verify this relation and thereby increase the understanding of K-deactivation. Based on the results obtained in this work, deactivation by K is discussed in Chapter 7.

In the third part of the experimental work, a deactivation test simulating the suggested ratios $\text{P/K}=2$ and $\text{P/Ca}=0.8$ has been carried out at the SCR pilot plant. The results are presented in Chapter 6 of this work. It is based mainly on this test that the potential effects of the addition process on the SCR catalysts are discussed. The work has been submitted for publication in the international peer-reviewed journal *Applied Catalysis B: Environmental*.

¹The integral version of the M.Sc. thesis is available at the Department of Chemical and Biochemical Engineering of the Technical University of Denmark.

Chapter 2

Literature Study

2.1 Introduction

Nitrogen oxides (NO_x) emitted from combustion and high temperature processes have been regarded during the last three decades as a major environmental concern, thus supporting a great amount of research to develop clean combustion techniques. Among the various technologies available for removing NO_x from stationary sources, the Selective Catalytic Reduction (SCR) process applied to fossil fuel combustion is the best-developed and worldwide applied [31, 32]. In this process, the NO_x fraction of the flue gas is reduced to nitrogen by ammonia on a catalyst surface. The commercial SCR catalysts are normally constituted by vanadia (the active phase) supported on high surface titania. WO_3 and MoO_3 are the most common compounds added to the catalysts in order to improve its performance both chemically and physically. The composition of the industrial catalyst, however, may vary according to the particular application and it is the result of a comprehensive research carried out in the last two decades.

Understanding of the mechanisms of catalyst deactivation has also been the aim of many investigations. Since their appearance in the 1980s, all the possible causes of both chemical and physical deactivation have been investigated. These studies have always been strictly correlated to the problems encountered at full-scale applications and have often conducted to the development of better catalysts. The number of these investigations is nowadays still increasing due to the requirement of NO_x abatement in processes (e.g biofuels and wastes combustion) where the catalyst life is not as long as desired. The interest in these *alternative* processes is in the last years increasing due to local environmental policy and regulations. In some cases, very fast rates of deactivation are observed resulting in great investments of resources aimed at overcoming the

encountered problems by developing new and more resistant catalysts.

The objective of the present Chapter is to review the open literature concerning the industrial SCR catalysts with a particular attention to the present knowledge about their deactivation mechanisms and promoters.

The present Chapter is composed by three parts. In the first part (Section 2.2 and Section 2.3) the NO_x sources and the available control technologies are presented. This part mainly deals with coal combustion, since the development of these technologies was mainly related to this fuel. The SCR process is also introduced in this first part.

The second part (Section 2.4) extensively deals with the vanadia-based catalysts. This is an attempt to point out from the open literature the characteristics and properties of this family of catalysts, which are relevant only for typical SCR conditions. The different proposed mechanisms of reaction and the respective kinetic models are also presented and discussed.

Finally, the third part (Section 2.5) deals with deactivation of vanadia-based catalysts. The different mechanisms of deactivation and the deactivation promoters are presented in this part. An attempt to correlate the different deactivation mechanisms to the particular SCR application is also made in this part.

2.2 NO_x Control Technologies

Nitric oxide and nitric dioxide, collectively termed NO_x , are acid rain precursors and participate in the generation of photochemical smog, thus constituting a major environmental concern. The need to comply with increasingly stringent regulations for the NO_x emissions has motivated a vast amount of research resulting in the development of different methods of NO_x control during the last decades. These methods are generally classified as *primary measures* when they act directly on the formation of NO_x in the boiler and furnace. On the other hand, the technologies that reduce the concentration of NO_x in the flue gas are known as *secondary measures*.

In the present section, after introducing the various sources of nitrogen oxides, both primary and secondary control measures of industrial interest are briefly presented.

2.2.1 Sources of Nitrogen Oxides

Fossil fuel combustion is identified as a major source of nitrogen oxides, NO and NO_2 . Another important source is biomass combustion. Together, these two *anthropogenic* sources cover about 75% of the total NO_x emission [26]. Beside these, *biogenic* emissions from soil are the third important source of NO_x .

2.2 NO_x Control Technologies

Table 2.1: Global inventory of NO_x sources [26].

| NO _x sources | Magnitude (TgN/year) | |
|-------------------------|----------------------|-------------|
| Fossil fuel combustion | 22.0 | (15-29) |
| Biomass Burning | 6.7 | (3-10.4) |
| Lightning | 2.0 | (1-4) |
| Stratospheric injection | 0.5 | (0.4-0.6) |
| Aircraft emissions | 0.6 | (0.5-0.6) |
| Ammonia oxidation | 1.0 | (0.5-1.5) |
| Total | 38.2 | (23.7-53.8) |

In this case, NO_x is the result of the natural process of nitrogen cycling. However, fertilizers and other agricultural practices perturb the natural process increasing the amount of NO_x emitted. Finally, other significant sources of NO_x are due to lightning, ammonia oxidation and aircraft exhausts. A global inventory of NO_x sources is presented in Table 2.1 [26].

The flue gas resulting from combustion processes mainly consists of NO and NO₂, with the former accounting for about 95% of the NO_x emissions from combustion. There are three different mechanisms for NO_x formation in combustion processes [33]:

1. *Thermal NO_x*. It is formed as a result of the reaction of nitrogen with molecular oxygen in the combustion air at peak flame temperature. Thermal NO_x increases according to the combustion temperature and generally accounts for about 5-25% of the NO_x formed during coal combustion.
2. *Fuel NO_x*. Its formation is due to oxidation of the nitrogen bound in the fuel. It highly depends on the local flame stoichiometry, whereas the temperature does not affect its production to any great extent. The nitrogen content in coal, ranging between 0.5 and 2%, can contribute up to 70-80% of NO_x formed during coal combustion.
3. *Prompt NO_x*. The formation of prompt NO_x takes place in the front of the flame first by reactions between nitrogen in the air and hydrocarbon fuel fragments forming intermediate HCN. This reaction is then followed by the oxidation of the HCN to NO. Prompt NO_x has a weak temperature dependence and is significant only in fuel-rich flames. In fact, for typical conditions the prompt NO_x portion from coal combustion accounts for only 5% of the total NO_x emissions.

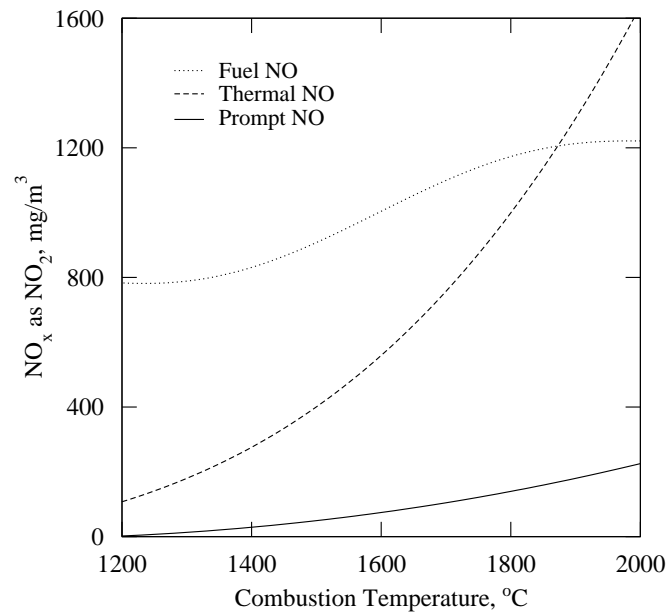


Figure 2.1: Temperature influence on the amount of NO_x produced from the three NO_x formation mechanism in the case of coal combustion. Data from [1].

In solid fuel systems, fuel NO is generally the major source of NO_x , with some contribution from thermal NO (Figure 2.1). The fuel nitrogen formation and conversion in solid fuel fired system was recently reviewed by Glarborg et al. [34].

2.2.2 Primary Measures

Primary measures, also known as combustion controls or clean technologies, are the first taken into consideration to lower the NO_x emissions due to their high effective-cost ratio compared to other control technologies.

The main targets for these measures are:

1. decreasing the oxygen level at peak temperature;
2. reducing the peak temperature and the residence time in the combustion zone;
3. reducing the level of fuel nitrogen.

The first two issues are in general achieved by adopting so-called *low- NO_x* burners. These are designed to control fuel and air mixing at each burner in

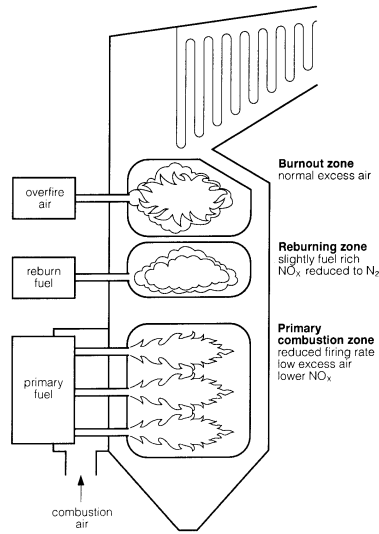


Figure 2.2: The three combustion zones in a reburning process [1].

order to create larger and more branched flames, reducing peak flame temperature.

The most effective combustion control is the *reburning* technique, shown in Figure 2.2 [1]. It consists of a three stage system and requires the injection of a secondary fuel, typically natural gas (also coal, oil and biomass can be used). In the first stage, the so-called “primary combustion zone”, the fuel is burnt at low excess air conditions, reducing initial NO_x formation. The secondary fuel is then introduced in the furnace at the second stage (the “reburning zone”) without combustion air. Here, the secondary fuel breaks down to produce hydrocarbon fragments which reduce NO_x from the first stage to HCN and NH₃. Then, according to the operating conditions at this stage, the formation of molecular nitrogen from these is favoured. Finally, at the third stage, overfire air is injected in order to consume the CO and the unreacted hydrocarbons leaving the reburning zone. This final stage is referred to as the “burnout zone”. The operating cost of this combustion control is highly influenced by the cost of the secondary fuel.

Another effective primary technique is *air staging*. It consists of the introduction of combustion air in two separate (primary and secondary) flow sections, in order to encourage the formation of N₂ rather than NO_x. Primary air (70-90%) is mixed with the fuel producing a relative low temperature, oxygen deficient, fuel-rich zone. In this manner, only moderate amounts of NO_x are formed. Secondary air (10-30%) is then injected above the combustion zone in order to complete the combustion of the fuel.

Literature Study

Table 2.2: Primary measure reduction capabilities in coal-fired boilers [1].

| Primary measure | De-NO _x (%) |
|--|------------------------|
| flue gas recirculation | <20 |
| burner fuel staging | 10-30 |
| low NO _x burners | 30-55 |
| low NO _x burners and overfire air | 35-70 |
| coal reburning | 40-60 |
| natural gas reburning with flue gas recirculation | 55-65 |
| natural gas reburning without flue gas recirculation | <60 |
| low NO _x burners with natural gas reburning | 60-70 |

Finally, other techniques are the *flue gas recirculation* and the *addition of steam or water*. Both of them decrease the peak temperatures in the combustion chamber and accordingly the production of thermal NO_x.

By combining different primary measures, NO_x removal up to 70% are possible [35]. Table 2.2 presents a list of primary methods and their respective NO_x reduction capabilities [1]. In some cases, however, some of these methods may not be viable for fuels like biomass or waste. These fuels are commonly burned on grates or in fluidized beds, and these technologies do not support, for example, the use of low-NO_x burners.

2.2.3 Secondary Measures

The secondary measures, also referred to as post-combustion control or flue gas treatment, offer moderate to high NO_x removal efficiency. They are categorized as follow:

- Selective Catalytic Reduction systems (SCR);
- Selective Non Catalytic Reduction systems (SNCR);
- hybrid SNCR/SCR systems;
- combined SO₂ and NO_x removal processes.

All these methods can be used independently or in combination with primary measures. In general, most of them relies on the injection of ammonia, urea or other compounds to react with the NO_x in the flue gas and reduce it to molecular nitrogen.

2.2 NO_x Control Technologies

Table 2.3: Simultaneous removal of SO_x and NO_x processes [1].

| Dry Processes | Wet Processes |
|-------------------------------|--------------------------------------|
| Mitsui-BF activated carbon | CombiNO _x process |
| RTI-Waterloo activated carbon | SOXAL process |
| Copper oxide process | Tri-NO _x -NoxSorb process |
| SNAP alumina-sodium process | LTO process |
| SNOX process | Iron-chelate process |
| SNRB process | |
| DESONOX process | |
| E-Beam process | |
| ANL alkali dry spray process | |
| LILAC process | |

In the SCR process, the reaction is carried out in the presence of a catalyst, which strongly enhances the rate of NO conversion at lower temperatures. This post-combustion control is capable of providing NO_x reductions in excess of 90%. The SCR process will be extensively discussed in the next sections.

On the contrary, in the SNCR process, nitric oxide and ammonia react in the absence of a catalyst. High conversions are only possible at higher temperatures (800-1000 °C) than the ones required by the SCR process (300-400 °C). For this reason, the reducing agent is introduced directly in the boiler, above the flame zone. NO_x removal up to 70% is possible using an efficient reagent injection control that avoids the decomposition of ammonia at higher temperatures, and an appropriate residence time in the reaction temperature range.

A hybrid SNCR/SCR system combines the injection of ammonia into the boiler with a SCR catalyst where the reaction between residual NO_x and ammonia slip takes place. In other words, the SNCR removes part of the NO_x while supplying the ammonia reagent required for the catalytic removal of more NO_x.

In order to achieve more cost effective systems with both high NO_x and SO₂ removal, several combined processes have been developed [1, 31], and are generally classified in dry and wet processes. Table 2.3 presents a list of the most important processes [1].

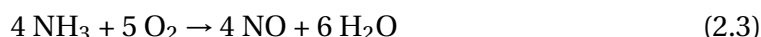
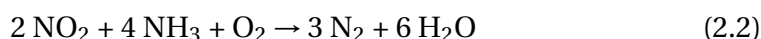
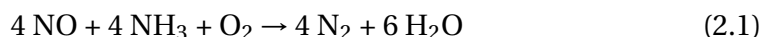
2.3 The SCR Process

Among flue gas treatment methods the Selective Catalytic Reduction (SCR) is the most world-wide used for controlling NO_x emissions from stationary combustion sources. It was first installed in Japan in the late 1970s on industrial and utility plants, whereas in Europe, the first commercial SCR process appeared in 1985. Based on the Japanese and European experience, the process was then adopted in the USA during the 1990s where it was first confined to gas turbines primarily located in California. [36–38].

The commercial use of the SCR process in the years has followed the introduction of stringent limits to regulate NO_x emissions in each country. In 2001, SCR commercial installations were in operation in the Japanese and European power companies for an estimated overall capacity close to 100 000 and 60 000 MW respectively [38]. However, in the last years the use of the SCR process has further increased due to its introduction to processes such as industrial and municipal waste incinerators, chemical plants and cement industries among the others. Moreover, SCR catalysts are also increasingly employed in biomass-fired boilers, stationary and non-stationary diesel and gas engines (i.e marine propulsion engines and locomotive engines) [38, 39].

2.3.1 The Reactions

In the SCR process, NO_x is reduced by ammonia directly injected into the flue gas over a catalyst in the presence of sufficient oxygen. The operating temperature is typically ranging between 300 and 400 °C. The NO_x reduction is then possible according to the following overall reactions:



Since NO constitutes more than 95% of NO_x in the flue gas, reaction (2.1) is the main SCR reaction and thus accounts for the overall stoichiometry of the process.

The ability of ammonia to react selectively with the NO_x fraction of the flue gas instead of being oxidized according to reaction (2.3) is a unique feature of this system, not observed in the case of other reagents such as CO and hydrocarbons [38].

The potentially most troublesome side reaction is the oxidation of SO₂ to SO₃ by the catalyst, which is greatly increased at temperatures above approximately 370 °C. Sulphur oxides in the flue gas may react in the presence of unreacted ammonia forming (NH₄)₂SO₄ and NH₄HSO₄. The formation of NH₄HSO₄

is possible at 235 °C in the usual SCR operating condition of 5 ppm NH₃ and 10 ppm SO₃, whereas (NH₄)₂SO₄ is formed if the temperature drops below 200 °C. These compounds are responsible for both (reversible) deactivation of the catalyst and damage of downstream equipment. This is a major problem with high sulphur coals.

From all this, it is clear that:

1. unreacted ammonia (ammonia slip) has to be avoided;
2. besides a high NO_x removal activity, selectivity is an extremely important parameter for SCR catalysts.

The first issue is accomplished by injecting around 0.9 parts of ammonia for each part of nitric oxide. Figure 2.3 shows the correlation between NO_x removal and ammonia slip [2]. From this, it is clear that to keep the ammonia slip below 5 ppm the NH₃/NO_x ratio have to be below 1. Furthermore, the temperature is typically kept below 370 °C, to avoid the oxidation of SO₂, but above 300 °C, to minimize ammonia slip and ensure efficient NO_x removal.

Different catalysts based on zeolite, iron oxide or activated carbon have been tested in laboratory scale. However, the most widely adopted are based on vanadia on a titanium oxide carrier [31, 32]. The characterization of this family of catalysts and their behaviour in the SCR reaction are extensively discussed in Section 2.4.

2.3.2 Process Design and Optimization

A typical SCR system includes: a storage, delivery, vaporization, and injection system for reagents; an SCR reactor housing the catalyst; soot blowers; and additional instrumentation. There are mainly three typical layout arrangements of SCR systems applied to fossil-fuel-fired power stations (Figure 2.4). The best configuration strongly depends on the particular application.

High dust configuration is the most widely used SCR configuration in coal-fired plants. The main advantage is that the temperature right after the boiler economizer is in the range suitable for the SCR reaction. The name “high dust” indicates that no particulates have been removed from the flue gas prior to the de-NO_x process. In this configuration, the catalyst is thus exposed to fly ash and chemical compounds present in the flue gas that can both plug the catalyst and degrade it mechanically and chemically. However, appropriate design of a high-dust SCR system can mitigate the impacts on the catalyst. If this was not the case, the cost of a high temperature electrostatic precipitator (H-ESP) placed in between the boiler and the SCR reactor could still be a convenient

Literature Study

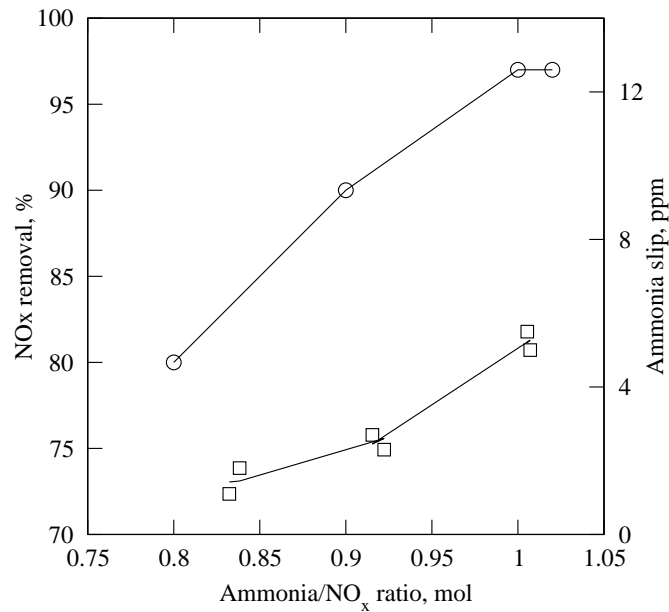


Figure 2.3: NO_x reduction (circles) and ammonia slip (squares) as a function of reagent normalized stoichiometric ratio. NO_x inlet: 425 ppm; temperature: 368 °C. Data from [2].

investment. This solution is known as *low dust* configuration. In a *tail end* configuration, the SCR reactor is placed between the Flue Gas Desulphurization plant (FGD) and the stack. In this case, the absence of SO₂ in the flue gas allows the use of more reactive catalyst formulations, mainly because the oxidation of SO₂ to SO₃ is not a problem. At the same time, the lifetime of the catalyst is also increased because of the low dust loading. However, the lower catalyst costs need to be compared with the investment in the heat exchangers and the energy needed in order to reheat the flue gas from about 60 to 370 °C.

Liquid ammonia is vaporized, diluted with air and injected into the flue gas through a grid located in the ductwork leading to the SCR reactor. The distance from the reactor is kept to a relative high value in order to ensure complete mixing of the reactants across the catalyst cross-section. The amount of ammonia injected is controlled by measuring the NO_x concentration in the flue gas at the economizer outlet, whereas the temperature of the flue gas reaching the SCR reactor is controlled by mixing the flue gas exiting the economizer with the flue gas from the economizer by-pass.

Industrial SCR reactors contain up to four catalyst layers with spacing in between (Figure 2.5). Each layer consists of different catalysts assembled in modules. The configuration of the applied SCR catalyst element and reactor depends on several factors. The SCR catalysts are designed for use in parallel

2.3 The SCR Process

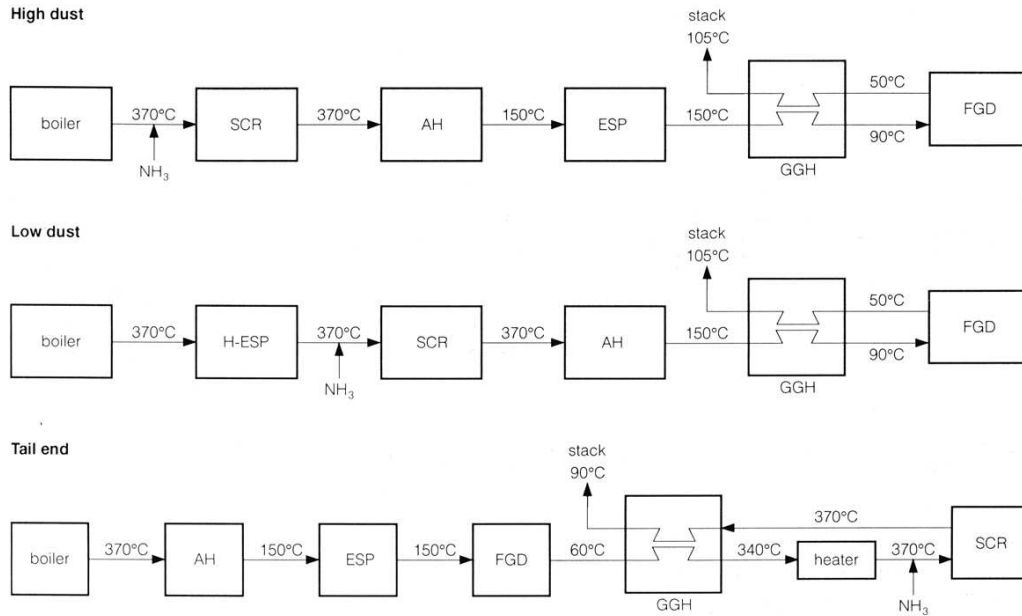


Figure 2.4: SCR process arrangements. SCR: selective catalytic reduction; AH: air preheater; ESP: electrostatic precipitator; H-ESP: high temperature ESP; GGH: gas-gas heater; FGD: flue gas desulphurisation. From [3].

flow and various types of geometry can be used. By using monolithic catalysts, both low pressure drops, large external surface, uniform flow and, most important for the treatment of flue gases, good resistance to attrition and dust deposition can be obtained. Each catalyst module contains a large number of parallel straight channels with openings of a few mm depending on dust concentration and properties. In high dust configurations, the channels have large channel openings (6-8 mm) and wall thickness (up to 1.5 mm) in order to prevent channel blocking and erosion by ash. In low dust and tail end configurations, the relative absence of particulate allows the use of catalysts with higher geometric surface. In all configurations, a typical honeycomb catalyst block is 50-100 cm long with a face area up to 50 cm by 50 cm. The flue gas normally has gas hourly space velocities (GHSV) in the 2000-7000 h^{-1} (STP) range [40].

In order to ensure high NO_x removal efficiency and low ammonia slip, great attention is paid to the fluid dynamics of the entire reactor. A uniform distribution of the reagents, and temperature and flat velocity profile of the flue gas need to be obtained over the entire cross-section of the catalyst layer. For these reasons, the SCR reactor is provided by guided vanes and distribution layers.

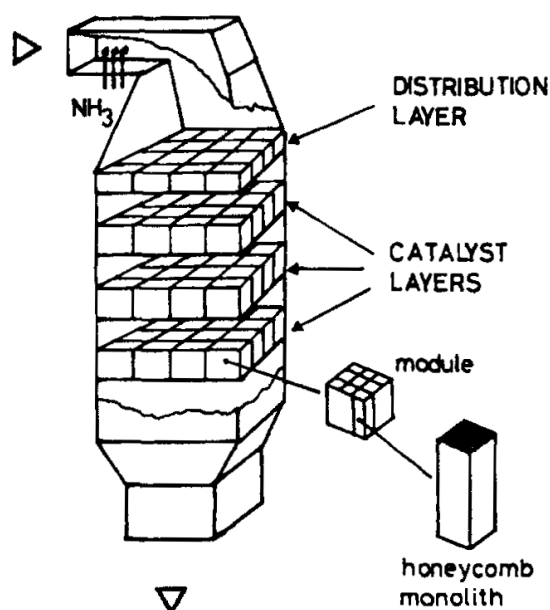


Figure 2.5: Structure of SCR reactors [4].

2.4 Supported-Vanadia Catalysts in the SCR of NO by NH_3

Among all the metal oxide catalysts applied in the SCR process of NO by NH_3 , the TiO_2 (anatase)-supported V_2O_5 catalyst is the most efficient one due to its high selectivity and high activity at relative low temperature [31]. Consequently, it has been subject to a great number of studies concerning reaction mechanisms and kinetics.

In the present section, a review of the information in the open literature about the catalyst properties and its behaviour in the selective catalytic reduction on NO by NH_3 is presented.

2.4.1 Catalyst Characterization

The name “supported vanadia catalyst” indicates a wide number of different systems that have in common the vanadium oxide as active component in the SCR reaction. The commercial catalysts present both different kind of supports and amounts of active component. Moreover, additives are used in order to improve their physicochemical properties and catalytic activity. On the other hand, in order to understand the influence of each single component in the

2.4 Supported-Vanadia Catalysts in the SCR of NO by NH₃

global catalyst, simplified systems have been studied. Pure vanadia catalysts and binary vanadia-titania systems have been prepared and characterized in order to clarify the role of the structure of the active phase and its influence on the behaviour of the catalyst [18, 41]. The behaviour of the single promoter has been displayed by analysing the activity in the SCR reaction of its pure phase [42]. Different authors have compared vanadia-titania system with promoters-titania and vanadia-promoter-titania systems [43–50] in order to address the optimal composition of the catalyst. Others have characterized commercial catalysts and compared them with the previous *ideal* systems [51, 52].

In the following sections, the properties of the support, the active phase and the most common promoters have been extracted and resumed from the data found in the open literature.

The Support

Even though pure titania catalysts have a low SCR activity [53], this has been preferred as optimal support for the active phase. Titania in the anatase form, despite its thermal instability, presents the highest surface area (BET \approx 70-100 m²/g).

IR studies of a pure titania catalyst after oxygen pretreatment revealed the presence on the surface of Ti–OH bonds mainly due to water molecules included in the atmosphere [53–55]. These species are the sites where the interaction between titania and vanadia takes place. Thus, their concentration determines the vanadia amount necessary to cover the support surface with a single monolayer and the dispersion of the vanadia species. As it will be clearer in the next section, both the amount of vanadia and its dispersion are essential parameters for the SCR activity and N₂ selectivity of the catalyst. A way to control the support properties is the preparation technique [56]. Among the others, the hydrolysis of titanium isopropoxide provides supports with the greatest surface area and highest concentration of Ti–OH sites [57].

The Active Phase

It is generally accepted that vanadia constitutes the active phase in the SCR process [6, 9, 10, 17, 31, 48, 58, 59]. A comprehensive review of the role and chemistry of supported vanadium oxides in heterogeneous catalysis has been recently published [5].

Supported vanadium oxides can be present in the following molecular configurations [5] depending on the load:

- isolated vanadium ions;

Literature Study

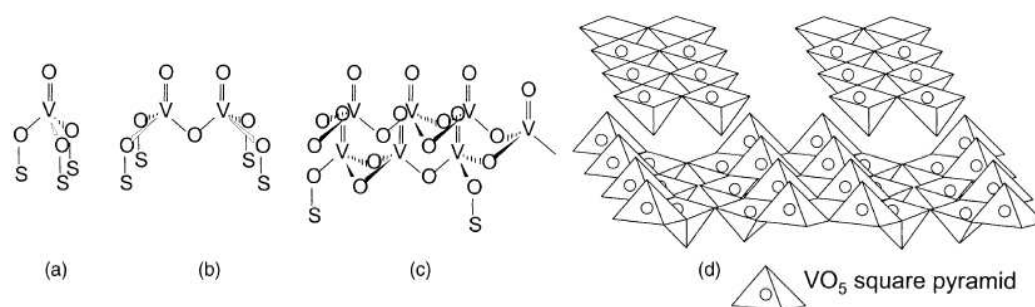


Figure 2.6: Possible molecular configurations for supported vanadium oxides (with S the support cation): (a) isolated vanadium oxide species; (b) dimeric vanadium oxide species; (c) two-dimensional vanadium oxide chains; (d) V_2O_5 crystals. From [5].

- dimeric or polymeric species;
- two-dimensional layer of supported vanadium oxides;
- crystalline or amorphous, three-dimensional vanadium oxides;
- mixed metal oxide phases with the support.

Each one of the previous species, shown in Figure 2.6, presents a different behaviour in the catalytic process. Went et al. [6] have first studied the dependence of vanadia load on the different molecular configurations and their behaviour in the SCR reactions. By means of Raman spectra, they showed that at low vanadia contents ($< 1\%$ wt) only *isolated* monomeric species are present on the support. For loading around 2% wt, *less isolated* monomers start reacting together producing polymeric vanadyl species. Finally, when the vanadia content is further raised above the dispersive capacity of anatase, the polymeric species increase in vanadia terminals and crystallites are also observed. In particular, the formation of the crystallites takes place at the expense of the polymeric entities as shown in Figure 2.7.

According to the Raman spectra obtained by the authors, both mono- and polymeric vanadates are characterized by $V=O$ bands at different frequencies. The crystallites, in addition, present $V-O-V$ bonds, where the O atoms are more labile than the ones present in the $Ti-O-Ti$ bonds of the support. The different energies of formation associated with the vanadate species were then used to explain the values of activity and N_2 selectivity according to the vanadia loading. These have been found to be optimal when one monolayer of vanadia is dispersed on the support surface [6, 48, 58], indicating a strong activity of the polymeric species characterized by terminal $V=O$ bonds in dry conditions and

2.4 Supported-Vanadia Catalysts in the SCR of NO by NH₃

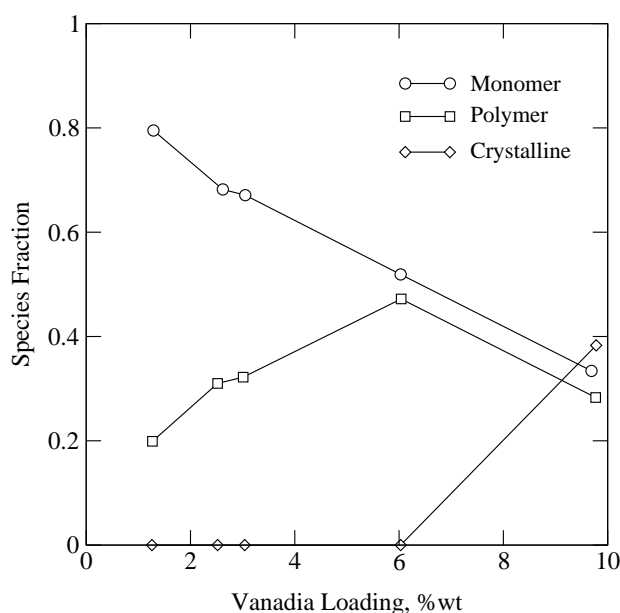


Figure 2.7: Distribution of monomeric, polymeric and crystalline vanadia species as a function of the vanadia surface density. Data from [6].

V–OH bonds in wet atmospheres. As a direct consequence of this result, and considering that vanadia is active in the undesired oxidation of SO₂ to SO₃, the vanadia content in the commercial catalysts for the SCR of NO by NH₃ usually does not exceed about 2%wt in the presence of SO₂ in the flue gas.

Topsøe et al. [54], analysing pure titania and vanadia-titania samples at different loads by means of Fourier Transform IR (FT-IR), have found that the deposition of vanadia takes place on the sites previously occupied by the Ti–OH bonds. Moreover, the resulting species are characterized by V–OH bonds (3500–3700 cm⁻¹), not observed on pure V₂O₅. The concentration of V–OH bonds is also very sensitive to the sample pretreatments and enhanced by oxidation. In fact extensive reduction in H₂ eliminated the V–OH species, reexposing the surface Ti–OH ones.

Additional Components

The industrial catalysts for the SCR process are based mainly on TiO₂-supported V₂O₅-WO₃ and/or V₂O₅-MoO₃. WO₃ and MoO₃ have been selected since they increase the acidity and reactivity of the V₂O₅/TiO₂ catalysts and can limit the oxidation of SO₂ to SO₃. Moreover, they also provide thermal stability to the catalyst, widening its temperature window and avoiding both the surface area

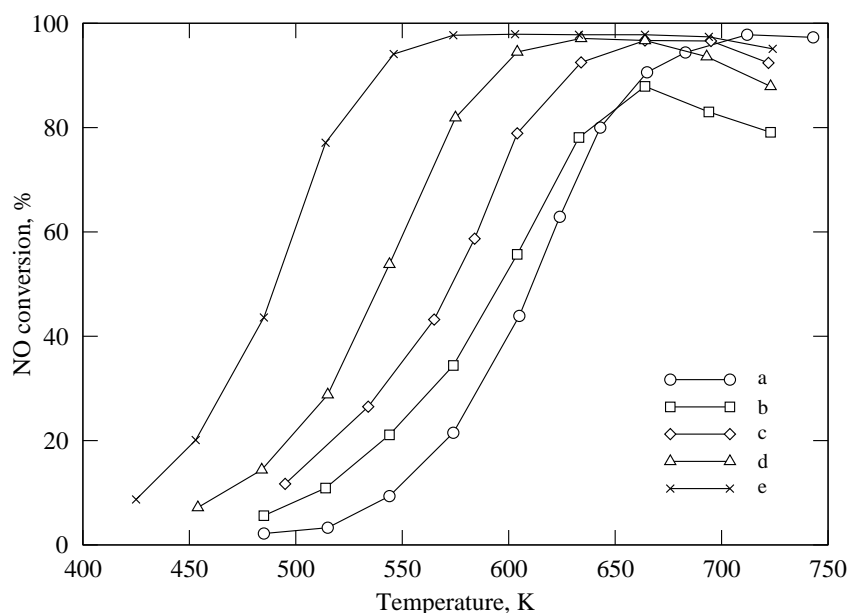


Figure 2.8: NO conversion versus temperature: (a) 9 %wt WO₃-TiO₂; (b) 0.78 %wt V₂O₅-TiO₂; (c) 1.4 %wt V₂O₅-TiO₂; (d) 0.78 %wt V₂O₅-9 %wt WO₃-TiO₂; (e) 1.4 %wt V₂O₅-9 %wt WO₃-TiO₂. Feed: He, 800 ppmv NH₃, 800 ppmv NO, 1 %v O₂. Data from Ref. [7].

loss of anatase and its transformation to the more stable rutile configuration [7, 31]. In addition to these compounds, silico-aluminates and glass-fibres are also added to improve the mechanical properties and strength of the catalysts.

WO₃ is added in substantial amounts ($\approx 10\%$ wt). While pure WO₃ or WO₃ supported on titania shows only limited SCR activity, when added to vanadia/titania catalysts it strongly improves their activity, as shown in Figure 2.8. The properties of this compound in the SCR reaction can be extracted from different studies on pure WO₃ [42], WO₃/TiO₂ [48, 50] and TiO₂(a)-supported V₂O₅-WO₃ [43, 44, 49, 51, 52] catalysts. From these studies, it is seen that WO₃ interacts with the titania supports forming W_xO_y clusters containing W–O–Ti and terminal W–OH and W=O bonds, the latter with a coordinative unsaturation [50]. On the other hand, it does not interact with vanadia. In fact, no evidence is found for V–W mixed oxides [52] indicating that interactions take place only through the support. When tungsten and vanadia are both present on the titania support, they instead form the same W=O and V=O bonds observed on the tungsten-titania and vanadia-titania catalysts respectively [49].

With an extensive characterization of V₂O₅-MoO₃/TiO₂ catalysts, Lietti et al. [60] showed that the addition of MoO₃ to V₂O₅/TiO₂ produces similar effects to those produced by the addition of WO₃. In this case, the surface is charac-

2.4 Supported-Vanadia Catalysts in the SCR of NO by NH₃

terized by Mo=O and Mo–OH bonds. Compared to the catalyst with tungsten, the V₂O₅-MoO₃/TiO₂ at high temperature becomes less active. Furthermore, in the presence of a dry feed, it also becomes less selective due to the formation of N₂O. However, this additive has had a great success since it limited arsenic deactivation of vanadia-based catalysts (2.5.5).

Finally, regarding the use of sulphated TiO₂ supports, Choo et al. [55] found that they enhance the activity of the catalyst by improving the polymer vanadate fraction on the surface. This fact was explained by the authors to be caused by the reduced surface area available for vanadia deposition in the presence of sulphates.

2.4.2 Adsorption and Surface Reaction Studies

From the characterization presented above, it is clear that, according to the vanadia loading and the addition of promoters, the catalyst surface presents both (V,W,Mo)–OH, (V,W,Mo)=O and V–O–V bonds. On the other hand, the Ti–OH bonds disappear with the formation of a monolayer of vanadia. Additionally, Ti–O–Ti bonds are present on the uncovered titania. All these species are responsible in different ways for the adsorption of the reacting compounds.

To elucidate such aspects, the adsorption characteristics of SCR reactants over vanadia-based catalysts have been extensively investigated in the literature by means of Laser Raman (LR) spectra and Fourier Transform IR (FT-IR) [9, 44, 48, 51, 53, 54, 61, 62], Diffuse Reflectance Infrared Fourier Transform Spectroscopy (DRIFTS) [63, 64] and isotopic labelling [65]. Temperature Programmed Desorption (TPD) and Temperature Programmed Surface Reaction (TPSR) studies have also been performed to display the reactions activated by the catalyst [10, 43, 48, 59]. In order to better follow the adsorption process under typical reaction conditions, in situ techniques have also been applied and the surface reaction was analysed combining on-line mass spectroscopy (MS) [10, 59]. Transient response methods have also been performed [39, 43, 66–68]. The following sections present the most relevant evidences in order to introduce the mechanistic and kinetic discussion that will follow.

NH₃ Adsorption

The different ways ammonia can adsorb on vanadia-titania catalysts are shown in Figure 2.9 [7]. Ammonia readily adsorbs at room temperature on the TiO₂ support in the coordinated form [53, 54, 58, 59], indicating the presence of only Lewis Acid sites (LA) on pure titania. No evidence was found by different authors for NH₄⁺ species, showing the absence on the support of Brønsted acid

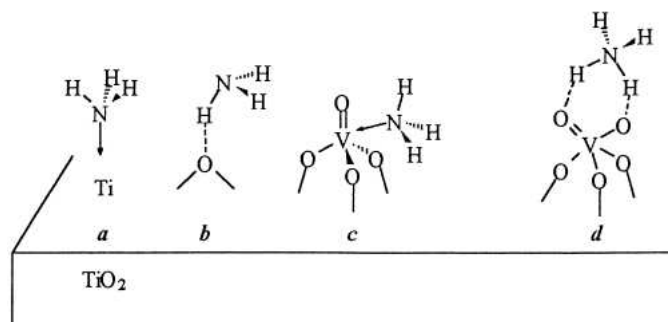


Figure 2.9: Proposed structures for NH_3 adsorbed on $\text{V}_2\text{O}_5\text{-TiO}_2$: (a) Lewis-bonded NH_3 at Ti sites; (b) H-bonded NH_3 on oxide sites; (c) Lewis-bonded NH_3 at vanadyl sites; (d) ammonium ions bonded at V Brønsted acid sites. From [7].

sites (BA). Instead, H-bonding between NH_3 and Ti-OH groups were detected by Topsøe et al. [54, 59].

On the contrary, pure vanadia is characterized mainly by Brønsted acid sites as indicated by the presence of ammonium ions upon ammonia adsorption. Besides the BA sites, small amounts of coordinated ammonia are present on pure vanadia catalysts. Their total amount increases after a reduction pretreatment due to more anion vacancies being created during reduction [54].

As expected from these results, titania-vanadia catalysts present both Lewis and Brønsted acid sites depending on the vanadia loading. In fact ammonia adsorbs on these catalysts both as coordinated ammonia and ammonium ions [9, 54]. Moreover, the relative amount of these sites is a function of the oxidation state of the catalyst: an oxidized catalyst will present much more BA sites than a reduced one. The contrary is true for the LA sites. H-bonding with oxide sites is also possible.

The effects of vanadia load on ammonia adsorption have been reported in several publications [9, 10, 54, 59]. The results showed that for catalysts with different vanadia loading treated with ammonia at room temperature the Brønsted acidity is greatly enhanced by the addition of vanadia [10, 54, 59]. The disappearance of the V-OH bands during the ammonia treatment suggests that the BA sites are directly associated to these species. Additionally, the upwards shifts of the frequencies due to NH_4^+ species in the vanadia/titania catalysts indicate that the interaction between titania and vanadia enhances the strength of the total Brønsted acidity [54]. Also the original Lewis acidity due to the support was found to increase somewhat by adding vanadia to the catalyst [54]. The disappearance in the recorded adsorption spectra of the peaks due to the V=O bonds indicated that ammonia is coordinated on vanadyl groups [9].

2.4 Supported-Vanadia Catalysts in the SCR of NO by NH₃

The influence of additional compounds on the ammonia adsorption was also investigated [43, 48, 50, 62]. All authors agree that the W=O and Mo=O species lead to the formation of Lewis acid sites stronger than the ones present on V₂O₅/TiO₂ surface. Additionally, protonated ammonia also adsorbs on the W–OH and Mo–OH sites, increasing the Brønsted acidity of the surface. Furthermore, under typical SCR conditions, the ammonia coverage of the WO₃-free catalyst is significantly lower [39], further pointing out the active role of the additives in the NH₃ adsorption.

Regarding the thermal stability of these acid sites, all the authors agree that LA sites are much stronger than BA sites: upon evacuation at 520 K, ammonium ions are not present on the catalyst, while coordinated ammonia is still observed [9]. Moreover, ammonia is more strongly adsorbed on the catalyst in the presence of WO₃ [39].

NO Adsorption

In principle, NO can adsorb on the titania support at least in three different ways [9, 53]: (i) it can coordinate on the Lewis sites of the titania oxide as nitrosyls; (ii) it can react on the catalyst surface and adsorb as coordinated N₂O; or (iii) as nitrate ions. On the other hand, vanadia-titania catalysts adsorb NO on exposed Ti⁴⁺ centres as NO₃⁻ species, the latter being produced by oxidation of NO on vanadyl cations. The oxidation state of the surface also plays an important role on NO adsorption [54]. In fact, no adsorption is possible on oxidized samples, whereas extensive adsorption is detectable only upon strong reduction in H₂ flow due to increased presence of Ti–OH bonds.

In any case, the interaction of NO with the surface is very weak and, as it will be clearer in the following section, it is negligible under typical SCR conditions, in particular in the presence of ammonia.

Surface Reaction Studies: Active Sites in the SCR Reaction

In order to better understand the mechanisms of the reaction, NH₃ and NO co-adsorption experiments were carried out by many investigators [9, 10, 39, 43, 44, 46, 54, 59, 61, 63–66]. From all these, it appears that under typical SCR conditions NO does only slightly adsorb on the catalyst surface. On the other hand, most authors agree that ammonia strongly adsorbs both as coordinated on Lewis acid sites and as protonated on Brønsted acid sites. However complete agreement on which one of these two acid sites is the active site during the SCR reaction has still not been reached.

Ramis et al. [9] using a standard FT-IR cell found that with increasing temperature, coordinated ammonia disappeared faster than the ammonium ions,

in contrast to the evidences from ammonia desorption studies. At the same time, the bands assigned to adsorbed nitrosamide (NH_2NO) and to hydroxyl groups, possibly due to the adsorption of water, were growing. They concluded that these two facts implied the presence of the SCR reaction: *coordinated ammonia* and gaseous NO were then identified as the active species in the reaction, with the latter passing through the formation of NH_2NO identified as a possible intermediate.

Contrarily, Topsøe et al. [59] concluded that *ammonium ions* are involved in the SCR reaction, mostly adsorbed on V–OH sites that are then indicated as the active sites of the reaction. To better follow the surface reaction and the formation of the products, they combined in situ FT-IR and Mass Spectroscopy and performed TPSR in O_2 , NO and O_2+NO atmosphere. As Ramis et al. [9], they also noticed the disappearance of the coordinated ammonia, but in their opinion under SCR conditions coordinated ammonia desorbs and readily re-adsorbs on BA sites. Furthermore, LA sites are also converted to BA sites by the water present in the feed. In any case, an important role in the catalytic activity of the catalyst was assigned to the V=O terminals. According to [59], these are responsible for the activation of adsorbed ammonia on BA sites.

The ammonia adsorbed on sites provided by the additional components does not seem to be directly involved in the SCR reaction. On the contrary, it has been shown by means of Transient Response Method that these sites provide an ammonia reservoir [39, 51, 66]. This ammonia needs to be transferred over the surface or desorb and re-adsorb on vanadia sites prior to reaction.

2.4.3 Reaction Mechanism

Since the first mechanism proposed by Takagi et al. [69] in 1977, different mechanisms have been presented in the literature, based both on experimental and theoretical studies [7, 32, 70]. In the present section a brief review of the main mechanisms is presented.

Since there is a general agreement that no NO adsorption is possible under typical SCR conditions, the reaction follows an Eley-Rideal mechanism between strongly adsorbed NH_3 and gaseous or weakly adsorbed NO. The possibility that the reaction would follow a Langmuir-Hinshelwood mechanism with both the reactants adsorbed on the catalyst, as first supposed by Takagi et al., has been completely excluded at high temperatures.

The first mechanism supposing a reaction between gaseous NO and NH_3 adsorbed on vanadia catalysts as ammonium ions was proposed by Miyamoto et al. [8]. Ammonia was supposed to adsorb on $\text{O}=\text{V}-\text{O}-\text{V}-\text{OH}$ species and then react with NO forming an activated complex. After the release of N_2 and H_2O , the starting species on vanadia were reestablished by gaseous oxygen (Fig-

2.4 Supported-Vanadia Catalysts in the SCR of NO by NH₃

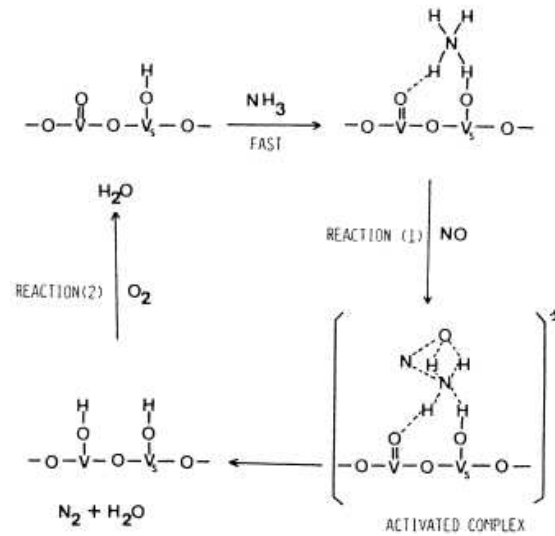
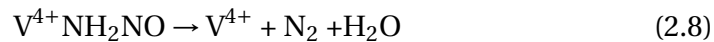
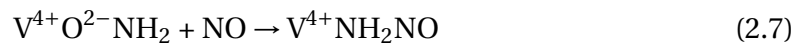
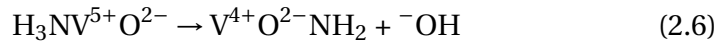
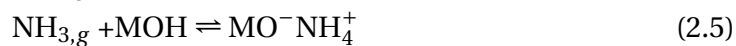
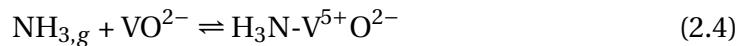


Figure 2.10: Mechanism of the NO-NH₃ reaction on vanadium oxide in the presence of oxygen. Miyamoto et al. [8].

ure 2.10). Similar mechanisms were later proposed by Gasior et al. [71] and Odenbrand et al. [72].

The first mechanism based on the reaction between gaseous NO and *co-ordinated* NH₃ was proposed by Ramis et al. [9], referred to as the “amide-nitrosamide” mechanism (Figure 2.11). The mechanism consists of the following steps:



where M=V,Ti,W,Mo and S according to the composition of catalyst (reactions (2.4) and (2.5)). In the first two steps ammonia is adsorbed reversibly on the surface of the catalyst both on Lewis and Brønsted acid sites, MO^{2-} and M-OH respectively. Then, only the ammonia adsorbed on vanadium Lewis sites reacts producing N₂ and H₂O via NH₂NO formation and decomposition (reactions (2.6), (2.7) and (2.8)). In reactions (2.9) and (2.10) the catalyst is finally

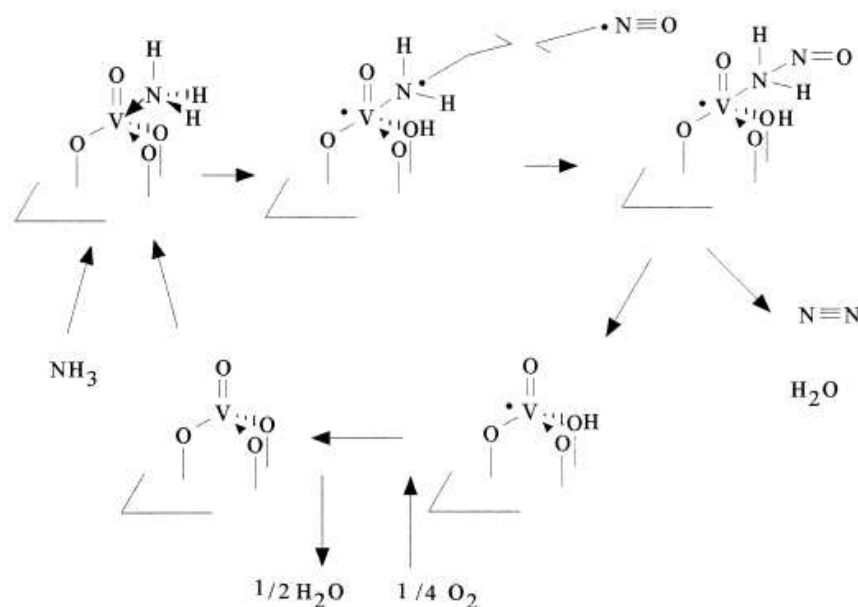
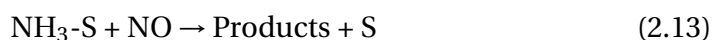
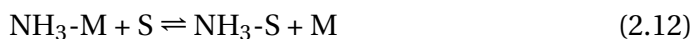


Figure 2.11: Mechanism of the NO-NH₃ reaction on vanadium oxide in the presence of oxygen. Ramis et al. [9].

reoxidized by gaseous oxygen.

In 1993, Topsøe et al. [73] showed that a simple two-step Eley-Rideal mechanism involving reaction between adsorbed NH₃ and gaseous NO is not able to describe correctly the experimental evidences obtained at typical SCR conditions. They thus proposed the following three-step mechanism:



consisting of equilibrated ammonia adsorption, followed by an activation step of the adsorbed ammonia and a subsequent reaction between the activated ammonia species and NO to form the products. The three-step mechanism was found to quantitatively describe both the ammonia conversion and the ammonia slip (see 2.4.4). However the authors pointed out that the three-step mechanism had to be regarded as semi-empirical in nature, since information concerning the nature of the M and S sites was still lacking.

In view of this situation, in situ FTIR spectroscopic studies of the surface chemistry for different vanadia-based catalysts were performed [10, 59] and the

2.4 Supported-Vanadia Catalysts in the SCR of NO by NH₃

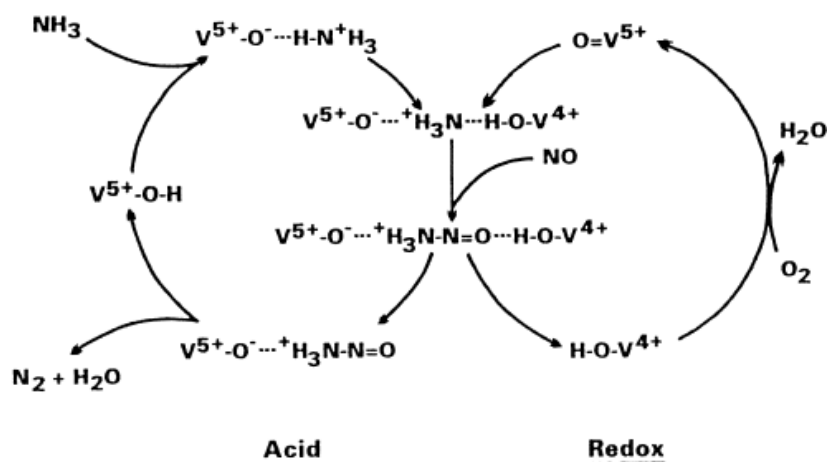
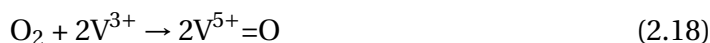
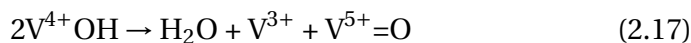
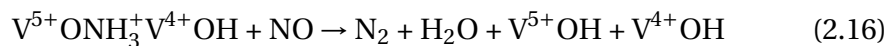
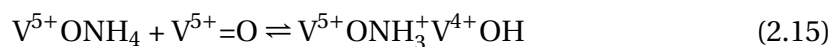


Figure 2.12: Mechanism of the NO-NH₃ reaction on vanadium oxide in the presence of oxygen. Topsøe et al. [10].

following mechanistic scheme was proposed (1995):



Clearly, the M-sites and S-site (reactions (2.11)-(2.13)) were associated to the V-OH and V=O sites respectively. Thus, the *BA sites* were found to be responsible for adsorption of *reacting* ammonia, whereas the V=O species, normally associated to LA sites, were found responsible for the required activation of the adsorbed ammonia (reaction 2.15): only this activated adsorbed ammonia can further react with gaseous NO giving the products of reaction. During this activation, the vanadyl groups are reduced and additional reduced V-OH are released upon reaction with NO (reactions 2.15 and 2.16). Again, the gaseous oxygen is then responsible for the reoxidation of the surface (reaction 2.18). Overall, the proposed mechanism involves an acid cycle and a redox cycle clearly shown in Figure 2.12. This fact strongly underlines the important role played in the SCR reaction by the redox state of the catalyst. In particular, when the oxygen concentration in the flue gas is high (i.e. >5%v) the acid cycle controls the overall reaction rate. This will be then faster at increasing number of V-

Literature Study

OH sites. On the other hand, at low oxygen concentrations, the redox cycle is the one controlling the reaction rate since the reoxidation of the surface is slow (reactions (2.17)-(2.18)).

The main criticism revolved to the mechanism proposed by Topsøe has been the lack of information about the chemical structure and the kinetic role of the intermediate specie NH_3^+ . According to Busca et al. [7], it is difficult to accept on a chemistry basis that this radical-cation specie, produced by the extraction of an electron from ammonia, is involved as such in the reaction with gaseous NO. In this sense, the research which the group of Topsøe is currently carrying out by using DFT calculations [74–76] is seen as a step toward an improvement of the mechanism proposed. From their results, more insight into both the nature of the BA sites and the intermediates are already available:

1. BA sites are favoured by the titania support by (i) stabilizing the H atoms bonded to vanadium oxide moieties; (ii) transferring H atoms from a Ti-OH group to a vanadium oxide moiety;
2. ammonia preferentially adsorbs on V-OH species as NH_4 which is then stabilized between two V=O species;
3. the NH_2NO species are the intermediate of reaction, as already stated in the mechanisms of Ramis, but in this case their formation involves the participation of both V=O and V-OH groups, and the formation of NH_4 species. Their decomposition to N_2 and water is then favoured by the transfer back and forth of hydrogen atoms.

While the mechanisms proposed by Takagi et al. and Miyamoto et al. still present interest only for their historical importance, the ones from Topsøe et al. and Ramis et al. are the ones on which the debate is nowadays still open. In particular, the following can be stated:

1. It has first to be mentioned that both the Ramis et al. [9] and Topsøe et al. [10] mechanism are supported by surface studies performed in the absence of water and SO_2 that can alter the acidity and redox state of the catalyst. Thus, care must be taken when extrapolating data to the real operating conditions.
2. The two mechanisms are in general very similar. They both have in common the fact that an acid cycle is coupled with a redox cycle. In particular the authors underline the importance of this redox cycle in order to clarify the influence of water and oxygen on the observed rate of reaction. This fact should even more stress what just said in the previous item.

2.4 Supported-Vanadia Catalysts in the SCR of NO by NH₃

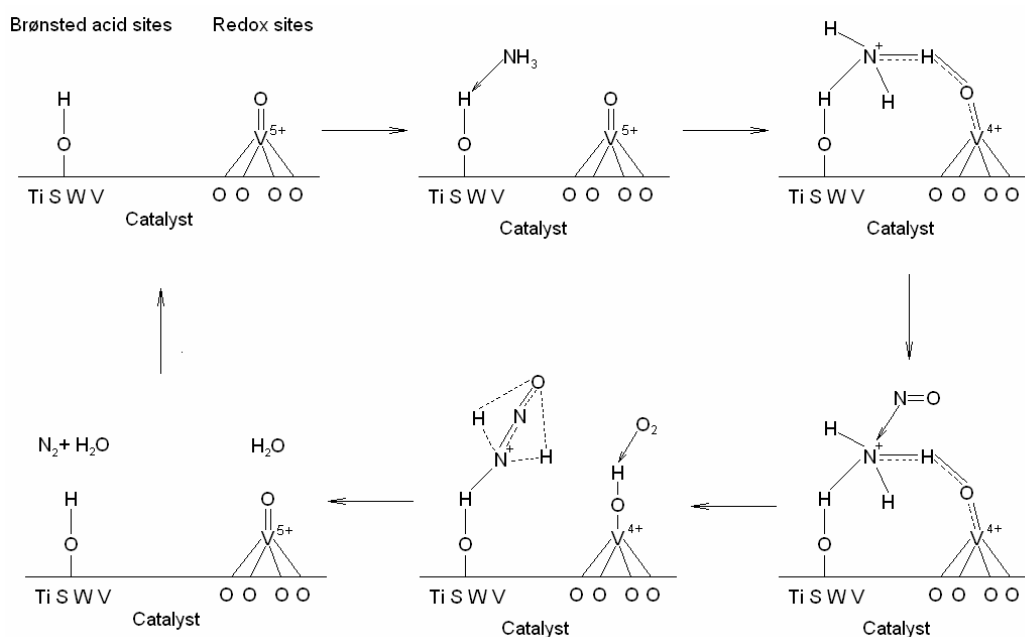


Figure 2.13: Scheme illustrating the cycle of the SCR reaction over V₂O₅/TiO₂ catalyst [11].

3. The surface studies were conducted using different techniques. In this sense the results obtained by Topsøe et al. are more interesting since they were obtained in situ.
4. The deactivation experience with vanadia-based catalysts should be considered as a viable way to better support a proposed mechanism of reaction.

Recently, most of these considerations have been taken into account by Guo in his study about poisoning and sulphation of vanadia SCR catalysts [11], which have led to a refined version of Topsøe dual acid-redox mechanism, shown in Figure 2.13. Here, it can be seen that the Brønsted acid sites where NH₃ is adsorbing are supplied by both tungsten, sulphate species, the support and vanadia. However, based on NH₃-NO coadsorption and NO reduction tests on sulphated both vanadia/titania and tungsten/titania catalysts, it was concluded that vanadia is not as active as W and S in this process. Instead, its main role is of providing the adjacent redox-sites where the reaction can happen. Increasing the number of the different Brønsted acid sites increases the NO reduction activity since a higher number of sites for the NH₃ chemisorption is created. Accordingly, decreasing their number or their strength by poisoning with alkali

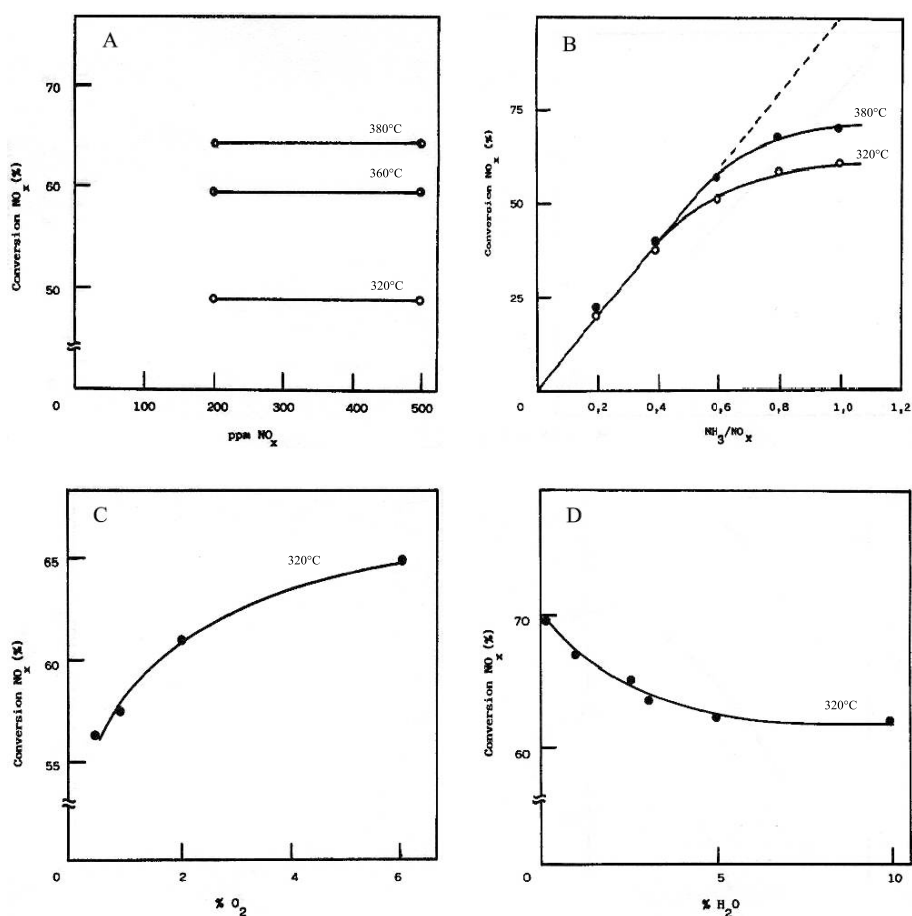


Figure 2.14: A: Effect of NO_x concentration on NO_x conversion; B: effect of NH_3/NO_x ratio, $\text{NO}_x=500$ ppm, on NO_x conversion; C: effect of O_2 concentration on NO_x conversion; D: effect of water concentration on NO_x conversion. From [12].

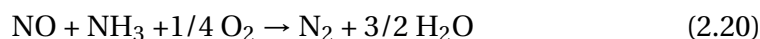
and alkaline earth metals decreases the catalyst activity. No change in activity can instead be correlated to Lewis acid sites population.

2.4.4 Kinetics of the SCR Reaction

Several kinetic studies have been reported in the literature for the SCR reaction, based on both empirical expressions [13, 77, 78] and mechanistic approaches [15, 16, 79–83]. The catalysts used were both model and commercial vanadia-based catalysts. In all cases, these were crushed and sieved to small particles (generally with diameters in the range 100–300 μm) in order to avoid internal mass transfer limitations. The NO and NH_3 concentrations were varying in the

2.4 Supported-Vanadia Catalysts in the SCR of NO by NH₃

range 50-2500 ppm. Kinetic expressions were generally proposed for temperatures in the range 120-350 °C. Only in few cases, the kinetic behaviour of the reaction was studied at higher temperatures. Even though water was not always added into the feed, in all the studies no evidence was found for the formation of N₂O and NO₂ and the only reaction considered was the following:



From an empirical point of view, without adopting any detailed reaction mechanism, the NO conversion rate can be simply assumed to depend on the concentrations of the reactants (i.e NO, NH₃ and O₂) and water according to the following expression:

$$-r_{\text{NO}} = k C_{\text{NO}}^{\alpha} C_{\text{NH}_3}^{\beta} C_{\text{O}_2}^{\gamma} C_{\text{H}_2\text{O}}^{\delta} \quad (2.21)$$

Different authors [13, 77, 78] have reported values for α in the range 0.5-0.8 for temperatures less than 300 °C. The order of dependence on C_{NH_3} also appeared with values of β larger than zero when the ratio NH₃/NO was less than 1, typical in the industrial applications. Moreover, γ was found to vary in the range 0.25-0.5 for vanadia-based catalysts.

On the other hand, for temperatures in the 300-380 °C range, working with NH₃/NO ≥ 1, more than 5%v of oxygen and 5%v of water, the rate of NO conversion is found to be independent of ammonia, oxygen and water. At these conditions, the following expression is then considered a good approximation:

$$-r_{\text{NO}} = k C_{\text{NO}} \quad (2.22)$$

The use of this expression is supported by the evidences showed in Figure 2.14, in which the effects of the reagents on the NO conversion measured on a commercial monolith are presented [12].

In order to obtain an expression that physically explains the behaviour of the catalyst in the SCR reaction in a wider domain, adsorption, surface reaction and mechanistic studies have to be considered. In particular, the effects due to ammonia, oxygen, nitric oxide and water concentrations need to be included in the kinetic model, since their effects become relevant.

In the following sections, each of these effects and the way they have been taken into account in the kinetic expressions found in the literature is presented. Furthermore, a summary of these expressions together with the conditions where they were validated is presented in Table 2.4.

Ammonia Effects

As discussed previously, ammonia is adsorbed on the catalyst prior to reaction, thus the coverage of ammonia under reaction conditions has to be considered.

Table 2.4: Proposed rate expressions for the SCR of NO by NH₃.

| $-r_{NO}$ | NO, ppm | NH ₃ /NO | O ₂ , %v | H ₂ O, %v | T, °C | Ref. |
|---|----------|---------------------|---------------------|----------------------|---------|------|
| a. $\frac{4k_R C_I P_{NO}}{1 + \frac{k_R P_{NO}}{8k_O P_{O_2}^{0.71}} + \sqrt{\frac{k_R P_{NO}}{8k_O P_{O_2}^{0.71}} \left(2 + \frac{k_R P_{NO}}{8k_O P_{O_2}^{0.71}} \right)}}$ | 400-1600 | 1-4 | 0.5-12 | - | 195-310 | [79] |
| b. $k \frac{K_{NO} K_{NH_3} P_{NO} P_{NH_3}}{1 + K_{NH_3} P_{NH_3} (1 + K_{NO} P_{NO})}$ | 100-1100 | 0.02-2 | excess | - | 200-250 | [80] |
| c. $k \frac{K_{NO} K_{NH_3} P_{NO} P_{NH_3}}{1 + K_{NH_3} P_{NH_3} (1 + K_{NO} P_{NO}) + K_{H_2O} P_{H_2O}}$ | 100-1100 | 0.02-2 | excess | - | 250-350 | [80] |
| d. $k \frac{K_{NH_3} C_{NH_3}}{1 + K_{NH_3} C_{NH_3}} \frac{K_{O_2} C_{O_2}}{1 + K_{O_2} C_{O_2}}$ | 50-1000 | 0.05-20 | 0.2-6.5 | - | 225-325 | [81] |
| e. $k \frac{K_{NO} P_{NO}}{1 + K_{NO} P_{NO}} \frac{\frac{K_{O_2} P_{O_2}}{1 + K_{O_2} P_{O_2}}}{\frac{K_{O_2} P_{O_2, 10\%}}{1 + K_{O_2} P_{O_2, 10\%}}}$ | 300-1000 | 0.3-3.3 | 0-11.5 | 0-7.5 | 120-200 | [15] |

2.4 Supported-Vanadia Catalysts in the SCR of NO by NH₃

| | | | | | | | |
|----|--|------------------------|---------|--------|-------|---------|------|
| f. | $k \frac{K_{O_2} P_{O_2}}{1 + K_{O_2} P_{O_2}} \frac{P_{NO}}{1 + K_{O_2} P_{O_2,10\%}}$ | 300-1000 | 0.3-3.3 | 0-11.5 | 0-7.5 | 200-290 | [15] |
| g. | $k_{2,11} P_{NO} \frac{K_{2,11} P_{NH_3} / P_{NO}}{1 + K_{2,11} P_{NH_3} / P_{NO} + K_{2,12} P_{NO} + K_{NH_3} P_{NH_3}}$ | SCR typical conditions | | | | | [73] |
| h. | $\frac{\alpha}{\beta} \left[\gamma - (\gamma^2 + \beta m / \alpha)^{1/2} \right]^2$ | 100-500 | 0.2-1 | 4 | 0-10 | 250-350 | [82] |
| i. | $\frac{m}{(1+m)^2} \frac{k_1 \theta_{NH_3}}{1 + \frac{P_{H_2O}^{1/2}}{K_{OX} P_{O_2}^{1/4}} + \frac{k_1 \theta_{NH_3}}{(1+m) k_2 P_{NO}}}$ | 80-1080 | 0-26 | 0.05-5 | - | 240-280 | [83] |
| l. | $k C_{NO} \theta_{NH_3}^* \left[1 - \exp \left(- \frac{\theta_{NH_3}}{\theta_{NH_3}^*} \right) \right]$ | 0-700 | 0-1 | 1 | 0-5 | 220-400 | [14] |

$$m = S_{V^{5+}=O} / S_{V^{5+}OH}$$

$$\alpha = k_9 k_{10} P_{NO} K_8 P_{NH_3} / [(k_{-9} + k_{10} P_{NO}) (1 + K_{13} P_{H_2O} + K_8 P_{NH_3}) + k_9 K_8 P_{NH_3}]$$

$$\beta = 16 k_{11} k_{12} P_{O_2}$$

$$\gamma = (2 k_{12} P_{O_2})^{1/2} + k_{11}^{1/2}$$

Literature Study

At low NH_3/NO , the coverage of NH_3 is not unity. At high temperatures ($\geq 300^\circ\text{C}$), the exothermicity of the adsorption reaction also implies that the coverage is not total. In order to consider the ammonia effects, most authors have added in their rate expression a term due to the ammonia coverage θ_{NH_3} . When the adsorption reaction is assumed to follow a Langmuir-type isotherm, the following expression can be derived:

$$\theta_{\text{NH}_3} = \frac{K_{\text{NH}_3} C_{\text{NH}_3}}{1 + K_{\text{NH}_3} C_{\text{NH}_3}} \quad (2.23)$$

If a simple Eley-Rideal mechanism is assumed with strongly adsorbed ammonia reacting with gaseous nitric oxide, the following expression is derived by considering the surface reaction as the limiting step and the ammonia concentration in equilibrium on the surface:

$$-r_{\text{NO}} = k C_{\text{NO}} \theta_{\text{NH}_3} \quad (2.24)$$

Figure 2.15 shows the progress of θ_{NH_3} versus the partial pressure of ammonia at different temperatures [13]. The values were obtained from activity measurements on powders assuming $\theta_{\text{NH}_3}=1$ in the case of maximum conversion, and comparing the conversion rate under different conditions as follow:

$$\theta_{\text{NH}_3} = \frac{k}{k_{\text{max}}} \quad (2.25)$$

Figure 2.15 clearly shows a typical Langmuir-type isotherm for the adsorption curve.

An expression similar to (2.24) was proposed by Nova et al. [14, 84], presented in Table 2.4 (expression (I)). By analysing the ammonia adsorption and the surface reaction on model vanadia-based catalysts by transient methods, they showed that the ammonia coverage affects the reaction rate only if θ is less than a critical NH_3 coverage value θ^* with $\theta^* < \theta$. This phenomenon is well shown in Figure 2.16A, where the NO outlet concentration is measured against step changes in the NH_3 inlet concentration. Notably, when NH_3 is added to the feed, the NO outlet concentration reaches its steady-state value well before NH_3 . Furthermore, when the ammonia inlet concentration is again decreased (trace b), the NO concentration remains unaffected for several minutes. All these facts demonstrate that NH_3 is stored on surface *spectator* sites as *non reacting* ammonia, from which is transferred to these active sites, as already affirmed by Kleemann et al. [39] and discussed in 2.4.2.

In any case, it is worth noting that, when the ammonia coverage can be assumed total (low temperatures/high ammonia partial pressures), 2.24 reduces to the first-order expression (2.22).

2.4 Supported-Vanadia Catalysts in the SCR of NO by NH₃

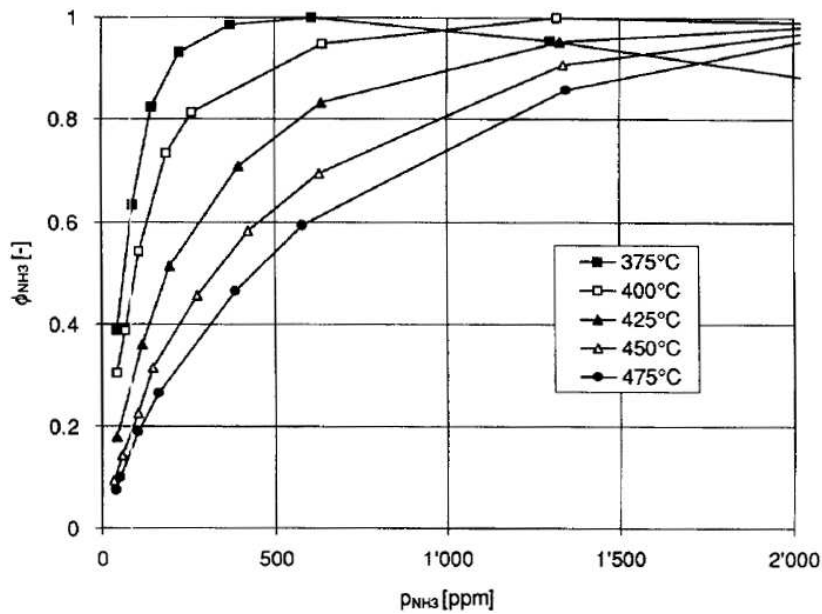


Figure 2.15: Experimental values of θ_{NH_3} , NO: 100 ppmv. From [13].

Topsøe et al. [73] found that a three-step Eley-Rideal mechanism ((2.11)-(2.13)) was more consistent with the data from typical SCR conditions than a simple two-step Eley-Rideal mechanism. They thus proposed the expression (g) presented in Table 2.4, assuming a fast ammonia adsorption and slow rates for the two remaining steps. This expression was found to quantitatively describe both the NO reduction and the ammonia slip for NH₃/NO varying in the range 0.7-1.1.

Oxygen Effects

All authors agree that oxygen has an enhancing effect on the NO conversion, as shown in Figure 2.14C. This effect is especially pronounced at low oxygen concentrations and levels off above $\approx 10\%v$ [15, 81]. Its effect is directly linked to the oxidation state of the catalyst surface. At lower O₂ concentrations, reoxidation reaction of the catalyst is the limiting step in the SCR reaction [85].

The effects due to oxygen have been considered in two different ways. By plotting the rate of NO conversion vs the oxygen concentration at different temperatures for a vanadia-tungsta-titania/sepiolite catalyst, Odenbrand et al. [81] showed that the oxygen adsorption follows a Langmuir behaviour comparable to that of ammonia. Thus they assumed that also the oxygen concentration was in equilibrium on different sites than NH₃ and added to the rate expression an

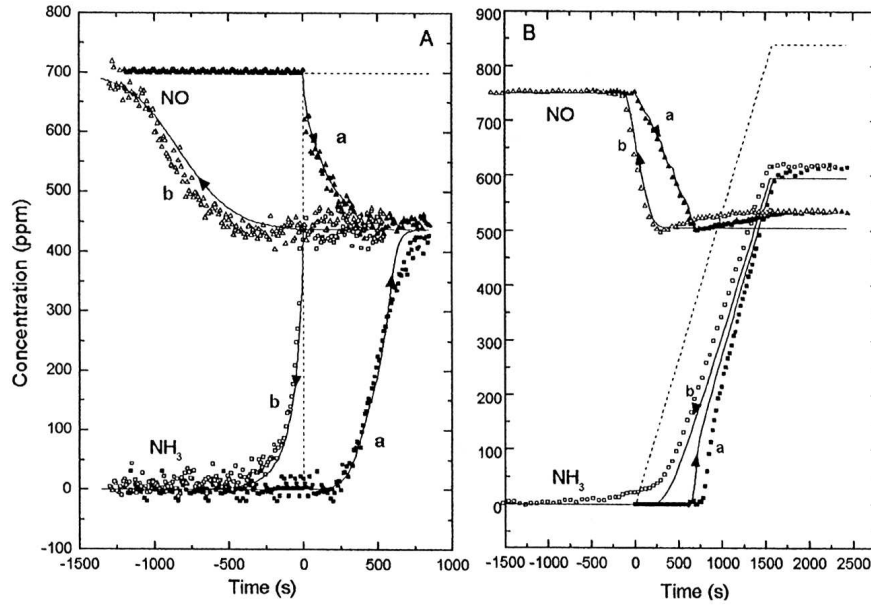


Figure 2.16: Dynamics of the $\text{NH}_3 + \text{NO}$ reaction. (A) Step changes of the NH_3 inlet concentration ($0 \rightarrow 700 \rightarrow 0$ ppm) in $\text{He} + \text{NO} + \text{O}_2$ at 493 K over model $\text{V}_2\text{O}_5\text{-WO}_3/\text{TiO}_2$ catalyst. (B) Linear changes of the NH_3 inlet concentration ($0 \rightarrow 840 \rightarrow 0$ ppm) in $\text{He} + \text{NO} + \text{O}_2$ at 573 K over model $\text{V}_2\text{O}_5\text{-WO}_3/\text{TiO}_2$ catalyst. From [14].

oxygen coverage θ_{O_2} term:

$$\theta_{\text{O}_2} = \frac{K_{\text{O}_2} C_{\text{O}_2}}{1 + K_{\text{O}_2} C_{\text{O}_2}}, \quad (2.26)$$

obtaining expression (d) in Table 2.4. In the presence of excess oxygen, the previous term can be neglected and the rate expression takes the Eley-Rideal form (2.24). In a similar way, the effect of oxygen was taken into account by Willi et al. [15]. In this case, the θ_{O_2} was normalized to 10% oxygen in the exhaust gas to allow an independent estimation of the constant k (expressions (e) and (f)). Figure 2.17 presents their experimental data and the good agreement between experimental results and simulations.

On the other hand, other authors [79, 82, 83] considered the effects of oxygen by assuming the re-oxidation of the catalyst as a rate determining step in the global SCR reaction rate. They assumed the reaction following a simplified version of the mechanism proposed by Inomata et al. [8] and the Acid-Redox mechanism proposed by Topsøe et al. [10]. The results are presented in Table 2.4 (expressions (a) and (i) respectively).

2.4 Supported-Vanadia Catalysts in the SCR of NO by NH₃

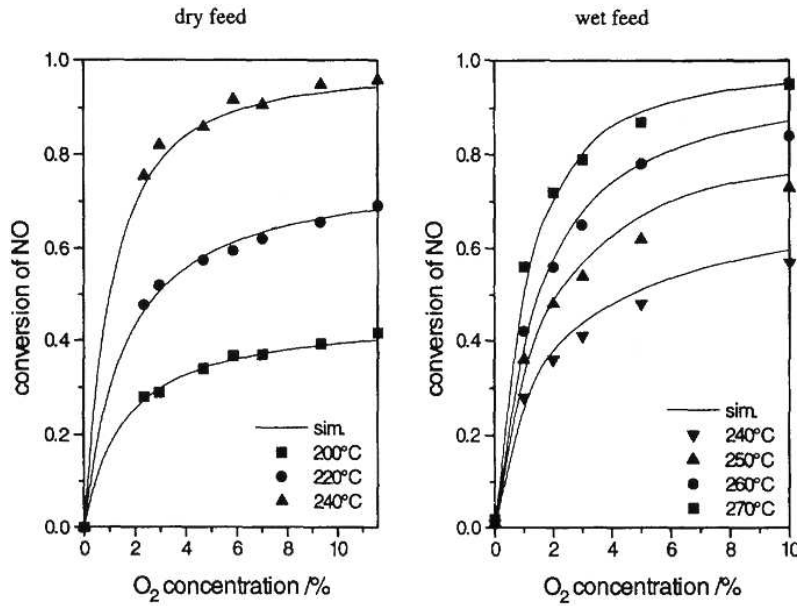


Figure 2.17: Conversion of NO versus oxygen concentration. Feed: 0-11.5%v O₂, 1000 ppmv NO, 1000 ppmv NH₃, 5%v H₂O, balance N₂. From [15].

Nitric Oxide Effects

At typical SCR conditions, NO does not adsorb on the catalyst. At lower temperatures, however, evidences for NO adsorbed species were found [13, 16].

As already mentioned, the order with respect to NO in (2.22) was found to decrease from unity with decreasing temperatures. This fact was explained by different authors [13] assuming a weak adsorption of NO on the catalyst. In particular, according to Koebel et al. [13], at low temperatures, a much better description of the kinetic behaviour of the catalyst is possible taking into consideration the adsorption of both NH₃ and NO on different sites. The same conclusion was reached by Willi et al. [15] and Tufano et al. [80]. As a matter of fact, the first group added to their rate expression valid for low temperature (expression (e)) the following term:

$$\theta_{NO} = \frac{K_{NO}C_{NO}}{1 + K_{NO}C_{NO}} \quad (2.27)$$

thus assuming that also the concentration of NO is equilibrated on the surface through a Langmuir-type isotherm on different sites than NH₃.

On the contrary, Tufano et al. derived a rate expression directly from the nitro-nitrosamide mechanism (reactions (2.4)-(2.10)) assuming the rate of decomposition of the amine species (reaction (2.8)) as the limiting step, resulting

Literature Study

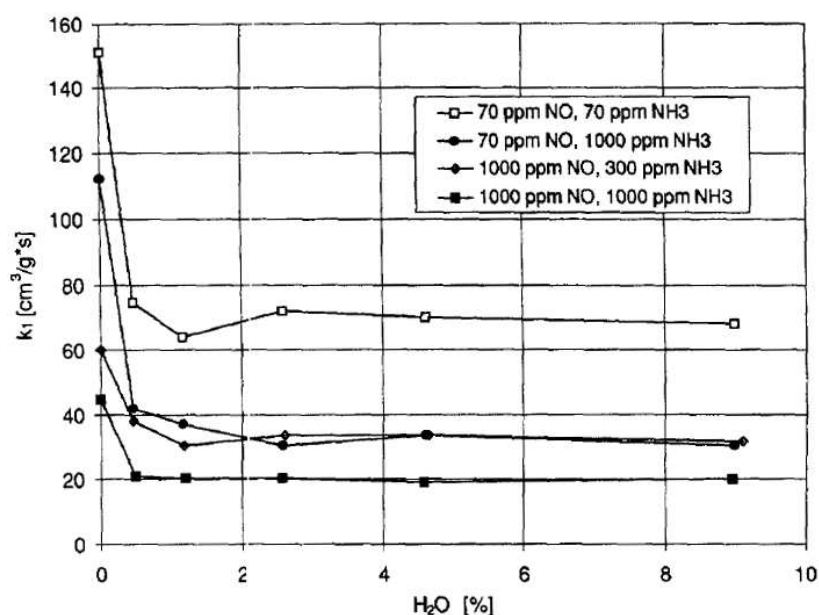


Figure 2.18: Influence of water on reaction rate, O₂=10%, T=250 °C. From [13].

in the rate expression (b) in Table 2.4. This expression best fitted the experimental data in the whole range of temperatures examined. However, at higher temperatures (i.e 300-350 °C), a similar fitting accuracy was obtained assuming instead the surface reaction (2.7) as the rate limiting of the global reaction, thus obtaining from the same mechanism a simple Eley-Rideal model ((2.24)). This fact was interpreted by the authors affirming that at lower temperatures the amide species are more strongly adsorbed on the catalyst surface and thus their decomposition becomes the limiting step in the global SCR reaction. Again, the strong influence of temperature on the reaction behaviour was pointed out.

Water Effects

The addition of water in the feed has an inhibiting effect on the NO conversion. A relative activity ($k_{obs,wet}/k_{obs,dry}$) of less than 0.50 was found in the presence of 2%v of water [13, 15]. However, this effect was found to level off at increasing concentrations (Figure 2.18).

This inhibiting effect has been considered in different ways. In the earlier studies, it was considered by assuming water competing with ammonia on the active sites [86]. Tufano et al. [80] found that at high temperatures this effect, if included in the rate expression by considering an adsorption constant for water, could better fit the experimental data. They thus proposed expression

2.4 Supported-Vanadia Catalysts in the SCR of NO by NH₃

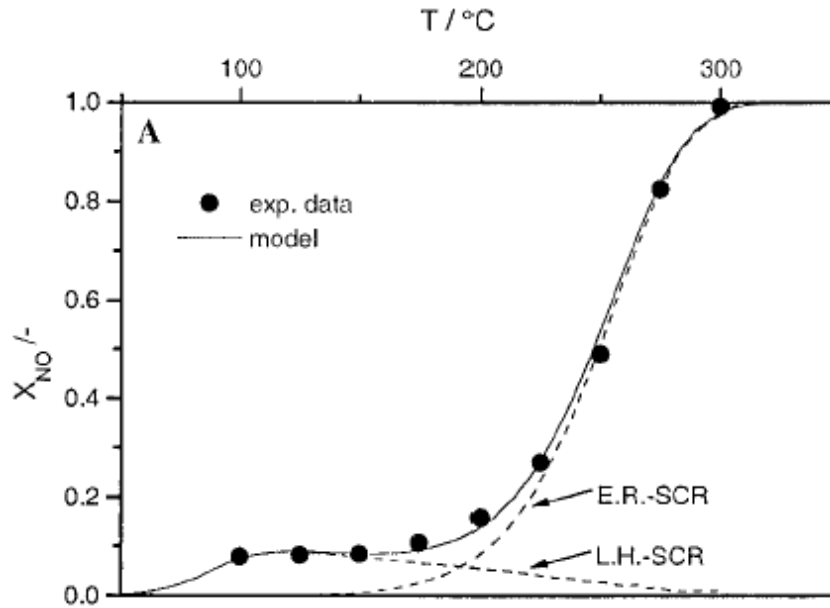


Figure 2.19: Conversion of NO versus temperature, LH-SCR and ER-SCR paths. Feed: 10% O₂, 5% H₂O, 1000 ppm NO, 1000 ppm NH₃, balance N₂. Catalyst weight: 4.41 g; particle size: 250 μ m; flow 260 L/h (NTP). From [16].

(c) in Table 2.4 at temperatures above 250 °C. However, water was not reported to have been added into the feed [80].

Nowadays, the possibility that water could compete with ammonia on the active sites is still matter of discussion. All authors agree that the interactions between water and the active sites are weak compared to the ammonia-vanadia interactions. On the other hand, water is present at higher concentrations, so that eventually the observed inhibiting effects of water appears plausible.

Recently, Nova et al. [14] observed the effect of water on the transient behaviour of the SCR reaction. They added 5% of water vapour into the feed and showed that the inhibiting effect could not be explained by the competitive adsorption of water. They rather concluded that this effect should be explained by considering the changes in the redox state of the catalyst due to the presence of water, as already affirmed by Topsøe [87], which is then the main responsible for the overall rate of reaction.

The models directly derived from the SCR mechanism proposed by Topsøe et al. [10] are the ones that better can account for the redox state of the catalyst. Kamata et al. [83] derived directly from equations (2.14)-(2.19) the expression (i) in Table 2.4. In this, the parameter m is defined as the ratio of $S_{V^{5+}=O}$ to $S_{V^{5+}OH}$ sites, considered as a function of P_{O_2} and P_{H_2O} . The authors calcu-

Literature Study

lated by data fitting the dependence of m with the oxygen pressure and found that this is proportional to $P_{O_2}^{1/4}$ at all temperatures. Dumesic et al. [82] also validated the mechanism under typical SCR conditions (5%v H₂O, 300 °C) and proposed expression (h), valid only if the water concentration is sufficiently low that reaction (2.17) is irreversible.

Temperature Effects

As already discussed in 2.4.4, the temperature has a direct influence on the general mechanism of reaction. At lower temperatures (i.e. < 250 °C), the mechanism follows a Langmuir-Hinshelwood path with both ammonia and nitric oxide reacting as adsorbed species [13], whereas at higher temperatures the Eley-Rideal path is the one followed by the reaction. This fact was clearly showed by Roduit et al. [16] by simulating the reaction assuming both the two possible paths. Figure 2.19 shows the results of their calculations and the good agreement with experimental data.

2.4.5 Catalyst Design and Reactor Modelling

From the previous discussion it is clear that the SCR reaction is dependent on various parameters and a single expression valid in a wide domain of temperatures (150-450 °C) and different flue gas compositions is not yet available. However, when limiting the domain at the conditions relevant for industrial applications, most of the expressions presented in Table 2.4 can be implemented in a general model simulating the entire SCR reactor.

Different authors [4, 12, 40, 88–92] have modelled the entire SCR reactor taking into account the reaction kinetics and both external and internal mass transfer limitations. A good introduction to the role of mass transfer in the SCR reaction over catalysts of different shapes can be found in [93].

The entire SCR reactor can be described with a one-dimensional model, neglecting axial diffusion and pressure drop [93]. Regarding the external mass transfer, at typical industrial conditions the flow in the channel is laminar with significant mass transfer limitation between the gas phase and the monolith wall. In order to evaluate the contribution of this external resistance, both experimental and theoretical approaches have been considered. Some correlations for the Sherwood number available in the literature are shown in Table 2.5. In the case of empirical expressions, the Sherwood number is given as an *average* number ($Sh_{av} = (k_{mt}d_h/D)$) over the entire monolith length ($z^* = LD/(d_h^2u)$).

Besides the external mass transfer limitations, monoliths also present intraporous diffusion limitations which strongly limit the performance of commer-

2.4 Supported-Vanadia Catalysts in the SCR of NO by NH₃

Table 2.5: Correlations for estimating the external mass transfer in monolith catalysts.

| Correlation | Type | Reference |
|--|------------------|---------------------|
| $Sh_{av} = 0.766 / [z^*]^{0.483}$ | empirical | Ullah |
| $Sh_{av} = 2.976 [1 + 0.139 / z^*]^{0.81}$ | empirical | Uberoi & Pereira |
| $Sh_{av} = 2.976 [1 + 0.095 / z^*]^{0.45}$ | semi-theoretical | Hawthorn |
| $Sh = 2.976 [1 + 0.206 / z]^{0.545}$ | theoretical | Tronconi & Forzatti |

cial SCR catalysts. This resistance is a function of the effective diffusivity of the reactants into the catalytic pores and, in order to model correctly the observed reaction rate, it is important to measure or predict its value [94]. Beeckman et al. [95] developed an experimental technique to measure the effective diffusion coefficient of nitric oxide through the porous walls of a monolith-type ceramic catalyst. It involves the passage of gas streams inside and outside of a particular monolith channel and measuring the net flux across its walls. The experimental data were then successfully compared with the prediction of the random pore model of Wakao and Smith [96] based on Hg porosimetry measurements.

This finding had mainly two consequences. The first one was that it was possible to estimate the effective diffusivity by Hg porosimetry measurements, which is easy to obtain. The second one was that the internal mass transfer limitations were then modelled as a function of micro- and macroporosity (expressed as volume fractions) and the volume-integral-averaged micro- and macropore radii [4, 12, 40, 90, 91, 93]. From the analysis of the numerical solutions, it is seen that SCR catalysts normally operate under inter- and intra-phase mass transfer limitations. The NO intra-phase diffusion coefficient has been found about two-orders of magnitude smaller than molecular diffusivity [93]. Accordingly, the effectiveness factor of the monolith catalyst is in the range 0.01-0.1, indicating that only a very thin layer (0.2 mm) of catalyst is active in the SCR reaction [91].

The adoption of the random pore model of Wakao and Smith [96] had also another important consequence. By the analysis of the influence of the pore distribution on the SCR activity, it was shown that the introduction of macroporosity strongly enhanced the effective diffusion coefficient. The reason was found in a larger effective diffusion coefficient provided by the macropores, which are able to more than offset the drop in volume-specific area, caused by the reduction of micropores. The necessity of a new pore structure was then revealed. In particular, Beeckman et al. [40] suggested to include a matrix of

Literature Study

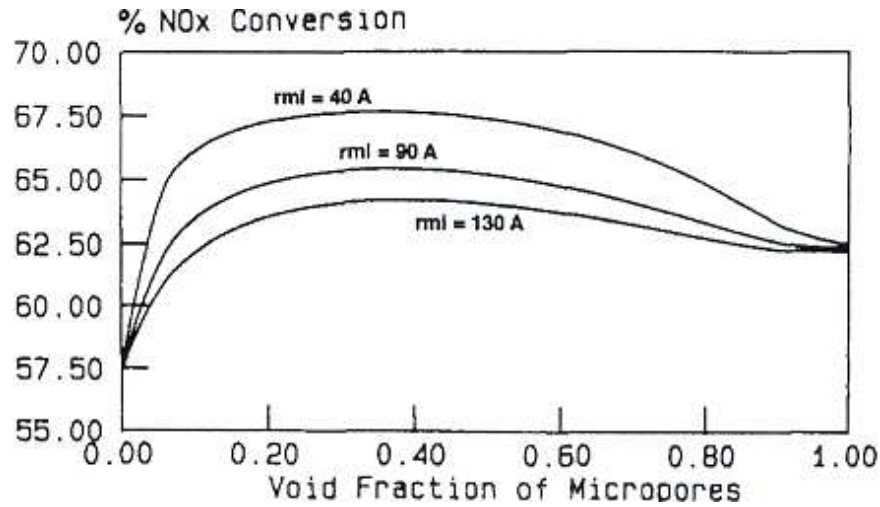


Figure 2.20: Calculated NO conversion vs. micropore void fraction for different values of micropore radius r_{mi} ; macropore radius = 200 nm. From [4].

silica in the catalyst, which is able to satisfy the calculated bimodal pore structure. Tronconi et al. [4] showed that up to 17% of the total catalyst volume can be saved by limiting the micropore fraction to 0.4 with a micropore radius of 4 nm, as shown in Figure 2.20. The total void fraction was fixed to 0.7 for mechanical reasons.

Based on these results it can be concluded that in order to increase the global efficiency of the whole SCR process different roads are possible:

1. From a chemical point of view, the development of new catalyst compositions should aim at increasing the activity of the catalyst at lower temperatures. In this case it would be more convenient to adapt a tail-end configuration limiting the problems due to deactivation by particulates. Another reason to develop new compositions should be to obtain catalysts which are more poison-resistant. This would favour the application of the SCR process to systems where nowadays the deactivation rate is so fast that the SCR process is not feasible.
2. From an engineering point of view, the reactor should permit a complete and uniform mixing of the reactants. The use of 3-D modelling during the design process has already given good results [97]. Moreover, both the micro- and macro-structure of the catalyst monolith could be even more improved by developing monoliths with optimal channels geometry and pore sizes distributions, according to the results of the simulations. In

this sense it could be more interesting to develop complete two- or three-dimensional models for the monoliths instead of using simplified one-dimensional models. The problems due to the high computational time due to these more complex models should nowadays not be an issue any more, as it was in the past when these models were first developed.

2.5 Deactivation of SCR Vanadia-based Catalysts

2.5.1 General Aspects

Catalyst deactivation is defined as the loss over time of catalytic activity and/or selectivity. Due to the high costs for catalyst replacement and process shut-down, this is one of the major problems related to the operation of catalytic processes. Deactivation is inevitable, but in a well-controlled process some of its consequences may be slowed, postponed or even prevented. Hence, research and understanding of the deactivation mechanisms are needed in order to optimize the development, design and operation of commercial processes.

There are many mechanisms of catalyst deactivation, both chemical and physical (thermal and mechanical) [98–100]. *Poisoning* is the strong chemisorption of reactants, products or impurities present in the feed on the active sites, which are then deactivated. A species act as a poison only if its adsorption strength is high compared to other species competing for catalytic sites. A poison may act simply by geometrically blocking an active sites, or by electronically altering the adsorption of other species. Moreover, in the presence of a poison, the chemical nature of the active sites can be altered by the formation of new compounds.

The loss of activity due to blockage of active sites and/or pores caused by the physical deposition of species from the fluid phase onto the catalyst surface is known as *fouling*.

Deactivation via structural modification of the catalyst is referred to as *sintering*. This mechanism generally takes place at high temperatures (e.g. >500 °C) and involves the agglomeration and coalescence of small crystallites into larger ones with lower surface-to-volume ratio. In general, sintering processes are difficult to reverse, but at moderate reaction temperatures their kinetics is slow. *Solid-state transformation* is also a deactivating mechanism leading to the transformation of a crystalline phase into a different one with less surface area. This process is favoured at high temperatures and could be considered as an extreme form of sintering. Moreover, it may occur due to the presence of foreign compounds in the lattice or even on the surface.

Beside these just mentioned, other deactivation mechanisms include *vola-*

tilization, erosion and attrition.

The SCR catalysts were mainly developed for purely fossil-fuel-fired systems with a lifetime up to 5 years in the case of an HD-SCR reactor. In this case, the main deactivating causes reported in the literature are the following [101]:

1. loss of surface area due to sintering and rutilization of titania after long-term operation at high temperature in *gas firing*;
2. poisoning by alkali metals in *oil firing*;
3. pore and channel blocking by calcium compounds in *coal firing*;
4. poisoning by As in the case of *wet bottom or recirculating boilers*;
5. accumulation of P components in lubricating oil in the case of *diesel engines*.

Recently, the thermal recycling of residues as secondary fuel is of increasing interest for power plant operators. Consequently, a variety of secondary fuels such as straw, wood, sewage sludge, meat and bone meal (MBM) and municipal waste are combusted. In all these cases, the lifetime of a conventional HD-SCR catalyst has been found to be drastically reduced and the major deactivating mechanism according to the different application are under study.

In the following sections, each of the previously mentioned mechanisms of deactivation are discussed according to the evidences available in the open literature in the case of vanadia-based SCR catalysts. The deactivating effects of different compounds are also reviewed.

2.5.2 Poisoning

In the case of vanadia-based catalysts applied at biomass firing, poisoning represents the main mechanism of deactivation. As discussed previously, the vanadia-based catalysts are characterized by both BA and LA sites on the active phase, the support and the promoters. Ammonia adsorbs on all these acid sites, but reacts with gaseous NO only if adsorbed on the vanadia sites. From this point of view, a poison is a species that can strongly adsorb on the vanadia sites, thus reducing the number of sites available for the adsorption of *reacting* ammonia. However, the same poison can adsorb on the different acid sites present on the support and/or due to the promoters, competing with the adsorption of *non-reacting* ammonia. Accordingly, the *total* amount of ammonia adsorbed decrease with the increasing level of poison. Care must be taken when correlating the strength of a poison with the total amount of adsorbed ammonia without considering the *selectivity* of the poison itself.

2.5 Deactivation of SCR Vanadia-based Catalysts

Alkali and alkaline earth metals, arsenic, phosphorus, HCl, zinc and lead are the main poisons for the vanadia-based catalysts. Their different contributions to the total deactivation rate strongly depend on the particular application, the fuel and the combustion process. In general, since the activity of the catalyst depends on its acidity, the poisoning strength is directly correlated to the basicity of the poison [19, 102]. Moreover, since vanadia is present in small concentrations on the commercial catalyst, even small amounts of poisons can produce drastic effects on the activity of the catalyst.

In order to prevent the effects of poisoning, two ways are available. The first one is the *partial* elimination of the poison from the flue gas. To this first class belong all the possible modifications of the combustion process and the fuel (e.g using additives) that can either avoid the release or favour the recapture of the poison. The second one is the reduction of the interactions between the poison and the active sites. This solution is mainly constituted by chemical modification of the catalyst composition. Introducing a component in the catalyst that forms non-active sites where the poison preferentially adsorbs, can preserve the active sites from the attacks. When prevention is not possible, the regeneration of the doped catalyst could still be an available way to reduce the cost compared to complete replacement of the catalyst unit.

2.5.3 Fouling and Channel Blocking

Fouling and catalyst plugging in the SCR process is primarily caused by both salt and fly ash deposition. The decrease of NO_x reduction associated with an increased pressure drop is the main indication of catalyst fouling. The determination of catalyst surface area, total pore volume and pore size distribution by mercury porosimetry and BET helps in distinguishing between pore blocking by ash and pore condensation.

In general, deactivation resulting from fouling presents a sharp initial decrease in the catalyst activity [103]. As a matter of fact, the initial salt deposition takes place on the catalytic active surface and, in the case of pore blocking, low amounts of salt can deactivate a great number of active sites. As the exposure time increases, the great part of the salt goes to thicken the already present deposit layer and the deposition on the fresh catalyst is limited.

Different compounds present in the flue gas are able to form salts that can solidify at SCR temperature and deposit on the catalyst, causing fouling of the surface and channel blocking. The most important are CaO, HCl, CaCO₃, NH₃ and SO₃. Free CaO in the fly ash reacts with SO₃ adsorbed on the catalyst forming CaSO₄, which is solid at SCR typical temperatures (i.e CaSO₄ melting point 1450 °C) and can plug the catalyst. This mechanism of deactivation is of particular interest during PRB coal combustion, since the ash produced are partic-

ularly rich in Ca-rich fine particles. Also NH_3 in the presence of SO_3 and H_2O can react forming ammonia bisulphate (NH_4HSO_4) and ammonium sulphate ($(\text{NH}_3)_2\text{SO}_4$). However, since these two ammonium salts have melting points lower than the typical SCR temperature (147 and 235 °C respectively), their deposition is a major concern for the equipment downstream the SCR reactor or at partial load. The ammonium chloride has a similar behaviour: it is formed from the reaction between gaseous NH_3 and HCl and has a melting point at 338 °C. However care must be taken when considering the melting points of the pure compounds, since in reality these compounds may not be pure and form a liquid phase at lower temperatures. Blockage of surface area and pores by phosphorus and arsenic were also reported [19, 21, 104].

According to the previous evidences, two ways are effective in order to decrease the effects of fouling and channel blocking. The first one is the proper selection of catalyst pitch and cell opening size according to the properties of dust and fly ash. Moreover, a temperature control in the SCR reactor can avoid the deposition of ammonium salts. The second one is the limitation of the SO_2 oxidation, since SO_3 is the main responsible for the formation of the most dangerous salts. In any case, efficient soot blowing systems installed at the inlet of each catalyst layers in the SCR reactor can strongly enhance the performance of the reactor and its resistance against fouling and channel blocking.

2.5.4 Sintering and Solid-state Transformation

Sintering and solid-state transformation due to ageing are the main mechanisms of deactivation for vanadia-based catalysts in the case of gas firing. In other applications (e.g coal and biomass/waste combustion) its importance is minor compared to poisoning and/or fouling, but not negligible considering the long life-time desired for the catalyst.

For the vanadia-based catalysts, both sintering and solid-state transformation are associated with the TiO_2 support and strongly depend on the thermal history [101] and on the composition of the catalyst [17, 18]. Titania is employed as support in the anatase form which presents a higher surface area than the rutile form. However, anatase is not a stable configuration and tends to convert into the rutile configuration.

The temperature has a direct influence on both sintering and rutilization. A catalyst which has experienced high temperatures (>500 °C, either during its initial calcination or during normal operation) presents bigger crystals and more rutile phase, and thus less specific surface area than a catalyst treated at lower temperatures [17, 18, 101].

Vanadia-loading also has an important influence on both sintering and rutilization. The influence of vanadia-loading on titania sintering has been studied

2.5 Deactivation of SCR Vanadia-based Catalysts

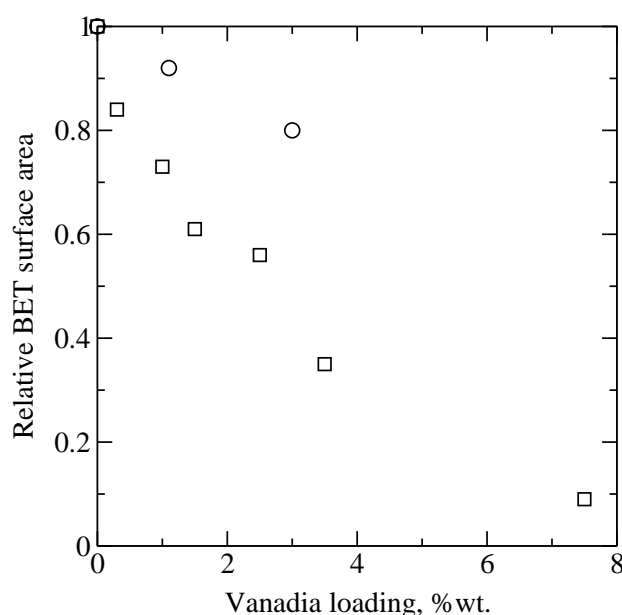


Figure 2.21: Effect of vanadia-loading on the relative BET surface area of model V_2O_5 - WO_3 - TiO_2 (circles) [17] and model V_2O_5 - TiO_2 (squares) [18] calcined at 500 and 600 °C respectively.

by Alemany et al. [18] on model V_2O_5 - TiO_2 and by Madia et al. [17] on model V_2O_5 - WO_3 - TiO_2 , using X-ray diffraction (XRD), X-ray photoelectron spectroscopy (XPS), Raman spectroscopy and BET surface area determination. Figure 2.21 shows the different values of relative BET surface area obtained by the authors. It can be noted that this latter was found to linearly decrease at increasing vanadia-loading. In particular, the specific surface area of the catalyst employed by Alemany et al. decreased from 85 m²/g (sample without vanadia) to 30 m²/g by adding only 3.5%wt. of vanadia. Since at the calcination temperatures adopted in these experiments (i.e. 500 °C for the experiments of Alemany et al. and 600 °C for those of Madia et al.) anatase was the only phase detected, it was concluded by both the authors that vanadia is a sintering promoter. This fact was further confirmed by the corresponding changes in the average crystal size, pore volume, and pore radius.

Vanadia is also able to lower the temperature of rutilization. Alemany et al. [18] found that a 1.5% V_2O_5 - TiO_2 catalyst calcined at 700 °C presented only 4% of rutile phase. When the vanadia content was raised to 7.5%, already at 600 °C the support was constituted by 72% of rutile. Its BET surface area was 8 m²/g.

The activity of a commercial (0.62%) V_2O_5 -(9%) WO_3 - TiO_2 calcined in the range 500-900 °C was tested in the laboratory by Nova et al. [101], in order to

correlate the sintering caused by temperature with the activity and selectivity of the catalyst. By analysing the catalysts by FT-IR, FT-Raman spectroscopy, it was concluded that the sintering of the support favours the aggregation of isolated vanadium ions. This fact resulted in higher activity at lower temperatures, but lower selectivity (i.e. -20% of the initial) at high temperatures, demonstrating the inapplicability of the common commercial catalysts in long-term high-temperature gas firing applications. Moreover the catalysts became more active in the SO_2 to SO_3 oxidation. However, it must be noted that the temperatures investigated in this work were higher than the melting point of V_2O_5 (690 °C).

Similar results were obtained by Madia et al. [17], further demonstrating that the temperature window of the vanadia-based catalysts decreases with the exposure time rendering the whole SCR process less flexible.

2.5.5 Performed Investigations on Deactivating Compounds

Due to their commercial success, vanadia-based catalysts have been subjected to numerous studies in order to understand and prevent the causes of their deactivation. A great part of the research has been carried out in the laboratory. Both model and commercial catalysts have been doped in situ by wet impregnation and their activities have been measured in lab-scale reactors [19, 20, 102, 105–107]. Although with this particular method of doping the results are far from simulating the real effects of a poison in the SCR reactor, these investigations can provide an useful first estimation of the *potential* poisoning effects of the single compound and they normally constitute the first step of a wider research program. However, since the deposition of a poison on the catalyst surface strongly depends on both the physical state (gaseous, solid, particle size, etc.) of the poison in the flue gas and the fluid dynamics within the SCR reactor, both pilot- and full-scale experiments have been performed. Here commercial catalyst module in full size have been exposed either to model flue gases containing the poisons under investigation [108] or to real flue gases from power plants [109, 110].

In the following sections, evidences reported in the literature about deactivation of vanadia-based catalysts are reviewed.

Alkali and Alkaline Earth Metals

Alkali (K, Na) metals are strong poisons for the vanadia-based catalysts. When the SCR is applied at biomass (co)-combustion, this is a major concern due to the high amount of water soluble alkali metal oxides present in the flue gas. These (mainly potassium) are released to form sulphates and chlorides which are water soluble and able to penetrate the catalyst pore structure [110, 111].

2.5 Deactivation of SCR Vanadia-based Catalysts

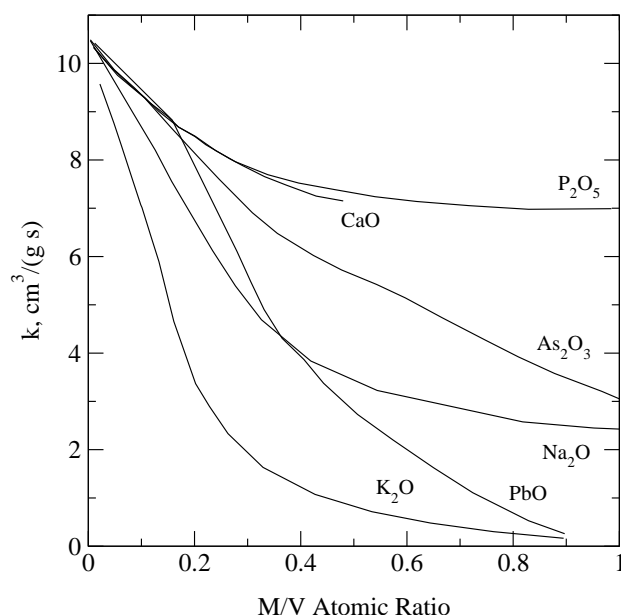


Figure 2.22: Activities of 5% V₂O₅/TiO₂ doped with different amounts of metal oxide poisons. Operating conditions: NO=NH₃=1000 ppm, O₂=2%, T=300 °C, space velocity=15000 h⁻¹ [19].

For purely coal-fired power plants, the effect of alkali deactivation is instead negligible since alkali content is relatively low and the alkali fractions in the fuel are usually bound as silicate and aluminate, which are very stable even at high temperatures.

According to Chen et al. [19, 102], the strength of the poison within this group follows the scale of basicity:

$$K > Na > Ca$$

as shown in Figure 2.22.

The effects of potassium were studied by different authors on both model vanadia/titania [19, 102, 105] and commercial catalysts [20, 106, 107, 112, 113]. The K-doped catalysts were prepared in laboratory by wet impregnation with aqueous solution of KNO₃ [19, 102, 106, 107], KOH and K₂CO₃ [105, 112, 113], and KCl and K₂SO₄ [20]. All the tests were conducted by measuring the rate of NO reduction at increasing K-content. Ammonia adsorption studies were also carried out. The amount of adsorbed ammonia was measured by TPD methods or by measuring the amount of NO reduced by a catalyst pre-saturated with ammonia. Both fresh and doped catalysts were then analysed by means of FT-IR in order to follow the changes in the measured spectra induced by the increasing levels of K deposited on the catalyst.

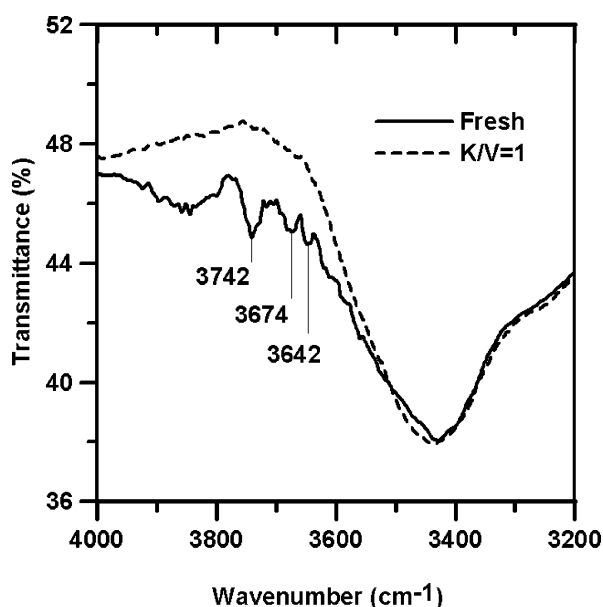


Figure 2.23: IR spectra in the OH region of the 1 %wt V₂O₅–WO₃–TiO₂ fresh catalyst and doped one with K/V=1 after activity measurement [20].

All authors find that due to K-doping a much lower amount of ammonia adsorbs on the vanadia-based catalyst, both in the coordinated and protonated form, resulting in a high decrease of NO conversion at even small addition of poison. For instance, up to 70% of the initial activity was lost when the K:V molar ratio in the catalyst was equal to 0.2 [19]. Furthermore, a K-doped 7.3 %wt V₂O₅ commercial catalyst plate became active in the oxidation of NH₃ to NO at temperatures > 300 °C[20].

FT-IR measurements made on K-doped catalysts suggested that potassium preferentially reacts with the V-OH species, as shown in Figure 2.23 [110], whereas the LA sites are not affected to great extent by the poisoning [106], indicating that the BA sites associated with the V-OH species are the active species in the SCR reaction. A recent study by Guo [11], however, has shown that the Brønsted acid sites, which are active in the SCR reaction and therefore attacked by the alkali metals, are mainly those formed by Ti, W and S and less by V. According to Nicosia et al. [113], apart from drastically affecting the acidity of the catalyst surface by interacting with the Brønsted acid sites, K also decreases the activity of V⁺⁵=O sites (which constitute the active sites of the redox cycle in both Ramis and Topsøe reaction mechanism), in agreement with Si-Ahmed et al. [114] and Due-Hansen et al. [115]. In particular, DFT calculations performed by the authors [113] have shown that one single K-atom is able to deactivate up to

2.5 Deactivation of SCR Vanadia-based Catalysts

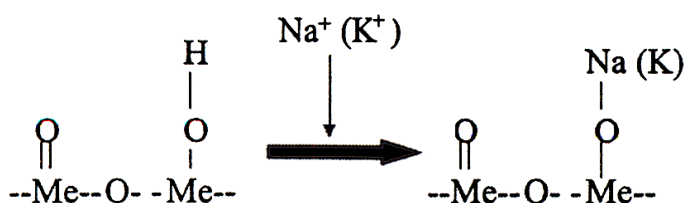


Figure 2.24: Model of alkali deactivation [21].

four vanadium centres, thus explaining the very low K:V molar ratio needed to deactivate the vanadia-based SCR catalysts. Figure 2.24 shows a schematic representation of alkali poisoning [21].

Similar behaviours were found for Na- and Ca-poisoning [19, 102, 107] when doping the catalysts by wet impregnation with aqueous solution of NaNO_3 and $\text{Ca}(\text{Ac})_2$.

As stated above, alkali metals are considered the main deactivating agents when the vanadia-based SCR catalysts are employed in plants burning biomass alone or with fossil fuels. The use of biomass as fuel in the power production is very common in countries like Sweden and Denmark. Here straw and wood are burned in the power plants in order to obey to the national regulations, however resulting in a lower performance of the whole combustion process [109, 110, 116]. The results obtained in the laboratory by wet impregnation are of course far from simulating the situation at full-scale. Here the alkali fraction is present as aerosol particles formed during homogeneous and heterogeneous condensation of alkali metals evaporated from the fuel during the combustion [117, 118]. Their interaction with the monolith is thus dependent on several different phenomena (e.g diffusion, evaporation, condensation, etc.), which are not simulated by the doping methods adopted in the laboratory. For this reason, investigations using catalysts exposed under more realistic conditions have recently started [108–110, 119].

Moradi et al. [108] exposed vanadia-supported monolith and wire-mesh catalysts to aerosol particles of KCl , K_2SO_4 and K_2CO_3 that were produced by a spray method. The de- NO_x activity of the exposed samples was then determined in the laboratory, and their surfaces were characterized by scanning electron microscopy and X-ray mapping. Hg-porosimetry and BET surface area determination were also performed. The investigation was aimed at correlating the deactivation with the melting temperature of the different K-salts. The aerosol particles produced had a constant average diameter around $0.066 \mu\text{m}$ and the load was around $15\text{--}20 \text{ mg/m}^3$ at room temperature, which are rather low if compared to the aerosol distribution measured at full-scale (straw grate-

firing), [117, 118]. After a total exposure of 31 hours at 300 °C, K-salts were found to penetrate the SCR catalyst wall to a depth of 1-1.5 μm . Since at that temperature these salts are solid, it was concluded that the fine particles were able to penetrate by diffusion. This conclusion was further supported by the increased amount of deposited K found when the exposure temperature was raised to 500 °C. The Hg-porosimetry and the BET analysis showed an increased value of the average pore diameter which suggested the occurrence of loss of meso- and micro-pores. Pore blocking by K-salts was then indicated as the main mechanism of deactivation. However, no significant decrease in activity was observed when the spent samples were used in the SCR reaction. Considering especially the very short exposure time adopted in these experiments, this result is not surprising and only suggests that experiments with longer exposure times are required in order to further clarify the process of deactivation.

The few references available in the open literature about SCR applied to biomass combustion are from Sweden [22, 109] and Denmark [110, 116, 119] where, as said before, the use of biomass in the power plant is highly motivated by local regulations. These references are the most important ones concerning the deactivation by alkali, in particular potassium.

Khodayari et al. [109] studied the activity of commercial $\text{V}_2\text{O}_5\text{-WO}_3\text{-TiO}_2$ ceramic honeycombs and plates as a function of exposure time (max 2100 h) at full-scale flue gases. The catalysts contained a higher amount of V_2O_5 than those normally used in coal combustion, due to the lower SO_2 levels in biomass combustion. The tests were carried out in a 125 MW_e circulating fluidized bed (CFB) plant burning forest residues, and in a 75 MW_e plant burning pulverized wood (PC). The catalysts were exposed either in a by-pass rig or in a test bench directly introduced into the flue gas duct. Activity measurements were performed on mini monoliths (3x3 channels) in an aluminium reactor chamber at a fixed temperature of 300 °C, and the exposed samples were characterized by BET surface analysis and SEM/EDX. In the case of the CFB plant where forest residues were burned, the catalysts lost 20% of their initial activity. Here K was found well distributed in the walls and constituted the 0.27 wt% of the whole catalyst mass. In the case of wood combustion at the PC plant, after only 1400 hours of exposure, the catalysts lost up to 80% of their initial activity. Here the total amount of K deposited was 0.8 wt%. The difference in deactivation between the two plants was found in the different composition of the fuels. Contrary to wood, forest residues present an ash with more than 40 wt% SiO_2 . Part of the K is then supposed to be bound to this silica in very stable fly ash, which does not interact with the active sites on the catalyst surface. These findings are in agreement with the experience developed in Denmark in cofiring coal and straw (20% on energy basis) [116].

Kling et al. studied the deactivation of three different vanadium-titanium

2.5 Deactivation of SCR Vanadia-based Catalysts

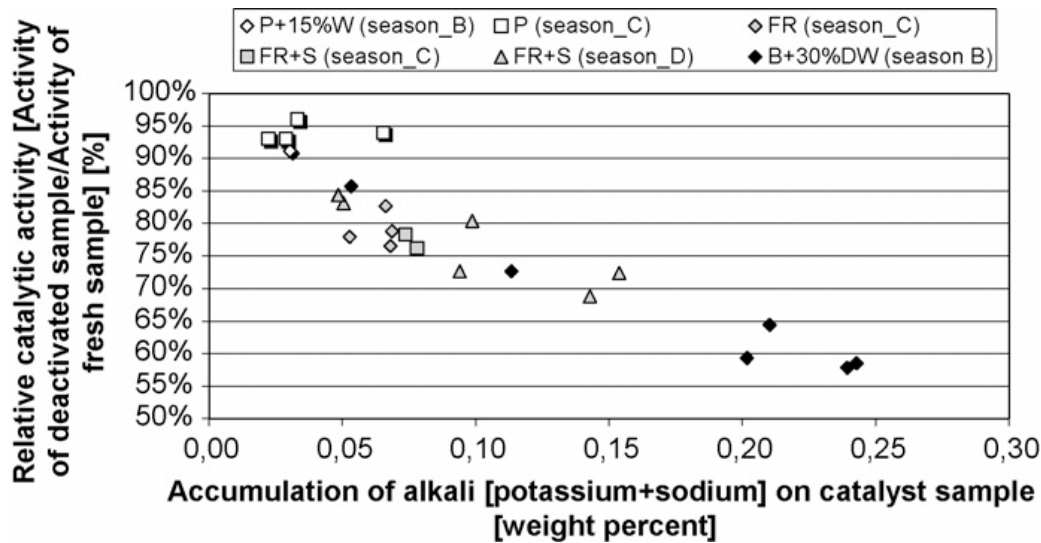


Figure 2.25: Accumulation of alkali on the SCR catalyst samples as function of the corresponding catalytic deNO_x activity (measured at a temperature of 300 °C). P, peat; FR, forest residues; B, bark; DW, demolition wood; S, sulphur. From [22].

SCR catalysts (low, medium and high V₂O₅-content) in high-dust position at three 100 MW-scale boilers during biofuel and peat combustion [22]. In the study, a linear correlation between exposure time in the boilers and alkali concentration (mainly potassium) on the samples was found, implying that mainly alkali in ultra fine particles (<100 nm) in the flue gas increased the alkali accumulation on the catalyst samples. The relative activity of the samples also linearly decreased at increasing alkali concentrations, as shown in Figure 2.25. In particular, 42% of the initial activity was lost in the case of the catalyst with the low V₂O₅-content when its alkali-content was only about 0.25 %wt after 1500 h of exposure to a flue gas from bark and demolition wood cofiring (deactivation rate equal to about 0.7%/day). The SEM-EDX test made with spent samples showed that K was evenly distributed in the catalyst wall, whereas no K-accumulation was found on the outer surface. These facts point out the penetration ability of K, which, however, cannot be associated to diffusion as solid particles, even considering the presence of ultra fine particles.

Zheng et al. studied the K-deactivation on commercial type V₂O₅-WO₃-TiO₂ monolith catalysts both at full-scale, under straw/wood combustion at a grate-fired power plant [110], and in a pilot plant by exposing the catalyst elements to a flue gas doped with KCl and K₂SO₄ aerosols [119]. The work involved aerosol measurements, periodic activity and ammonia chemisorption tests, and characterization by SEM-EDX and BET of the exposed catalysts. Re-

Literature Study

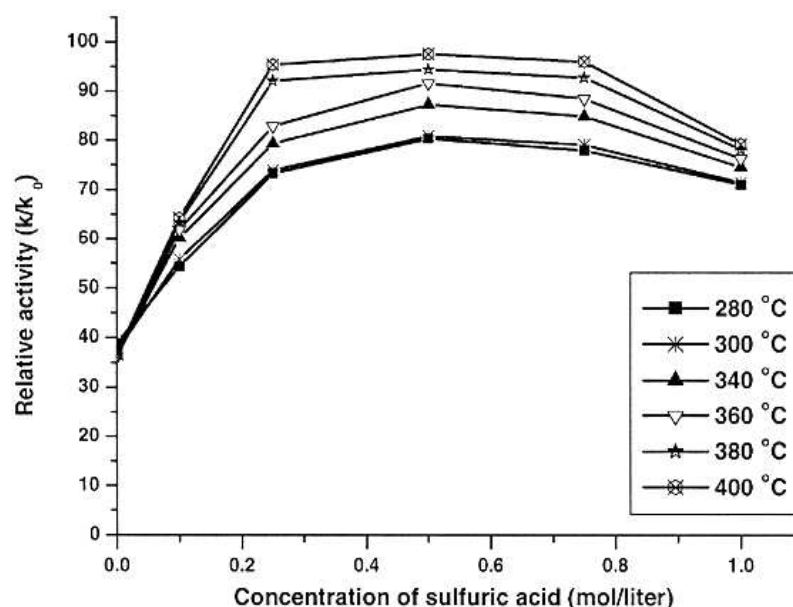


Figure 2.26: Relative activity vs. concentration of sulphuric acid at different temperatures. From [23].

Regardless the different particle size distributions and concentrations measured at the two setups, i.e. both lower particle mean diameter and concentration at the pilot plant, the deactivation proceeded at similar rates (i.e. about 1%/day). This result is in agreement with the study by Kling et al. [22] and further indicates that it is only the K present in the ultra fine particles that contributes to the deactivation. Again, K was able to penetrate the catalyst structure and a K/V ratio higher than 0.3 was found. According to Figure 2.22 this ratio is already able to reduce the catalyst intrinsic activity to 30% of the initial one.

Based on the results here presented, it is likely that the fast deactivation rates measured during biomass combustion are the result of both the high chemical affinity between K and V, when K is bound to water soluble salts, and the ability of K-salts in forming pure submicron particles.

In general, it can be said that overcoming K-deactivation at biomass combustion is a very challenging process. So far, regeneration of K-poisoned catalysts has been indicated as a viable solution for minimizing the total cost of the SCR process applied to biofuels (co)-combustion. Khodayari et al. [23, 120] studied the regeneration effects of washing with different aqueous solutions (i.e. of sulphuric acid, sulphuric acid and vanadyl sulphate, sulphuric acid and vanadyl sulphate and ammonium paratungstate) and sulphation with SO₂. From their activity tests on a commercial vanadia-based catalyst, they con-

2.5 Deactivation of SCR Vanadia-based Catalysts

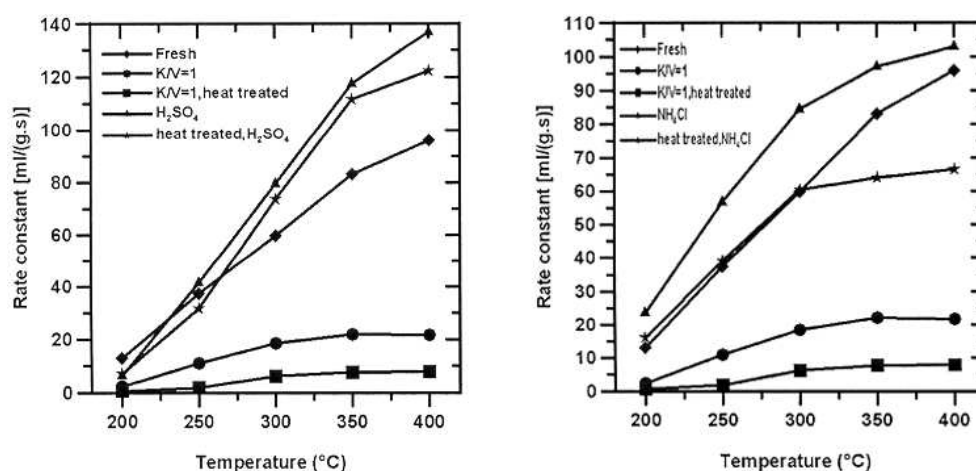


Figure 2.27: Effects of washing by 0.5 M H₂SO₄ and 1 M NH₄Cl on the activity of K-poisoned 1 wt% V₂O₅(WO₃)/TiO₂ catalysts. From [20].

cluded that the most effective method is washing with aqueous solution of H₂SO₄. As shown in Figure 2.26, a catalyst washed with 0.5 M of H₂SO₄ almost regained its initial activity at 400 °C. Similar results were obtained by Zheng et al. [20]. Again, washing by 0.5 M H₂SO₄ resulted an effective way to regenerate the catalyst. Beside this, the regeneration by 1 M NH₄Cl also showed good results (Figure 2.27). However, the textural properties of the catalyst after regeneration were found to degrade, indicating a limit in the number of possible regenerations [23].

Arsenic

Arsenic is a coal mineral matter constituent with serious impact on SCR design and operation [121–124]. Arsenic deactivation was first identified as a problem in wet bottom boilers or in the presence of ash recirculation: in some German installations, 50% loss of activity has been reported after 10 000 operating hours in the case of vanadia-tungsten based catalysts [122]. Due to this great impact of arsenic on the activity of SCR catalysts, many investigations have been carried out in order to elucidate the mechanism of As-deactivation and propose viable solutions [21, 124–128].

All authors agree that the poison is constituted by gaseous As₂O₃ released during fuel combustion. It is thus clear that the problems experienced in the presence of ash recirculation were related to the concentrating mechanism due to recirculation, which was able to cause high gaseous arsenic levels (10 times the initial level) in the flue gas. However it was also found that a correlation

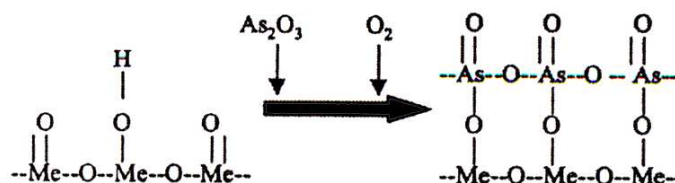


Figure 2.28: Model of gaseous arsenic deactivation [21].

between gaseous As and Ca in the fuel exists [121]. By analysing the ash composition, it was concluded that in the presence of free CaO in the gas, much of the As_2O_3 reacts with this to form calcium arsenide $\text{Ca}(\text{As}_2\text{O}_3)_2$. Since this compound is a stable solid material, it becomes boiler bottom ash or fly ash. In this case, only a small part of the As_2O_3 remains gaseous and reaches the SCR catalyst. Experience now indicates that if free CaO in the fly ash is below 2%, all the arsenic present in the fuel contributes to gaseous As_2O_3 [121]. In this case the addition of limestone to the fuel is necessary.

Research on the mechanism of deactivation by gaseous As_2O_3 lead to the development of the so-called As-resistant SCR catalysts [21, 124–128]. It was found that gaseous As tends to condense on the catalyst surface blocking the active sites (as shown in Figure 2.28), and altering the pore structure of the catalyst, indicating the co-presence of both chemical and physical deactivation [125, 128].

Further research on the deactivating effects of As on different catalysts compositions showed that vanadia-molybdenum-titania catalysts were more resistant to As poisoning than vanadia-tungsten-titania catalysts [127]: it is now demonstrated that arsenic preferentially reacts with MoO_3 and, while there are free Mo-OH on the catalyst surface, the vanadia sites are not attacked.

Based on these findings, arsenic poisoning was best abated by both catalyst formulation and pore design. Molybdenum was added to the catalyst up to 6% w/w and a deactivation rate up to three times slower compared to the $\text{V}_2\text{O}_5\text{-WO}_3/\text{TiO}_2$ catalyst was obtained. However, the resulting catalysts were less active compared to vanadia-tungsten-titania catalysts. Moreover, by reducing the average pore diameter, the diffusion of gaseous As_2O_3 was also limited due to the high volume occupied by the molecules [21, 121, 122]. This result is however in contrast with Jensen et al. [129], who showed that diffusion and pore condensation of As_2O_3 constitute the main mechanism of As-accumulation, and that a larger fraction of large pores can prevent fouling of the surface. According to the authors [129], As deactivation can be reversed by periodically switching to coal types with lower As concentrations.

2.5 Deactivation of SCR Vanadia-based Catalysts

Table 2.6: Ash analysis: MBM and sewage sludge. Data from CATDEACT final report.

| | Sewage Sludge | MBM |
|------------------------------------|---------------|------|
| <i>Ash composition, wt.% (ash)</i> | | |
| P ₂ O ₅ | 20.4 | 32.7 |
| SiO ₂ | 29.9 | 0.9 |
| Fe ₂ O ₃ | 13.0 | 0.5 |
| Al ₂ O ₃ | 12.8 | 0.1 |
| CaO | 14.3 | 56.0 |
| MgO | 3.0 | 1.1 |
| Na ₂ O | 0.6 | 2.2 |
| K ₂ O | 1.8 | 1.7 |
| TiO ₂ | 1.1 | <0.1 |

Phosphorus

Phosphorus is a typical constituent of coal. However, during coal combustion its deactivating effects are not relevant compared to other deactivation mechanisms. On the other hand, the increasing interest in (co-)firing with P-rich fuels like, for instance, sewage sludge and meat and bone meal (MBM) (Table 2.6), has led to new interest in its effect on the SCR activity of vanadia-based catalysts [24].

The deactivating effect of P were studied on both model (5 wt%)V₂O₅-TiO₂ [19] and commercial (1 wt%)V₂O₅-WO₃-TiO₂ catalysts [130]. Phosphorus was added to the catalysts by wet impregnation of aqueous solution of H₃PO₄. The activity of the doped catalysts was then measured in the laboratory and the samples were characterized by means of FT-IR and Raman spectroscopy, XPS and N₂ adsorption. The poison was found to disperse well over the catalyst surface without significant agglomeration up to 5 wt% load [130]. The activity tests performed on model high-vanadia-content catalysts [19] showed that P₂O₅ formed during heating is a very weak poison as compared with the alkali metal oxides (Figure 2.22) at typical SCR temperatures. At lower temperatures, however, its poisoning strength was found relatively higher as shown by Figure 2.29 [19]. Low addition of P₂O₅ to commercial V₂O₅(WO₃)/TiO₂ catalyst did not cause a pronounced deactivation effect either [130]. This effect was found to gradually increase according with the P₂O₅ content.

The following deactivating mechanisms by phosphorus were proposed by Kamata et al. [130]:

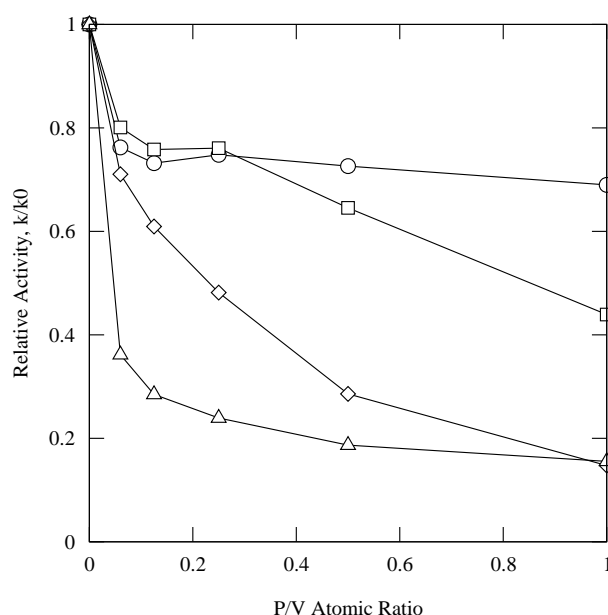


Figure 2.29: Effects of P_2O_5 doped on 5% V_2O_5/TiO_2 catalyst in the SCR reaction at 150 (triangles), 200 (diamonds), 250 (squares) and 300 °C (circles). Data from [19].

- by decreasing the specific surface area and pore volume of the catalyst, in agreement with previous observation by Blanco et al. [104] on vanadia catalysts extruded with H_3PO_4 ;
- by replacing the surface hydroxyl groups (V-OH and W-OH) with P-OH groups: FT-IR evidences of NH_3 adsorption showed that these groups still present a Brønsted acidity and participate in the activation of adsorbed ammonia [130], but this acidity is much weaker than the one due to the replaced groups;
- by removing sulphur species from the catalyst surface which are known to contribute to some extent to the acidity of the catalytic surface.

Recently, Beck et al. [24] analysed different high-dust vanadia-based catalysts employed in the treatment of flue gas produced by sewage sludge and MBM co-combustion. From the results of BET analysis of the exposed samples, they concluded that pore condensation in combination with pore blocking is the prevailing deactivation mechanism by phosphorus. The main responsible for this mechanism were identified by equilibrium calculations considering primary flue gas constituents (i.e. SO_2 , H_2O and CO) together with the fly ash components (i.e. CaO , Al_2O_3 and SiO_2) in the temperature range of 400-1400 °C.

2.5 Deactivation of SCR Vanadia-based Catalysts

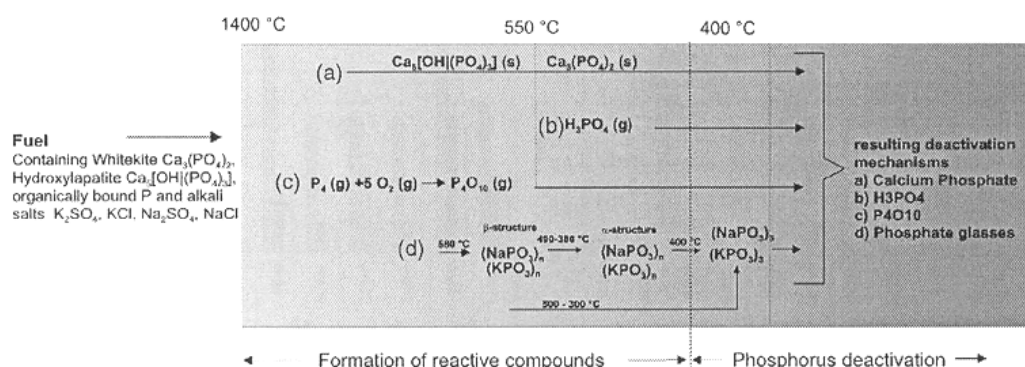


Figure 2.30: Proposed reactions of calcium phosphates along the flue gas path. From [24].

The results are shown in Figure 2.30. As it can be seen from this, the following deactivating species were proposed:

- *Solid calcium phosphates.* These compounds are due to heterogeneous reactions between gaseous P and fly ash, or they come directly from the fuel, especially in the case of MBM where a large part of the P is bound to high melting point calcium phosphates. These particles can be regarded as pore- and channel-blocking agents.
- *Condensed phosphoric acid.* When present in the gas-phase at high temperatures, the phosphoric acid forms poly-phosphates which have melting points higher than the typical SCR temperature. They can thus form aerosols which can diffuse into the pore structure and deactivate the catalysts both by poisoning and pore-condensation. Moreover, these poly-phosphates are known to form insoluble salts with ammonia and the alkali fraction present in the flue gas forming glassy deposits on the catalyst surface.
- *Gaseous phosphorus oxide and phosphoric acid.* Since these compounds are present in the gas phase, they can *easily* diffuse into the wall and poison the catalyst.

The relative activities of the different catalysts analysed were also plotted against the amount of phosphorus found on the surface of the exposed catalyst (i.e without considering the total amount of P deposited *in* the catalysts) in order to verify any relation between the two variables. However, in the case of P the test was not really successful as shown in Figure 2.31: in some cases better correlations were instead found for the alkali and alkaline earth metals. In general, considering that bulk concentrations for K_2O were found in the range

Literature Study

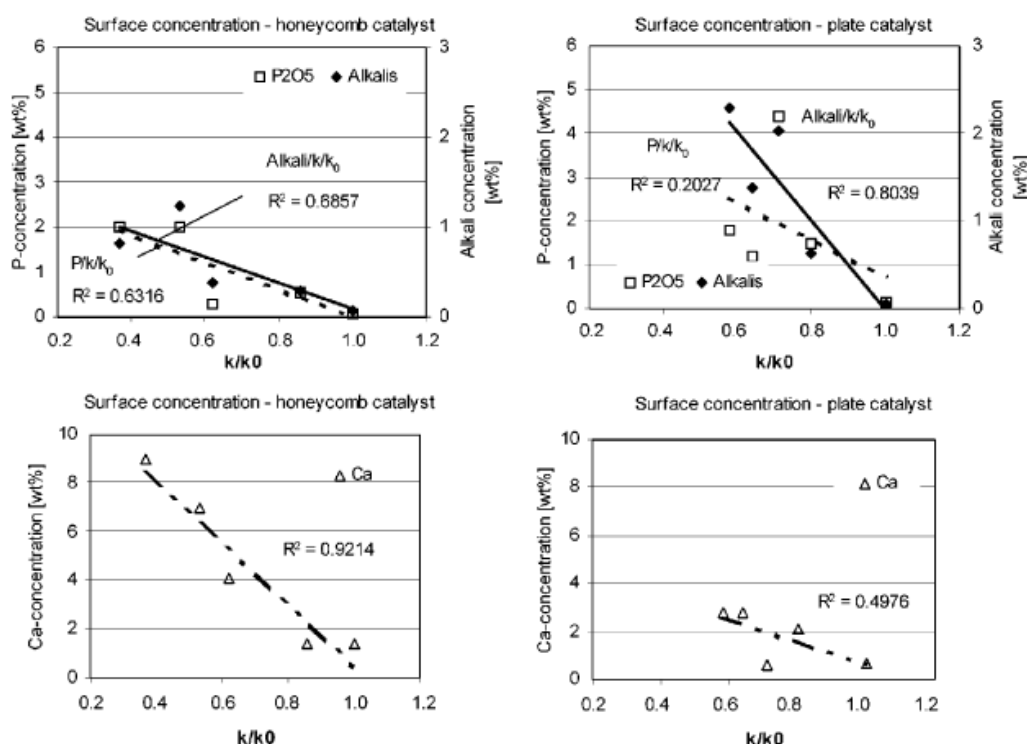


Figure 2.31: Relation of surface P, alkali and Ca concentration compared to k/k_0 of honeycomb and plate catalysts exposed to sewage sludge and MBM co-combustion. From [24].

0.2-0.7 wt%, which may be expected to cause significant deactivation, it is difficult to address the influence of P on the observed deactivation. Moreover, the catalysts were in fact poisoned under poorly defined conditions: Both honeycomb and plate type catalysts were exposed to flue gases from either wet bottom or dry ash boilers burning coal mixed to either MBM or sewage sludge. The exposure times were also varying between 2000 and 55000 hours.

From this work, however, it was clear that the P-chemistry could be an issue in the upcoming years since more interest has been focusing on the utilization of P-rich secondary fuels for energy production. Recently another work from Beck et al. concerning the behaviour of P in flue gases from coal and MBM and sewage sludge co-combustion and the SCR catalysts has been published [131]. In this study, by analysing at full-scale both the flue gas and particle composition at both the inlet and outlet of the SCR reactor, an increase of S-content in the particles at the outlet of the reactor was noted. Correspondingly an increase in phosphoric acid concentration at the outlet was also measured. The

2.5 Deactivation of SCR Vanadia-based Catalysts

following reaction occurring on the SCR catalyst was then proposed:



where a possible influence of P on SO₂ capture due to the SCR catalyst were hypothesized. More research in this field is needed in the future.

Lead, Zinc and Hydrogen Chloride

The poisoning effects of PbO, ZnO and ZnCl₂ are reported as the worst poisons for the SCR catalysts used at waste incineration plants [132]. Moreover, the flue gases from these plants can contain significant amount of hydrogen chloride [107].

Elemental analysis of the catalysts employed in the Swedish incinerator located in Sysav after 2000 hours of exposure revealed deposition of Pb and Zn on the catalyst *surface* up to 0.15 and 0.36 wt%.

Khodayari et al. [133] studied the effects of lead on the reduction of NO over a commercial vanadia-based catalyst by SCR activity tests and ammonia chemisorption determination. The samples were doped by wet impregnation with different aqueous solutions of Pb(NO₃)₂. In order to grant complete decomposition of the nitrate into the oxide, the samples were calcined at 420 °C for 14 h. At this temperature all lead should exist as PbO. In order to lessen the influence of mass transfer on the reaction rate for the fresh and impregnated catalysts, activity test were performed also over crushed and sieved samples. In the case of monolith samples, low lead loads (comparable with the amount found in the Swedish incinerator plant) caused only small changes in the activity. For higher lead coverage, a more significant drop (i.e. $k/k_0 \approx 0.35$ at 400 °C as calculated from the NO conversion data reported and assuming first order reaction in a plug flow) was observed when 1.85 wt% of PbO was deposited in the catalyst. At even higher lead concentrations (i.e. 2.31 and 2.88 wt%) no additional decrease in activity was found, indicating a saturation point. As expected, the crushed samples were found to be deactivated more than the monolith: only 10 wt% of the original activity was still present at 400 °C when again 1.85 wt% of PbO was present. The ammonia chemisorption tests revealed that the amount of NH₃ adsorbed and the activity of the catalysts were decreasing in the same way according to the Pb-load. Based on this result, it was concluded that Pb does not *selectively* react with the active sites but does deposit indistinguishably on the surface area, rendering the the active sites inaccessible to the gas phase.

Khodayari et al. [132] also tested in the laboratory the deactivating effects of ZnCl₂. Commercial catalysts were doped by ZnCl₂ using a gas phase impregnation technique at 650 °C. To avoid oxidation of ZnCl₂ to ZnO, the activ-

ity measurements were performed at temperature lower than 340 °C. At this temperature, the relative activity for the catalyst with the same concentration found in the Swedish incinerator plant was around 10-15%. A minimum in relative activity at the same temperature was then found at a concentration around 1.5 wt%, where the catalyst reached its ZnCl_2 saturation point. BET analysis showed a decrease in surface area at increasing Zn load and as in the case of Pb it was concluded that zinc non-selectively deposited over the catalyst surface. Increasing the temperature above 340 °C resulted in losing of weight due to evaporation of ZnCl_2 : after degassing for 16 hours at 400 °C, 50% of the Zn was already removed.

Moradi et al. [108] exposed vanadia supported catalysts to submicron aerosols of ZnCl_2 . The particles were prepared by spraying an aqueous solution of ZnCl_2 (25 g/l) and had a mean diameter equal to 0.70 μm . The particle load was around 20 mg/m^3 at room temperature and the total exposure time was 31 hours. SEM pictures and X-ray mapping of Zn of the catalysts exposed at 300 °C showed the formation of a layer of 6-8 μm thickness on the catalysts outer surface and an entire penetration depth around 5 μm . This ability in penetrating the pore structure of the wall was explained considering the fact that at these temperature the ZnCl_2 is a melt (melting point 275 °C) and can easily move through the porous structure of the catalyst. The activity of the doped catalysts was not found to decrease considerably. However no data about the final Zn concentration were reported.

Regarding the effects of hydrogen chloride, HCl, on the SCR activity, these are different and dependent on the reaction temperature [19]. According to the definition of poison, HCl can be considered as such for vanadia-based catalysts since it can react with the lower vanadium oxides formed by the reduction of V_2O_5 by NH_3 . Their interaction with gaseous HCl forms both VCl_4 and VCl_2 which are volatile and can be found in the outlet gas. Thus HCl “removes” the vanadia active sites from the catalyst surface. Moreover, Lisi et al. [107] reported that this effect is more evident at increasing vanadia contents. They thus concluded that weaker V=O terminals associated with polyvanadate species at higher V contents are more easily attacked by HCl.

2.6 Conclusions

In the last two decades, a tremendous amount of work has been carried out in order to find the best solution for NO abatement at stationary combustion processes. Both primary and secondary measures have been developed with different results. Among these cleaning techniques, the SCR of NO by NH_3 on vanadia-based catalysts is an effective process which has obtained an incredi-

ble commercial success, even though it presents disadvantages, like the use of an expensive and toxic reagent (i.e. NH_3), and has activity in the SO_2 oxidation.

Thanks to the above mentioned commercial success, a great amount of resources has been invested in the development of more performing vanadia-based catalysts, through the understanding of the nature of the active sites, the mechanisms of reaction under different conditions, and the evidences of the deactivation rates experienced at full-scale.

Nowadays, the main challenge for this family of catalysts is their application to fuels different from coal or oil and to non-stationary processes. Power plants firing secondary fuels (e.g biomass, wastes) are increasing in number. When applied to these systems, the vanadia-based catalysts quite often present unacceptable deactivation rates. The causes of deactivation are many and not yet fully understood. Both chemical and physical deactivation can play a role depending on the different compounds introduced by the fuels used in the combustion process. It is concluded from the deactivation studies carried out, that alkali and alkaline earth metals and arsenic are the most dangerous poisons for the vanadia-based catalysts. However, especially in the case of waste-firing, deactivation by phosphorus and heavy metals (e.g. Pb, Zn) has to be carefully taken into consideration. Only by understanding the different deactivation mechanisms, effective measures to slow these down as much as possible could be adopted. Moreover, also the regeneration of the spent catalysts could become a more used practice.

Chapter 3

Experimental

3.1 The Catalyst

Commercial corrugated-type monoliths and plates obtained from Haldor Topsøe A/S were used in this study. The catalysts were based on V_2O_5 (up to 5 wt%) and tungsten oxide (WO_3 , up to 9 wt%) dispersed on a fibre reinforced TiO_2 carrier. The monoliths had a size of 75 mm x 75 mm x 500 mm. The hydraulic diameter of the channels was about 6.5 mm and the wall thickness was 1.0 mm.

3.2 SCR Pilot Plant

In order to simulate the exposure conditions at full-scale, commercial SCR full-length monoliths have been exposed in a pilot-scale SCR setup to a flue gas containing aerosols of the different deactivating compounds under investigation. The aerosols are formed by spraying directly into the hot flue gas a water solution of the different compounds.

A schematic of the SCR pilot plant is shown in Figure 3.1. This mainly consist of a 50 kW natural gas burner for flue gas production, a lance for injecting liquid solutions, a square duct hosting a full length commercial monolith, an NH_3 supply system and a soot blowing system running with compressed air installed at the SCR reactor inlet.

The setup runs slightly below atmospheric pressure (5-8 mbar) for safety reasons. Natural gas is burned in the presence of excess air. The flue gas exiting the burner at 950-1000 °C is then led to a high temperature pipe, where the aqueous solutions are injected. This is done by pumping the solution through a water-cooled lance inserted in the high temperature pipe having a two-fluid nozzle at the outlet. Here the water solution meets a flow of compressed air (also added through the lance) and is thus sprayed into the flue gas.

Experimental

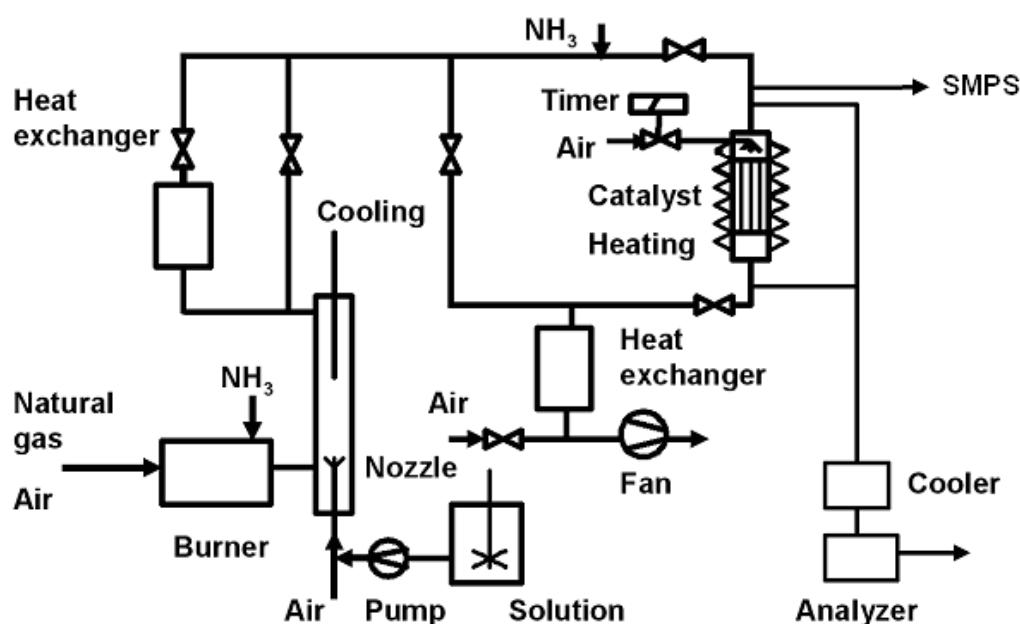


Figure 3.1: The pilot-scale SCR setup.

The temperature of the flue gas at the inlet of the SCR reactor can be controlled by adjusting the flow passing through a heat exchanger. For minor adjustments, or to avoid corrosion of the metal pipes, the temperature can be controlled by simply adjusting the position of a bayonet heat exchanger inserted on the other end of the high temperature pipe. The gas flow is measured by a pitot tube situated at the inlet of the SCR reactor. A throttle valve is used to bypass part of the flue gas and get the desired flow through the reactor.

Ammonia is added into the burner in order to obtain a NO concentration of ≈ 500 ppmv at the SCR reactor inlet. If NH_3 was not added, only about 80 ppmv of NO would have been present in the flue gas.

The reactor is a squared duct, where the catalyst element is vertically supported. In order to have a constant temperature along the whole element, two electric heating wires with temperature control are installed around the reactor. In this way the temperature difference between the inlet and the outlet of the reactor can be kept less than 3 °C.

Plate-shaped catalysts can be also exposed to the flue gas by placing them in the pipe downstream the SCR reactor using a squared-plate-holder designed for the purpose.

3.3 Laboratory Gas Flow Setup

In the laboratory, the activities of the catalysts were measured by means of the setup shown in Figure 3.2. This mainly consisted of three sections: a gas metering and mixing section, a reactor, and an analyser section. The flow rates of the individual gases were controlled by mass flow controllers providing a constant flow, and measured by a bubble flowmeter. Mixing was then performed with a flow panel. Normally, two different gas streams were made and directed to the reactor. Water was added by passing part of the nitrogen gas through an evaporator consisting of a PermaPure tube placed in a thermostated water bath.

The reactor was a fixed-bed reactor made of quartz shown in Figure 3.3. The inner and bottom tubes of the reactor were removable. Ammonia, O₂, H₂O, and half of N₂ were added through the bottom (1 in Figure 2), which functions as a preheating section, whereas NO and the other half of N₂ were added from the top of the reactor inlet (2 in Figure 3.3). With this arrangement, reactive gases could be kept separated until they were mixed, just above the catalysts placed on the porous quartz plate. This minimises homogeneous and wall-catalysed reactions in the pre-heating section, which, in any case, were negligible at the temperatures used here. The reactor temperature was measured below the porous quartz plate by a thermocouple shielded in a quartz tube. The reactor was placed in a three-zone oven for effective temperature control. Nitric oxide was analysed by a conventional UV analyser. No NH₃ measurements have been performed.

3.4 Activity Measurements

The rate of SCR reaction at typical industrial reacting conditions has been assumed to follow an Eley-Rideal mechanism of reaction with NH₃ adsorbed on the catalyst surface and NO reacting from the gas phase. The following expression for the rate of reaction, r_{NO} , can then be derived:

$$-r_{NO} \left[\frac{\text{mol}}{\text{m}^3_{\text{cat}} \text{s}} \right] = k c_{NO} \frac{K_{\text{NH}_3} c_{\text{NH}_3}}{1 + K_{\text{NH}_3} c_{\text{NH}_3}} \quad (3.1)$$

where k [1/s] is the rate constant, c_{NO} and c_{NH_3} [mol/m³] are the concentrations of NO and NH₃ respectively, and K_{NH_3} [m³/mol] is the adsorption constant for NH₃ on the catalyst surface. The fraction term on the right-hand side of 3.1 is the NH₃ coverage of the catalytic surface, θ_{NH_3} . At the reaction conditions adopted during the measurements, introduced below, the NH₃ coverage

Experimental

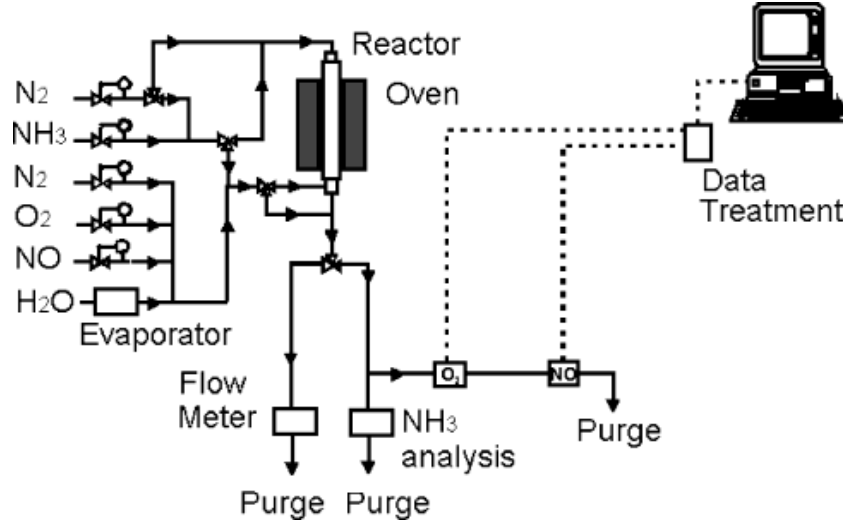


Figure 3.2: The laboratory gas flow setup.

can be assumed equal to 1 and the reaction rate can be regarded as pseudo-first order with respect to NO and zero order with respect to NH_3 . Therefore, directly from the fractional NO conversion, X , it is possible to calculate an observed catalyst activity constant, k' , that includes both the influence of external and internal mass transfer:

$$-k' \left[\frac{\text{ml}}{\text{g}_{\text{cat}} \text{s}} \right] = -\frac{F_{\text{gas}}}{m_{\text{cat}}} \ln(1 - X) \quad (3.2)$$

where F_{gas} is the gas flow rate (ml/s), m_{cat} is the weight of catalyst (g). The degree of deactivation can be then calculated as the ratio k/k_0 between the activity constant of the catalyst measured at different exposure times, k , and the one measured for the fresh element, k_0 , right before starting the poison addition.

Pilot Plant

At the pilot plant, the NO conversions were measured at 350 °C in the presence of about 500 ppmv NO, 600 ppmv NH_3 , 10%v O_2 , 6%v CO_2 , and about 10%v H_2O . During the measurements (where not stated differently) the flow through the SCR reactor was kept at 40 Nm^3/h , corresponding to a GHSV equal to about 14200 h^{-1} . At this flow the gas velocity in the channel was about 6.5 m/s at 350 °C, thus similar to the velocities used at full scale applications, and up to 50% external mass transfer limitations have been estimated.

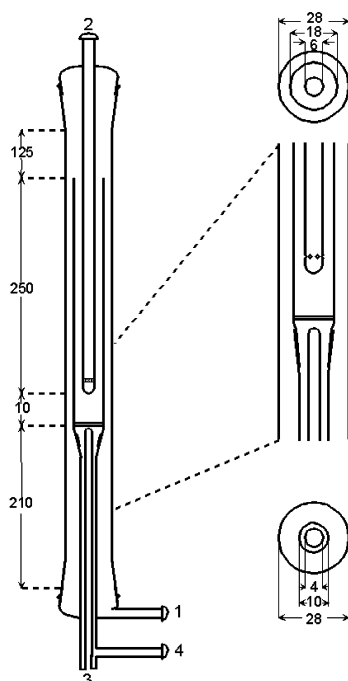


Figure 3.3: Sketch of the laboratory reactor. All shown measures are in millimetres. (1) Bottom gas inlet. (2) Top gas inlet. (3) Thermocouple. (4) Gas outlet.

Laboratory

In the laboratory, powdered samples have been tested for activity in a packed bed quartz micro-reactor with an internal diameter equal to 10 mm. Around 0.07 g of powder has been used during activity measurement. This has been mixed with sand of the same particle size in order to have a particle bed of about 10 mm, thus ensuring the applicability of the here assumed integral reactor model. In all experiments, the total flow was equal to 2.8 NL/min and was constituted by 500 ppmv NO, 600 ppmv NH₃, 5% O₂ and 1.4% H₂O in N₂. Activity measurements have been performed in the temperature range 250-400 °C. The catalyst activity has been calculated according to 3.2 and the deactivation as the ratio between the activity constant of the spent catalyst and the one measured for the fresh one. At 350 °C, the observed activity constant for the fresh catalyst was found only 10% less than the one calculated in the total absence of mass transfer limitations. The latter value was calculated by extrapolating at higher temperatures the Arrhenius fitting obtained in the range 250-330 °C.

In the case of the catalyst plates, the activity tests were carried out in another quartz reactor with an internal diameter equal to 18 mm. The plates were

Experimental

cut into 15 mm x 15 mm bits. Only one bit, corresponding to around 0.17 g of catalyst, was used for each measurement. This was placed in the centre of the reactor and supported by small glass indentations especially designed for the purpose. The total flow and gas composition used during the activity measurements on plates were the same as the ones used for the powders. In previous tests carried out at different flows, it has been shown that when 2.8 NL/min were used, the rate of reaction could be assumed not limited by external mass transfer limitations up to 350 °C.

During all activity measurements, the NO concentration in the dry mixture was measured by conventional UV analysers (Rosemount NGA 2000). Due to the presence of water in the feed during all activity measurements, no N₂O formation is expected [134]

3.5 Ammonia Chemisorption Tests

As discussed in Chapter 2, NH₃ chemisorption constitutes the first step of the SCR reaction mechanism. Therefore, NH₃ chemisorption studies have been systematically carried out during the different exposures, in order to identify possible deactivation mechanisms proceeding by blocking of the active sites for the NH₃ chemisorption.

These tests have been carried out both in the laboratory, using the fixed bed quartz reactor and the catalyst plates, and at the pilot plant, using the entire monolith during exposure. In both cases, the complete SCR gas mixture described in the previous section was used. All the mixture components except NO (i.e. no NH₃ was added at the burner at this stage) were first let into the reactor and passed over the catalyst for 30 minutes. During this time, the catalyst surface was saturated with NH₃. After this saturation period, the NH₃ addition was shut off and the NO flow was added to the rest of the mixture (i.e. at the pilot plant NH₃ was added only in the burner). Reaction between NO and the previously chemisorbed NH₃ then took place and the amount of NH₃ on the catalyst was calculated from the total amount of NO reduced.

3.6 Catalyst Characterization

Small pieces of catalyst were cut from the ends of both fresh and exposed monoliths. These were then characterized by different techniques.

Chemical Analysis

The chemical composition was obtained by ICP-OES at the laboratory of DONG Energy A/S and Haldor Topsøe A/S. Prior to the measurements, the samples were cut to $1.5 \times 1.7 \text{ cm}^2$ and dried at 105°C for 2 h before analysis.

Hg-porosimetry

The total pore volume and the pore size distribution of the different catalyst sample were made by mercury intrusion in a Micromeritics Autopore II 9220 porosimeter.

Scanning Electron Microscopy

SEM-EDX analysis were performed at the Danish Technological Institute using a Zeiss Ultra55 and an Oxford ISIS with a Pentafet X-ray detector.

In situ Electron Paramagnetic Resonance Spectroscopy

During the investigation reported in Chapter 4, the redox state of the catalyst surface were studied by in situ Electron Paramagnetic Resonance Spectroscopy (EPR). Samples ($\approx 0.030 \text{ g}$) of both the fresh and the exposed monoliths at the pilot plant were placed into a micro reactor cell specially designed for high temperature EPR measurements using a Bruker ER 4114 HT cavity. The spectra were recorded in situ at 350°C in a flow of around 100 ml/min simulated flue gas. After thermal equilibration, the catalysts were first exposed to a reactant gas composition consisting of 1000 ppmv NO , $3.5\% \text{v O}_2$, $3\% \text{v H}_2\text{O}$ in N_2 . After acquisition of a spectrum at stationary conditions, 1000 ppmv NH_3 was added to the gas mixture. Again after acquisition at stationary conditions, NO was omitted from the reactant gas and the final spectrum was recorded. Spectra were recorded with 1024 points from 2500-4500 Gauss, using a time constant of 82 ms and a total sweep time of 84 seconds. The resonance frequencies were around 9.534 GHz. Modulation frequency and amplitude were 100 KHz and 8.12 Gauss respectively.

3.7 Aerosol Measurements

Scanning Mobility Particle Sizer

A Scanning Mobility Particle Sizer (SMPS, TSI Inc.), which included an Electrostatic Classifier (Model 3080) and a Condensation Particle Counter (Model

Experimental

3775) was used to measure the particle concentration and size distribution during the exposure. Particle sampling was carried out at the inlet of the SCR reactor by an ejector sampler running with dry, particle-free air. In this system the particle-containing flue gas was at the same time cooled and diluted thereby preventing: i) water condensation; ii) particle coagulation in the sample line by effectively decreasing its rate by several orders of magnitude; iii) overloading of both the impactor and the SMPS. The dilution ratio, required to know the real particle concentration in the flue gas, was obtained by measuring the CO₂ concentration both in the flue gas and in the diluted sample.

Low Pressure Cascade Impactor

A 10-stage Berner-type low pressure cascade impactor (LPI) with an aerodynamic diameter range of 0.03-12.7 μm connected to a vacuum pump was used. The flow through the LPI was controlled by a critical orifice and was equal to 22.49 L/min at 25 °C and atmospheric pressure. The flue gas was sampled directly at the reactor inlet without any dilution. In order to avoid water condensation, the sampling line and the LPI were heated to 90 °C. Deposited particles were collected on aluminium foils coated with a thin film of Apiezon H grease. The grease served to limit bouncing of the particles and was added using a dilute toluene solution of the grease. The toluene was evaporated from the foils by drying these in an oven at 140 °C for 2 hours. The sampling time was equal to 60 minutes, which allowed a suitable collection of particle mass. The weight gains from the deposited particles on each foil were determined by a Sartorius M5D-000V001 microbalance. The foils were finally analysed by electron dispersive X-ray analysis for chemical composition.

Chapter 4

Deactivation by Polyphosphoric Acids

The work reported in this chapter has been published in *Applied Catalysis B: Environmental* [135]. The paper is included in Appendix A.

4.1 Introduction

Deactivation of SCR catalyst can be due to poisoning, fouling, surface masking, and sintering according to the particular application. Phosphorus is known as a poison for the vanadia-based catalysts. Its poisoning strength was tested in the laboratory both using model V_2O_5 - TiO_2 and commercial vanadia-based catalysts [19, 130]. Generally authors report that poisoning by P is moderate. At 300 °C, a model 5% V_2O_5 - TiO_2 catalyst wet impregnated with aqueous solution of H_3PO_4 lost about 30% of activity when $P/V=1$ [19]. Moreover, Kamata et al. [130] found that P is able to some extent to form Brønsted acid sites, which are still able to adsorb ammonia, and could then actively participate in the SCR reaction. Blanco et al. [104] pointed out the negative influence of P on the surface area of vanadia-based honeycomb catalysts extruded with phosphoric acid. However, catalysts extruded with H_3PO_4 and having up to 12.3 %wt P showed almost the same activity as a P-free catalyst. Beck et al. [24] analysed SCR catalysts exposed at full-scale plants to flue gases from co-combustion of P-rich fuels (i.e. MBM, sewage sludge) and coal. The catalysts had up to 4.9 wt% P_2O_5 on the external surface and both a decreased surface area and total pore volume. The authors regarded P as one of the main components responsible for the deactivation of the catalysts and hypothesized the following mechanisms of deactivation by P: (i) poisoning by gaseous P_2O_5 and/or H_3PO_4 ; (ii) pore condensation by polyphosphoric acids; (iii) deposition of alkali phosphates glasses.

Deactivation by Polyphosphoric Acids

However, the catalysts were exposed to ill defined conditions and in the presence of other known poisons (e.g. K). Hence it was not possible to clearly point out the main mechanism of deactivation by P and its importance in the simultaneous presence of other deactivating species.

The main objective of this work was to investigate the deactivating effect of P under well defined and realistic operating conditions. Full length commercial SCR monoliths have been exposed for more than 800 hours to a flue gas doped with different concentrations of orthophosphoric acid in the pilot-scale SCR setup and the deactivation mechanisms by P have been pointed out.

4.2 Experimental

In order to verify the condensation of ortho-phosphoric acid and have an on-line measurement of the activity of a SCR catalyst, a water solution of H_3PO_4 has been injected in a hot flue gas from a natural gas burner. The resulting mixture was then passed over a commercial SCR monolith, and the activity was periodically measured.

The addition of H_3PO_4 to the flue gas was performed by spraying different acid water solutions through a nozzle as described above. The solutions were prepared by diluting 85% H_3PO_4 (Fluka Inc.) with distilled water. Three catalyst elements have been exposed to 10, 100 and 1000 ppmv H_3PO_4 . In this work they will be identified by the labels “P10”, “P100” and “P1000” respectively. The letters “T” and “B” added at the end of the labels will indicate a sample cut respectively from the top (first 5 cm) or the bottom (last 5 cm) of element. In all tests, the solution feed was fixed at 1.25 litre/hour and the acid concentrations were 0.018, 0.18 and 1.8 mol/litre respectively. During the 100 ppmv test, 5 catalyst plates were also exposed. They will be referred as P100plate in this work.

Plate-shaped catalysts were doped with H_3PO_4 at three different levels by a wet-impregnation method at room temperature under a vacuum of 0.8 bar absolute pressure to allow the solution to evenly penetrate into the catalyst pores. The catalyst plates had a dimension of 1 mm x 50 mm x 150 mm. They were dried at 120 °C for 1 h and then calcined at 400 °C for 4 h under a stream of 1 L/min of N_2 . The different P/V ratios obtained were measured by inductively coupled plasma optical emission spectroscopy (ICP-OES) and were equal to 1.8, 2.9 and 4.7.

Table 4.1: Performed SMPS experiments.

| Experiment | | SMPS Results | | | |
|---|--------------------------------|--------------------------------|--|---|----------------------------|
| H ₃ PO ₄ Added (ppmv) | P-added (g/m ³) | Particle Mean Diameter (nm) | Particle Total Concentration (#/m ³) | P-content ^a (g/m ³) | P-inlet Fraction (%) |
| 10 | 0.006 | 25.0 | 3.76E+14 | 0.003 | 50 |
| 20 | 0.012 | 31.8 | 4.63E+14 | 0.008 | 66 |
| 30 | 0.018 | 36.2 | 5.20E+14 | 0.013 | 72 |
| 40 | 0.024 | 39.7 | 5.42E+14 | 0.018 | 75 |
| 50 | 0.030 | 42.8 | 5.82E+14 | 0.024 | 80 |
| 70 | 0.042 | 46.9 | 6.30E+14 | 0.034 | 81 |
| 100 | 0.061 | 50.1 | 6.14E+14 | 0.041 | 67 |
| 200 | 0.121 | 59.4 | 7.13E+14 | 0.085 | 70 |
| 300 | 0.181 | 63.6 | 7.63E+14 | 0.103 | 57 |
| 400 | 0.243 | 66.9 | 8.14E+14 | 0.127 | 52 |

^aThe P-content of the particles has been calculated by assuming the particles at the azeotropic mixture (P₂O₅ = 92.4 wt%). T=350 °C.

4.3 Results

4.3.1 Aerosol Measurements at the Pilot-scale Setup

Table 4.1 summarizes the main results of the SMPS measurements carried out. In Figure 4.1 the particle size distribution (PSD) for the tests with 10 and 100 ppmv of H₃PO₄ are shown. In all the measurements the PSD consisted of only one clear peak. The mean particle size, which was calculated from the total number concentration, was found to vary in the range 25-70 nm and was increasing with the acid concentration in the flue gas. The order of magnitude of the total particle number concentration was equal to $1 \cdot 10^{14}$ #/m³. A blank measurement where only distilled water was sprayed into the setup has also been performed. The results of this measurement showed the presence of particles with a mean diameter equal to 5.81 nm. The total particle number concentration was more than 10 times lower than the one measured when adding 10 ppmv of acid. Table 4.1 also reports the total P-concentration in the particles measured by the SMPS, together with the ratio between this concentration and the total P injected as H₃PO₄. The P-content of the particles has been calcu-

Deactivation by Polyphosphoric Acids

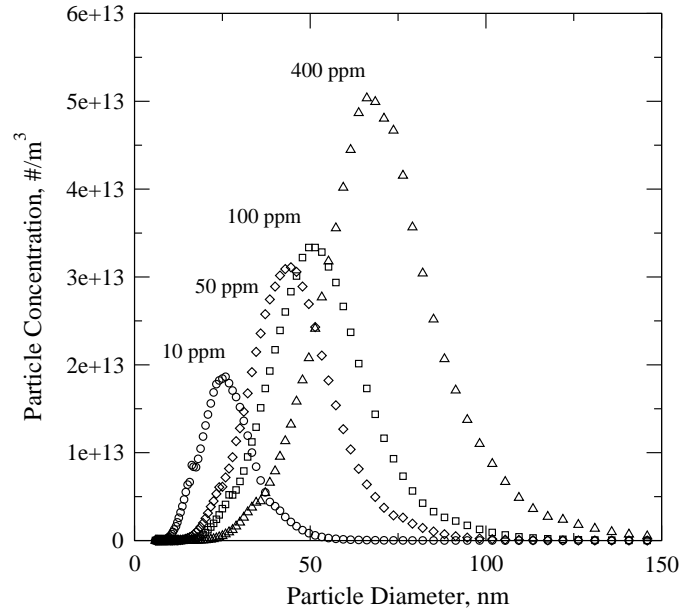


Figure 4.1: Particle size distribution of polyphosphoric acids measured at the SCR reactor inlet at different H_3PO_4 addition by SMPS. $T = 350^\circ\text{C}$.

lated by assuming the particles constituted by 92.4 wt% P_2O_5 . The reasons for this assumption will be clearer in the section 4.1. The particle density, ρ , has then been calculated as:

$$\rho = (0.7102 + 0.01617 \cdot \text{P}_{2\text{O}_5, \text{wt}\%}) - (11.7\text{E} - 4 - 6.0\text{E} - 6 \cdot \text{P}_{2\text{O}_5, \text{wt}\%}) \cdot T \quad (4.1)$$

where T is the temperature in $^\circ\text{C}$ [136]. From the values reported in Table 4.1, it can be seen that 50-81% of the injected P reaches the catalyst in the particles. Apparently, the mass-fraction of P that reaches the inlet of the SCR reactor goes through a soft maximum around 70 ppmv. The remaining may be in the gas phase or is deposited on the walls of the setup before the catalyst.

4.3.2 Activity Tests at the Pilot-scale Setup

The three catalyst elements P10, P100 and P1000 have been exposed for 819, 38 and 24 hours respectively. Prior to exposure, each element has been exposed to a clean flue gas for at least 1 week or until its activity had reached a stable value. The different values of activity for the fresh elements have then been used to calculate the relative activity of each catalyst element.

The results of the different deactivation tests are presented in a chronological order.

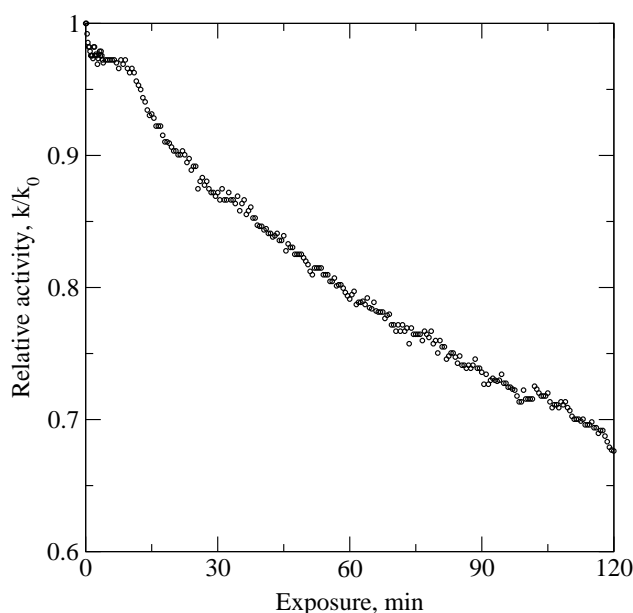


Figure 4.2: Relative activity of the P1000 element during the first 2 hours of exposure. $T = 350$ °C. Total flow: $40 \text{ Nm}^3/\text{h}$. Gas composition on dry basis: $\text{NO} = 496 \text{ ppmv}$, $\text{NH}_3 = 735 \text{ ppmv}$, $\text{O}_2 = 10\% \text{v}$, $\text{CO}_2 = 6\% \text{v}$, N_2 balance. $10\% \text{v H}_2\text{O}$.

Exposure to 1000 ppmv H_3PO_4

The addition of 1000 ppmv H_3PO_4 was carried out for 24 hours. During the first 2 hours of exposure, the activity of the catalyst element was continuously measured. The results of the measurement are shown in Figure 4.2. As it can be seen from this, the relative activity rapidly decreased as soon as the P-rich flue gas was flowing through the SCR reactor. After only 2 hours the element lost already 33% of its original activity. At the end of the acid addition, the monolith showed no activity at all. The results show that high level of P in the flue gas may be very harmful to the catalyst.

This test had a tremendous impact on the whole setup. A lot of acid was found deposited on the setup pipe walls and therefore an extensive cleaning was carried out before starting the test at lower acid concentrations.

Exposure to 10 ppmv H_3PO_4

The addition of 10 ppmv H_3PO_4 corresponds to about 32 mg/Nm^3 of P_4O_{10} in the flue gas, which is well below the expected P_4O_{10} concentration (3500 mg/Nm^3) assuming a 4% co-firing thermal share of sewage sludge with a P-content of 7% and a solid-gas conversion equal to 50% [24]. Figure 4.3 shows

Deactivation by Polyphosphoric Acids

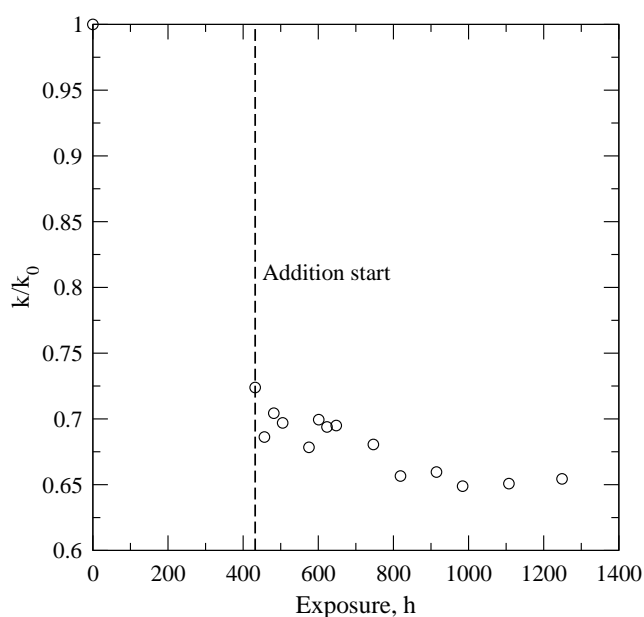


Figure 4.3: Relative activity of P10 at 350 °C as a function of exposure time. Total flow: 40 Nm³/h. Average gas composition: NO = 500 ppmv, NH₃ = 735 ppmv, O₂ = 10%v, CO₂ = 6%v, and 10%v H₂O in N₂.

the decrease in relative activity of the exposed catalyst element. A fresh monolith was charged and exposed to a clean flue gas for about 430 hours. This time was required in order to get a steady value for the NO conversion. However, the element had already lost about 28% of its original activity, probably due to deposit remaining in the setup even after the cleaning. The addition of 10 ppmv H₃PO₄ was then started. The exposure to the flue gas containing 10 ppmv H₃PO₄ further deactivated the catalyst. However this deactivation was found to be rather slow. Globally, the relative activity levelled off at around 65%, meaning that the element lost 7% of activity since the start of the exposure to 10 ppmv H₃PO₄. The results indicate that low levels of P in the flue gas may not be very harmful to the catalyst. During the activity measurements, a transient in the NO conversion was noted when NH₃ was added. This phenomenon was even more evident during the exposure to 100 ppmv H₃PO₄, and will be therefore presented in the next section.

Exposure to 100 ppmv H₃PO₄

The addition of 100 ppmv H₃PO₄ was carried out for only 38 hours. After this time, the element was exposed to a clean flue gas for additional 433 hours. Ta-

4.3 Results

Table 4.2: Results of the activity measurements performed with the P100 element.

| Operating time (h) | H ₃ PO ₄ addition (h) | X | | k/k ₀ | |
|--------------------|---|-------|--------------|------------------|--------------|
| | | Max | Steady state | Max | Steady state |
| 0 | 0 | 0.585 | 0.585 | 1 | 1 |
| 20 | 20 | 0.569 | 0.390 | 0.957 | 0.562 |
| 134 | 38 | 0.549 | 0.312 | 0.905 | 0.425 |
| 158 | 38 | 0.531 | 0.366 | 0.861 | 0.518 |
| 180 | 38 | - | 0.369 | - | 0.523 |
| 471 | 38 | 0.535 | 0.388 | 0.871 | 0.558 |

ble 4.2 reports the activity measurements carried out. During all the measurements, the NO conversion was found to first go through a maximum and then reach a steady level at lower values as a function of time. In Table 4.2, both the maximum and steady state are reported. Figure 4.4 shows the activity measurement carried out after 134 hours of operating time. Here, the NO concentration in the flue gas is plotted against the time of the activity measurement. For times less than 0, no ammonia is present in the flue gas and about 514 and 484 ppmv NO are present at the reactor inlet and outlet respectively. This difference was simply due to dilution of the flue gas with ambient air entering the setup from the pipe flanges. At time 0, around 600 ppmv of NH₃ are added to the flue gas and, as a result of the SCR reaction, the NO concentration starts decreasing until it reaches a concentration of 218 ppmv, corresponding to a NO conversion, X, of 55% and a relative activity, k/k_0 , of 0.91. However, right after reaching this value, the NO concentration in the flue gas starts increasing and reaches a steady state value at 333 ppmv after about 1 hour. In the meantime, the NO concentration at the inlet was measured twice in order to verify that the NO transient was not due to changes in the inlet values. In both cases, this was found equal to about 504 ppmv. This value was only 10 ppmv lower than the initial one and could have been caused by only few degrees change in the burner. At steady state, neglecting the small change in NO inlet concentration, the NO conversion, X, was equal to 0.31, corresponding to a relative activity, k/k_0 , equal to 42%. After having reached the steady state, the amount of NH₃ to the SCR reactor was doubled. Interestingly, the relative activity of the element increased to 50%. Since ammonia is introduced as a pure gas, it is excluded that the drop in NO concentration shown in Figure 4.4 is due to dilution of the flue gas. This

Deactivation by Polyphosphoric Acids

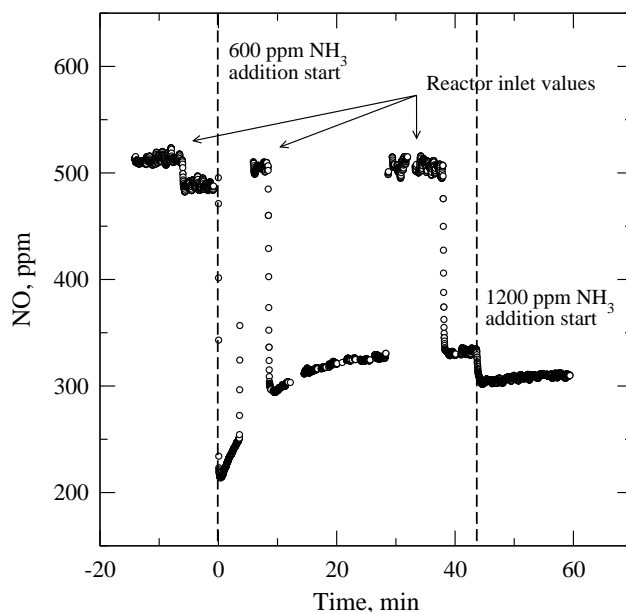


Figure 4.4: Activity measurement for P100 at 350 °C and 50 Nm³/h after 134 hours of operating time. Gas composition on dry basis: NO = 515 ppmv, NH₃ = 600 - 1200 ppmv, O₂ = 11%v, CO₂ = 5.6%v, N₂ balance. 10%v H₂O.

effect is more likely related to changes in the NH₃ adsorption properties of the P100 surface.

From the analysis of the activity measurements reported in Table 4.2, it is possible to see that at increasing time of H₃PO₄ exposure, both the maximum and the steady state value of NO conversion are decreasing. However, when the element was exposed to a H₃PO₄-free flue gas for some time, it slowly regained some activity. In fact, both the maximum and the steady state values of NO conversion increased, indicating that part of the deposited acid causing the deactivation is slowly leaving the catalyst.

As it will be discussed later, it is believed that this element is clearly showing effects of chemical deactivation due to polyphosphoric acids associated with the transient in NO conversion and due to the formation of V-P-O-NH₃ species, which are not or less active in the reduction of NO than the original sites. Finally, it is worth noting that the NO transient was fully reproducible provided that the NH₃ was shut off for about 1 hour. If the element was exposed to an NH₃-free flue gas for shorter times before NH₃ was reintroduced in the flue gas, the NO transient was still present, but the measured maximum NO conversion was lower. This shows that it takes quite some time for the surface complexes to be consumed.

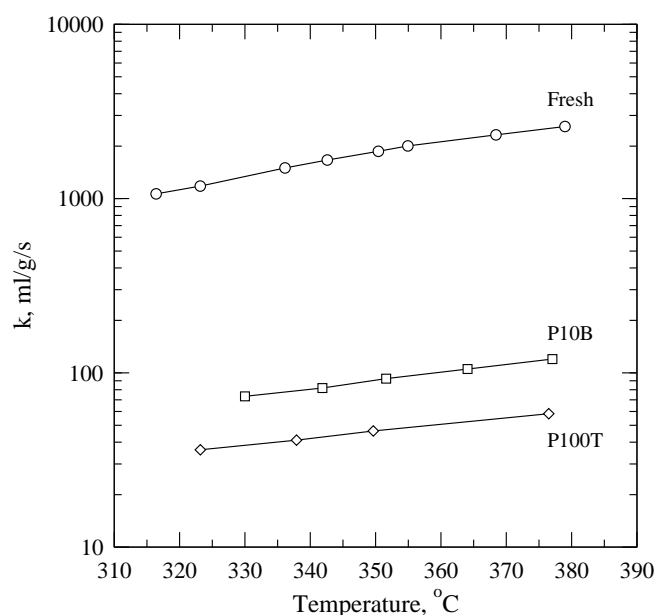


Figure 4.5: Activity test on powdered samples. Total flow: 2.8 NL/min. NO = 521 ppmv, NH₃ = 622 ppmv, O₂ = 5.2%v, H₂O = 1.47%v, N₂ balance. Catalyst mass W = 0.072 g.

4.3.3 Lab-scale Investigations

Activity Tests on Catalyst Deactivated at the Pilot-scale Setup

The activity tests on powdered spent and fresh monoliths are shown in Figure 4.5. The plot only reports the results in the temperature range 320-380 °C, where external and internal mass transfer have been estimated not to limit the observed reaction rate. Therefore, the values reported in the plot represent the pseudo-first order intrinsic reaction rate constants. Both the powdered P10B and P100B showed an extreme deactivation: at 350 °C they retained only 5 and 2.6% of their original activity respectively.

Activity Tests on Wet Impregnated Plates

The relative activities of the three different impregnated plates were found in the range 0.85-0.90. Even though the P/V ratios (i.e. 1.8, 2.9 and 4.7) for these plates were comparable to the ones measured on the monoliths P10 and P100 (Table 4.3), their deactivation was much lower, in agreement with other works [19, 130] where both model and commercial catalysts have been doped by a wet impregnation method. The results indicate that when P does not experience temperatures higher than the calcination temperature used during the

Deactivation by Polyphosphoric Acids

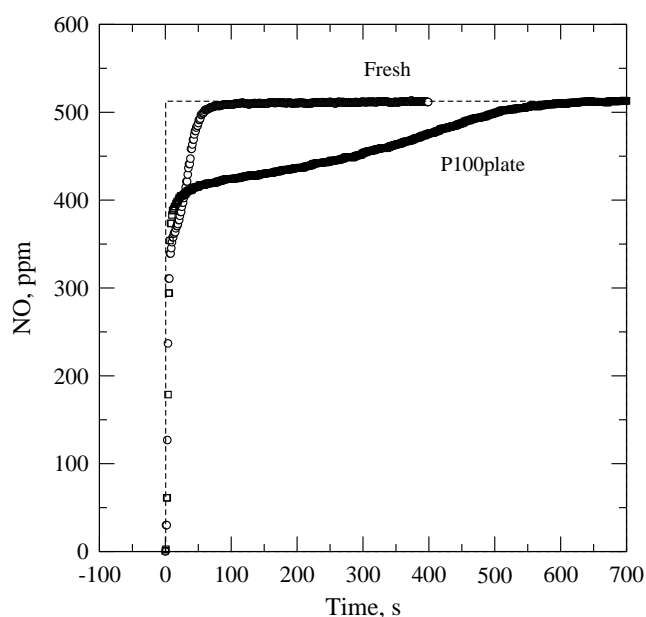


Figure 4.6: NH_3 chemisorption test on fresh and P100plate samples at 350 °C. Total flow: 2.75 NL/min. NO = 501 ppmv, NH_3 = 601 ppmv, O_2 = 5%v, N_2 balance. Catalyst mass W = 0.45 g.

doping process, it is not present on the catalyst surface as a polyphosphate. Its deactivating strength is therefore limited.

NH_3 Chemisorption Tests

Figure 4.6 shows the results of the NH_3 chemisorption test performed at 350 °C with a sample cut from P100plate and a fresh plate of the same type. As it can be seen from the plot, the amount of NH_3 adsorbed on the P-deactivated sample was much higher than on the fresh sample. In fact, the P-deactivated sample is able to adsorb about 5 times more NH_3 than the fresh catalyst. This is in agreement with the increased acidity of the catalyst surface due to deposition of the polyphosphoric acids. However, the activity measurements show that the NH_3 adsorbed on the polyphosphates is much less active (or even non active), which indicates that in the chemisorption test this NH_3 acts mainly as a reservoir.

4.3.4 In-situ EPR Spectroscopy

Figure 4.7 shows the in-situ EPR spectra of VO_2^+ present on the samples taken from exposure tests of the fresh, P10 and P100 elements measured at 350 °C.

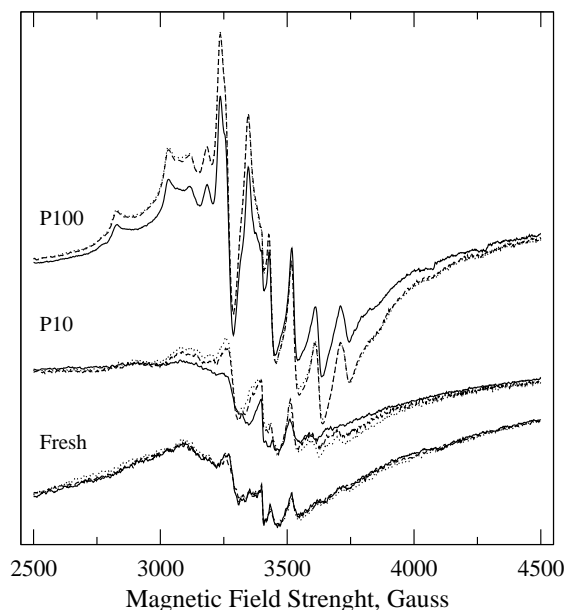


Figure 4.7: In situ EPR spectra acquired at 350 °C of catalyst samples taken from pilot plant tests fresh, P10 and P100, exposed to various simulated flue gas compositions. Gas composition: 1000 ppmv NO (—), 1000 ppmv NO + 1000 ppmv NH₃ (···), 1000 ppmv NH₃ (- - -) and 3.5%v O₂, 3%v H₂O in N₂.

Vanadium in oxidation states +5 and +3 are both invisible in EPR at these temperatures. The oxidizing mixture NO, O₂, H₂O in N₂ is leaving the active oxovanadium species present on the catalyst surface mainly in their oxidation state +5. Under these conditions, the spectrum of the fresh catalyst exhibits a broad band from polymeric surface vanadium species. Superimposed on this, a spectrum exhibiting poorly resolved hyperfine structure is observed. The latter appears to be from dimeric V(IV) species, with only the most significant peaks clearly visible. No significant presence of monomeric V(IV) species at this temperature under oxidizing conditions is observed. During exposure to gases containing NH₃, the redox chemistry of the fresh catalyst surface is not altered at all, as shown by the identical spectra, which were recorded during exposure to the different gas mixtures.

The P10 sample essentially shows the same spectrum as the fresh catalyst after equilibration in the oxidizing NO, O₂, H₂O, N₂ atmosphere. However, unlike the uncontaminated sample, the exposure to an NH₃-containing mixture caused an increase in VO₂⁺ (or (VO₂⁺)_n) content. In particular, the spectrum of the sample equilibrated in the SCR gas mixture exhibited the greatest difference from oxidizing conditions.

Deactivation by Polyphosphoric Acids

Contrarily to the previous results, P100 showed a significantly increased broad band of polymeric $(VO_2^+)_n$ species even during exposure to the oxidizing gas mixture. Superimposed on this signal, a new but recognizable contribution from monomeric VO_2^+ species is observed.

4.3.5 Catalyst Characterization

The V- and P-content on both the surface and bulk of the fresh and doped catalyst are shown in Table 4.3. The results of the mercury porosimetry are also reported in Table 4.3. In all the tested cases, the P-levels in the bulk were found slightly higher at the inlet compared to the outlet of the catalyst element, according to both the higher particle concentration and the higher mass transfer due to the developing flow and higher level of turbulence.

The P-content of the P100 element was found slightly higher than the one measured for the P10 (i.e. about 4%wt against 3%wt.). Considering the big difference in exposure time for the two experiments (819 hours vs. only 38 hours), and assuming a linear and constant deposition of P vs. time, it can be calculated that the overall accumulation rates have been 0.09%/day and 2.6%/day for P10 and P100 respectively. Assuming a first order process for the particle deposition (i.e. the fraction of deposited particles not depending on the total particle concentration number) and making the conservative assumption that the particle formed during the addition of 10 ppmv H_3PO_4 have the same diffusivity of the bigger particles formed in the presence of 100 ppmv H_3PO_4 , the deposition rate for the 100 ppmv H_3PO_4 test should have been only 10 times higher than the one with 10 ppmv H_3PO_4 . As calculated before, the P-accumulation on P100 was instead found 29 times the P-accumulation on P10. This fact, as it will be discussed later, is considered as an indication that the overall P-accumulation is the result of a balance between particle deposition and deposit hydrolysis followed by P-vaporization from the sample.

According to the results obtained by Hg-porosimetry shown in Figure 4.8, the deposition of polyphosphoric acid produced a shift toward smaller pore diameters in the pore size distribution for the different monoliths, pointing out the occurrence of physical deactivation due to pore blocking and condensation. In fact, it appears that the smaller pores at 40-50 nm of the bimodal mesoporous system are filled during P-addition, and a partial blocking of the interparticulate pore structure happened for P10 and P100. Furthermore, large crystalline formation has filled the void space in the macro-cracks above 100 μm . For the P10 a shift towards smaller macropores is observed due to this, whereas for the P100, a more dispersed destruction of the entire pore system is observed.

Table 4.3: Results of the bulk and surface chemical analysis, and of the Hg-porosimetry for the fresh and spent monoliths.

| | Monolith | | | | | | | Plate | |
|------------------------------------|----------|-------|-------|-------|-------|--------|--|-------|-----------|
| | Fresh | P10T | P10B | P100T | P100B | P1000B | | Fresh | P100plate |
| Bulk chemical analysis | | | | | | | | | |
| V, % wt/wt | 1.60 | 1.66 | 2.85 | 3.12 | 1.80 | 0.70 | | 1.00 | 0.87 |
| P, % wt/wt | 0.01 | 3.29 | 3.02 | 4.17 | 4.19 | 18.70 | | 0.10 | 6.07 |
| P/V, mol/mol | | 3.26 | 1.74 | 2.20 | 2.10 | 43.94 | | | 11.48 |
| Surface chemical analysis | | | | | | | | | |
| V, % wt/wt | 2.1 | 3.1 | 3.3 | 3.9 | 2.7 | 1.1 | | | |
| P, % wt/wt | 0.0 | 5.4 | 4.4 | 7.9 | 6.3 | 21.8 | | | |
| P/V, mol/mol | 0.0 | 2.8 | 2.2 | 3.3 | 3.9 | | | | |
| Hg porosimetry | | | | | | | | | |
| Total Intrusion Volume, ml/g | 0.71 | 0.57 | 0.58 | 0.42 | 0.53 | 0.06 | | 0.82 | 0.44 |
| Total Pore Area, m ² /g | 36.84 | 31.16 | 22.77 | 19.60 | 30.67 | 5.42 | | 73.05 | 17.19 |
| Catalyst Bulk Density, g/ml | 0.96 | 1.15 | 1.14 | 1.38 | 1.17 | 2.11 | | 0.89 | 1.20 |
| Porosity, % | 68.60 | 65.27 | 66.47 | 57.73 | 61.96 | 11.83 | | 73.02 | 53.02 |

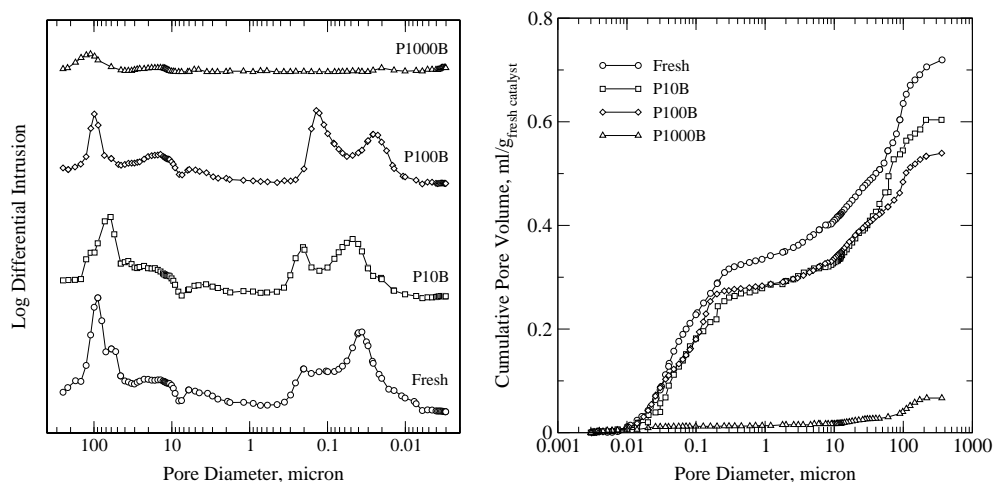


Figure 4.8: Pore size distribution and cumulative intrusion volume measured by Hg porosimetry with different monolithic samples.

Overall, the total intrusion volume (TIV) was found to decrease at increasing P-content (Figure 4.9).

The physical deactivation revealed by the Hg-porosimetry measurements has also been confirmed by SEM analysis of the exposed catalysts (Figure 4.10). From these it can be seen that the surface of P100 looks uniformly covered by a glassy layer, whereas the porous structure of titania is more defined on the surface of P10. Instead, on this latter, some needle-shaped crystals are present. The analysis of these crystals by EDX showed enrichment in both P and V.

Figure 4.11 shows the distribution of P into the walls of P10B and P100B as measured by EDX at the points showed in Figure 4.10. P was found to penetrate the whole catalyst wall in both cases. In particular, the P-content in P100B was found constant around a value of 6.1 wt%. Differently, the concentration profile measured on P10B showed a gradient in P-concentration in the proximity of the surface, normally indicating a diffusion limited process in P-accumulation. However, in some points in the middle of the wall, especially in the proximity of a macropore, the P-concentration was found again higher. Overall, the average P-content in P10B wall was equal to 3.1wt%.

4.4 Discussion

A higher degree of deactivation was obtained by exposure to polyphosphoric acid aerosols at the pilot plant compared to the one obtained by wet impregnation of H_3PO_4 aqueous solutions. This indicates the importance in understand-

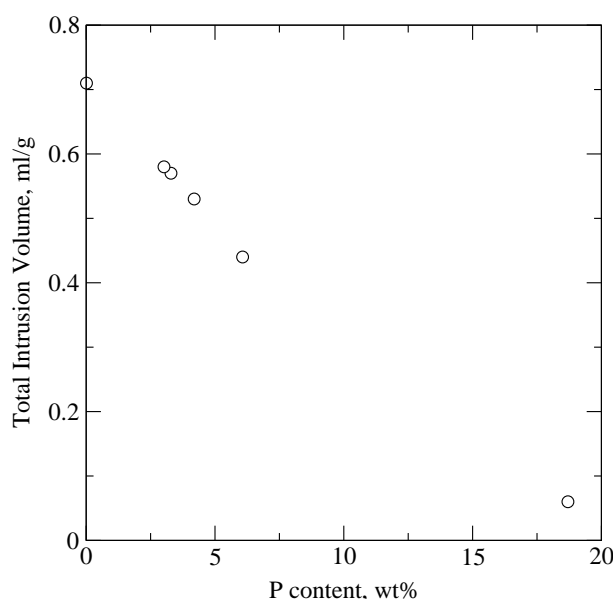


Figure 4.9: Total intrusion volume measured by Hg-porosimetry as a function of P-content measured in the bulk of the different spent monoliths.

ing the mechanism of formation of these particles and their influence on the activity of the vanadia-based catalysts. Apparently the real poisoning strength of P is not reproduced by the wet impregnation method normally used to dope both model and commercial catalysts.

4.4.1 Polyphosphoric Acids Formation and Deposition

The measured particles had very small mean diameters and a total particle number concentration in the order of $1 \cdot 10^{14} \text{ \#/m}^3$ indicating their formation by homogeneous nucleation from the gas-phase. Condensation on particles already present (i.e. the ones measured during the blank measurement) cannot be completely excluded. However, this cannot be regarded as the main mechanism of particle formation since already at the lower acid concentrations (i.e. 10 ppmv), the particle number concentration was more than 10 times higher than the one found during the blank test. Furthermore, due to the very small size of the particles measured during the blank test, their mass fraction in the deposits can be neglected. In order to explain the particle formation experienced, the formation of polyphosphoric acid will be presented [137]. The phosphoric acid molecule H_3PO_4 can be written as $0.5\text{P}_2\text{O}_5 \cdot 3\text{H}_2\text{O}$ and thus be considered as a 72.5% P_2O_5 solution having a boiling point temperature at 255 °C. When ex-

Deactivation by Polyphosphoric Acids

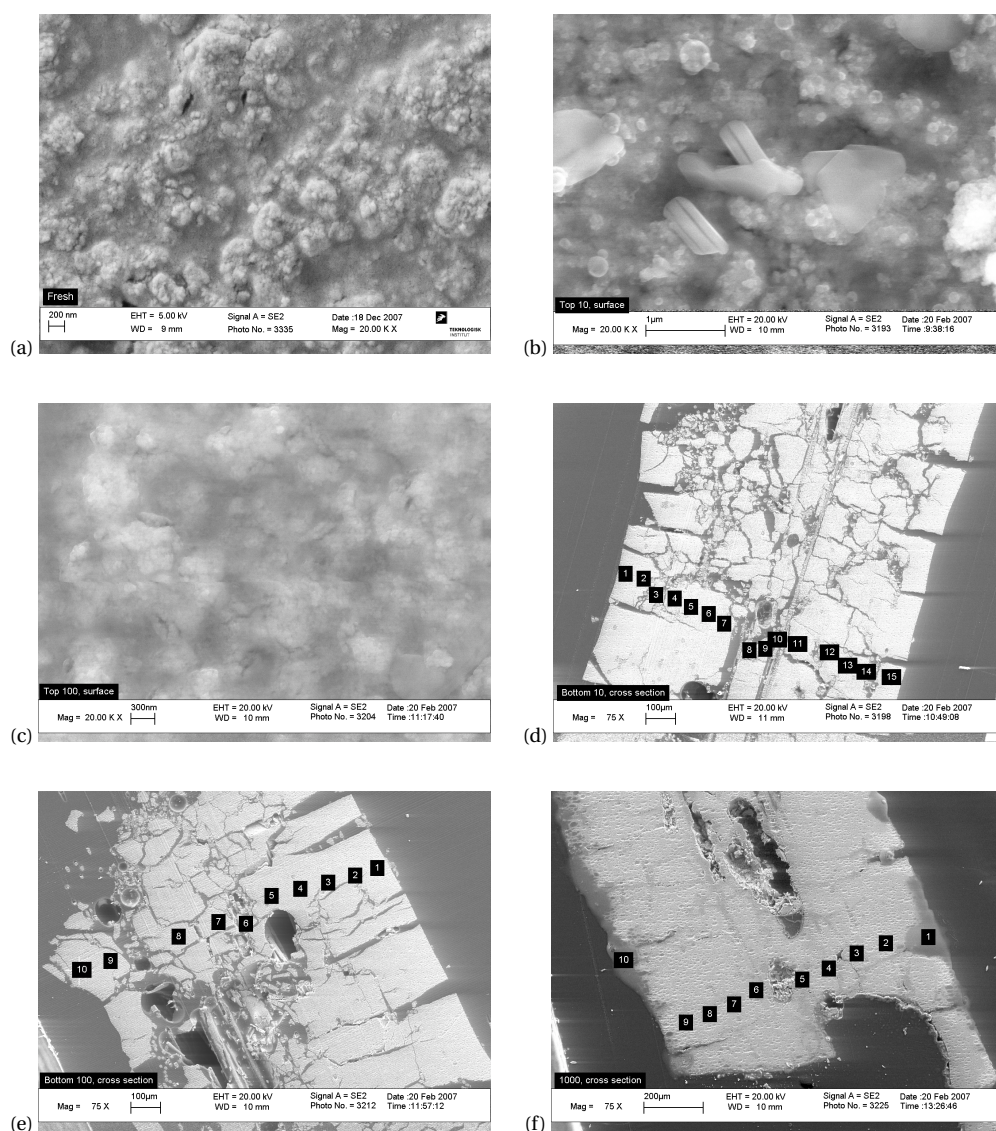


Figure 4.10: SEM analysis of fresh and spent catalyst: (a) fresh surface; (b) P10T surface; (c) P100T surface; (d) P10B wall cross section; (e) P100B wall cross section; (f) P1000B wall cross section.

posed to higher temperatures, water can evaporate until an azeotropic mixture consisting of 92.4% P_2O_5 is formed. This azeotropic mixture has a much higher boiling point at 864 °C. This water evaporation and the subsequent increase of P_2O_5 concentration is the result of condensation reactions taking place between the H_3PO_4 molecules in the gas phase producing chains of poly-, pyro-,

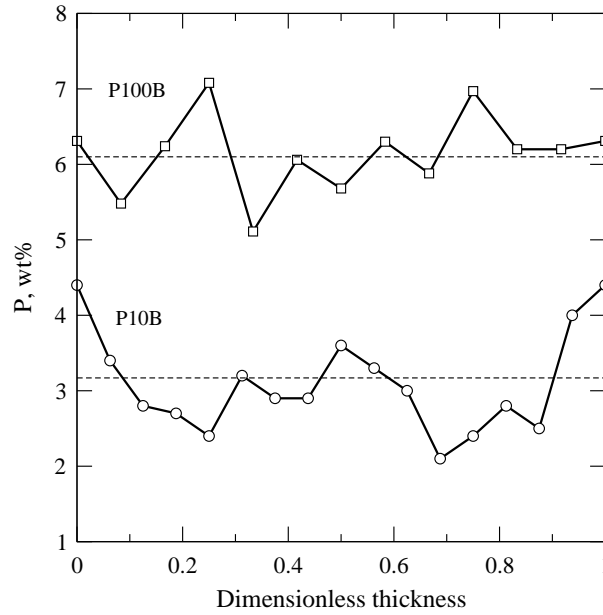
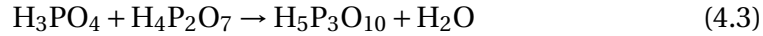


Figure 4.11: P-content measured by EDX across some catalyst walls showed in Figure 4.10.

tri-, and meta-phosphoric acid, as follows:



Due to their higher boiling point temperatures, the polyphosphoric acids may condense according to their vapour pressure when the gas cools down to the SCR reactor temperature.

Figure 4.12 shows a plot of the partial pressure of different polyphosphoric acids as a function of P_2O_5 content [25]. Since particles have been found at the reactor inlet even at the lowest acid concentration of 10 ppmv, and considering the high temperatures ($>850^\circ\text{C}$) experienced in the spraying section of the setup, it is assumed that the composition of the deposited particles is equal to the azeotropic mixture. In this way, around 50-81% of the injected P-mass, was collected at the inlet of the SCR reactor. In the absence of a direct measurement of the P-content in the gas phase, it is difficult to completely exclude and/or quantify the presence of gaseous P-species at the reactor inlet. Considering the equilibrium between the gas- and the liquid-phase as described by Figure 4.12, no condensation with 10 ppmv H_3PO_4 is expected since this would have needed a supersaturated atmosphere in order to take place. However, this was not the case. Moreover, the fraction of P calculated from the particle number concentration measured by the SMPS was found in the range 50-81%. If it

Deactivation by Polyphosphoric Acids

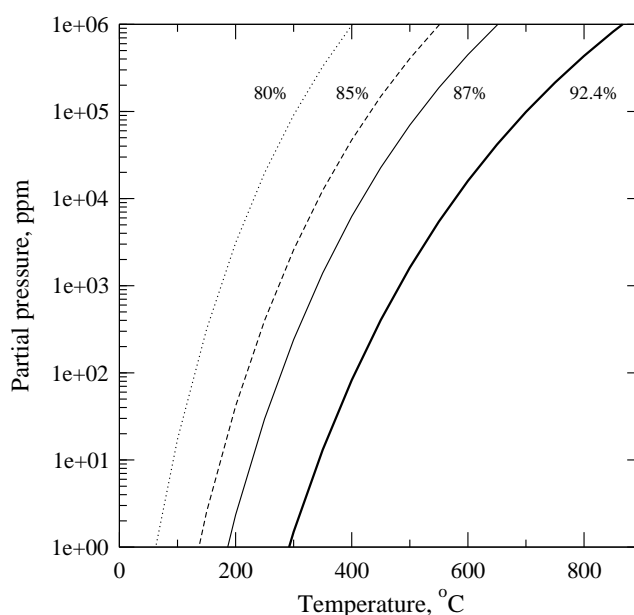


Figure 4.12: Vapour pressure of polyphosphoric acids as a function of temperature at different P_2O_5 weight content. The lines are calculated by extrapolating at lower pressures the equation fitting the experimental data found at higher partial pressures [25].

is assumed that at low acid concentrations the rest of the injected P is in the gas phase, this should have been close to zero at increasing acid concentrations. However, as shown in Table 1, the collected P-fraction at 400 ppmv H_3PO_4 was almost the same as the one at 10 ppmv.

It is therefore assumed that: (i) the injected H_3PO_4 reacted in the gas phase forming an azeotropic mixture of polyphosphoric acids; (ii) nucleation of polyphosphoric acid happened at temperatures $< 500\text{ }^{\circ}\text{C}$; (iii) almost all the acid was present in the liquid phase and iv) the differences found between the total P-mass injected and the P-mass measured at the SCR reactor inlet was mainly due to particle deposition on the pipe walls leading to the SCR reactor.

Due to their submicron dimensions, the particles are very mobile and can diffuse towards the catalyst walls, deposit on the catalyst surface and even penetrate into the pore structure by capillary forces. Once deposited, however, some of the deposited polyphosphoric acid may be hydrolysed in the presence of the flue gas moisture forming H_3PO_4 which evaporates from the catalyst. The resulting P-accumulation rate is therefore a balance between the particle deposition and evaporation of phosphoric acid. The hydrolysis of polyphosphoric acid in water is known to be a slow process and dependent on different factors, such temperature, chain length and pH [16]. Therefore the P-accumulation in

the catalyst walls will be mainly controlled by the particle deposition rate at high total particle numbers, while deposit evaporation at low deposition rates and low total particle number concentrations becomes relatively more important.

Taking into account all these facts, together with the different P-profiles measured by EDX on P10 and P100 (Figure 4.11), it is possible to conclude that evaporation of phosphorus compounds effectively limited the P-accumulation in the P10 case and that the profile measured in the wall is the net result of deposition and evaporation. The deposition rate during the 100 ppmv H_3PO_4 addition was much faster than evaporation leading to a fast accumulation of P in the wall.

4.4.2 Deactivation Mechanism

The high P-concentration found in the bulk of the exposed catalysts, the even P-distribution measured along the catalyst walls, the decrease in TIV measured by Hg-porosimetry at increasing P-concentrations and the SEM analysis of the different catalyst surfaces, all point to the occurrence of physical deactivation due to surface masking, pore blocking and condensation, in agreement with previous investigations about P-deactivation. However, the transient in NO conversion observed during every activity measurements clearly points out the occurrence of a simultaneous chemical deactivation mechanism.

The in situ EPR measurements carried out with the fresh catalyst samples have shown that the different gas compositions are not able to change the redox properties of the surface. In particular, during the SCR reaction, the V(V) species are continuously reduced during formation of the reaction intermediates and then re-oxidized by O_2 [10, 59]. The fact that this sample, when exposed to the complete SCR mixture, does not show an increased number of V(IV) species can be explained assuming that at 350 °C the rate of re-oxidation of the active V(IV) species in the redox cycle of the mechanism is high enough to keep the vanadium as V(V). In other words, this behaviour confirms the literature consensus [32] that at this temperature, the order of reaction of oxygen is zero.

Under oxidizing conditions, P10 practically exhibited the same spectrum as the fresh sample. However, when P10 was exposed to the complete SCR gas mixture, the number of $(\text{VO}_2^+)_n$ species slightly increased. This indicates that the SCR-reaction is occurring, but that the re-oxidation step is significantly slower than for the fresh catalyst. Contrarily to the previous results, $(\text{VO}_2^+)_n$ species are present as a stable phase on the catalyst surface of the P100 sample already under oxidizing conditions, suggesting that the VO_2^+ on P10 and P100 are exposed to two distinctly different phosphor species. Furthermore,

Deactivation by Polyphosphoric Acids

the concentration of V(IV) is increased when NH_3 is added to the mixture and the SCR reaction takes place. The most likely explanation for this is that the intermediate V(IV) species, which are consistently formed during the SCR reaction [10, 59], are being trapped by phosphate interactions, since it appears unlikely that phosphates alone should be able to reduce the V(V) compounds. This indicates that the deposited phosphates interact with parts of the active oxo-vanadium species, forming vanadyl-phosphate species which will not take part in the reaction anymore, thus inducing chemical deactivation by titration of the active species.

By considering this chemical deactivation, together with the effect of intra-particle diffusion limitations, the transient in NO conversion can be explained. As shown in Figure 4.4, at the very beginning of the NH_3 addition, the monolith P100 still presents a relative good activity. As reported in Table 4.2, when the NO conversion goes through the maximum, the relative activity is equal to 0.91. The lost 9% of activity is mainly due to physical deactivation only. However, the V(IV) species which were initially formed during the SCR reaction, are then stabilized in complexes which are formed with the deposited polyphosphoric acids. NH_3 can then be considered as the responsible for this titration of active sites since it initiates their reduction due to the SCR reaction. This titration is assumed to happen first at the outer catalyst wall, since it is where the SCR reaction is first happening. The intrinsic rate of reaction then starts decreasing at the outer wall due to the formation of NH_3 -P-V species and the reagents have to diffuse further into the catalyst walls in order to find active sites where to react. The steady-state is finally reached when equilibrium between the formed P-V-complexes, the active V-species and NH_3 is reached along the catalyst wall. In the case shown in Figure 4.4 and reported in Table 4.2, the additional 48% of activity which has been lost has to be considered due to chemical deactivation.

NH_3 is controlling the stability of the formed and inactive complexes. In fact, the NO transient during the activity measurement can only be reproduced if NH_3 has been taken off the flue gas for the time required by these complexes to completely disappear. Moreover, as shown in Figure 4.4, further NO conversion can be obtained by increasing the NH_3 partial pressure, but again this will first show a maximum and then a steady-state level at lower values. This additional activity at higher NH_3 partial pressures can be related to the NH_3 adsorption constant of the catalyst surface, which is changed due to the presence of the polyphosphoric acids. As shown in Figure 4.6, the amount of chemisorbed NH_3 is increased due to the polyphosphoric acid deposition. However this additional adsorbed NH_3 can be assumed either less active, in agreement with Kamata et al. [130], or inactive, simply constituting an NH_3 -storage on the surface. In the latter case, it has first to jump on an active site prior to react. Regarding the increased activity, which was measured when the NH_3 concentration was

increased, it can then be argued that, due to the increased number of sites for the NH_3 chemisorption, the coverage of NH_3 appearing in equation (1.4) has become less than 1 at the typical condition of our activity measurements. Finally, the reason for P100 for showing a more pronounced transient than P10 has to be found in: (i) a higher P-content in P100 and a consequent slower diffusivity due to the decreased pore sizes; (ii) a higher degree of polymerization of the deposits in P100 due to the faster deposition compared to the hydrolysis rate; (iii) a more uniform distribution of P in the P100 walls.

4.5 Conclusions

When exposed to the high temperatures of a combustion process, the H_3PO_4 molecules eventually released in the gas phase start condensation reactions forming polyphosphoric acids. These species are characterized by higher melting point temperatures than the typical SCR reaction temperatures, and are found in a liquid-phase at the SCR reactor inlet. Condensation of these species has been estimated to happen at temperatures lower than 500 °C. Therefore, there is a high probability that the formed aerosols will be characterized by high number concentrations of submicron liquid particles, due to the short time passing between the nucleation burst and the SCR reactor inlet. These particles therefore have high diffusivities and a high deposition rates on the monolith walls. Deactivation by polyphosphoric acid has been found to follow both a physical and a chemical deactivation. Surface masking, fouling, pore blocking and condensation are definitely important contributions to catalyst deactivation. Once deposited on the catalyst outer surface, they are very mobile and can even be sucked into the walls by capillary forces. The P-accumulation, and consequently the implied deactivation, is however limited by the rate of hydrolysis of the deposits themselves. The H_2O present in the flue gas, at the SCR temperatures can break down the polyphosphoric acid chains and free some H_3PO_4 back in the gas-phase.

The physical deactivation, however is not the only effect responsible for the overall measured deactivation levels. Supported by the NO reduction transient measured during activity tests with mass transfer-limited-catalysts, and in-situ EPR analysis of the spent catalysts, it has been found that the deposited polyphosphoric acids tend to both increase and stabilize the number of non active V(IV) species, which are formed as intermediate during the SCR reaction. Moreover, part of the NH_3 present in the gas phase preferentially adsorbs on the polyphosphoric acids and is only less active in the reduction of NO.

The results obtained in this work constitute the first reference about deactivation of vanadia-based catalysts explicitly due to polyphosphoric acid alone.

Deactivation by Polyphosphoric Acids

It is believed they show the real deactivating potential of P, when this is present in the flue gas during post-treatment of combustion processes, which has been found much more poisonous than indicated by wet impregnated tests.

Chapter 5

Deactivation by Potassium Phosphates

The work reported in this chapter has been published in *Applied Catalysis B: Environmental* [138]. The paper is included in Appendix B.

5.1 Introduction

Deactivation of vanadia-based catalysts can be due to poisoning, fouling, surface masking, pore blocking and sintering according to the particular application. In most of these cases, however, the fly ash plays an important role since it may act both as physical deactivating agent, and as a carrier for different chemical deactivating species. For instance K, which according to different studies is a very strong poison for the vanadia-based SCR catalysts [19, 20, 102, 105, 106, 109, 110, 112, 113, 119], is present as solid particles at the SCR reactor inlet. The observed rate of deactivation is thereby directly related to the fluid dynamics controlling the rate of particle deposition. As well important is the rate of particle/poison penetration into the catalyst walls, which is more likely related to the way the K-fraction is bound to the particle itself. For instance, up to 1%/day deactivation has been measured both at a biomass-fired combined heat and power plant [110] and in a pilot plant [119] where K was present as aerosols of pure KCl and K₂SO₄. Contrary, accordingly to coal firing experience, when K is mainly bound to non-soluble silica-aluminates, the deactivation proceeds at much slower rates. In order to explain the influence of the particle composition on the different deactivation rates experienced, Zheng et al. [110] suggested that this is related to the K-mobility at the SCR temperatures. The reason for the good mobility of KCl and K₂SO₄ was found in the Hüttig and Tamman temperatures of these compounds. These two temperatures are normally used

to estimate the temperatures at which sintering starts [103] and are calculated with the following empirical expressions:

$$T_{\text{Hüttig}} = 0.3 T_{\text{melting}} \quad (5.1)$$

$$T_{\text{Tamman}} = 0.5 T_{\text{melting}} \quad (5.2)$$

When the Hüttig temperature is reached, atoms at vacancies start being mobile. When the Tamman temperature is eventually reached, the atoms in the bulk start showing mobility. According to their Hüttig and Tamman temperatures, the atoms forming the KCl and K₂SO₄ deposits may then be expected to be mobile at the SCR temperatures, and therefore react with the catalyst surface and further diffuse on it.

The discussion above indicates that binding K to ashes with higher melting temperatures by the addition process may reduce the rate of deactivation by decreasing the poison penetration in the catalyst walls. In order to verify this possibility, full-length commercial SCR monoliths have been exposed to a flue gas doped with K₃PO₄ in a pilot-scale SCR setup for up to 700 hours.

A parallel investigation on poisoning by K₃PO₄ has been carried out in the laboratory, where catalyst plates have been doped with different amounts of K and P by wet impregnation with K₃PO₄ aqueous solutions.

Apart from estimating the potential effect of the addition process on the SCR catalysts, the tests shown in this chapter offer the possibility: (i) to provide further input to the mechanism of K-deactivation by aerosols; (ii) to determine the possible formation of polyphosphoric acids and thereby provide additional information about the P-release during combustion.

5.2 Experimental

The addition of K₃PO₄ to the flue gas was performed by spraying water solutions through a two-fluid nozzle. The solutions were prepared by dissolving K₃PO₄ (reagent grade ≥98%, Sigma®) in distilled water. Two catalyst elements have been exposed to 100 and 200 mg/Nm³ K₃PO₄. In this work they will be identified by the labels “KP100” and “KP200” respectively. The letters “T” and “B” added at the end of the labels will indicate a sample cut respectively from the top (first 10 cm) and the bottom (last 10 cm) of the element. In all tests, the salt concentration in the solutions was fixed at 21 g/litre and the solution feed rate was then varied in order to obtain the desired concentration in the flue gas (i.e. 0.25 and 0.5 litre/h to get 100 and 200 mg/Nm³ respectively).

Plate-shaped catalysts were doped with K₃PO₄ at five different levels by a wet impregnation method at room temperature for 16 h under a vacuum of 0.8

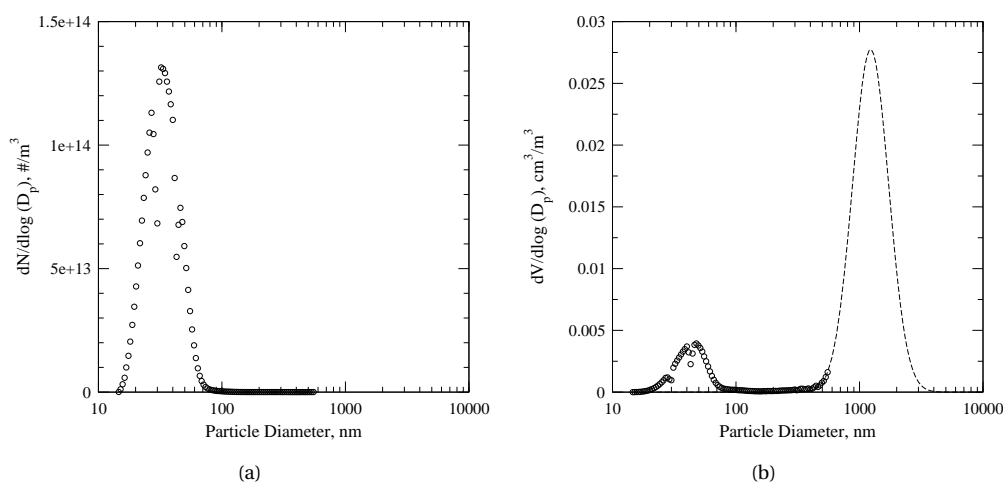


Figure 5.1: Number-based (a) and volume-based (b) particle size distributions measured by SMPS at the reactor inlet during addition of $100 \text{ mg/Nm}^3 \text{ K}_3\text{PO}_4$. $T = 350 \text{ }^\circ\text{C}$.

bar absolute pressure to allow the solution to evenly penetrate into the catalyst pores. The catalyst plates had a dimension of $1 \text{ mm} \times 50 \text{ mm} \times 150 \text{ mm}$. They were dried at $120 \text{ }^\circ\text{C}$ for 1 h and then calcined at $400 \text{ }^\circ\text{C}$ for 4 h under a stream of 1 L/min of N_2 . The different K/V and P/V ratios obtained were measured by inductively coupled plasma optical emission spectroscopy (ICP-OES). In order to study the effect of the wet impregnation method on the fresh activity, a catalyst sample was simply wet impregnated with water.

The doped catalyst plates have been washed with a 0.5 M sulphuric acid aqueous solution in order to see whether regeneration was possible. Each sample was washed in 100 ml of the acid solution at 0.8 bar and $25 \text{ }^\circ\text{C}$ for 30 min. After washing, the samples were dried at $150 \text{ }^\circ\text{C}$ for 15 h. The same regeneration method was also applied to a fresh sample in order to see the effects of the method on the initial activity.

5.3 Results

5.3.1 Aerosol Measurements at the Pilot-scale Setup

SMPS Measurements

Figure 5.1 shows the number-based and volume-based particle size distributions measured during the addition of $100 \text{ mg/Nm}^3 \text{ K}_3\text{PO}_4$. According to the number-based particle distribution, the aerosols were characterized by a peak at around 30 nm . However, when the volume-based distribution is plotted in-

Deactivation by Potassium Phosphates

Table 5.1: K- and P-content measured on the impactor stages by EDX. The particles were collected during addition of 100 mg/Nm³ K₃PO₄.

| Stage (#) | Particle Diameter (nm) | K (mol%) | P (mol%) | K/P (mol/mol) |
|-----------|------------------------|----------|----------|---------------|
| 4 | 1488 | 47.31 | 13.80 | 3.48 |
| 5 | 754 | 51.22 | 15.39 | 3.33 |
| 6 | 382 | 48.66 | 16.65 | 2.92 |
| 7 | 193 | 48.49 | 14.82 | 3.27 |
| 8 | 98 | 47.49 | 14.80 | 3.21 |
| 9 | 49 | 44.08 | 14.71 | 3.00 |

stead, a second peak at higher diameter appears. In particular, it can be seen in Figure 5.1b that this second peak almost entirely extends outside the upper detection limit of the SMPS used. By assuming a density for these particles equal to the density of K₃PO₄ (i.e. 2.564 g/cm³), the total mass measured by the SMPS would be equal to around 8% of the injected one. This low value indicates that a great part of the injected mass is present at the larger diameters not detectable by the SMPS. By fitting the data obtained with a lognormal distribution, the curve showed in Figure 5.1b can be obtained. The fitting has been made by minimization of:

$$\sum_{d_p} [\Psi_{V,SMPS}(d_p) - \Psi_{V,logn}(d_p)]^2 \quad 300 \text{ nm} \leq d_p \leq 500 \text{ nm} \quad (5.3)$$

where $\Psi_{V,SMPS}(d_p)$ is the volume distribution $dV/d(\log d_p)$ calculated from the SMPS measurement, $\Psi_{V,logn}(d_p)$ is the fitted distribution. The mean diameter of the lognormal distribution is equal to 1.25 μm . Overall, the total mass calculated is equal to around 40% of the injected K₃PO₄. Both the mean diameter and the total mass at the reactor inlet would then be comparable to previous tests carried out at this setup [119]. As will be discussed later, the presence of this dual mode particle distribution is related to the presence of mainly two different species, whose formation has followed different mechanisms.

Cascade Low Pressure Impactor Measurements

Tests with the LPI have been performed during both the KP100 and KP200 experiments. In all cases, the particles collected at the different stages were very liquescent and were therefore melting as soon as they were exposed to ambient air. The determination of the weight of the different foils was therefore

problematic. Not only the foils were increasing their weight due to water adsorption. Some of them were at some point even losing weight during their mass determination. This fact indicates that during exposure to ambient air at room temperature some gaseous species were released by the deposit. Due to these problems, the only partly useful indications obtained from the tests were those provided by the EDX analysis of the different foils reported in Table 5.1. Here, values of the K:P molar ratio in the range 3-3.5 were measured, which are slightly higher than the expected value of 3. Interestingly, the K:P values were increasing with the collected particle size (apart from the value measured on stage #6). These values may differ from the expected value of 3 simply because experimental uncertainty of the EDX measurements, but, recalling the particle size distribution measured by the SMPS, they may also indicate that part of the P was not collected on the lower impactor stages, probably because the remaining fraction was present in even smaller particles or in the gas phase.

5.3.2 Catalyst Characterization

Bulk and Surface Chemical Analysis

Table 5.2 reports the results of both the bulk and surface chemical analysis for the elements KP100 and KP200. The K-content in the bulk was varying in the range 0.8-2.5 wt%, whereas the P-content was varying in the range 0.4-0.8 wt%. Apart from the K-content in KP200, both the levels of K and P found in the bulk of the two elements were decreasing from the top to the bottom in agreement with both the higher particle concentration and the higher mass transfer due to the developing flow and higher level of turbulence at the top. About double levels of K were found on KP100 compared to KP200, whereas the levels of P were roughly the same. The calculated bulk K:P molar ratios were in the range 0.85-2.52 and therefore less than 3, which is the value introduced into the system by the K_3PO_4 molecule, indicating a different path for the accumulation of K and P in the catalyst walls.

Regarding the external surface composition measured by SEM-EDX shown in Table 5.2, very high concentrations of P have been found. In particular, the element KP200 reported P-concentrations up to 12.6 %wt. In the case of KP100, the P-content was ranging between 1.0 and 2.8 %wt. The cross sections of the samples KP100B and KP200T have also been analysed by SEM-EDX in order to measure the distributions of K and P along the catalyst walls. The results of the EDX measurements are shown in Figure 5.2a and Figure 5.2c. As shown in the plots, both the K- and P-content decrease as a function of catalyst wall depth, indicating a diffusion limited process. Only in the case of KP100B, the K-content is almost constant around 0.7 %wt throughout the analysed wall thick-

Deactivation by Potassium Phosphates

ness. However, the major difference between the K- and P-distributions is that, in the case of K, the concentration in the walls always appears to level off at a finite K-level (i.e. 0.7 %wt in the cases shown in Figure 5.2a), whereas the P-concentration decreases to zero. From these profiles, it appears that K tends to penetrate and remain in the catalyst wall, whereas P either is characterized by a slower mobility compared to K, or its penetration is counterbalanced by simultaneous evaporation of P as it was shown in the previous chapter. As expected, in the presence of higher total K_3PO_4 concentrations in the flue gas, both K and P tend to accumulate on the outer catalyst surface.

Finally, Figure 5.2b and Figure 5.2d shows the calculated values for the K:V and P:V molar ratios, which can be used to estimate the local activities of the catalyst wall. According to values found in the literature [19, 102], for K:V molar ratios equal to 0.2, up to 70% deactivation in the absence of mass transfer limitations can be expected.

Hg-porosimetry

The pore size distribution of the fresh and spent catalysts has been measured in order to clarify the presence of physical deactivation by pore blocking due to deposition of K-P particles. Figure 5.3 reports the results of this investigation. The PSD of the fresh catalyst is clearly a dual-mode distribution, with the first peak found in the region 0.6-300 μm at 90 μm , and the second one in the region 0.003-0.6 μm at 0.03 μm . This dual mode distribution is basically conserved in all spent catalyst samples. No major differences indicating pore blocking are found between the fresh and spent samples apart from the region 0.6-8 μm . Here, the spent samples consistently show almost no pores, whereas the fresh one has a considerable amount of them. In particular, the porosity for the fresh sample in this diameter range has been calculated to be equal to 6.93%. This value dropped to 1.35 and 0.89% for KP100T and KP100B respectively, and 1.32 and 1.19% for KP200T and KP200B respectively. However, no major difference in the total intrusion volume of the spent catalysts compared to the fresh sample was found (Table 5.2). This fact may indicate that the sample outer wall layer, which is the first that gets in contact with Hg during the measurement, had no pores in that range due to deposit build-up and/or pore blocking, but kept the original structure of the inner wall.

5.3 Results

Table 5.2: Bulk, surface and Hg-porosimetry analysis for the fresh and spent monoliths.

| | Sample | | | | |
|--------------------------------------|--------|--------|--------|--------|--------|
| | Fresh | KP100T | KP100B | KP200T | KP200B |
| Total exposure time ^a (h) | | 720 | 720 | 189 | 189 |
| Bulk chemical analysis | | | | | |
| V (% wt/wt) | 1.60 | 2.46 | 1.61 | 1.76 | 2.70 |
| K (% wt/wt) | 0.0 | 2.45 | 1.44 | 0.80 | 0.90 |
| P (% wt/wt) | 0.01 | 0.77 | 0.46 | 0.75 | 0.40 |
| K/P (mol/mol) | | 2.52 | 2.46 | 0.85 | 1.79 |
| K/V (mol/mol) | | 1.30 | 1.17 | 0.59 | 0.44 |
| P/V (mol/mol) | | 0.31 | 0.47 | 0.70 | 0.24 |
| Surface chemical analysis | | | | | |
| V (% wt/wt) | 2.1 | 2.1 | 3.5 | 2.4 | 2.2 |
| K, (% wt/wt) | 0.0 | 1.7 | 0.8 | 6.2 | 2.1 |
| P (% wt/wt) | 0.0 | 2.8 | 1.0 | 12.6 | 6.2 |
| K/P (mol/mol) | | 0.5 | 0.7 | 0.4 | 0.3 |
| K/V (mol/mol) | 0.0 | 1.1 | 0.3 | 2.7 | 1.2 |
| P/V (mol/mol) | 0.0 | 2.2 | 0.5 | 7.1 | 4.5 |
| Hg porosimetry | | | | | |
| Total Intrusion Volume (ml/g) | 0.71 | 0.71 | 0.67 | 0.67 | 0.64 |
| Total Pore Area (m ² /g) | 36.84 | 37.04 | 37.65 | 48.66 | 39.46 |
| Catalyst Bulk Density (g/ml) | 0.96 | 0.94 | 1.01 | 1.03 | 1.11 |
| Porosity (%) | 68.60 | 66.92 | 67.66 | 69.64 | 70.78 |

^aThis exposure time does not include the lance blocking.

5.3.3 Deactivation at the Pilot-scale Setup

Activity Measurements

The results of the activity measurements carried out during exposure to 100 and 200 mg/Nm³ K₃PO₄ are shown in Figure 5.4. Overall the measured deactivation rate was increasing according to the K₃PO₄ concentrations in the flue gas. In both cases, the deactivation was very fast at the beginning of the exposure: The

Deactivation by Potassium Phosphates

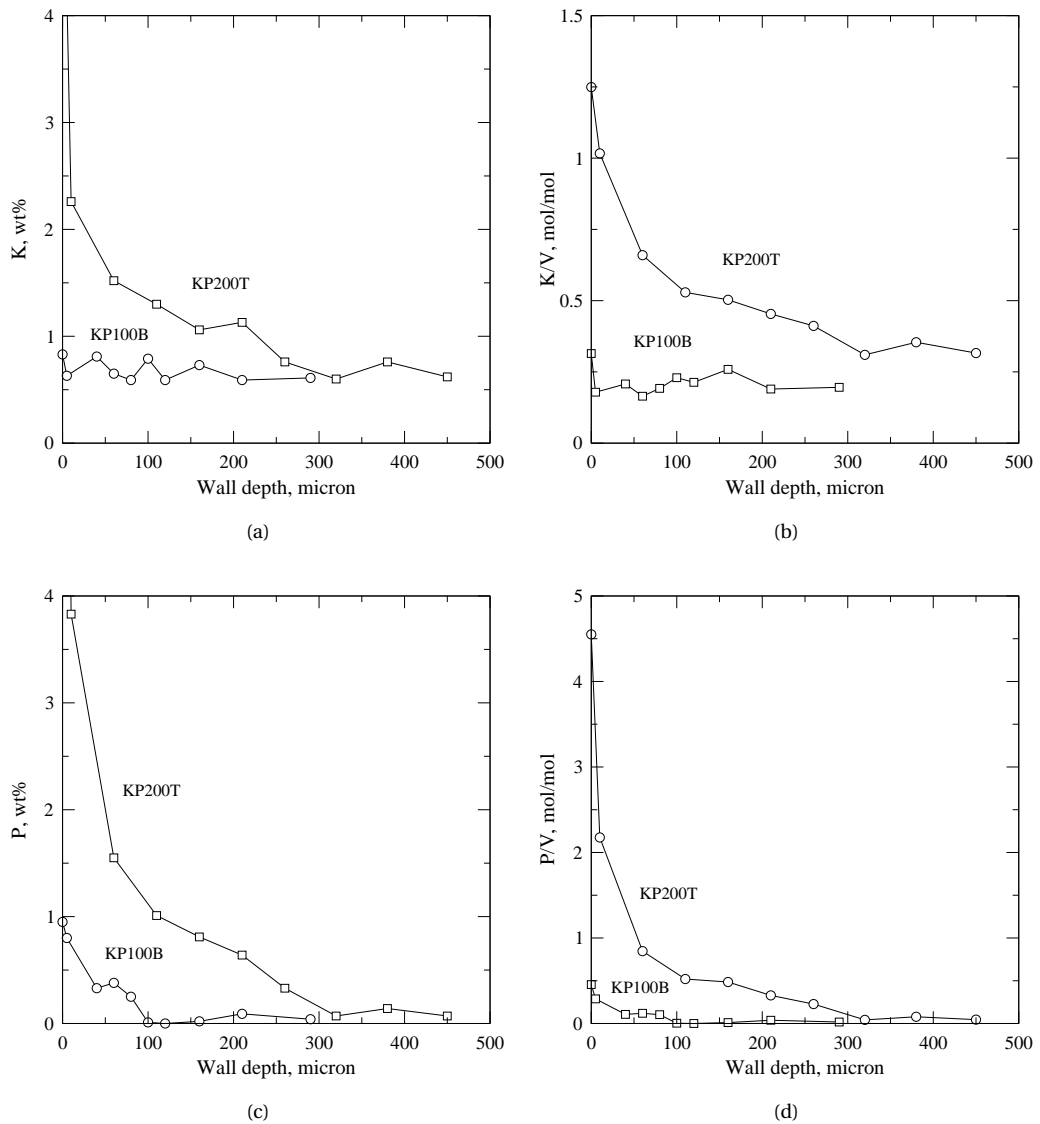


Figure 5.2: K- and P-content and K:V and P:V molar ratios along the KP100B and KP200T walls as measured by SEM-EDX.

two elements lost respectively 26 and 31% of their original activity during the first 72 h. After this initial period, the deactivation proceeded at slower but still appreciable rates.

The addition of 100 mg/Nm^3 was carried out for 720 h. After this period of time, the element was exposed to clean flue gas for additional 288 h, before it was taken out and characterized. The relative activity at the end of the addition time was 62%, corresponding to an overall deactivation rate of about 1.3%/day.

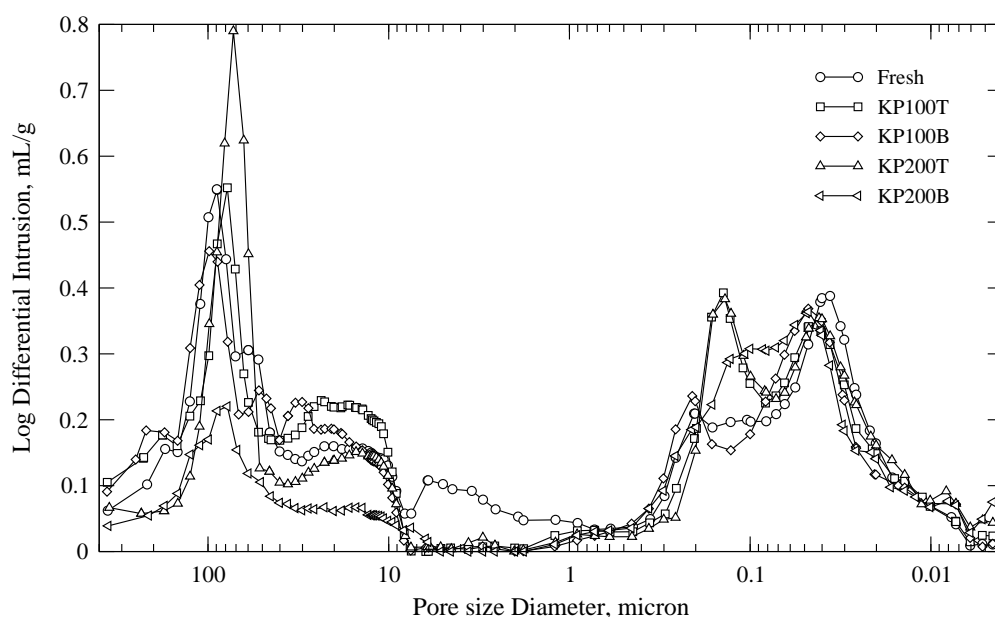


Figure 5.3: Pore size distribution for fresh and spent samples measured by Hg-porosimetry.

During the subsequent exposure to the clean flue gas, the element regained 9% of relative activity. In particular, 7% was regained after the first 24 h after the addition was shut off. During these 24 hours, the pressure drop over the monolith decreased by 11% indicating some cleaning of the channels due to soot blowing, which was continued after the addition stopped.

The addition of 200 mg/Nm³ was carried out for only 280 h and was more problematic than the previous test. Due to the higher K₃PO₄ load, the two-fluid nozzle used for atomizing the water solution tended to clog due to salt deposition. In particular, the compressed air line right at the meeting point with the liquid solution was the one that had the higher tendency in getting clogged. When this happened, the solution was not correctly atomized and was eventually introduced as a liquid jet. The jet was then simply hitting the hot pipe walls right after the lance and forming massive deposits of salt. Clogging of the nozzle mainly happened two times: After 89 and 284 h from the addition start. In both cases, the activity measurement performed after the clogging showed an increased relative activity of the element compared to the previous test. These facts are in agreement with the result obtained with the element KP100, when this latter was exposed to a clean flue gas as discussed before. Overall, at the end of the experiment, the element KP200 had lost 22% of its original activity. However, the minimum relative activity was measured after 284 h during the last activity measurement before the nozzle clogged for the second time.

Deactivation by Potassium Phosphates

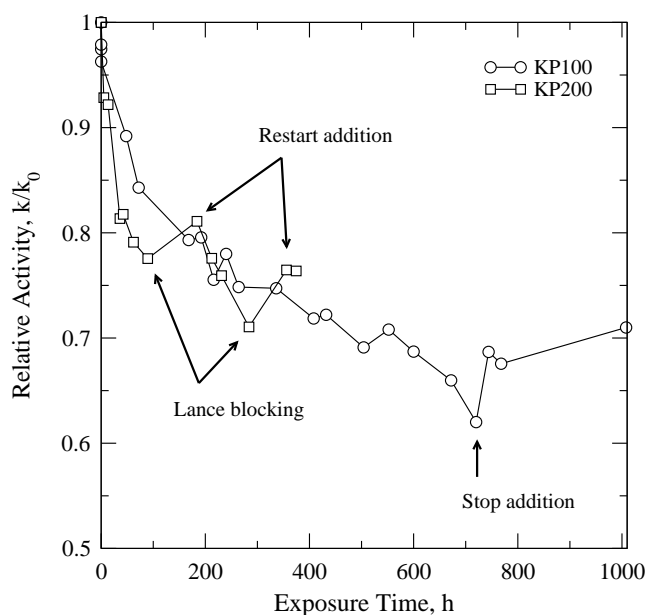


Figure 5.4: Relative activity as a function of exposure time. Total flow: 40 Nm³/h. Gas composition: NO = 500 ppmv, NH₃ = 600 ppmv, O₂ = 10%v, CO₂ = 6%v, and 10%v H₂O in N₂.

Here the relative activity was equal to 73%, corresponding to a deactivation rate equal to about 2.3 %/day.

NH₃ Chemisorption Tests

Figure 5.5 shows the results of NH₃ chemisorption tests made with the element KP100 and KP200 during the addition of K₃PO₄. Since the amount of reduced NO is assumed equal to the amount of NH₃ chemisorbed on the catalyst surface, a longer time for the NO measured at the outlet to equalize to the value measured at the inlet indicates that more NH₃ is chemisorbed on the catalyst. From Figure 5.5 it can be seen that the fresh element was able to chemisorb a higher amount of NH₃, and that this was decreasing as a function of the exposure to K₃PO₄. In particular, after 408 h of exposure the amount of chemisorbed NH₃ on KP100 was about 54% of the fresh one. After 720 h, this further dropped to 47%. These results indicate that the deactivation was proceeding by deactivation of the sites for the NH₃ chemisorption.

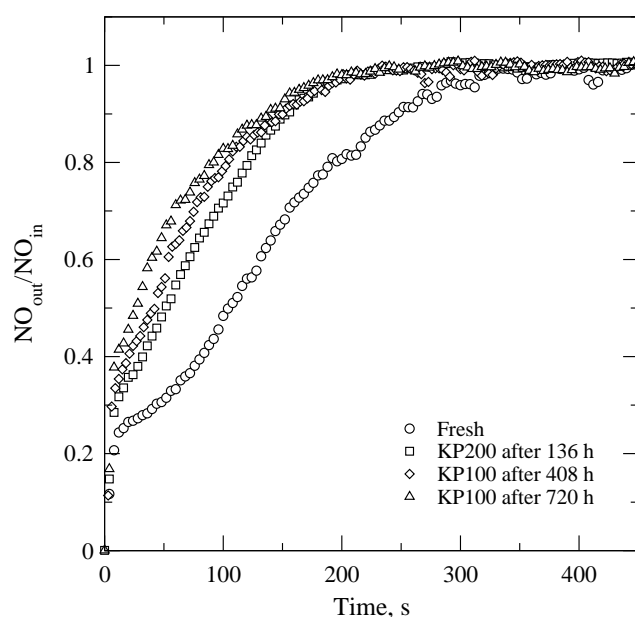


Figure 5.5: NH_3 chemisorption test for the element exposed to $100 \text{ mg/Nm}^3 \text{ K}_3\text{PO}_4$ at different times during the exposure.

5.3.4 Deactivation at the Lab-scale Setup

Activity Tests with Powder

Figure 5.6 shows the activity measurements made with powdered samples cut from the top and the bottom of the element KP100, together with a measurement made on a fresh catalyst. The plot only reports the results in the temperature range 250-400 °C, where external and internal mass transfer have been estimated not to limit the observed reaction rate for the doped samples. Due to its very high activity, the fresh sample is subjected to some mass transfer limitations (i.e. $\approx 10\%$ at 350 °C). As expected from the K- and P-content of the KP100 monolith, the top of the catalyst is more deactivated than the bottom. At 350 °C the relative activities for the top and the bottom of the element are equal to 9.1% and 30.0% respectively.

Activity, NH_3 Chemisorption and Regeneration Test with Plates

As stated above, fresh catalyst plates have been wet impregnated with 5 different K_3PO_4 aqueous solutions. Moreover, one plate was also wet impregnated with distilled water. All the results have then been compared to the ones obtained with this latter catalyst in order not to include in the deactivation the

Deactivation by Potassium Phosphates

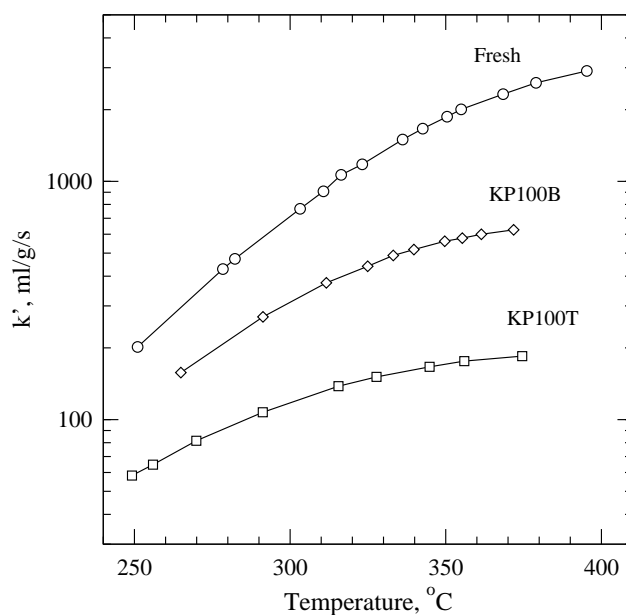


Figure 5.6: Activity measurements on powder samples. Total flow: 2.8 NL/min. NO = 521 ppmv, NH₃ = 622 ppmv, O₂ = 5.2%v, H₂O = 1.47%v, N₂ balance. Catalyst mass W = 0.072 g.

effect of the impregnation itself. The K/V and K/P molar ratios were then determined by ICP-OES. The results are shown in Figure 5.7. As it can be seen, P accumulated in the catalyst walls more than the expected if compared with the K found in the different samples, especially in the K/V molar ratio range 0.4-1.2.

Figure 5.8 shows the decrease of relative activity measured at different temperatures in the range 250-400 °C with the plates doped in the laboratory at increasing K/V molar ratios. No clear correlation between the loss in activity and the P-levels measured (i.e. P/V molar ratios varying in the range 0.6-0.9) for the doped samples was found, indicating that K was the main responsible for the deactivation. As it can be seen, at 350°C, the catalyst having a K/V molar ratio equal to about 2.5 showed no activity. When the K/V ratio was instead equal to 1, the relative activity was equal to about 35% of the initial activity. Comparing Figure 5.8 with Figure 2.22, it can be seen that in the case of plates, the decrease in relative activity is not as steep as the one measured with powders. This fact is due to the masking effect played by internal diffusion limitations during testing with plates. Further confirming this fact is the lower deactivation measured at increasing temperatures, as shown in Figure 5.8.

Ammonia chemisorption tests were made with the doped samples at 250 °C. The relative amount of chemisorbed NH₃ was then calculated as the ratio between these measurements and the one made with a fresh catalyst wet impreg-

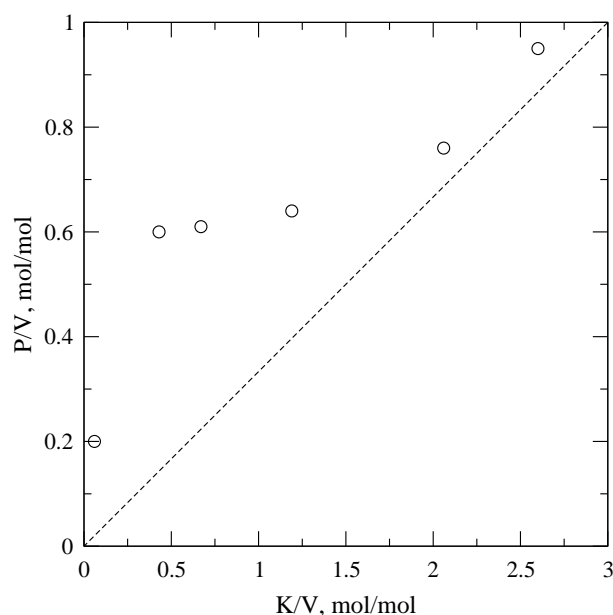


Figure 5.7: K/V and P/V molar ratios measured on catalyst plates doped by wet impregnation with K_3PO_4 aqueous solutions.

nated with water, and plotted in Figure 5.9. As it can be seen, the chemisorbed NH_3 was found to decrease at increasing K/V molar ratios. However, by comparing this decrease with the loss in activity at the same temperature shown in Figure 5.8, it can be seen that the relative chemisorbed NH_3 has never been found lower than the relative activity, as it would have been expected. Considering the higher amounts of P deposited on the catalysts, it can then be concluded that part of the chemisorbed NH_3 was sitting on non/less active Brønsted P-OH acid sites. In particular, it is worth noting that when the catalyst is completely dead at K/V molar ratio equal to 2, about 27% of the initial chemisorbed NH_3 can still be found on the catalyst surface.

Comparing these results with the chemisorption tests made with the monoliths, it can be argued that in that case most of P found in the catalyst walls was “deactivated” by K itself and therefore was not improving the chemisorption ability of the catalyst surface. The different behaviour seen in the laboratory is definitely due to the wet impregnation method here used, which favours the independent distribution of the different compounds. This fact, once again, stresses the importance of adopting the most realistic conditions for doping the catalysts.

As expected from the type of deactivation seen and the results of previous investigations [20, 23, 120], regeneration of the doped plates was successful. As

Deactivation by Potassium Phosphates

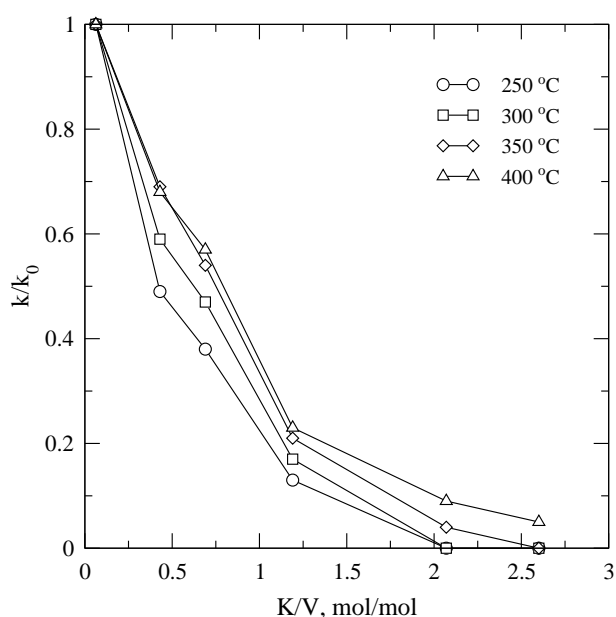


Figure 5.8: Relative activity measured as a function of K/V molar ratios with catalyst plates doped in the laboratory with K_3PO_4 . Total flow: 2.8 NL/min. Gas composition: 500 ppmv NO, 600 ppmv NH_3 , 5% O_2 in N_2 . Catalyst mass: 0.17 g.

shown in Figure 5.10, both the regenerated fresh and regenerated doped sample became more active than the fresh catalyst. Interestingly, the regenerated activity in the case of the doped sample having a K/V molar ratio equal to 2, was higher than the one obtained regenerating a fresh sample. For all regenerated samples, the amount of chemisorbed ammonia was equal to 95-100% of the amount chemisorbed on a fresh catalyst wet impregnated with distilled water. Considering the higher activities measured, it is believed that the regeneration methods used here has mainly changed the *type* of the Brønsted acid sites. For instance, lower amounts of V (i.e. about 60%) were found in the doped samples compared to the water-doped fresh sample. It could be argued that the lost V-sites have been replaced by S-sites, which, according to Guo [11], constitute a more active Brønsted acid site than the V-OH.

5.4 Discussion

5.4.1 K- and P-accumulation and Penetration Mechanisms

The bulk chemical analysis of the catalyst composition has shown a K:P molar ratio less than the theoretical value of 3, varying in the range 0.85-2.5. The

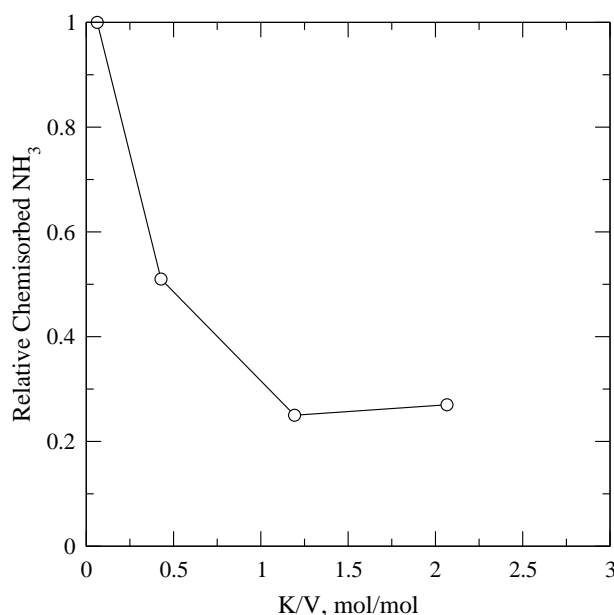


Figure 5.9: Relative chemisorbed NH₃ measured as a function of K/V molar ratios with catalyst plates doped in the laboratory with K₃PO₄. Total flow: 2.8 NL/min. Temperature: 250 °C. Gas composition: 500 ppmv NO, 600 ppmv NH₃, 5% O₂ in N₂. Catalyst mass: 0.17 g.

same ratio was always lower than 1 on the outer surface. Assuming a reaction between the catalyst surface and the K₃PO₄ particles leading to accumulation of K in the wall and release of H₃PO₄ in the gas phase, in a similar way as the release of HCl from KCl on the catalyst surface [110], the resulting K:P molar ratio should have then been found higher than 3. This fact is clearly in contrast with the results of the bulk chemical analysis and indicates that the deposited particles are not only constituted by K₃PO₄.

Further confirming this fact is the dual-mode particle size distribution measured by the SMPS. As discussed above, both particles with a volume-based mean diameter around 30 nm and particles with diameters exceeding the upper limiting range of the SMPS were present in the gas. Simply based on their size, the following can be assumed for these two classes of particles:

1. Low particle diameters and high number concentrations indicate particle formation due to homogeneous nucleation in the gas phase. In other words, the particles with mean diameters of 30 nm are constituted by species which can be found in the gas phase at relatively high temperatures. Contrarily, particles with diameters up to 1 μm are more likely formed due to salt crystallization during water evaporation from the atomized aqueous solution according to their different solubilities.

Deactivation by Potassium Phosphates

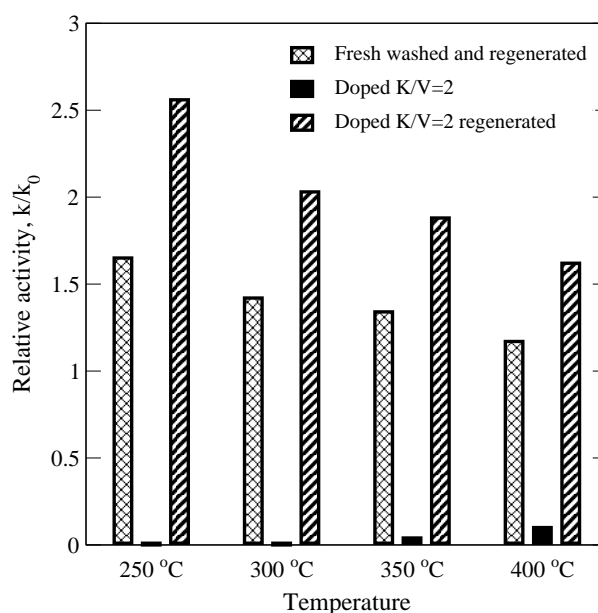
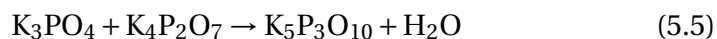
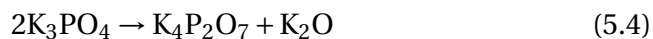


Figure 5.10: Activity vs. temperature for different catalyst plates relative to a fresh sample wet impregnated with water. Total flow: 2.8 NL/min. Gas composition: 500 ppmv NO, 600 ppmv NH₃, 5% O₂ in N₂. Catalyst mass: 0.17 g.

- The deposition rate of the smaller particles is higher due to the higher diffusion coefficients for these particles. In the presence of differences in the chemical composition as a function of particle size, the element characterizing the population with the higher number concentration and smaller particle diameters will accumulate faster on the catalyst surface.

In the absence of a detailed determination of the particle chemical composition due to the encountered experimental limitations, the scenario plotted in Figure 5.11 is proposed.

- Condensate phosphates formation.* Potassium phosphates are reported to form condensate phosphates [137], here referred to as KPO_x:



From these reactions K₂O is formed. According to equilibrium calculations performed in this work by using the commercial software FactSage 5.2, the formed K₂O will be converted to KOH by reacting with the flue gas moisture. At lower temperatures K₂CO₃ will be formed by reaction with CO₂.

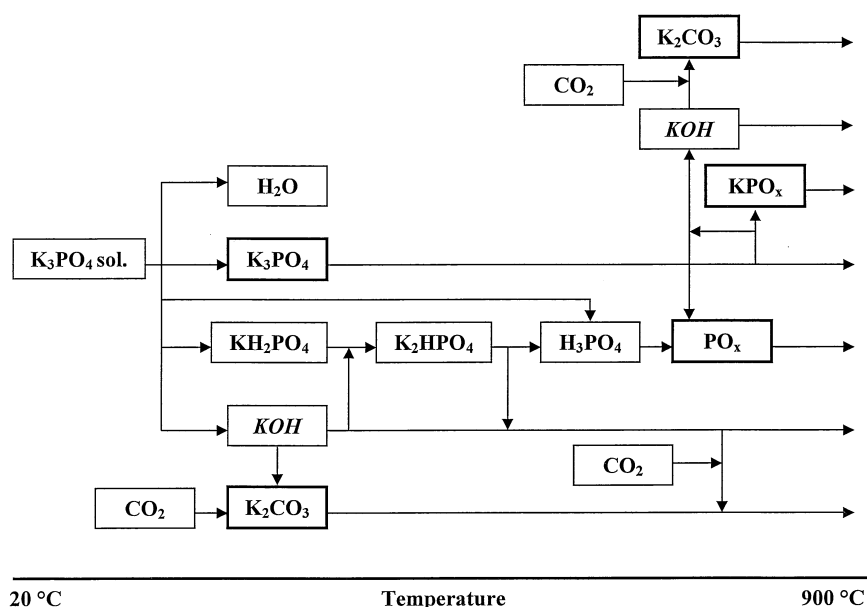


Figure 5.11: Possible reactions during heating of K_3PO_4 solution droplets. The compounds in bold boxes are the ones most likely found at the SCR reactor inlet.

2. *KH_2PO_4 formation.* Crystallization of salts which are not the thermodynamic stable phases under the conditions of crystallization is reported to be rather common for the potassium orthophosphate system [137]. This means that the salts formed during the fast water evaporation from every single K_3PO_4 solution drop sprayed into the flue gas may differ from the initial K_3PO_4 . Table 5.3 shows the known P-K salts and their solubility in water. In this, the solubility for KOH is also reported. As it can be seen, KH_2PO_4 is the salt with the lowest solubility. This indicates that this compound is the first that precipitates when water evaporates from a drop in the hot flue gas. The remaining K, which is not bound to the formed KH_2PO_4 will later precipitate as KOH . Part of the P may also lead to some H_3PO_4 . After water evaporation, the formed aerosols will be heated by the surrounding flue gas, and both the formed KH_2PO_4 and KOH are then converted to the more stable K_2HPO_4 and K_2CO_3 . At temperatures higher than 465 °C the K_2HPO_4 will finally decompose. This decomposition may lead to formation of gaseous H_3PO_4 and solid K_2CO_3 by reaction with CO_2 .

Both of these two scenarios foresee the formation of H_3PO_4 , KPO_x , K-P-salts with K:P molar ratios lower than 3 and some K_2CO_3 , at the expenses of some of

Deactivation by Potassium Phosphates

Table 5.3: Solubility and melting temperature for different K-species.

| | Solubility (g/100 g H ₂ O) | Melting Temperature (°C) |
|---------------------------------|---------------------------------------|--------------------------|
| K ₃ PO ₄ | 106 | 1340 |
| K ₂ HPO ₄ | 168 | dec. |
| KH ₂ PO ₄ | 25 | 253 |
| KOH | 121 | 406 |
| K ₂ CO ₃ | 111 | 891 |

the original K₃PO₄. Among these species, H₃PO₄ can be regarded as responsible for the formation of the aerosols with mean diameter equal to 30 nm. Similar results have in fact been obtained during the exposure to H₃PO₄ reported in the previous Chapter. In this way, the high P-content on the outer catalyst surface measured by SEM-EDX would be explained, since it would be due to the higher deposition rates for these small particles compared to the bigger ones, where K is concentrated.

Regarding the presence of K₂CO₃, this cannot be proved by the tests carried out in this work. However, the relatively high K:P molar ratios measured on the impactor stages may be considered as an indication of the presence of P-free K-particles. Moreover, it can be argued that the gas released by the deposits collected with the impactor was CO₂. Most of the compounds present in Figure 5.11 are deliquescent, and therefore form a liquid solution when exposed to the ambient air, in agreement with the experience of the collected deposits. In this liquid solution then, release of CO₂ could be possible due to recombination of the species in the liquid phase, and could be favoured by the presence of acid compounds like the polyphosphoric acids.

The SEM-EDX of the catalyst wall cross sections indicate a faster net penetration for K compared to the one measured for P. Even though there still is an uncertainty about the real composition of the aerosols involved in the performed tests, and the presence of different species have been assumed, these different penetration rates are not likely associated to the presence of different species with different particle sizes and mobilities in the solid state. These are instead more likely associated with the different affinities between the elements K and P towards the acidic surface of the catalyst. It is here assumed that *solid-state acid-base reactions* are the major driving force responsible for reaction between the K-atoms from the particles and the catalyst surface. Since particles are deposited at the outer layers of the catalyst walls, a K-surface-gradient in

the wall is first formed. This gradient is then responsible for the further penetration/distribution of the K-atoms by surface diffusion. On the other hand, P is included in acidic compounds. Consequently, acid-base reactions between the P-containing particles and the catalyst surface are not expected. The penetration of P is then mainly controlled by capillary forces applied on the viscous liquid phase the polyphosphoric acids are made of, and possibly K-P solid particle diffusion in the external layers of the catalyst walls. Furthermore, considering that the PO_x are hydrolysed by the flue gas moisture at the reactor temperature releasing gaseous H_3PO_4 (see Chapter 4), the P-concentration in the wall will approach zero as observed. This would in fact be the result of combined particle deposition and P-evaporation. The P which is included in K-P salts might also leave the particle as H_3PO_4 when the K reacts with the catalyst surface.

5.4.2 Deactivation Mechanism

The exposure of the commercial monoliths used in this work to a flue gas containing aerosols of K- and P-species has rapidly lowered the activity of the tested elements. In the absence of particles, the deactivation did not continue any further. On the contrary, when the exposure was performed without any K_3PO_4 addition, some reactivation of the catalysts was observed (9%). These facts indicate that (i) the aerosols are necessary to get any deactivation; (ii) reversible physical deactivation by outer surface fouling is contributing to the measured deactivation. According to the K-content measured by SEM-EDX analysis and the activity measurements made on powders, an agreement with the poisoning data from the literature has been found. For instance, the SEM-EDX analysis for the sample KP100B showed a constant K:V value of 0.2 along the whole wall. For the same sample, the relative intrinsic activity measured on powder was equal to 30% at 300 °C (Figure 5.6), in good agreement with previous studies of K-poisoning [19, 102] shown in Figure 2.22. The same agreement was found with the results obtained in the laboratory shown in Figure 5.8. These facts and the results of the NH_3 chemisorption tests indicate that the deactivation measured is mainly due to poisoning by K via blocking of the active sites for NH_3 chemisorption and those for NH_3 activation. The influence of poisoning by polyphosphoric acid at the pilot plant is not significant in this work due to: (i) the relative low levels of P found due to simultaneous hydrolysis of the deposited acids; (ii) their relative low poisoning strength compared to K; (iii) a possible lowering of the deactivation strength of the polyphosphates due to the presence of K.

Since the mechanism of deactivation follows the same path seen during poisoning by KCl and K_2SO_4 in previous works [19, 102, 105, 106, 109, 110], the same regeneration method proposed in the literature [109, 110] has resulted

highly effective also in this work.

Physical deactivation due to pore blocking or surface masking by particle deposition is not likely to be the main mechanism responsible for the deactivation measured, but it is clearly contributing to the overall deactivation as indicated by the partial reactivation obtained by exposing the spent monoliths to clean flue gas while soot blowing. In particular, the almost complete disappearance of the pores in the range 0.6-8 μm for all the spent catalysts, together with the small loss (i.e. 6%) of the total intrusion volume are indications of the formation of an outer fouling layer. With up to 12 %wt P found on the outer catalyst surface, and since the polyphosphoric acids are viscous liquids at the SCR temperature (see Chapter 4), it is believed that they are playing an important role in the formation of this fouling layer by gluing together the different deposited particles. In general, an efficient soot blowing system is required not only to keep the channels opened, but also to clean their external surface.

5.5 Conclusions

K_3PO_4 has been indicated as a potential product of combustion of biomass mixed with P- and Ca-based K-getter additives for reducing fouling and corrosion problems on superheater surfaces at power stations. In order to evaluate whether the formation of this compound might also have a positive effect on the vanadia-based SCR catalysts by limiting the fast rate of deactivation normally experienced with KCl or K_2SO_4 , K_3PO_4 has been added in a hot flue gas at a SCR pilot scale setup and the activity of two commercial vanadia-based monoliths has been followed as a function of exposure time. A study about poisoning by K_3PO_4 following the more classical wet impregnation method has also been carried out in the laboratory.

During the tests carried out at the pilot plant, different K- and P-compounds have been formed from the originally injected K_3PO_4 . A dual-mode volume-based particle distribution with peaks at around 30 nm and at diameters > 1 μm has been measured at the SCR reactor inlet. The distribution of K and P in the different particles has thereby influenced the rate of deposition and accumulation of the species in the exposed catalysts. In order to explain the high P-concentrations and low K:P molar ratios found on the outer catalyst surface, the smaller particles have been associated with liquid phase phosphates (PO_x and KPO_x), whereas the larger ones have been associated to potassium phosphates formed during evaporation of water from the injected droplets.

Deactivation rates up to 3%/day have been measured. K has been found to penetrate the whole catalyst wall indicating that this is not strongly bound to the particles and relatively fast reacts with the catalyst surface and subse-

quently penetrates the catalyst wall by surface diffusion. The NH_3 chemisorption studies have shown that the deactivation has mainly proceeded via K-poisoning by blocking the sites for NH_3 adsorption and activation. All these data recall the mechanism of deactivation previously reported during exposures to KCl and K_2SO_4 and therefore indicate that binding K to P by the addition process does not seem to be an advantageous solution with respect to the vanadia-based SCR catalysts.

Poisoning by polyphosphoric acids is not clearly seen in this investigation due to both the relatively low P-content in the catalyst and the low poisoning strength compared to K. However, Hg-porosimetry has revealed the occurrence of fouling and pore mouth blocking at the outer catalyst surface. It is believed that the polyphosphoric acids play an important role in the formation of this layer by gluing together the deposited particles and should therefore be considered a fouling promoter.

In the laboratory, K was again the main responsible for the deactivation measured at increasing K/V molar ratios. According to the NH_3 chemisorption study, the deactivation is caused by K-blocking of the Brønsted acid sites, as known from the literature. Phosphorus, which has accumulated more relatively to K, increased the amount of chemisorbed NH_3 , probably via formation of P-OH Brønsted acid sites. However, these species are not active enough to compensate for the loss of activity originated from the deactivation of the original Brønsted acid sites.

Based on the tests carried out in the laboratory, washing with a H_2SO_4 aqueous solution may be a viable solution for re-establishing the original activity.

Chapter 6

Deactivation by Additives Mixture

The work reported in this chapter has been published in *Applied Catalysis B: Environmental* [139]. The paper is included in Appendix C.

6.1 Introduction

The addition of P- and Ca-compounds during biomass combustion and the corresponding changes in both ash load and composition may have a beneficial effect on the fast SCR catalyst deactivation normally experienced during biomass combustion [22, 110]. Here K, which is known as one of the strongest poisons for the vanadia-based catalysts normally used in the SCR process [19, 20, 102, 105, 106, 109, 119], once deposited as submicron particles of KCl and K_2SO_4 , is found to easily diffuse inside the catalyst wall and thereby deactivate the active sites. The transfer of K to the catalyst, as shown in Chapter 5, apart from being related to the submicron particles, is directly dependent on how strongly K is bound to the particle itself. In this sense, capturing K into P-K-Ca particles may decrease the amount of K that is released to the catalyst surface and deactivate it. These particles will in fact have higher melting temperatures, lower water solubilities and potentially a higher stability.

On the other hand, both Ca and P are known as deactivating compounds for the vanadia-based SCR catalysts [19, 24, 102, 104, 130, 135]. Having a relatively weak poisoning strength, Ca is normally considered as a physically deactivating specie since during combustion it forms very stable compounds constituting the fly ash, which tend to block the pore structure of the catalyst wall. Furthermore, sulphation of the deposited Ca is often referred to form a fouling layer on the outer catalyst surface. On the other hand, P may act both as chemical and physical deactivating species according to the compounds it may form during combustion [135] (Chapter 4). When polyphosphoric acids (PO_x) are formed,

physical deactivation by pore blocking and surface masking is enhanced by the liquid viscous nature of these compounds. Furthermore, chemical deactivation at high concentrations (i.e. >100 ppmv) may be very fast, involving blocking of the catalytic cycle via formation of non-active V(4+) species [135] (Chapter 4). Increasing the concentration in the flue gas of P and Ca by the addition process, which as stated above may require an excess of both species compared to K, may then lead to undesired deactivating effects. These may counterbalance the possible positive effects obtained by binding K into P-K-Ca particles.

The aim of this study is to evaluate the potential effects of the P, Ca addition process on the SCR catalysts by exposing a commercial vanadia-based SCR monolith to a flue gas doped with K, Ca and P for 1000 hours and following its activity as a function of exposure time. The exposed catalysts are further characterized by a range of techniques.

6.2 Experimental

A water solution of KCl, Ca(OH)₂, H₃PO₄ and H₂SO₄ has been injected in a hot flue gas (T > 900 °C) from a natural gas burner. The resulting flue gas was then passed over a commercial SCR monolith, and the activity was periodically measured.

In order to simulate the addition process, the molar P:K and P:Ca ratios in the flue gas have been fixed to 2 and 0.8 respectively. The KCl concentration has been fixed to 10 mg/Nm³. Accordingly, 13, 26 and 20 mg/Nm³ of Ca(OH)₂, H₃PO₄ and H₂SO₄ have been added. The addition has been carried out by preparing a water solution of the above listed compounds with the following concentrations: KCl = $6.7 \cdot 10^{-3}$ mol/litre, Ca(OH)₂ = $1.7 \cdot 10^{-2}$ mol/litre, H₃PO₄ = $1.3 \cdot 10^{-2}$ mol/litre, H₂SO₄ = $1.0 \cdot 10^{-2}$ mol/litre. Since the total flue gas flow at the injection point was equal to 50 Nm³/h, the solution feed has been fixed to 1 litre/h. Only 40 Nm³/h were then let through the catalyst element during the whole exposure.

6.3 Results

6.3.1 Aerosol Measurements at the Pilot-scale Setup

SMPS Measurements

Figure 6.1 shows the particle size distribution (PSD) measured by the SMPS. The number-based distribution (Figure 6.1a) is characterized by a peak around 9 nm. Due to their small sizes, these particles are very mobile and are expected

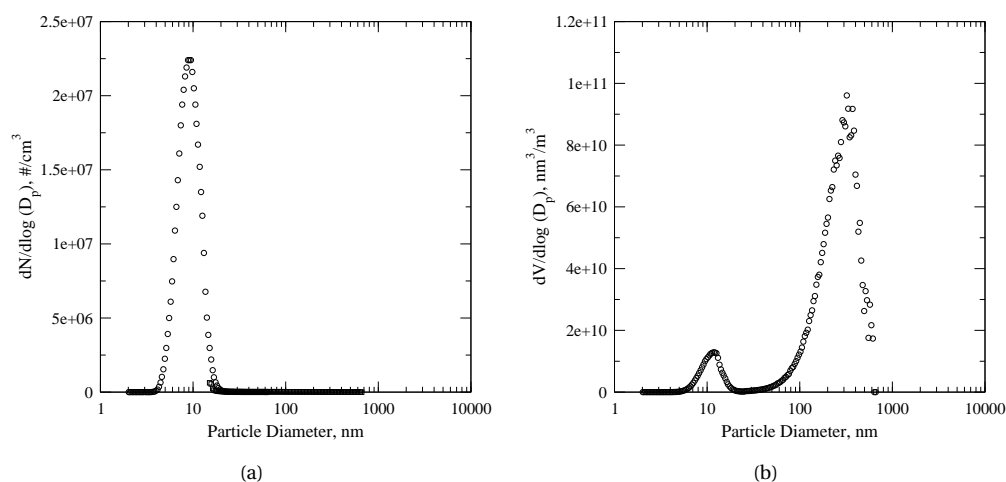


Figure 6.1: Number-based (a) and volume-based (b) particle size distributions measured by SMPS at the reactor inlet during addition of KCl (10 mg/Nm³), Ca(OH)₂ (13 mg/Nm³), H₃PO₄ (26 mg/Nm³) and H₂SO₄ (20 mg/Nm³). T = 350 °C.

to have fast deposition rates on the catalyst surface. The volume-based distribution (Figure 6.1b), which is proportional to the mass carried by the different particles, shows instead the presence of two distinct peaks. The first one has a mean diameter equal to 12 nm, whereas the second one has a peak around 300 nm. This second peak is clearly representing most of the volume/mass of the total PSD.

The dual-mode volume-based PSD measured by SMPS indicate the presence of mainly two classes of compounds:

1. The first peak is constituted by small particles and high concentration numbers due to homogeneous nucleation of gaseous species. This class of particles accounts for about 6% of the total volume measured by the SMPS.
2. The second class is constituted by bigger particles with low total concentration numbers. Their formation is likely due to salt crystallization during water evaporation from the atomized solution droplets at the injection point. This class accounts for about 94% of the total volume measured by the SMPS.

Due to their different mobility and number concentrations, these two particle classes contribute differently to the species accumulation and penetration into the catalyst walls.

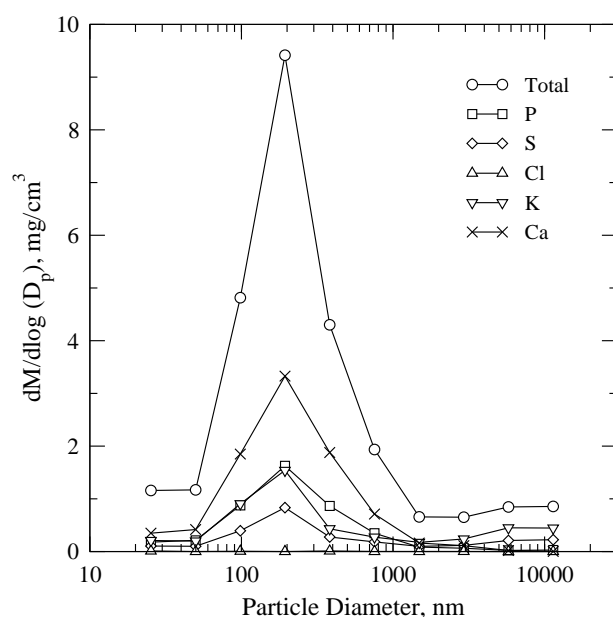


Figure 6.2: Particle size distribution measured by a LPI at the reactor inlet during simultaneous addition of KCl (10 mg/Nm³), Ca(OH)₂ (13 mg/Nm³), H₃PO₄ (26 mg/Nm³) and H₂SO₄ (20 mg/Nm³). T = 90 °C. The curves for each single element have been obtained knowing their concentration on each single stage from EDX analysis.

Low Pressure Cascade Impactor Test

The results of the tests made with the LPI are shown in Figure 6.2 and reported in Table 6.1. Here a mass based particle size distribution with a peak at around 200 nm can be seen. This value is lower than the one measured by the SMPS, and the difference is believed to be due to experimental uncertainties associated with the different sampling techniques and equipments. Particle deposition was found to happen at every single impactor stage as indicated by the non-zero particle concentration in the whole particle diameter range. The total mass concentration was about 10 mg/Nm³. The EDX chemical analysis of the collected deposits showed no Cl in any of the impactor stages, indicating that Cl was effectively released to the gas phase prior to enter the SCR reactor. From the analysis of the element distribution shown in Figure 6.2, it can be seen that both Ca and P are distributed in the particle diameter range 25-3000 nm and are instead not found at higher diameters, where only K and S are found, probably due to the formation of some K₂SO₄. For each impactor stage, the different P:K, P:Ca, K:S and K:Ca molar ratios have been calculated and compared with the ones present in the injected solution. As it can be seen in Table 6.1, both P:Ca and K:S molar ratios have been found constant at around

6.3 Results

Table 6.1: EDX analysis performed on the foils of the impactor stages.

| Stage (#) | Particle Diameter (nm) | P/K (mol/mol) | P/Ca (mol/mol) | K/S (mol/mol) | K/Ca (mol/mol) |
|-----------|------------------------|---------------|----------------|---------------|----------------|
| 1 | 11391 | 0.08 | 17.22 | 1.63 | 211.61 |
| 2 | 5773 | 0.06 | 1.42 | 1.76 | 23.63 |
| 3 | 2931 | 0.33 | 0.72 | 1.67 | 2.18 |
| 4 | 1488 | 0.62 | 0.68 | 1.44 | 1.10 |
| 5 | 754 | 1.60 | 0.63 | 1.23 | 0.39 |
| 6 | 382 | 2.53 | 0.60 | 1.28 | 0.24 |
| 7 | 194 | 1.33 | 0.63 | 1.52 | 0.47 |
| 8 | 98 | 1.22 | 0.61 | 1.88 | 0.50 |
| 9 | 50 | 1.35 | 0.66 | 1.63 | 0.49 |
| 10 | 25 | 1.08 | 0.66 | 1.64 | 0.61 |
| Addition | | 2.00 | 0.80 | 0.67 | 0.40 |

0.65 and 1.55 respectively throughout the whole particle size range, with only some exceptions for the P:Ca ratio at the first and second impactor stage. Simply based on these values it is not possible to identify the exact composition of the formed salts. However, by comparing the results with both the P:K and P:Ca injected, it is possible to conclude that some P is missing. This result might indicate the formation of gaseous P-compounds or the preferential formation of particles with diameters out of the impactor range, for instance those with volume-based mean diameter at 12 nm measured by the SMPS.

6.3.2 Catalyst Characterization

Bulk and Surface Chemical Analysis

Table 6.2 reports the results of both the bulk and surface analysis of samples taken from the exposed monolith at two different exposure times. According to the results obtained from the bulk elemental analysis, P is, among the different species, the element that has accumulated the most in the catalyst walls: On average, the P-accumulation rate is equal to $1.4 \cdot 10^{-3}$ wt%/h, corresponding to about 4% of the incoming P mass. Regarding the Ca and S, the elemental bulk analysis did not show any important increase of these two species in the exposed samples. In fact, apart from ADD1T, the contents of Ca and S were

Deactivation by Additives Mixture

Table 6.2: Bulk and surface analysis for the fresh and spent monoliths.

| | Sample | | | | |
|---------------------------|--------|-------|-------|-------|-------|
| | Fresh | ADD1T | ADD2B | ADD2B | ADD2T |
| Axial Position (cm) | | 5 | 10 | 40 | 45 |
| Additive exposure (h) | | 453 | 1000 | 1000 | 453 |
| Bulk chemical analysis | | | | | |
| V (% wt/wt) | 1.60 | 2.4 | 1.9 | 1.8 | 1.7 |
| K (% wt/wt) | 0.0 | 0.1 | 0.2 | 0.1 | <0.1 |
| P (% wt/wt) | 0.01 | 0.7 | 1.8 | 1.3 | 0.5 |
| Ca (% wt/wt) | 1.7 | 2.1 | 1.9 | 1.7 | 1.8 |
| S (% wt/wt) | 0.3 | 0.4 | 0.4 | 0.3 | 0.3 |
| Cl (% wt/wt) | < 0.1 | < 0.1 | < 0.1 | < 0.1 | < 0.1 |
| Surface chemical analysis | | | | | |
| V (% wt/wt) | 2.1 | 3.84 | 3.35 | 1.93 | 2.04 |
| K (% wt/wt) | 0.0 | 0.22 | 0.25 | 0.33 | 0.12 |
| P (% wt/wt) | 0.0 | 1.67 | 4.67 | 3.10 | 1.72 |
| Ca (% wt/wt) | 0.0 | 0.41 | 0.36 | 1.17 | 0.11 |
| S (% wt/wt) | 0.66 | 0.67 | 0.71 | 1.39 | 0.36 |
| Cl (% wt/wt) | 0.0 | 0.0 | 0.0 | 0.0 | 0.0 |

similar to the ones measured for the fresh catalyst, indicating very low accumulation rates for these two elements. The same can be said for the Cl, where the levels were below the lower detection limits for all tested samples.

The results of the EDX surface chemical analysis showed the presence of all the added elements on the outer surface of the catalyst wall. P was again the most abundant element with a concentration in the range 1.7-4.7 wt%. These values are higher than the total P found in the bulk. As it will be seen later, the reason for the difference is in the decreasing P-concentrations measured along the cross-section of the catalyst wall. As stated before, Ca and S are normally found in the bulk of the fresh catalyst, but are not seen on the outer surface of the walls by EDX. This fact indicates that their presence might be due to the glass fibres, which are reinforcing the catalyst support. All the exposed samples showed instead some Ca and S also on the outer surface indicating that some deposition of these elements did happen during the exposure to the additive

mixture. K was also found on the outer surface. The highest level was found on ADD2B, where this was equal to 0.3 wt%, corresponding to a K:V molar ratio equal to 0.2. Comparing the P:K and P:Ca ratios on the catalyst surface with the ratios in the injected solution indicates an enhanced accumulation of P in the catalyst walls.

SEM Analysis

Aerosol deposition on the outer catalyst surface has been confirmed by the SEM pictures taken of the different samples, shown in Figure 6.3. In the case of ADD1T shown in Figure 6.3a, most of the characteristic macro-cracks were filled with particles. However, these particles which were deposited in the catalyst macro-cracks were able to penetrate the pores for only 20-30 μm , as shown in Figure 6.3b for ADD1B, indicating that clogging of the macro-cracks did not necessarily require the complete filling of their pore volume. Figure 6.3c shows a picture at higher magnifications of the deposits found in the macro-cracks.

At the end of the exposure, the aspect of the catalyst surface had changed. The SEM analysis made after 1000 h of exposure revealed the presence of layer on the outer catalyst surface. Figure 6.4 shows the surface of the catalyst at different magnifications, together with pictures taken of a fresh sample at the same magnifications for comparison. This layer was revealed by the presence of unusual cracks on the surface as shown in Figure 6.4a and Figure 6.4b. As can be seen from these pictures, this layer appears as a compact phase about 2-3 μm thick. The comparison with the fresh sample surface clearly confirms the presence of this deposit covering the original catalyst surface. In fact, only the zones revealed by the deposit breakage somewhat recall the porous structure seen on the fresh sample. The EDX analysis of the zones underneath the formed layer, which were revealed by the outer layer cracks, had a reduced content of P compared to the top of the compact layer itself: In the zones opened to the original catalysts material, the P-content was found equal to around 1 wt%, whereas the average P-content of the surface was equal to 3 wt%.

Cross-sections of the catalyst sample have also been analysed by SEM-EDX in order to measure the distribution of the different elements inside the catalyst walls. The P-distribution for the sample ADD1B and ADD2T are shown in Figure 6.5. The measured profiles were those typical for diffusion limited processes, with the P-concentrations levelling off within the first 100 μm of the catalyst wall. In the figure, it can also be seen how the P-levels have increased according to the longer exposure in the sample ADD2T.

Regarding K and Ca, they were not found inside the catalyst walls indicating the inability of these elements in diffusing into the catalyst material. Sulphur was constantly ranging inside the walls between 0.4 and 0.5 wt%, identical to

Deactivation by Additives Mixture

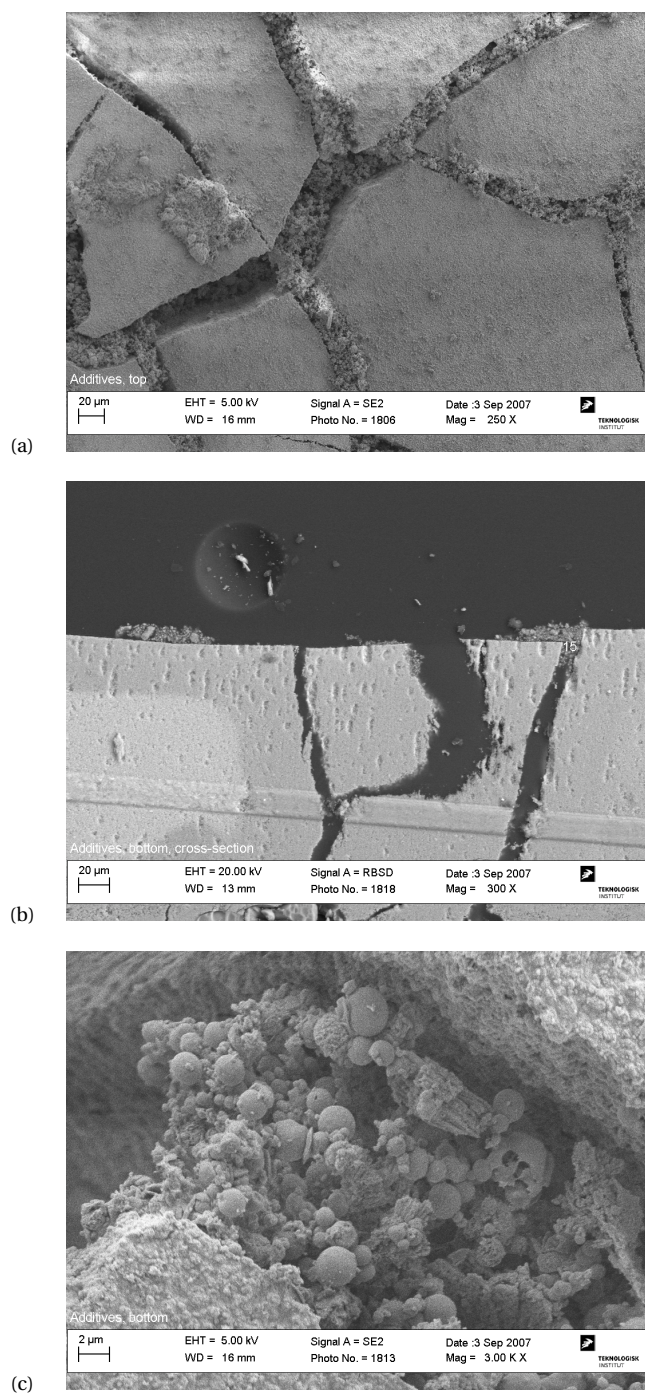


Figure 6.3: SEM images of catalyst samples taken after 453 h of exposure: a) ADD1T; b) ADD1B; c) ADD1B.

6.3 Results

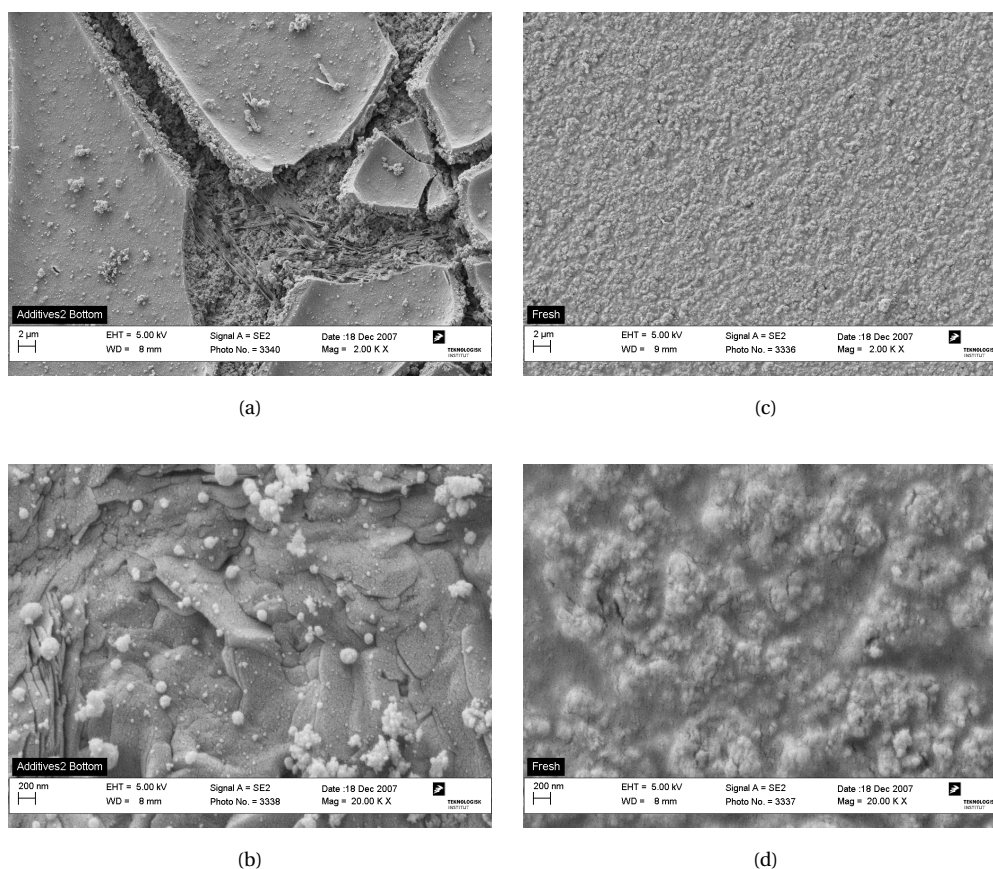


Figure 6.4: SEM images of: a,b) catalyst sample taken after 1000 h of exposure (ADD2B); c,d) fresh sample. Magnification: a,c) 2 kX; b,d) 20 kX.

the values found for a fresh sample.

Overall, the results obtained from the analysis of the catalyst cross-sections clearly indicate (i) the ability of P in penetrating the whole catalyst wall; (ii) the inability of K and Ca, although deposited on the outer surface, to further diffuse inside the wall.

6.3.3 Deactivation at the Pilot-scale Setup

Activity Measurements

Three activity measurements made after 0, 191 and 1 000 h of exposure respectively are shown in Figure 6.6. As it can be seen, apart from the different final conversions obtained, which are also dependent on different total catalyst mass due to the cut after 453 h, the conversion curve obtained at 1000 h dif-

Deactivation by Additives Mixture

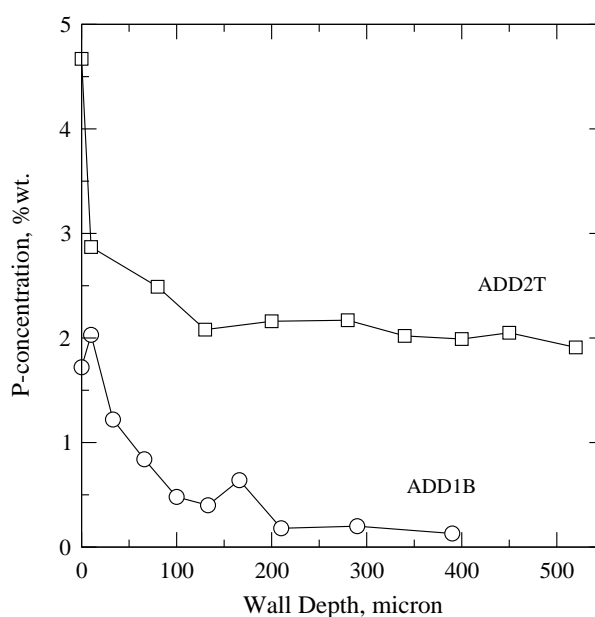


Figure 6.5: P-concentration profile inside the spent catalyst walls.

fers from the other two curves because it first goes through a maximum value right after the NH_3 introduction, and then reaches a steady-state value after about 2 minutes of exposure to NH_3 . All the activity measurements made after around 300 h of exposure to the additive mixture have shown this behaviour. No NO conversion transient was instead measured at shorter exposure times, as shown by the activity tests made at 0 and 191 h of exposure. This NO transient was found in a previous investigation to be related to the accumulation of polyphosphoric acids in the catalyst wall and the subsequent titration of V(5+) active sites by formation of P-V(4+) species during exposure to NH_3 [135] (Chapter 4). From both the aerosol measurements and the catalyst characterization presented so far, it is clear that also in this case the transient can be associated to the PO_x . In order to isolate the PO_x effect on the overall degree of deactivation, for each activity measurement both a maximum and a steady-state relative activity have been calculated. The results of the calculation are shown in Figure 6.7. As it can be seen, the two curves started been distinguishable from each other after about 300 h of exposure. Figure 6.8 shows a plot of the difference between the “Max X” and the “Steady-state” curve shown in Figure 6.7. In the plot, the y-axis has been labelled “Relative activity - PO_x effect” in order to underline that the curve represents the deactivation explicitly due to the polyphosphoric acids poisoning. As it can be seen, this mechanism of deactivation first increased at a calculated rate of 0.2 %/day, and then started

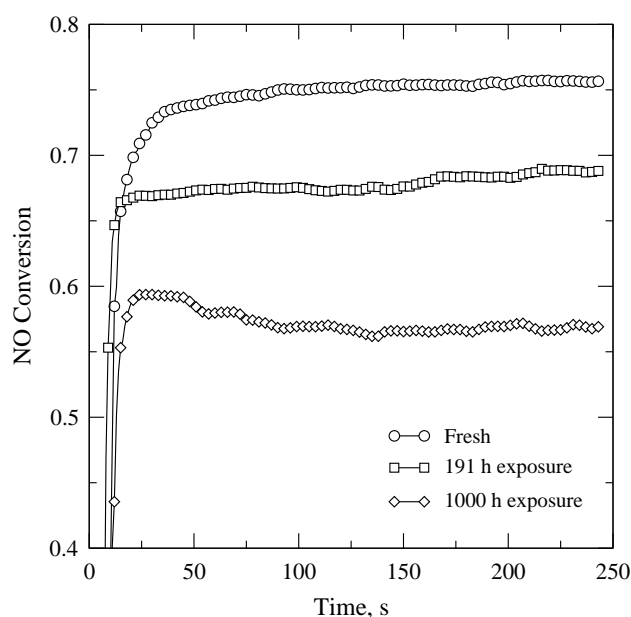


Figure 6.6: Activity measurement made on fresh and spent monolith at 350 °C. Gas dry composition: NO = 500 ppmv, NH₃ = 600 ppmv, O₂ = 10 %v, CO₂ = 6 %v. H₂O = 10 %v. Flow: 40 Nm³/h.

levelling off after about 750 h of exposure, indicating a steady-state between P-deposition and loss by hydrolysis. At the end of the exposure, the percentage of total deactivation that could be associated to poisoning by PO_x can be estimated equal to about 6-7%.

Apart from the quantification of the so called “PO_x effect”, another important conclusion can be made from Figure 6.7. Since the appearance of the NO conversion transient, the “Max X” relative activity has constantly remained around 81% throughout the whole exposure. In fact, 19% of the original activity was lost after the first 191 h of exposure, where no NO transient was measured. This result indicates that the components causing the fast drop of activity at the beginning of the exposure did not cause any further deactivation during the rest of exposure.

NH₃ Chemisorption Tests

The NH₃ chemisorption tests made before the first cut off of the top and bottom 5 cm are reported in Table 6.3, together with the observed steady-state relative activity for comparison, in order to understand the mechanism of deactivation that caused the steep initial decrease in relative activity. According to

Deactivation by Additives Mixture

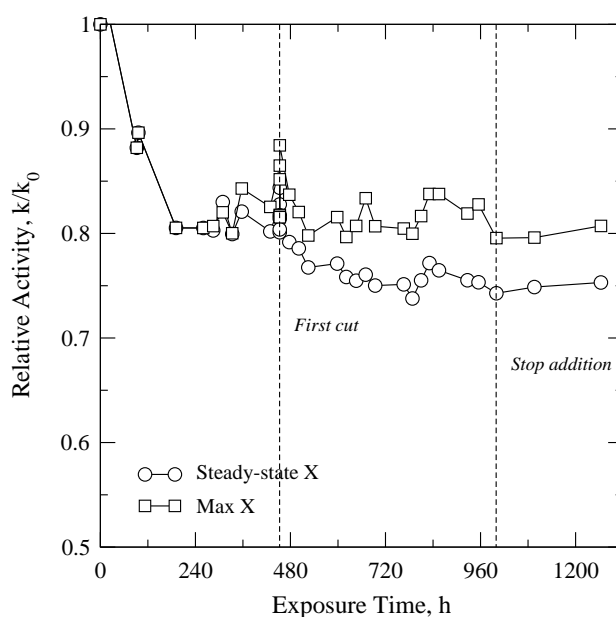


Figure 6.7: Relative activity as a function of exposure time. The activity measurement were made at 350 °C. Gas dry composition: NO = 500 ppmv, NH₃ = 600 ppmv, O₂ = 10 %v, CO₂ = 6 %v, H₂O = 10 %v. Flow: 40 Nm³/h.

the NH₃ chemisorption tests, the 19% decrease of activity measured after 260 h of exposure was accompanied by a loss of only 16% in the total chemisorbed NH₃. A higher decrease in the relative amount of chemisorbed NH₃ compared to the decrease in relative activity would have been measured, if poisoning by K and/or Ca was the main responsible for the measured deactivation. This is because the monolith is operating under both external and internal mass transfer limitations, which are partially masking the effect of chemical deactivation on the intrinsic rate of reaction. Assuming (i) a square root dependency between intrinsic rate of reaction and the observed rate of reaction, valid for mass-transfer-limited reactions; and (ii) a linear relation between the chemisorbed NH₃ and the intrinsic activity, it can be calculated that poisoning only accounted for 8% of the lost activity. The remaining 11% was instead due to physical deactivation by pore blocking and surface masking.

After the first cut of material, a relative increase of chemisorbed NH₃ was measured. For instance, the element increased its capacity in chemisorbing NH₃ of about 39% in the last 600 h of exposure. This increase in chemisorbed NH₃ was found in our previous investigation to be related to the presence of polyphosphoric acids in the catalyst [135] (Chapter 4), which form P-sites where NH₃ can chemisorb. However, these sites are either less active, in agreement

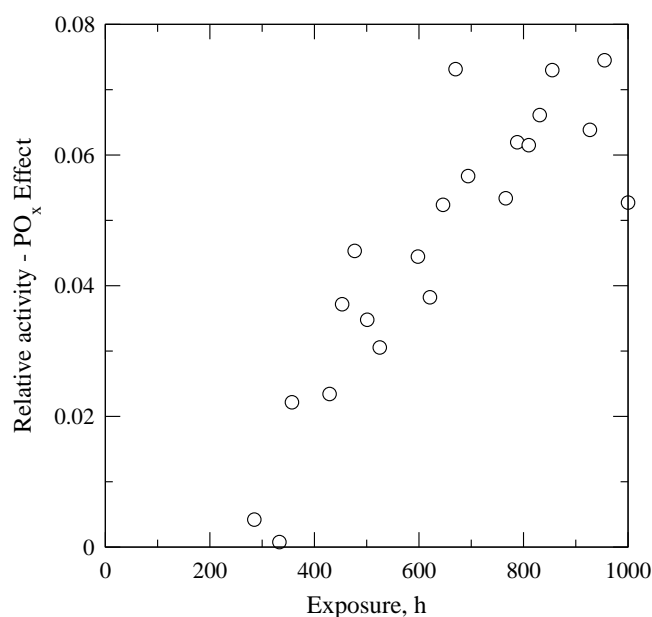


Figure 6.8: PO_x deactivation effect as a function of exposure time. The data points represent the difference between “Max X” and “Steady-state X” curves in Figure 6.7.

with Kamata et al. [13], or inactive, thus simply constituting an NH₃-storage on the surface.

Similarly to our previous investigation [135] (Chapter 4), higher NO conversions could be obtained by increasing the NH₃ partial pressure in the flue gas, as shown in Figure 6.9, where a standard activity measurement made after 1096 h of total exposure (i.e. after 1000 h exposure to the doped flue gas and 96 hours exposure to a clean flue gas) followed by a test with the double amount of NH₃ introduced (i.e. 1200 ppmv) is reported. This additional activity at higher NH₃ partial pressures is related to changes in the NH₃ adsorption constant of the catalyst surface. It can then be argued that, due to the increased number of sites for the NH₃ chemisorption, the coverage of NH₃ appearing in 3.1 has become less than 1 at the typical condition of our activity measurements.

6.3.4 Laboratory Activity and Hg-porosimetry Tests

Activity tests on powder samples have been carried out in the laboratory in order to more clearly identify the extent of deactivation measured on the monolith due to poisoning. Figure 6.10 shows an Arrhenius plot of the activities of the fresh and spent catalyst samples exposed for 453 h. The samples ADD1T and ADD1B had a relative activity of 27% and 75% respectively. These values

Deactivation by Additives Mixture

Table 6.3: Relative chemisorbed NH_3 and relative activity as a function of exposure time.

| Exposure Time (h) | NH_3^* (mol/kg) | $\text{NH}_3^* / \text{NH}_{3,0}^*$ | $k_{s,s} / k_0$ |
|-------------------|--------------------------|-------------------------------------|-----------------|
| 0 | 0.033 | 1.00 | 1.00 |
| 260 | 0.028 | 0.84 | 0.81 |
| 333 | 0.028 | 0.84 | 0.80 |
| 357 | 0.029 | 0.86 | 0.82 |

were constant in the whole temperature range as indicated by the same activation energy calculated from the Arrhenius plot (i.e. 63 kJ/mol), pointing at the occurrence of non-selective poisoning [16].

Physical deactivation by formation of the external layer has been pointed out by the Hg-porosimetry analysis. Figure 6.11 shows the pore size distribution for the fresh sample and ADD2B, which, as shown by the SEM pictures, presented a fouling layer on its external surface. As it can be seen in the figure, the ADD2B sample did not present any pores in the range 0.3-8 μm . However the total intrusion volume did not differ between the two samples. This fact indicates that the outer surface of the ADD2B sample only presents pores smaller than 0.3 μm due to the formation of the fouling layer causing pore mouth closure.

6.4 Discussion

6.4.1 Polyphosphoric Acids Formation

Based on the results obtained in a previous investigation about deactivation by polyphosphoric acids [135] (Chapter 4) and the results just described in this work (i.e. aerosol formation by homogeneous nucleation, NO conversion transient, increased amount of chemisorbed NH_3 , activity dependency on NH_3 partial pressures), there is no doubt about their formation during the exposure to the additive mixture in this work. The reasons for their formation during this particular test can be various, but they would all require the formation of gaseous H_3PO_4 and its exposure to temperatures higher than 600-700 $^\circ\text{C}$. It is believed that some of the compounds which were formed during evaporation of the water from the atomized droplets went through decomposition at increasing temperatures and released some H_3PO_4 in the gas phase. This latter might also have been formed directly during the spraying process. At the

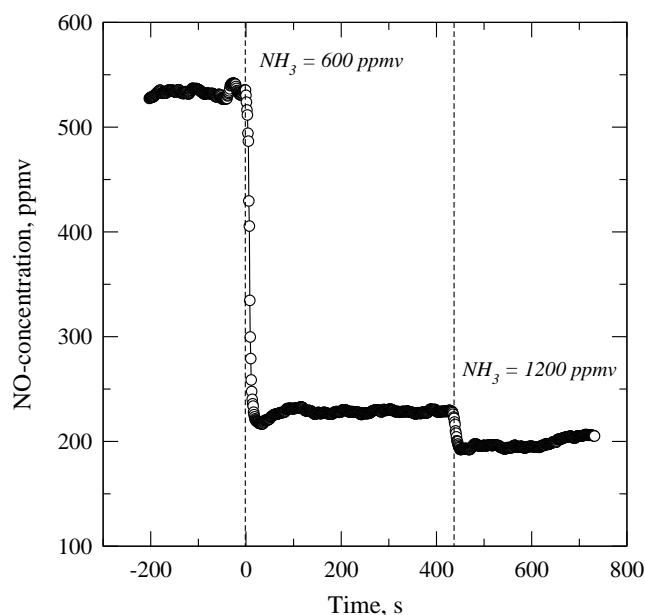


Figure 6.9: Activity measurement on spent catalyst exposed for 1000 hours to the doped flue gas and 96 additional hours to a clean flue gas. $T = 350^{\circ}\text{C}$. Gas dry composition: $\text{NO} = 500 \text{ ppmv}$, $\text{NH}_3 = 600 \text{ ppmv}$, $\text{O}_2 = 10 \text{ \%v}$, $\text{CO}_2 = 6 \text{ \%v}$, $\text{H}_2\text{O} = 10 \text{ \%v}$. Flow: $40 \text{ Nm}^3/\text{h}$.

end of the polyphosphoric acid investigation [135] (Chapter 4), it was not clear whether the formation would have been possible in a system including other different elements, or whether the formation was the result of the simplified flue gas composition used in those tests. The results obtained in this investigation have shown that the formation of polyphosphoric acids was possible in our system at the given P/K and P/Ca ratios. Depending on their concentration, polyphosphoric acids may constitute a high risk for a fast deactivation of the vanadia-based SCR catalysts, since for concentrations corresponding to $100 \text{ ppmv H}_3\text{PO}_4$, their deposition might already be too fast compared to the rate of hydrolysis at SCR reaction conditions.

6.4.2 Particle Deposition and Penetration

The volume-based particle size distributions measured by the SMPS and the SEM pictures of the deposits have shown the presence of two distinct classes of particles. The first one with a volume-based mean diameter equal to 12 nm , and the second one with a volume-based mean diameter equal to 400 nm . Due to both a higher number concentration and a higher diffusion coefficient, the first class of particles is depositing faster than the other. By associating these

Deactivation by Additives Mixture

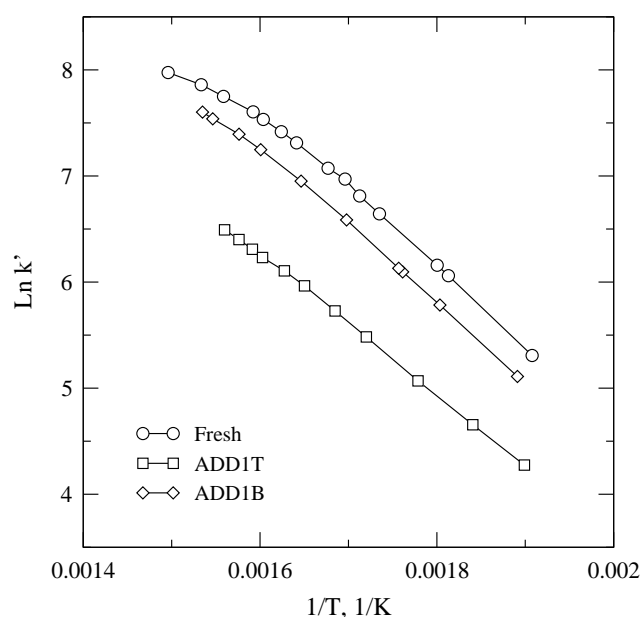


Figure 6.10: Activity test on powder samples. Catalyst mass, $W = 0.07$ g. Total flow $F = 2.8$ Nlitre/min. Gas composition: $\text{NO} = 500$ ppmv, $\text{NH}_3 = 600$ ppmv, $\text{O}_2 = 5\%$, $\text{H}_2\text{O} = 1.4\%$ in N_2 .

particles to the polyphosphoric acids, which are liquid at the SCR temperatures, it can be assumed that the P found inside the catalyst walls is mainly due to their depositions and penetration due to capillary forces. On the other hand, the complete absence of Ca and K inside the walls is an indication that: (i) these elements are present in the bigger particles (i.e. $d_p > 0.1 \mu\text{m}$) which have lower deposition rates and practically no penetration ability; (ii) they are tightly bound to the particles themselves. This latter indication is particularly interesting since it further supports the mechanism of deactivation by K proposed in previous works [3,11]. It is now clear that the K present in the particles which are deposited on the outer surface of the catalyst needs to be released from the particles on atomic scale by interactions with the catalyst surface. It is only afterwards that K can diffuse inside the walls by surface concentration gradients. Particle diffusion is not likely to happen since the same mechanism would have also been active in this investigation, due to the similar particle sizes involved in the tests. K and Ca are instead accumulating on the outer surface. Due to the higher concentration of P found on the formed fouling layer, it is likely that the K-Ca-(P) crystals are glued together by deposited polyphosphoric acids forming the molten-looking layer. This fact would then indicate that the polyphosphoric acids can be regarded as fouling promoters. From the present data it is not possible to know whether this outer layer would have con-

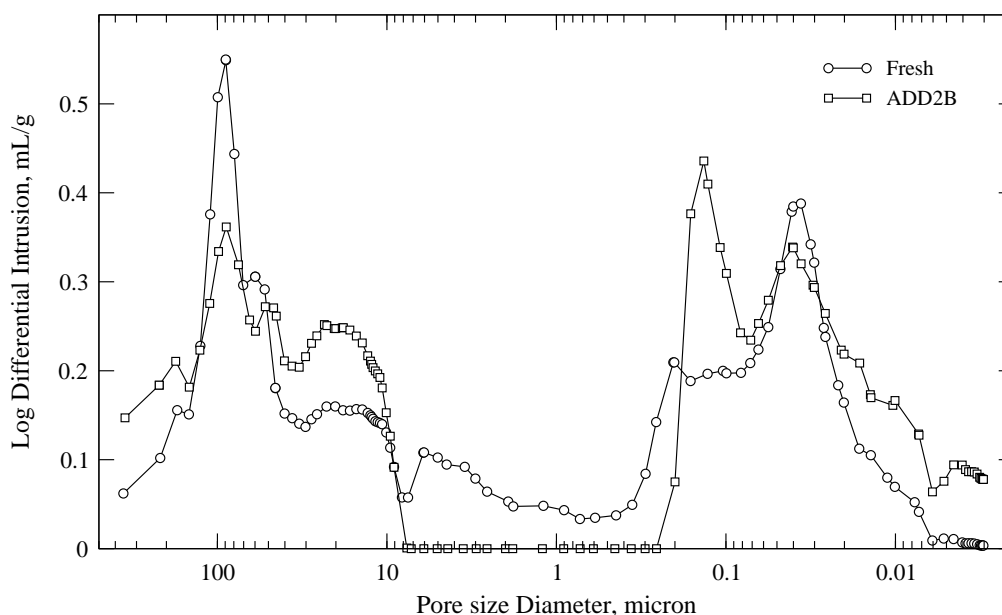


Figure 6.11: Pore size distribution measured by Hg-porosimetry.

tinued growing or whether its thickness had reached a steady value. From the cracks found during the SEM analysis, it appears that some of it has fallen apart, but this could have happened during the cooling of the monolith and may not happen during normal operation.

Regarding the S-content, the SO_2 levels measured in the flue gas were approximately the same as those calculated by assuming the entire S added by the solution to be completely converted to SO_2 . Therefore it is believed that the additional S found on the outer surface of the catalyst is due to sulphation reactions between the deposits and the gaseous SO_2 . Moreover, since no additional S has been found inside the catalyst wall where only P had accumulated, it is assumed that the sulphation reaction preferentially takes place with K and Ca giving K_2SO_4 and CaSO_4 respectively.

6.4.3 Deactivation Mechanism

Based on the results presented, it can be concluded that the deactivation measured during this investigation followed different mechanisms, each of them acting in different periods of time. During the first 200 h of exposure, the steep decrease in observed deactivation (i.e. - 2.4%/day) was mainly due to physical deactivation surface fouling and blocking of the macro-cracks caused by particle deposition on the catalyst outer surface, with subsequent direct and indirect

blocking of the active sites. Due to the pore blocking, the diffusion of both reactants and products is slowed down and, even though the inner layers of the wall are still very active since not attacked by the poison, they are less accessible. This mechanism of deactivation, however, is not expected to cause any further deactivation in the long term provided that the formed deposit layer will (i) keep some porosity, and (ii) not increase its thickness. For exposure time > 300 h, the observed deactivation was instead due to poisoning by polyphosphoric acids and initially proceeded at 0.2 %/day and reached a steady-state level after about 750 h of exposure. Based on both the size and number concentration of the particles which have been assigned to the polyphosphoric acids (i.e. the peak around 9 nm) and the aerosols measurements made at different H_3PO_4 concentrations in a previous investigation [135] (Chapter 4), it can be estimated that these were counting for about 3-4 ppmv P during the test reported in this work, i.e. half of the total P injected in the flue gas. At these low concentrations, P-accumulation in the catalyst walls is limited by the hydrolysis of the polyphosphoric acids at the SCR temperature by the gas moisture [135] (Chapter 4). Therefore, it is believed that the relative activity levelled off due to a steady-state PO_x -level in the catalyst wall obtained due to simultaneous deposition and hydrolysis.

Based on these considerations, it is not expected that further deactivation due to the just discussed mechanisms would have been measured if the exposure was continued.

6.5 Conclusion

Simultaneous addition of KCl, H_3PO_4 , $\text{Ca}(\text{OH})_2$ and H_2SO_4 in a hot flue gas has been carried out for 1000 h and a commercial SCR catalyst has been exposed to the resulting flue gas while the activity was followed as a function of exposure time. The test has been used to estimate the effects of the potential products of the K-getter additives during biomass combustion. In the test carried out, the P/K and P/Ca molar ratios have been fixed to values of 2 and 0.8 respectively suggested in the literature.

At the end of the exposure, the catalyst element lost about 25% of the original activity. However, about 80% of the total deactivation was lost already after 240 h of exposure. Either K or Ca did penetrate the catalyst walls but only accumulated on the external catalyst surface. Poisoning by K and Ca was therefore limited to the most outer wall layers. It has been estimated that 8% of initial relative activity (i.e. about 1/3 of the overall deactivation measured at the end of the test) was lost due to this mechanism, whereas 11% was lost due to physical deactivation by fouling and pore blocking.

At the chosen experimental conditions, formation of polyphosphoric acids has been favoured and about half of the total P has been estimated to be present in these compounds, which formed aerosols with volume-based mean diameter equal to 12 nm. The known deactivating effects of the polyphosphoric acids (i.e. NO transient, activity dependency on NH_3 partial pressures) have been identified: After the initial loss of activity, they controlled the overall deactivation rate, which was about 0.2 %/day. However, due to their relatively low concentration and the simultaneous occurrence of hydrolysis at the SCR reaction condition, the catalyst activity reached a steady-state after about 750 h of exposure. No additional deactivation was then measured in the following 250 h of addition.

Based on the results obtained in this work, it can be concluded that binding K into P-K-Ca compounds is an effective way of reducing the deactivation rates normally experienced during biomass combustion. Reactions between K and the V active sites are in fact prevented, and so is the penetration of K in the catalyst walls by surface diffusion. However, in real applications, the formation of polyphosphoric acids needs to be controlled, since this may counter-balance the just mentioned positive effects by promoting fouling and by poisoning the active sites. In particular, regarding the poisoning, PO_x levels in the range 1-10 ppmv may still be acceptable since their accumulation will be limited by their simultaneous hydrolysis, and a steady-state level in the catalyst wall will be reached. This situation could however be different in the presence of higher K-concentrations in the flue gas. If the fraction of P forming the PO_x is mainly controlled by the P/K and P/Ca ratios, at higher K-contents the amount of formed PO_x could be higher and thereby lead to faster deactivation rates. More tests at different P/K and P/Ca ratios would be necessary to understand the formation of PO_x , and suggest the conditions to limit it.

Chapter 7

Further Discussion of the Results

The potential effects of the P,Ca-additives on commercial SCR catalysts have been studied both in the laboratory and in a SCR pilot plant. By carrying out the tests under well defined and realistic conditions, it has been possible to obtain a better understanding of the deactivation mechanisms that may be encountered at full-scale during the addition of K-getter compounds, or of such compounds experienced during firing of K, P-rich fuels.

In this Chapter, the main findings described in Chapter 4, Chapter 5 and Chapter 6 are represented in order to further underline the mechanism of deactivation by P, K and the ones expected by the P,Ca-additives.

7.1 Deactivation by P

The effect of phosphorus on the vanadia-based catalysts have been extensively investigated first by adding H_3PO_4 in a hot flue gas, and then by adding it in the co-presence of other species like K, Ca, Cl and S. The addition of H_3PO_4 described in Chapter 4 has provided the possibility to simulate the release of gaseous P-species during combustion, and thereby to isolate the deactivating effects of the formed species on the vanadia-based SCR catalysts. According to the results obtained, gaseous H_3PO_4 , when exposed to temperatures higher than 800 °C, forms polyphosphoric acids that are liquid at the typical SCR temperatures. These species can then deposit in the catalyst walls and deactivate it both physically and chemically. Moreover, in the presence of deposited fly ash, they can act as fouling promoters by gluing the different particles together and thereby decreasing the porosity of the formed fouling layer.

Accumulation of the PO_x in the catalyst wall is to some extent limited by hydrolysis of these species due to the water content of the flue gas, with subsequent release of gaseous P-species. Counterbalancing the deposition, this reac-

Further Discussion of the Results

tion may slow down or even stop the deactivation experienced. Following this, alternating the use of fuels, or mixtures, rich in P with others short of P may be used to auto-regenerate the catalysts. According to our tests, up to 10-20 ppmv of vaporised-P in the flue gas may be acceptable¹. At higher concentrations, the observed deactivation will instead be too fast.

At full scale, the formation of polyphosphoric acids will depend on several parameters, but it will be mainly proportional to the amount of vaporised P² that experiences high combustion temperatures. In general, high P-contents in the raw fuel can give a first estimation of the probability to experience deactivation by PO_x. For instance, the P-content occurring in form of P₂O₅ in the low temperature ashes of different coal samples may vary between 0.3-2.5 wt%, whereas in the ashes of sewage sludge, they normally reach levels >20 wt% [140]. Therefore, P-deactivation may in principle be neglected in the case of coal combustion (as it has been done so far), whereas it constitutes great concern during sewage sludge, or other biofuels rich in P, co-combustion.

More important than the P-concentration in the fly ash is, however, the type of compounds in which P is present in the raw fuels. When P is bound to organic compounds, rapid vaporisation even during low temperature pyrolysis has been measured [140]. This will then be the case of sewage sludge, MBM and even PRB coals where the organic P fraction is not negligible. Once P is present in the gas phase, reactions with O₂ and H₂O may then form H₃PO₄, which may then start condensation reactions and lead to the formation of the ultra-fine particles measured in this work. Instead, when the P organic fraction is negligible, like for instance in the case of bituminous coals, vaporisation of P is controlled by both the mode of occurrence of P-bearing species in the raw fuel, and the combustion temperatures. In particular, when P is bound to minerals like for instance apatite (Ca₃(PO₄)₂), this will not vaporise even at 1800 °C. On the other hand, when P is present in complex forms containing Si, Al, Ca, Fe, P and O at non stoichiometric ratios, the vaporisation will instead start at 1200 °C, and will gradually increase at higher temperatures [140]. The reasons for this vaporization have been found in the partial melting of the complexes with liberation of P from the melt liquid.

At the light of these facts, in order to apply the evidences found in this work about deactivation by PO_x, a detailed fuel analysis aiming at estimating the P-concentrations in the gas phase may be required.

¹The use of extruded monoliths having lower porosities than the corrugated monoliths employed in this work may require lower P-concentrations.

²In the literature, the amount of vaporised P is normally related to the amount of submicron particles measured at room temperature.

7.2 Deactivation by K

Since the use of biomass at central power station has become more popular, various investigations have been carried out in order to clarify the deactivation mechanism due to alkali, and in particular due to K, and to propose some viable ways to limit the deactivation and even regenerate the spent catalysts. When this project was first initiated, discussion about the nature of the deactivation, i.e. chemical or physical, was still open. The poisoning tests carried out by wet impregnation methods in the laboratory have always indicated K as a very strong poison for the vanadia-based SCR catalysts, no matter which compound was used to dope the catalysts. At full scale, however, K is present in the particles constituting the fly ash, which first have to diffuse towards the catalyst outer surface, and then have to penetrate the catalyst pore structure prior to deactivate the active sites. Even though K, especially during biomass combustion, forms submicron particles whose size often overlaps with the size of the catalyst pores, it is not likely that the diffusion of these particles can explain the presence of K beyond the most outer μm of wall. On the other hand, as discussed in Chapter 2, the analysis of catalysts employed at full-scale during biomass combustion has always indicated K to be well distributed along the whole wall cross-section. In order to explain the fast penetration of K inside the catalyst wall, Zheng et al. [110] reviewed different accumulation and penetration mechanisms, i.e. by potassium vapours, by formation of low melting point $\text{K}_2\text{S}_2\text{O}_7\text{-V}_2\text{O}_5$ species and by surface diffusion. While the first two mechanisms were judged not relevant at typical SCR conditions, surface diffusion was instead indicated as the responsible for the K-penetration. In particular, the mobility of the K-compound was related to the melting point of the K-compound itself via their Tamman and Hüttig temperatures. By relating the penetration of K to the melting temperature of the K-compound also served as an explanation for the negligible deactivation due to K during coal (co-)combustion, where K is normally bound to alumina and silicates having high melting point temperatures.

The investigations reported in Chapter 5 were partially meant to verify the influence of melting temperature on the K-penetration. However the original K_3PO_4 went through some transformations (see Figure 5.11) and the real composition of the particles entering the SCR reactor in the tests is unknown. Besides, all the compounds that could have formed, shown in Figure 5.11, have lower melting point temperatures than the original K_3PO_4 and could have then be responsible for the fast K-penetration. Even so, however, it is hard to imagine that the diffusion as *solid particle* was so fast to explain the flat profiles found in the case, for instance, of KP100B (Figure 5.2a). Therefore it seems more likely that the melting temperature is not the main parameter influenc-

Further Discussion of the Results

ing the K-penetration. Instead, *atomic diffusion* seems to be a more realistic mechanism for K-penetration. The following chain of events is then proposed:

1. K-particles deposit on the acidic surface of the SCR catalyst, mainly on the most outer wall;
2. reaction at the particle interface between K and the –OH terminals of the catalyst surface takes place with extraction of K-atoms from the particle;
3. atomic surface diffusion of the extracted K-atoms favoured by the dense population of –OH sites at typical SCR reaction conditions.

In this way both the aerosols, and the affinity between the K-particle and the catalyst surface are responsible for the deactivation. The smaller the particles are, the larger the interface relative to the particle mass where the extraction of K-atoms can happen will be. Moreover, in the absence of aerosols in the flue gas, the already deposited particles will more likely sinter reducing the amount of K that could be extracted and no further deactivation will be seen. Regarding the affinity with the catalyst surface, the reaction happening at the interface appears to be an acid-base reaction. Therefore, the solubility of the K-compounds (or more generally the ash) in water or in acid solution may give a more useful indication regarding the potential deactivation effect.

From all this discussion, it can be concluded that chemical deactivation is the main mechanism of deactivation by K when this is present in water soluble compounds and fine particles. In all the other cases, the K-particles will simply contribute to the physical deactivation (i.e. fouling, surface masking and pore blocking) due to fly ash.

7.3 Deactivation by Additives

Deactivation of vanadia-based SCR catalysts during utilisation of the P/Ca-based additives will be mainly controlled by (i) the amount of vaporised P, and (ii) by the amount of K which will still be present at the SCR reactor inlet in water soluble fine particles. Both these two quantities are highly dependent on the P/K and P/Ca molar ratios employed during the addition process. In particular, the P/Ca molar ratio employed appears to be very important. In fact, on one side it ensures capturing of all the K while releasing the Cl in the gas phase, thus preventing fouling and corrosion of the superheater exchangers with Cl-rich particles. Provided that the alkali fraction gets efficiently captured in Ca-K-P salts with affinity for the catalyst sites, instead of, for instance, the highly soluble (even hygroscopic) K-P salts formed during the tests with K_3PO_4 , the additives process may even solve the problems normally experienced with the

7.3 Deactivation by Additives

SCR vanadia-based catalysts at biomass combustion. On the other side, the adopted P/Ca molar ratio has to limit vaporisation of P, thus preventing formation of PO_x and deactivation of the SCR catalysts. In this regard, according to a recent study about P-vaporisation, also the combustion temperature may assume a determinant role.

Overall, it is believed that, if the optimal conditions, at which all the K and P are captured in relatively high melting point Ca-K-P-compounds having low water solubility, are found, no enhanced deactivation of the SCR catalysts will be measured. The only deactivation mechanisms which may be experienced will then be fouling, channel and pore blocking by fly ash, which are already well controlled by choosing catalyst elements with an appropriate channel size, based on coal combustion experience.

Chapter 8

Summary, Conclusions and Suggestions to Further Work

The objective of this work is to contribute to the knowledge about vanadia-based SCR catalysts deactivation. In particular, the deactivation induced by K, P and Ca has been studied under realistic condition of exposure, providing useful information when planning the addition of K-getter P,Ca-additives to biomass, or when burning fuels rich in those compounds. The results are summarised below and suggestion for further work are given.

8.1 Deactivation by Polyphosphoric Acids

In order to simulate the release of P-compounds during combustion, H_3PO_4 aqueous solutions have been injected in a hot flue gas at a SCR pilot-scale setup. The H_3PO_4 concentration in the resulting flue gas has been fixed to 10, 100 and 1000 ppmv and three monoliths have been exposed for 819, 38 and 24 h respectively. Separate particle measurements have shown that the injected H_3PO_4 formed polyphosphoric acids, which have higher melting point temperatures than the typical SCR reaction temperatures, and are found in a liquid-phase at the SCR reactor inlet. In particular, condensation of these species has been estimated to happen at temperatures lower than 500 °C. The formed aerosols were characterised by high number concentrations and sub-micron particle sizes, and thereby high diffusivities and high deposition rates on the monolith walls. The P-accumulation, and consequently the implied deactivation, was however limited by the rate of hydrolysis of the deposits themselves by the H_2O present in the flue gas. At the SCR temperatures, this can in fact break down the polyphosphoric acid chains and free some H_3PO_4 back in the gas-phase.

Summary, Conclusions and Suggestions to Further Work

Deactivation by polyphosphoric acids has been found to follow both a physical and a chemical deactivation. Surface masking, fouling, pore blocking and condensation are important contributions to catalyst deactivation. The measured overall deactivation is however also due to chemical deactivation. Supported by the NO reduction transient measured during activity tests with mass transfer-limited-catalysts, and in-situ EPR analysis of the spent catalysts, it has been found that the deposited polyphosphoric acids tend to both increase and stabilize the number of non-active V(IV) species, which are formed as intermediate during the SCR reaction. Moreover, part of the NH_3 present in the gas phase preferentially adsorbs on the polyphosphoric acids and is only less active in the reduction of NO.

Based on the results obtained in this work, the release of P during combustion needs to be kept as low as few tens ppmv of H_3PO_4 . At these levels, deactivation by polyphosphoric acids will be limited by simultaneous evaporation of H_3PO_4 from the catalyst surface. At higher concentrations, both the accumulation of P and the deactivation rate will be too fast.

8.2 Deactivation by Potassium Phosphates

K_3PO_4 has been indicated as a potential product of combustion of biomass mixed with P- and Ca-based K-getter additives for reducing fouling and corrosion problems on superheater surfaces at power stations. Its effect on the vanadia-based SCR catalysts has therefore been investigated in this work, both at a SCR pilot-scale setup and in the laboratory.

At the pilot plant, K_3PO_4 has been injected directly in a hot flue gas as an aqueous solution. Two monoliths have been exposed during the addition of 100 and 200 mg/Nm^3 K_3PO_4 for 720 and 189 h respectively. Particle measurements carried out with a SMPS system have revealed a dual-mode volume-based particle distribution with peaks at around 30 nm and at diameters $> 1 \mu\text{m}$ at the SCR reactor inlet. According to SEM-EDS analysis of the exposed catalyst surfaces, high P-concentrations and low K:P molar ratios were found on the outer catalyst surface. Therefore, the smaller particles measured by the SMPS have been associated with liquid phase phosphates (PO_x and KPO_x), whereas the larger ones have been associated to potassium phosphates formed directly during evaporation of water from the injected droplets.

At the end of the addition of 100 mg/Nm^3 K_3PO_4 , the element continuously exposed for 720 h lost 38% of its original activity. In the case of the addition of 200 mg/Nm^3 , the catalyst exposed for only 189 h lost 27% of activity. In both cases, the deactivation rates were very fast and deactivation rates up to 3%/day have been measured. The causes of the deactivation have been associated to

8.3 Deactivation by Additives Mixture

K-poisoning, as indicated by NH_3 chemisorption studies, and fouling, as indicated by Hg-porosimetry measurements. Poisoning by polyphosphoric acids is not clearly seen in this investigation due to both the relatively low P-content in the catalyst and the low poisoning strength compared to K. However, it is believed that the polyphosphoric acids play an important role in the formation of the fouling layer by gluing together the deposited particles and should therefore be considered a fouling promoter.

In the laboratory, K was again the main responsible for the deactivation measured at increasing K/V molar ratios. According to the NH_3 chemisorption study carried out, the deactivation involved blocking by K of the Brønsted acid sites present on the catalyst surface, as known from the literature. Phosphorus, which during the wet impregnation process has accumulated more relatively to K, increased the amount of chemisorbed NH_3 , probably via formation of P-OH Brønsted acid sites. However, these species are not active enough to compensate for the loss of activity originated from the deactivation of the original Brønsted acid sites.

Based on the information gained in this work, it can be said that binding K to P by the addition process does not seem to be an advantageous solution with respect to the vanadia-based SCR catalysts. Regeneration, however, may still be possible. As indicated by the tests carried out in the laboratory, the original activity of the spent catalyst samples was re-established by washing them with a H_2SO_4 aqueous solution.

8.3 Deactivation by Additives Mixture

A flue gas resulting from biomass combustion in the presence of P/Ca-additives has been simulated in terms of P/K and P/Ca molar ratios by simultaneous addition of KCl, H_3PO_4 , $\text{Ca}(\text{OH})_2$ and H_2SO_4 in a hot flue gas at the SCR pilot-scale setup. A commercial SCR monolith has been exposed to the resulting flue gas for 1000 h and its activity has been followed as a function of exposure time. The test has been used to estimate the effects of the potential products of the K-getter additives during biomass combustion. In the test carried out, the P/K and P/Ca molar ratios have been fixed to values of 2 and 0.8 respectively suggested in the literature.

At the end of the exposure, the catalyst element lost about 25% of the original activity. However, about 80% of the total deactivation was lost already after 240 h of exposure and no deactivation was measured in the last 250 h of exposure. The reasons for the deactivation have been various. Neither K or Ca did penetrate the catalyst walls but only accumulated on the external catalyst surface. Poisoning by K and Ca was therefore limited to the most outer wall

Summary, Conclusions and Suggestions to Further Work

layers. It has been estimated that 8% of initial relative activity (i.e. about 1/3 of the overall deactivation measured at the end of the test) was lost due to this mechanism, whereas 11% was lost due to physical deactivation by fouling and pore blocking. The remaining deactivation has been assigned to poisoning by polyphosphoric acids. In fact, at the chosen experimental conditions, about half of the total P has been estimated to form polyphosphoric acids, and their known deactivating effects (i.e. NO transient, activity dependency on NH_3 partial pressures) have been identified. After the initial loss of activity, they controlled the overall deactivation rate, which was about 0.2 %/day. However, due to their relatively low concentration and the simultaneous occurrence of hydrolysis at the SCR reaction condition, the catalyst activity reached a steady-state after about 750 h of exposure. No additional deactivation was then measured in the following 250 h of addition.

Based on the results obtained in this work, it can be concluded that binding K into P-K-Ca compounds is an effective way of reducing the deactivation rates normally experienced during biomass combustion. Reactions between K and the V active sites are not favoured, and thereby, the penetration of K in the catalyst walls by atomic surface diffusion is prevented. Attention, however, must be paid in real applications to the formation of polyphosphoric acids. This may in fact counterbalance the just mentioned positive effects by promoting fouling and by poisoning the active sites. PO_x levels in the range 1-10 ppmv, as those estimated during this test, may still be acceptable. Their accumulation will in fact be limited by their simultaneous hydrolysis, and a steady-state level in the catalyst wall will be reached. This situation could however be different in the presence of higher K-concentrations in the flue gas. If the fraction of P forming the PO_x is mainly controlled by the P/K and P/Ca ratios, at higher K-contents the amount of formed PO_x could be higher and thereby lead to much faster deactivation rates.

8.4 Suggestions to Further Work

The tests carried out in this work, especially those involving addition of H_3PO_4 at the SCR pilot-scale setup, have shown the importance of being able to foresee, based on fuel analysis and combustion technique, the formation of polyphosphoric acids and to estimate their concentrations at the SCR reactor inlet. This may not be an easy task due to both the complexity of the combustion process and the lack of thermodynamic data, however further work in this field is recommended. In particular, regarding the additive process, more tests at different P/K and P/Ca ratios would be necessary to understand the formation of PO_x , and suggest the conditions to limit it. Full-scale tests may also be required

8.4 Suggestions to Further Work

in order to study the influence of the particular combustion technique on the P-release. Useful knowledge may be gained from these tests, that could then be applied to various applications, like for instance MBM and sewage sludge combustion.

In the various tests reported in this work, P, in the form of polyphosphoric acids, has been indicated as a fouling promoter. Deactivation by fouling is known to be the main deactivation mechanism during combustion of PRB coals. In these applications, the formation of this fouling layer has always been indicated to be due to sulphation of the Ca(OH)_2 deposited on the outer catalyst surface. However, apart from being rich in Ca, these coals are also rich in P, which, according to the evidences reported in this work, may play an active role in the formation of the fouling layer. It may therefore be worth running experiments at the pilot-scale setup where the addition of Ca(OH)_2 and SO_2 is compared with the simultaneous addition of Ca(OH)_2 , SO_2 and H_3PO_4 .

Deactivation by K has now been extensively studied in the laboratory, and both at pilot- and full-scale, under very different conditions. Even though the overall picture about the deactivation mechanism is nowadays quite clear, it is believed that lab-scale investigations involving single monolith channels, well classified particles sizes and realistic exposure times may still be worth trying. The experimental setup may resemble the one used by Moradi et al. [108] and may even involve different gas compositions, for instance dry and reducing mixtures, in order to study the influence of H_2O and the oxidation state of the catalyst surface on K-diffusion in the catalyst wall.

Bibliography

- [1] H.N. Soud and K. Fukasawa. Developments in the NO_x abatement and control. IEA Coal Research, London, United Kingdom, 1996.
- [2] H. Flora, J. Barkley, G. Janik, B. Marker, and Cichanowicz. Status of 1 MW SCR pilot plant tests at Tennessee valley authority and new york state electric & gas. Proceeding of the 1991 joint symposium on stationary combustion NO_x control, March 1991.
- [3] J. Ando. Flue gas cleaning technology of the world. Coal Mining Research Institute, 1990.
- [4] E. Tronconi. Interaction between chemical kinetics and transport phenomena in monolithic catalysts. *Catalysis Today*, 34:421–427, 1997.
- [5] B.M. Weckhuysen. Chemistry, spectroscopy and the role of supported vanadium oxides in heterogeneous catalysis. *Catalysis Today*, 78:25–46, 2003.
- [6] G.T. Went, L.-J. Leu, and A.T. Bell. Quantitative structural analysis of dispersed vanadia species in TiO₂(Anatase)-supported V₂O₅. *Journal of Catalysis*, 134:479–491, 1992.
- [7] G. Busca, L. Lietti, G. Ramis, and F. Berti. Chemical and mechanistic aspects of the selective catalytic reduction of NO_x by ammonia over oxide catalysts: A review. *Applied Catalysis B: Environmental*, 18:1–36, 1998.
- [8] A. Miyamoto, M. Inomata, A. Hattori, T. Ui, and Y. Murakami. A molecular orbital investigation of the mechanism of the NO- NH₃ reaction on vanadium oxide catalyst. *Journal of Molecular Catalysis*, 16(3):315–333, 1982.
- [9] G. Ramis, G. Busca, F. Bregani, and P. Forzatti. Fourier transform infrared study of the adsorption and coadsorption of nitric oxide, nitrogen dioxide and ammonia on vanadia-titania and mechanism of selective catalytic reduction. *Applied Catalysis*, 64:259–278, 1990.

Bibliography

- [10] N.-Y. Topsøe, H. Topsøe, and J. A. Dumesic. Vanadia/Titania catalysts for selective catalytic reduction (SCR) of nitric oxide by ammonia. Studies on active sites and formulation of catalytic cycle. *Journal of Catalysis*, 151:241–252, 1995.
- [11] X. Guo. *Poisoning and sulfation on vanadia SCR catalyst*. PhD thesis, Department of Chemical Engineering, Brigham Young University, August 2006.
- [12] J. Svachula, N. Ferlazzo, P. Forzatti, E. Tronconi, and F. Bregani. Selective reduction of NO_x by NH₃ over honeycomb deNO_xing catalysts. *Ind. Eng. Chem. Res.*, 32:1053–1060, 1993.
- [13] M. Koebel and M. Elsener. Selective catalytic reduction of NO over commercial deNO_x-catalysts: experimental determination of kinetic and thermodynamic parameters. *Chemical Engineering Science*, 53(4):657–669, 1998.
- [14] I. Nova, L. Lietti, E. Tronconi, and P. Forzatti. Transient response method applied to the kinetic analysis of the DeNO_x-SCR reaction. *Chemical Engineering Science*, 56:1229–1237, 2001.
- [15] R. Willi, B. Roduit, R.A. Koeppl, A. Woakun, and A. Baiker. Selective reduction of NO by NH₃ over vanadia-based commercial catalyst: parametric sensitivity and kinetic modelling. *Chemical engineering science*, 51(11):2897–2902, 1996.
- [16] B. Roduit, A. Wokaun, and A. Baiker. Global kinetic modeling of reactions occurring during selective catalytic reduction of NO by NH₃ over vanadia/titania-based catalysts. *Ind. Eng. Chem. Res.*, 37:4577–4590, 1998.
- [17] G. Madia, M. Elsener, M. Koebel, F. Raimondi, and A. Wokaun. Thermal stability of vanadia-tungsta-titania catalysts in the SCR process. *Applied Catalysis*, 39:181–190, 2002.
- [18] L.J. Alemany, M.A. Bañares, M.A. Larrubia, M.C. Jiménez, F. Delgado, and J.M. Blasco. Vanadia-titania systems: morphological and structural properties. *Materials Research Bulletin*, 31(5):513–520, 1996.
- [19] J.P. Chen, M.A. Buzanowski, and R.T. Yang. Deactivation of the vanadia catalyst in the selective catalytic reduction process. *J. Air Waste Manage. Assoc.*, 40:1403–1409, 1990.

- [20] Y. Zheng, A.D. Jensen, and J.E. Johnsson. Laboratory investigation of selective catalytic reduction catalysts: deactivation of potassium compounds and catalyst regeneration. *Ind. Eng. Chem. Res.*, 43:941–947, 2004.
- [21] S. Pritchard, S. DiFrancesco, S. Kaneko, N. Kobayashi, K. Suyama, and K. Iida. Optimizing SCR catalyst design and performance for coal-fired boilers. Presented at EPA/EPRI 1995 joint symposium stationary combustion NO_x control, May 16-19 1995.
- [22] Å. Kling, C. Andersson, Å. Myringer, D. Eskilsson, and S.G. Järås. Alkali deactivation of high-dust SCR catalysts used for NO_x reduction exposed to flue gas from 100 MW-scale biofuel and peat fired boilers: Influence of flue gas composition. *Applied Catalysis B: Environmental*, 69(3-4):240–251, 2007.
- [23] R. Khodayari and C.U.I. Odenbrand. Regeneration of commercial TiO₂-V₂O₅-WO₃ SCR catalysts used in bio fuel plants. *Applied Catalysis B: Environmental*, 30:87–99, 2001.
- [24] J. Beck, J. Brandenstein, S. Unterberger, and K.R.G. Hein. Effects of sludge and meat and bone meal co-combustion on SCR catalysts. *Applied Catalysis B: Environmental*, 49:15–25, 2004.
- [25] E.H. Brown and C.D. Whitt. *Industrial and Engineering Chemistry*, 44:615–618, 1952.
- [26] R. Delmas, D. Serca, and C. Jambert. Global inventory of NO_x sources. *Nutrient Cycling in Agroecosystems*, 48:51–60, 1997.
- [27] L. Sørensen, J. Fjellerup, and U. Henriksen. International Patent Number WO 01/05911 A2, 2001.
- [28] P. Henderson, C. Andersson, and H. Kassman. VGB PowerTech 58, 2004.
- [29] IACM, Swedish Patent SE 9903656-8, 2001; IACM, International Patent PCT WO0127593, 2001; IACM, European Patent EP1221036, 2002.
- [30] P.A. Jensen, L.H. Sørensen, G. Hu, J.K. Holm, F. Frandsen, and U.B. Henriksen. KT-report 0504, Technical University of Denmark, 2005.
- [31] H. Bosch and F. Janssen. Catalytic reduction of nitrogen oxides - A review on the fundamentals and technology. *Catalysis Today*, 2(4):369–532, 1988.

Bibliography

- [32] V.I. Parvulescu, P. Grange, and B. Delmon. Catalytic removal of NO. *Catalysis Today*, 46:233–316, 1998.
- [33] J.A. Miller and C.T. Bowman. Mechanism and modeling of nitrogen chemistry in combustion. *Prog. Energy Combust. Sci.*, 15:287–338, 1989.
- [34] P. Glarborg, A.D. Jensen, and J.E. Johnsson. Fuel nitrogen conversion in solid fuel fired systems. *Progress in Energy and Combustion Science*, 29:89–113, 2003.
- [35] Coalpower: world coal fired power plants and FGD and NO_x control installations database on cd-rom. IEA Coal Research, London, United Kingdom, 1995.
- [36] R. Rodenhausen. Case study: choosing selective catalytic reduction as a preferred technology for the destruction of NO_x. *Environmental Progress*, 18:260–266, 1999.
- [37] S. Khan, G. Shroff, J. Tarpara, and R. Srivastava. Scr applications: addressing coal characteristic concerns. EPRI-DOE-EPA, 1997.
- [38] P. Forzatti. Present status and perspectives in de-NO_x SCR catalysis. *Applied Catalysis A: General*, 222:221–236, 2001.
- [39] M. Kleemann, M. Elsener, M. Koebel, and A. Wokaun. Investigation of the ammonia adsorption on monolithic SCR catalyst by transient response analysis. *Applied Catalysis*, 27:231–242, 2000.
- [40] J.W. Beeckman and L.L. Hegedus. Design of monolith catalysts for power plant NO_x emission control. *Ind. Eng. Chem. Res.*, 30:969–978, 1991.
- [41] G. Busca, G. Ramis, and V. Lorenzelli. FT-IR study of the surface properties of polycrystalline vanadia. *Journal of Molecular Catalysis*, 50:231–240, 1989.
- [42] G. Ramis, C. Cristiani, A.S. Elmi, P. Villa, and G. Busca. Characterization of the surface properties of polycrystalline WO₃. *Journal of Molecular Catalysis*, 61:319–331, 1990.
- [43] L. Lietti. Reactivity of V₂O₅-WO₃/TiO₂ de-NO_x catalysts by transient methods. *Applied Catalysis B: Environmental*, 10:281–297, 1996.
- [44] L. Lietti, J.L. Alemany, P. Forzatti, G. Busca, G. Ramis, E. Giamello, and F. Bregani. Reactivity of V₂O₅-WO₃/TiO₂ catalysts in the selective catalytic reduction of nitric oxide by ammonia. *Catalysis Today*, 29:143–148, 1996.

- [45] L.J. Alemany, L. Lietti, N. Ferlazzo, P. Forzatti, G. Busca, E. Giammello, and F. Bregani. Reactivity and physicochemical characterization of V_2O_5 - WO_3 /TiO₂ De-NO_x catalysts. *Journal of Catalysis*, 155:117–130, 1995.
- [46] L. Casagrande, L. Lietti, I. Nova, P. Forzatti, and A. Baiker. SCR of NO by NH₃ over TiO₂-supported V_2O_5 -MoO₃ catalysts: reactivity and redox behavior. *Applied Catalysis B: Environmental*, 22:63–77, 1999.
- [47] P. Ciambelli, M.E. Fortuna, D. Sannino, and A. Baldacci. The influence of sulphate on the catalytic properties of V_2O_5 -TiO₂ and WO_3 -TiO₂ in the reduction of nitric oxide with ammonia. *Catalysis Today*, 29:161–164, 1996.
- [48] L. Lietti, J. Svachula, P. Forzatti, G. Busca, G. Ramis, and F. Bregani. Surface and catalytic properties of vanadia-titania and tungsta-titania systems in the selective catalytic reduction of nitrogen oxides. *Catalysis Today*, 17:131–140, 1993.
- [49] G. Ramis, G. Busca, and P. Forzatti. Spectroscopic analysis of titania-tungsta-vanadia deNO_xing catalysts. *Applied Catalysis B: Environmental*, 1:L9–L13, 1992.
- [50] G. Ramis, G. Busca, C. Cristiani, L. Lietti, P. Forzatti, and F. Bregani. Characterization of tungsta-titania catalysts. *Langmuir*, 8:1744–1749, 1992.
- [51] L. Lietti, G. Ramis, F. Berti, G. Toledo, D. Robba, G. Busca, and P. Forzatti. Chemical, structural and mechanistic aspects on NO_x SCR over commercial and model oxide catalysts. *Catalysis Today*, 42:101–116, 1998.
- [52] L.J. Alemany, F. Berti, G. Busca, G. Ramis, D. Robba, G.P. Toledo, and M. Trombetta. Characterization and composition of commercial V_2O_5 - WO_3 -TiO₂ SCR catalysts. *Applied Catalysis B: Environmental*, 10:299–311, 1996.
- [53] G. Ramis, G. Busca, V. Lorenzelli, and P. Forzatti. Fourier transform infrared study of the adsorption and coadsorption of nitric oxide, nitrogen dioxide and ammonia on TiO₂ Anatase. *Applied catalysis*, 64:243–257, 1990.
- [54] N.-Y. Topsøe. Characterization of the nature of surface sites on vanadia-titania catalysts by FTIR. *Journal of Catalysis*, 128:499–511, 1991.
- [55] S.T. Choo, Y.G. Lee, I.-S. Nam, S.-W. Ham, and J.-B. Lee. Characteristic of V_2O_5 supported on sulfated TiO₂ for selective catalytic reduction of NO by NH₃. *Applied Catalysis A: General*, 200:177–188, 2000.

Bibliography

- [56] L.J. Alemany, M.A. Bañares, E. Pardo, F. Martín-Jiménez, and J.M. Blasco. Morphological and structural characterization of a titanium dioxide system. *Materials Characterization*, 44:271–275, 2000.
- [57] I. Georgiadou, N. Spanos, Ch. Papadopoulou, H. Matralis, Ch. Kordulis, and A. Lycourghiotis. Preparation and characterization of various titanias (anatase) used as supports for vanadia-supported catalysts. *Colloids and Surfaces A: Physicochem. Eng. Aspects*, 98:115–165, 1995.
- [58] G.T. Went, L.-J. Leu, R.R. Rosin, and A.T. Bell. The effects of structure on the catalytic activity and selectivity of V_2O_5/TiO_2 for the reduction of NO by NH_3 . *Journal of Catalysis*, 134:492–505, 1992.
- [59] N.-Y. Topsøe, H. Topsøe, and J. A. Dumesic. Vanadia/Titania catalysts for selective catalytic reduction (SCR) of nitric oxide by ammonia. Combined temperature programmed in situ FTIR and on-line mass spectroscopy studies. *Journal of Catalysis*, 151:226–240, 1995.
- [60] L. Lietti, I. Nova, G. Ramis, L. Dell’Acqua, G. Busca, E. Giamello, P. Forzatti, and F. Bregani. Characterization and reactivity of $V_2O_5-MoO_3/TiO_2$ de- NO_x SCR catalysts. *Journal of Catalysis*, 187:419–435, 1999.
- [61] G. Ramis, L. Yi, and G. Busca. Ammonia activation over catalysts for the selective catalytic reduction of NO_x and selective catalytic oxidation of NH_3 . an FT-IR study. *Catalysis Today*, 28:373–380, 1996.
- [62] M.A. Larrubia, G. Ramis, and G. Busca. An FT-IR study of the adsorption of urea and ammonia over $V_2O_5-MoO_3-TiO_2$ SCR catalysts. *Applied Catalysis B: Environmental*, 27:L145–L151, 2000.
- [63] M.A. Centeno, I. Carrizosa, and J.A. Odriozola. $NO-NH_3$ coadsorption on vanadia/titania catalysis: determination of the reduction degree of vanadium. *Applied Catalysis B: Environmental*, 29:307–314, 2001.
- [64] S.M. Jung and P. Grange. DRIFTS investigation of V=O behavior and its relations with the reactivity of ammonia oxidation and selective catalytic reduction of NO over V_2O_5 catalyst. *Applied Catalysis B: Environmental*, 36:325–332, 2002.
- [65] U.S. Ozkan, Y. Cai, and M.W. Kumthekar. Mechanistic studies on vanadia catalysts for the selective catalytic reduction of nitric oxide using N-15 and O-18 isotopic labeling. Symposium on NO_x reduction 207th National Meeting, American Chemical Society, March 1994.

- [66] I. Nova, L. Lietti, E. Tronconi, and P. Forzatti. Dynamics of SCR reaction over TiO₂-supported vanadia-tungsta commercial catalyst. *Catalysis Today*, 60:73–82, 2000.
- [67] L. Lietti, I. Nova, S. Camurri, E. Tronconi, and P. Forzatti. Dynamics of the SCR-DeNO_x reaction by transient-response method. *AIChE Journal*, 43(10):2559–2570, October 1997.
- [68] L.G. Pinaeva, A.P. Suknev, A.A. Budneva, E.A. Paukshtis, and B.S. Bal'zhinimaev. On the role of oxygen in the reaction of NO reduction by NH₃ over monolayer V₂O₅-TiO₂ catalyst. *Journal of Molecular Catalysis A: Chemical*, 112:115–124, 1996.
- [69] M. Takagi, T. Kawai, M. Soma, T. Onishi, and K. Tamaru. The mechanism of the reaction between NO_x and NH₃ on V₂O₅ in the presence of oxygen. *Journal of Catalysis*, 50(3):441–446, 1977.
- [70] M. Calatayud, B. Mguig, and C. Minot. Modeling catalytic reduction of NO by ammonia over V₂O₅. *Surface science reports*, 55:169–236, 2004.
- [71] M. Gasior, J. Haber, T. Machej, and T. Czeppe. Mechanism of the reaction NO + NH₃ on V₂O₅ catalysts. *Journal of Molecular Catalysis*, 43(3):359–369, 1988.
- [72] C.U.I. Odenbrand, S.T. Lundin, and L.A.H. Andersson. Catalytic reduction on nitrogen oxides 1. The reduction of NO. *Applied Catalysis*, 18(2):335–352, 1985.
- [73] J.A. Dumesic, N.-Y. Topsøe, T. Slabiak, P. Morsing, B.S. Clausen, E. Tornqvist, and H. Topsøe. Proc. of 10th International Congress on Catalysis, Budapest, 1993.
- [74] N.-Y. Topsøe, M. Anstrom, and J.A. Dumesic. Raman, FTIR and theoretical evidence for dynamic structural rearrangements of vanadia/titania DeNO_x catalysts. *Catalysis Letters*, 76:11–20, 2001.
- [75] M. Anstrom, J.A. Dumesic, and N.-Y. Topsøe. Theoretical insight into the nature of ammonia adsorption on vanadia-based catalyst for SCR reaction. *Catalysis Letters*, 78:281–289, 2002.
- [76] M. Anstrom, N.-Y. Topsøe, and J.A. Dumesic. Density functional theory studies of mechanistic aspects of the SCR reaction on vanadium oxide catalysts. *Journal of Catalysis*, 213:115–125, 2003.

Bibliography

- [77] J. Marangozis. Comparison and analysis of intrinsic kinetics and effectiveness factors for the catalytic reduction of NO with ammonia in the presence of oxygen. *Ind. Eng. Chem. Res.*, 31:987–994, 1992.
- [78] A.M. Efstathiou and K. Fliatoura. Selective catalytic reduction of nitric oxide with ammonia over V_2O_5/TiO_2 catalyst: A steady-state and transient kinetic study. *Applied Catalysis B: Environmental*, 6:35–59, 1995.
- [79] L.J. Pinoy and L.H. Hosten. Experimental and kinetic modelling study of DeNO_x on an industrial $V_2O_5-WO_3/TiO_2$ catalyst. *Catalysis Today*, 17:151–158, 1993.
- [80] V. Tufano and M. Turco. Kinetic modelling of nitric oxide reduction over a high-surface area $V_2O_5-TiO_2$ catalyst. *Applied Catalysis B: Environmental*, 2:9–26, 1993.
- [81] C.U.I. Odenbrand, A. Bahamonde, P. Avila, and J. Blanco. Kinetic study of the selective reduction of nitric oxide over vanadia-tungstania/sepiolite catalyst. *Applied Catalysis B: Environmental*, 5:117–131, 1994.
- [82] J.A. Dumesic, N.-Y. Topsøe, H. Topsøe, Y. Chen, and T. Slabiak. Kinetics of selective catalytic reduction of nitric oxide by ammonia over vanadia/titania. *Journal of Catalysis*, 163:409–417, 1996.
- [83] H. Kamata, Takahashi K., and C.U. Odenbrand. Kinetics of the selective reduction of NO with NH_3 over a $V_2O_5(WO_3)/TiO_2$ commercial SCR catalyst. *Journal of Catalysis*, 185:106–113, 1999.
- [84] L. Lietti, I. Nova, E. Tronconi, and P. Forzatti. Transient kinetic study of the SCR-DeNO_x reaction. *Catalysis Today*, 45:85–92, 1998.
- [85] J. Brück and H.-G. Lintz. Combined kinetic and potentiometric measurements of the reduction of nitrogen monoxide on vanadia titania catalysts. *Chemical Engineering and Processing*, 38:571–577, 1999.
- [86] M.D. Amiridis, I.E. Wachs, G. Deo, J.-M. Jehng, and D.S. Kim. Reactivity of V_2O_5 catalysts for the selective catalytic reduction of NO by NH_3 : influence of vanadia loading, H_2O , and SO_2 . *Journal of Catalysis*, 161:247–253, 1996.
- [87] N.-Y. Topsøe. Influence of water on the reactivity of vanadia/titania for catalytic reduction of no_x . *Journal of Catalysis*, 134:742–746, 1992.

- [88] M.A. Buzanowski and R.T. Yang. Simple design of monolith reactor for selective catalytic reduction of NO for power plant emission control. *Ind. Eng. Chem. Res.*, 29:2074–2078, 1990.
- [89] E. Tronconi and P. Forzatti. Adequacy of lumped parameter models for SCR reactors with monolith structure. *AIChE Journal*, 38:201–210, 1992.
- [90] E. Tronconi, P. Forzatti, J.P. Gomez Martin, and S. Malloggi. Selective catalytic removal of NO_x: a mathematical model for design of catalyst and reactor. *Chemical Engineering Science*, 47:2401–2406, 1992.
- [91] A. Santos, A. Bahamonde, M. Schmid, P. Avila, and F. Garcia-Ochoa. Mass transfer influences on the design of selective catalytic reduction (SCR) monolithic reactors. *Chemical Engineering and Processing*, 37:117–124, 1998.
- [92] A. Beretta, C. Orsenigo, N. Ferlazzo, E. Tronconi, and P. Forzatti. Analysis of the performance of plate-type monolithic catalysts for selective catalytic reduction deNO_x applications. *Ind. Eng. Chem. Res.*, 37:2623–2633, 1998.
- [93] E. Tronconi and A. Beretta. The role of inter- and intra-phase mass transfer in the SCR-DeNO_x reaction over catalysts of different shapes. *Catalysis Today*, 52:249–258, 1999.
- [94] S.T. Kolaczkovski. Measurement of effective diffusivity in catalyst-coated monoliths. *Catalysis Today*, 83:85–95, 2003.
- [95] J.W. Beekman. Measurement of the effective diffusion coefficient of nitrogen monoxide through porous monolith-type ceramic catalysts. *Ind. Eng. Chem. Res.*, 30:428–430, 1991.
- [96] N. Wakao and J.M. Smith. Diffusion in catalyst pellets, 1962.
- [97] B. Roduit, A. Baiker, F. Bettoni, J. Baldyga, and A. Wokaun. 3D modeling of SCR of NO_x by NH₃ on vanadia honeycomb catalysts. *AIChE Journal*, 44:2731, 1998.
- [98] C.H. Bartholomew. Mechanisms of catalyst deactivation. *Applied Catalysis A: General*, 212:17–60, 2001.
- [99] P. Forzatti and L. Lietti. Catalyst deactivation. *Catalysis Today*, 52:165–181, 1999.

Bibliography

- [100] A.K. Neyestanaki, F. Klingstedt, T. Salmi, and D.Y. Murzin. Deactivation of postcombustion catalysts, a review. *Fuel*, 83:395–408, 2004.
- [101] I. Nova, L. dall’Acqua, L. Lietti, E. Giamello, and P. Forzatti. Study of thermal deactivation of a de-NO_x commercial catalyst. *Applied Catalysis B: Environmental*, 35:31–42, 2001.
- [102] J.P. Chen and R.T. Yang. Mechanism of poisoning of the V₂O₅/TiO₂ catalyst for the reduction of NO by NH₃. *Journal of Catalysis*, 125:411–420, 1990.
- [103] J.A. Moulijn, A.E. van Diepen, and F. Kapteijn. Catalyst deactivation: is it predictable? What to do? *Applied Catalysis A: General*, 212:3–16, 2001.
- [104] J. Blanco, P. Avila, C. Bahamonde, J.A. Odrizola, J.F. Garcia de la Banda, and H. Heinemann. Influence of phosphorus in vanadium-containing catalysts for NO_x removal. *Applied Catalysis*, 55:151–164, 1989.
- [105] L. Lietti, P. Forzatti, G. Ramis, G. Busca, and F. Bregani. Potassium doping of vanadia/titania de-NO_x catalysts: Surface characterization and reactivity study. *Applied Catalysis B: Environmental*, 3:13–35, 1993.
- [106] H. Kamata, K. Takahashi, and C.U.I. Odenbrand. The role of K₂O in the selective reduction of NO with NH₃ over V₂O₅(WO₃)/TiO₂ commercial selective catalytic reduction catalyst. *Journal of Molecular Catalysis A: Chemical*, 139:189–198, 1999.
- [107] L. Lisi, G. Lasorella, S. Malloggi, and G. Russo. Single and combined deactivating effect of alkali metals and HCl on commercial SCR catalysts. *Applied Catalysis B: Environmental*, 50:251–258, 2004.
- [108] F. Moradi, J. Brandin, M. Sohrabi, M. Faghihi, and M. Sanati. Deactivation of oxidation and SCR catalysts used in flue gas cleaning by exposure to aerosols of high- and low melting point salts, potassium salts and zinc chloride. *Applied Catalysis B: Environmental*, 46:65–76, 2003.
- [109] 5th European Conference on Industrial Furnace and Boilers. *Deactivation and regeneration of SCR catalysts used in bio fuel plants*, volume II, April 2001.
- [110] Y. Zheng, A.D. Jensen, and J.E. Johnsson. Deactivation of V₂O₅-WO₃-TiO₂ SCR catalyst at a biomass-fired combined heat and power plant. *Applied Catalysis B: Environmental*, 60:261–272, 2005.

- [111] L.L. Baxter, T.R. Miles, T.R. Miles Jr., B.M. Jenkins, T. Milne, D. Dayton, R.W. Bryers, and L.L. Oden. The behavior of inorganic material in biomass-fired power boilers: field and laboratory experiences. *Fuel Processing Technology*, 54:4778, 1998.
- [112] O. Kröcher and M. Elsener. Chemical deactivation of V_2/WO_3-TiO_2 SCR catalysts by additives and impurities from fuels, lubrication oils, and urea solution. I. Catalytic studies. *Applied Catalysis B: Environmental*, 75:215–227, 2008.
- [113] D. Nicosia, I. Czekaj, and O. Kröcher. Chemical deactivation of V_2/WO_3-TiO_2 SCR catalysts by additives and impurities from fuels, lubrication oils, and urea solution. II. Characterization study of the effect of alkali and alkaline earth metals. *Applied Catalysis B: Environmental*, 77:228–236, 2008.
- [114] H. Si-Ahmed, M. Calatayud, C. Minot, E. Lozano Diz, A.E. Lewandowska, and M.A. Bañares. Combining theoretical description with experimental in situ studies on the effect of potassium on the structure and reactivity of titania-supported vanadium oxide catalyst. *Catalysis Today*, 126:96–102, 2007.
- [115] J. Due-Hansen, S. Boghosian, A. Kustov, P. Fristrup, G. Tsilomelekis, K. Ståhl, C.H. Christensen, and R. Fehrmann. Vanadia-based SCR catalysts supported on tungstated and sulphated zirconia: Influence of doping with potassium. *Journal of Catalysis*, 251:459–473, 2007.
- [116] K. Wieck-Hansen, P. Overgaard, and O.H. Larsen. Cofiring coal and straw in a 150 MW_e power boiler experiences. *Biomass and Bioenergy*, 19:395–409, 2000.
- [117] K.A. Christensen and H. Livbjerg. A field study of submicron particles from the combustion of straw. *Aerosol Science and Technology*, 25:185–199, 1996.
- [118] K.A. Christensen, M. Stenholm, and H. Livbjerg. The formation of submicron aerosol particles, HCl and SO₂ in straw-fired boilers. *Aerosol Science and Technology*, 29:421–444, 1998.
- [119] Y. Zheng, A.D. Jensen, and J.E. Johnsson. Deactivation of $V_2O_5-WO_3-TiO_2$ SCR catalyst at biomass fired power plants: Elucidation of mechanisms by lab- and pilot-scale experiments. *Applied Catalysis B: Environmental*, 83:186–194, 2008.

Bibliography

- [120] R. Khodayari and C.U.I. Odenbrand. Regeneration of commercial SCR catalysts by washing and sulphation: effect of sulphate groups on the activity. *Applied Catalysis B: Environmental*, 33:277–291, 2001.
- [121] J.E. Staudt, T. Engelmeyer, W.H. Weston, and R. Sigling. The impact of arsenic on coal fired power plants equipped with SCR. Presented at ICAT Forum 2002, Houston, February 12-13 2002.
- [122] *SCR catalyst design issues and operating experience: coals with high arsenic concentrations and coals from Powder River Basin*, July 2000.
- [123] M. Ichiki. Poisoning kinetics by arsenic on the DeNO_x catalysts. Proceedings of the international conference on power engineering, Kobe, Japan, November 9-13 2003.
- [124] F.C. Lange, H. Schmelz, and H. Knözinger. Infrared-spectroscopic investigations of selective catalytic reduction catalysts poisoned with arsenic oxide. *Applied Catalysis B: Environmental*, 8:245–265, 1996.
- [125] E. Hums. Effects of As₂O₃ on the phase composition of V₂O₅-MoO₃-TiO₂ (anatase) DeNO_x catalysts. *Ind. Eng. Chem. Res.*, 30:1814–1818, 1991.
- [126] E. Hums. Mechanistic effects of arsenic oxide on the catalytic components DeNO_x catalysts. *Ind. Eng. Chem. Res.*, 31:1030–1035, 1992.
- [127] E. Hums. Deactivation behavior of SCR DeNO_x catalysts - basis for the development of a new generation of catalysts. Symposium on NO_x Reduction, 207th National Meeting, American Chemical Society, San Diego, CA, March 13-18 1994.
- [128] E. Hums. Understanding of deactivation behavior of DeNO_x catalysts: a key to advanced catalyst applications. *Kinetics and Catalysis*, 39:603–606, 1998.
- [129] J. Jensen, T. Slabiak, and F. Hansen. In *Modern Power Conference*, May 2005.
- [130] H. Kamata, K. Takahashi, and C.U.I. Odenbrand. Surface acid property and its relation to SCR activity of phosphorus added to commercial V₂O₅(WO₃)/TiO₂ catalyst. *Catalysis Letters*, 53:65–71, 1998.
- [131] J. Beck, R. Muller, J. Brandenstein, B. Matschenko, J. Matschke, S. Unterberger, and K.R.G. Hein. The behaviour of phosphorus in flue gases from coal and secondary fuel co-combustion. *Fuel*, 84:1911–1919, 2005.

- [132] R. Khodayari. *Selective Catalytic Reduction of NO_x: Deactivation and Regeneration Studies and Kinetic Modelling of Deactivation*. PhD thesis, Department of Chemical Engineering II, Lund University, Institute of Technology, April 2001.
- [133] R. Khodayari and C.U.I. Odenbrand. Deactivating effects of lead on the selective catalytic reduction of nitric oxide with ammonia over a V₂O₅/WO₃/TiO₂ catalyst for waste incineration applications. *Ind. End. Chem. Res.*, 37:1196–1202, 1998.
- [134] N.-Y. Topsøe, T. Slabiak, B.S. Clausen, T.Z. Srnak, and J. A. Dumesic. *Journal of Catalysis*, 134:742–746, 1992.
- [135] F. Castellino, S.B. Rasmussen, A.D. Jensen, J.E. Johnsson, and R. Fehrmann. Deactivation of vanadia-based SCR catalysts by polyphosphoric acids. *Applied Catalysis B: Environmental*, 83:110–122, 2008.
- [136] T.D. Farr. Phosphorus properties of the element and some of its compounds. Technical report, Tennessee Valley Authority, Chemical Engineering Report No. 8, U.S. Government Printing Office, Washington, D.C., 1950.
- [137] J.R. Van Wazer. *Phosphorus and Its Compounds*. Interscience Publisher, New York, 1958.
- [138] F. Castellino, A.D. Jensen, J.E. Johnsson, and R. Fehrmann. Influence of reaction products of K-getter fuel additives on commercial vanadia-based SCR catalysts. Part I. Potassium phosphate. *Applied Catalysis B: Environmental*, 86:196–205, 2009.
- [139] F. Castellino, A.D. Jensen, J.E. Johnsson, and R. Fehrmann. Influence of reaction products of K-getter fuel additives on commercial vanadia-based SCR catalysts. Part II. Simultaneous addition of KCl, Ca(OH)₂, H₃PO₄ and H₂SO₄ in a hot flue gas at a SCR pilot-scale setup. *Applied Catalysis B: Environmental*, 86:206–215, 2009.
- [140] L. Zhang and Y. Ninomiya. Transformation of phosphorus during combustion of coal and sewage sludge and its contribution to PM₁₀. *Proceedings of the Combustion Institute*, 31:2847–2854, 2007.

Appendix A

Deactivation of vanadia-based commercial SCR catalysts by polyphosphoric acids

Francesco Castellino^a, Søren Birk Rasmussen^{b,1}, Anker Degn Jensen^{a,*},
Jan Erik Johnsson^a, Rasmus Fehrmann^b

^aDepartment of Chemical Engineering, Technical University of Denmark, Building 229, DK-2800 Kgs. Lyngby, Denmark

^bChemistry Department, Technical University of Denmark, Building 207, DK-2800 Kgs. Lyngby, Denmark

Received 7 January 2008; received in revised form 8 February 2008; accepted 13 February 2008

Available online 17 February 2008

Abstract

Commercial vanadia-based SCR monoliths have been exposed to flue gases in a pilot-scale setup into which phosphoric acid has been added and the deactivation has been followed during the exposure time. Separate measurements by SMPS showed that the phosphoric acid formed polyphosphoric acid aerosols, which were characterized by particle number concentrations in the order of $1 \times 10^{14} \text{ \#}/\text{m}^3$ at 350 °C and diameters $<0.1 \text{ \mu m}$. Three full-length monoliths have been exposed to flue gases doped with 10, 100 and 1000 ppmv H_3PO_4 for 819, 38 and 24 h, respectively. At the end of the exposure the relative activities were equal to 65, 42 and 0%, respectively. After exposure, samples of the spent monoliths have been characterized by ICP-OES, Hg-porosimetry, SEM–EDX and in situ EPR. The results showed that the polyphosphoric acids chemically deactivate the vanadia-based catalysts by decreasing the redox properties of the catalyst surface and by titrating the number of V(V) active species. When plate-shaped commercial catalysts have been wet impregnated with different aqueous solutions of H_3PO_4 obtaining P/V ratios in the range 1.5–5, the relative activity for the doped catalysts in the whole P/V range was 0.85–0.90 at 350 °C. These results show that the presence of phosphor compounds in the flue gas may be much more harmful than indicated by simple wet chemical impregnation by phosphoric acid. The reason has been found in the nature of the polyphosphoric acid aerosol formed in the combustion process, which cannot be reproduced by the wet impregnation process.

© 2008 Elsevier B.V. All rights reserved.

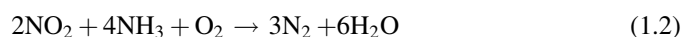
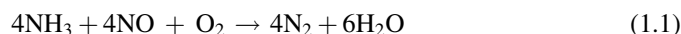
Keywords: SCR catalyst deactivation; Polyphosphoric acid; Vanadia; EPR; SMPS

1. Introduction

Biomass and waste (co)-firing with fossil fuels and NO_x reduction by selective catalytic reduction (SCR) are two practices of increasing application at stationary power stations, which, however, present some economical and technical challenges. Firing of secondary fuels such as biomass, meat and bone meal (MBM), sewage sludge and urban wastes is seen as a way to recover energy while decreasing the net CO_2 emissions. In countries like Denmark and Sweden this practice is forced by local regulations. NO_x emissions are also strictly

limited by national regulations, rendering the utilization of secondary measures like the SCR process necessary.

In the SCR process ammonia is injected into the flue gas and the gas is passed over a catalyst at 300–400 °C [1]. Here the undesired NO_x is reduced to molecular nitrogen according to the following global reactions:



Since NO accounts for roughly 95% of the total NO_x fraction at typical SCR conditions, reaction (1.1) can be considered the dominant SCR reaction.

Commercial catalysts are mainly constituted by vanadium oxide (V_2O_5) supported on a titania (TiO_2) carrier. The total load of V_2O_5 is around 1–5 wt.% depending on the specific application. WO_3 and MoO_3 are also added to the final composition improving both chemical and physical properties

* Corresponding author. Tel.: +45 45 25 28 41; fax: +45 45 88 22 58.

E-mail address: aj@kt.dtu.dk (A.D. Jensen).

¹ Present address: Instituto de Catálisis y Petroleoquímica, CSIC, c/Marie Curie 2, Cantoblanco 28049 Madrid, Spain.

of the catalyst. The catalysts are normally shaped into channels with hydraulic diameters up to 9 mm depending on the fly ash load. A widely accepted mechanism of reaction for these catalysts at typical industrial operating conditions was proposed by Topsøe et al. [2,3]. This involves adsorption of NH_3 on Brønsted acid sites, activation of adsorbed ammonia by $\text{V}=\text{O}$ species and subsequently reaction with gaseous or weakly adsorbed NO.

The SCR technology was first developed and optimized for fossil fuels applications: in the case of pure coal combustion, a catalyst at high dust position has an expected lifetime of up to 5 years. However, when applied at biomass or waste firing the SCR catalysts are reported to experience much faster rates of deactivation [4,5].

Deactivation of SCR catalyst can be due to poisoning, fouling, surface masking, and sintering according to the particular application. Phosphorus is known as a poison for the vanadia-based catalysts. Its poisoning strength was tested in the laboratory both using model $\text{V}_2\text{O}_5\text{--TiO}_2$ and commercial vanadia-based catalysts [6,7]. Generally authors report that poisoning by P is moderate. At 300 °C, a model 5% $\text{V}_2\text{O}_5\text{--TiO}_2$ catalyst wet impregnated with aqueous solution of H_3PO_4 lost about 30% of activity when $P/V = 1$ [6]. Moreover, Kamata et al. [7] found that P is able to some extent to form Brønsted acid sites, which are still able to adsorb ammonia, and could then actively participate in the SCR reaction. Blanco et al. [8] pointed out the negative influence of P on the surface area of vanadia-based honeycomb catalysts extruded with phosphoric acid. However, catalysts extruded with H_3PO_4 and having up to 12.3 wt.% P showed almost the same activity as a P-free catalyst. Beck et al. [9] analyzed SCR catalysts exposed at full-scale plants to flue gases from co-combustion of P-rich fuels (i.e. MBM, sewage sludge) and coal. The catalysts had up to 4.9 wt.% P_2O_5 on the external surface and both a decreased surface area and total pore volume. The authors regarded P as one of the main components responsible for the deactivation of the catalysts and hypothesized the following mechanisms of deactivation by P: (i) poisoning by gaseous P_2O_5 and/or H_3PO_4 ; (ii) pore condensation by polyphosphoric acids; (iii) deposition of alkali phosphates glasses. However, the catalysts were exposed to ill defined conditions and in the presence of other known poisons (e.g. K). Hence it was not possible to clearly point out the main mechanism of deactivation by P and its importance in the simultaneous presence of other deactivating species.

At the time of the writing, the addition of phosphorus compounds to biomass combustion processes is under investigation by Danish power companies [10,11]. It is suggested that this could be an effective measure to reduce the deposition of fly ash on the superheater surfaces, increasing the efficiency of biomass firing. In fact, during biomass combustion the fly ash is rich in K (mainly KCl and K_2SO_4) and has low melting points that make it particularly sticky at the temperatures of the superheater section. Addition of P and Ca has been found to form ashes in the P–K–Ca system with higher melting points and consequently lower tendency to deposit on the superheater exchangers. However, in this case the flue gas

could experience an important increase in total P-concentration [12]. Therefore all the potential drawbacks of this addition process have to be carefully examined at both lab- and pilot-scale, prior to any full-scale applications in the presence of an SCR reactor.

The main objective of this work was to investigate the deactivating effect of P under well defined and realistic operating conditions, thus helping the Danish power companies in foreseeing the potential effects of the P addition process on the SCR catalysts. Full-length commercial SCR monoliths have been exposed for more than 800 h to a flue gas doped with different water solutions of *ortho*-phosphoric acid in a pilot-scale SCR setup. The activity of the monoliths has been periodically tested during exposure and the deactivation mechanisms by P have been pointed out.

2. Experimental

In order to verify the condensation of *ortho*-phosphoric acid and have an online measurement of the activity of a SCR catalyst, a water solution of H_3PO_4 has been injected in a hot flue gas from a natural gas burner. The resulting mixture was then passed over a commercial SCR monolith, and the activity was periodically measured.

2.1. Catalysts

Commercial corrugated-type monoliths and plates obtained from Haldor Topsøe A/S were used in this study. The catalysts were based on V_2O_5 (up to 5 wt.%) and tungsten oxide (WO_3 , up to 9 wt.%) dispersed on a fiber reinforced TiO_2 carrier. The monoliths had a size of 75 mm × 75 mm × 500 mm. The hydraulic diameter of the channels was 6.44 mm and the wall thickness of about 1.0 mm. Pieces of both the fresh and spent monoliths have been cut from both the inlet and the outlet in order to study their local properties under well defined reacting conditions in a laboratory fixed bed reactor. In order to run activity tests on powdered samples, they have been gently crushed in a mortar and the particle fraction in the range 105–125 μm has been collected by sieving. Plate-shaped catalysts were doped with H_3PO_4 at three different levels by a wet impregnation method at room temperature under a vacuum of 0.8 bar absolute pressure to allow the solution to evenly penetrate into the catalyst pores. The catalyst plates had a dimension of 1 mm × 50 mm × 150 mm. They were dried at 120 °C for 1 h and then calcined at 400 °C for 4 h under a stream of 1 L/min of N_2 . The different P/V ratios obtained were measured by inductively coupled plasma optical emission spectroscopy (ICP-OES) and were equal to 1.8, 2.9 and 4.7.

2.2. SCR pilot plant

A schematic of the SCR pilot plant is shown in Fig. 1. The setup runs slightly below atmospheric pressure (5–8 mbar) for safety reasons. Natural gas is burned in the presence of excess air. The flue gas exiting the burner at 950–1000 °C is then led to a high temperature pipe, where the phosphoric acid solution is

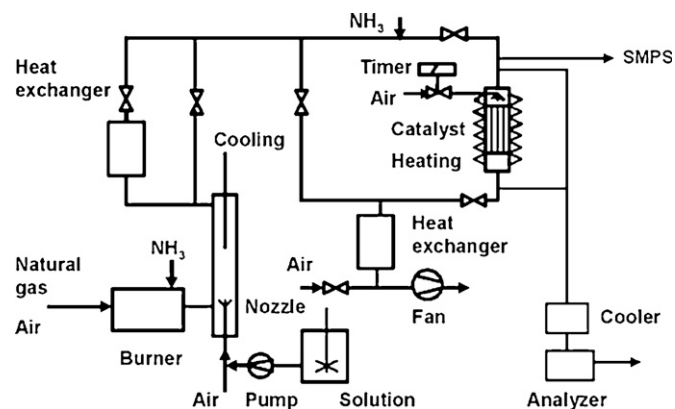


Fig. 1. Schematic drawing of the pilot-scale setup for catalyst monolith deactivation test.

injected. This is done by pumping the desired solution through a water-cooled lance inserted in the high temperature pipe having a two-fluid nozzle at the outlet. Here the water solution meets a flow of compressed air (also added through the lance) and is thus sprayed into the flue gas.

The temperature of the flue gas at the inlet of the SCR reactor can be controlled by adjusting the flow passing through a heat exchanger. For minor adjustments, or simply to avoid that a fraction of the flue gas experiences too low temperature affecting particle condensation rates, the temperature can be controlled by simply adjusting the position of bayonet heat exchanger inserted on the other side of the high temperature pipe. The gas flow is measured by a pitot tube situated at the inlet of the SCR reactor. A throttle valve is used to bypass part of the flue gas and get the desired flow through the reactor.

Ammonia is added into the burner in order to obtain a NO concentration of ~ 500 ppmv at the SCR reactor inlet. If NH_3 was not added, only 80 ppmv of NO would have been present.

The reactor is a squared duct where the catalyst element is vertically supported. In order to have a constant temperature along the whole element, two electric heating wires with temperature control are installed around the reactor. In this way the temperature difference between the inlet and the outlet of the reactor was always kept less than 3°C .

Plate-shaped catalysts have been exposed to the P-rich flue gases by placing them in the pipe downstream the SCR reactor using a squared-plate-holder designed for this purpose.

2.3. H_3PO_4 addition

The addition of H_3PO_4 to the flue gas was performed by spraying different acid water solutions through a nozzle as described above. The solutions were prepared by diluting 85% H_3PO_4 (Fluka Inc.) with distilled water. Three catalyst elements have been exposed to 10, 100 and 1000 ppmv H_3PO_4 . In this work they will be identified by the labels “P10”, “P100” and “P1000”, respectively. The letters “T” and “B” added at the end of the labels will indicate a sample cut respectively from the top (first 5 cm) or the bottom (last 5 cm) of element. In all tests, the solution feed was fixed at 1.25 L/h and the acid concentrations were 0.018, 0.18 and 1.8 mol/L, respectively.

During the 100 ppmv test, five catalyst plates were also exposed. They will be referred as P100plate in this work.

2.4. Activity measurements

The rate of SCR reaction at typical industrial reacting conditions has been assumed to follow an Eley-Rideal mechanism of reaction with NH_3 adsorbed on the catalyst surface and NO reacting from the gas-phase. The following expression for the rate of reaction, r_{NO} , can then be derived:

$$-r_{\text{NO}} \left(\frac{\text{mol}}{\text{m}^3\text{s}} \right) = k c_{\text{NO}} \frac{K_{\text{NH}_3} c_{\text{NH}_3}}{1 + K_{\text{NH}_3} c_{\text{NH}_3}} \quad (1.3)$$

where k (1/s) is the rate constant, c_{NO} and c_{NH_3} (mol/m^3) are the concentrations of NO and NH_3 , respectively, and K_{NH_3} (m^3/mol) is the adsorption constant for NH_3 on the catalyst surface. The fraction term on the right-hand side of Eq. (1.4) is the NH_3 coverage of the catalytic surface, θ_{NH_3} .

At the pilot plant, the activities of the catalysts were measured at 350°C in the presence of about 500 ppmv NO, 600 ppmv NH_3 , 10 vol.% O_2 , 6 vol.% CO_2 , and about 10 vol.% H_2O . During activity measurements (where not stated differently) the flow through the SCR reactor was normally kept at $40 \text{ Nm}^3/\text{h}$. At this flow the gas velocity in the channel was about 6.5 m/s at 350°C , thus similar to the velocities used at full-scale applications, and up to 50% external mass transfer limitations have been estimated.

Since ammonia in our measurements is added in excess with respect to NO (i.e. $\text{NH}_3/\text{NO} \approx 1.2$), the NH_3 coverage, θ_{NH_3} , can be assumed equal to one and the reaction rate can be regarded as pseudo-first order with respect to NO and zero order with respect to NH_3 . Therefore, directly from the fractional NO conversion, X , it is possible to calculate an observed catalyst activity constant, k' , that includes both the influence of external and internal mass transfer:

$$k' \left(\frac{\text{mL}}{\text{g s}} \right) = - \frac{F_{\text{gas}}}{m_{\text{cat}}} \ln(1 - X) \quad (1.4)$$

where F_{gas} is the gas flow rate (mL/s), m_{cat} is the weight of catalyst (g). The degree of deactivation can be then calculated as the ratio k/k_0 between the activity constant of the catalyst during exposure, k , and the one measured for the fresh element, k_0 , right before starting the poison addition.

In the laboratory, powdered samples have been tested for activity in a packed bed quartz micro-reactor with a diameter equal to 10 mm. Around 0.07 g of powder has been used during activity measurement with a total flow equal to $2.8 \text{ NL}/\text{min}$ constituted by 500 ppmv NO, 600 ppmv NH_3 , 5% O_2 and 1.4% H_2O in N_2 . Activity measurements have been performed in the temperature range $250\text{--}400^\circ\text{C}$. The catalyst activity has been calculated according to Eq. (1.5) and the deactivation as the ratio between the activity constant of the spent catalyst and the one measured for the fresh one. At 350°C , the observed activity constant for the fresh catalyst was found only 10% less than the one calculated in the total absence of mass transfer limitations. The latter value was calculated by extrapolating at higher

temperatures the Arrhenius fitting obtained in the range 250–330 °C. No NH₃ oxidation has been measured up to 350 °C during an empty reactor test. In the case of the plates, the activity tests were carried out in another quartz reactor with a diameter equal to 18 mm. The plates were cut into 15 mm × 15 mm bits. Only one bit, corresponding to around 0.17 g of catalyst, was used for each measurement. This was placed in the center of the reactor and supported by small glass indentations especially designed for the purpose. The total flow and gas composition used during the activity measurements on plates were the same as the ones used for the powders. In previous tests carried out at different flows, it has been shown that when 2.8 NL/min were used, the rate of reaction could be assumed not limited by external mass transfer limitations up to 350 °C.

During all activity measurements, the NO concentration in the dry mixture was measured by conventional UV analyzers (Rosemount NGA 2000).

2.5. Ammonia chemisorption

NH₃ chemisorption is the first step of the reaction mechanism [2,3]. Therefore, NH₃ chemisorption studies have been made to investigate the mechanism of deactivation due to polyphosphoric acid deposition. The tests were carried out in our laboratories using the fixed bed quartz reactor and the catalyst plates. The complete SCR gas mixture described in the previous section was prepared. All the mixture components but NO were then let into the reactor and passed over the catalyst for 30 min. During this time, the catalyst surface got saturated with NH₃. After this saturation period, the NH₃ addition was shut off and the NO flow was added to the rest of the mixture. Reaction between NO and the previously chemisorbed NH₃ then took place and the amount of NH₃ on the catalyst was calculated from the amount of NO reduced.

2.6. Aerosol measurements

To get a better understanding of polyphosphoric acids formation, aerosols measurements have been carried out at the SCR pilot plant. The particle concentration and size distribution were measured by a Scanning Mobility Particle Sizer (SMPS, TSI Inc.), which included an Electrostatic Classifier (Model 3080) and a Condensation Particle Counter (Model 3775). Particle sampling was carried out at the inlet of the SCR reactor by an ejector sampler running with dry, particle-free air. In this system the particle-containing flue gas was at the same time cooled and diluted. In this way: (i) water condensation was prevented by keeping the sample well above the water dew point; (ii) the rate of coagulation in the sample line was effectively decreased by several orders of magnitude; (iii) overloading of both the impactor and the SMPS was prevented. The dilution ratio, needed to know the real particle concentration in the flue gas, was obtained by measuring the CO₂ concentration both in the flue gas and in the diluted sample. The aerosol measurements were carried out during addition of H₃PO₄ in the range 10–400 ppmv.

2.7. Catalyst characterization

Small pieces of catalyst were cut from the ends of both fresh and exposed monoliths and characterized with respect to bulk chemical composition, mercury porosimetry and physical appearance by a scanning electron microscope (SEM).

The chemical composition was obtained by ICP-OES at the laboratory of DONG Energy A/S and Haldor Topsøe A/S. Prior to the measurements, the samples were cut to 1.5 cm × 1.7 cm and dried at 105 °C for 2 h before analysis.

The total pore volume and the pore size distribution of the different catalyst sample were made by mercury intrusion in a Micromeritics Autopore II 9220 porosimeter. SEM–EDX analysis was performed at the Teknologisk Institut using a Zeiss Ultra55 and an Oxford ISIS with a Pentafet X-ray detector.

2.8. In situ EPR spectroscopy

Samples (~0.030 g) of both the fresh and the exposed monoliths at the pilot plant (P10 and P100) were placed into a micro-reactor cell specially designed for high temperature EPR measurements using a Bruker ER 4114 HT cavity [13,14]. The spectra were recorded in situ at 350 °C in a flow of around 100 mL/min simulated flue gas. After thermal equilibration, the catalysts were first exposed to a reactant gas composition consisting of 1000 ppmv NO, 3.5% O₂, 3% H₂O in N₂. After acquisition of a spectrum at stationary conditions, 1000 ppmv NH₃ was added to the gas mixture. Again after acquisition at stationary conditions, NO was omitted from the reactant gas and the final spectrum was recorded. Spectra were recorded with 1024 points from 2500 to 4500 G, using a time constant of 82 ms and a total sweep time of 84 s. The resonance frequencies were around 9.534 GHz. Modulation frequency and amplitude were 100 kHz and 8.12 G, respectively.

3. Results

3.1. Aerosol measurements at the pilot-scale setup

Table 1 summarizes the main results of the SMPS measurements carried out. In Fig. 2 the particle size distribution (PSD) for the tests with 10, 50, 100 and 400 ppmv of H₃PO₄ are shown. In all the measurements the PSD consisted of only one clear peak. The mean particle size, which was calculated from the total number concentration, was found to vary in the range 25–70 nm and was increasing with the acid concentration in the flue gas. The order of magnitude of the total particle number concentration was equal to 1×10^{14} particles/m³. A blank measurement where only distilled water was sprayed into the setup has also been performed. The results of this measurement showed the presence of particles with a mean diameter equal to 5.81 nm. The total particle number concentration was more than 10 times lower than the one measured when adding 10 ppmv of acid. Table 1 also reports the total P-concentration in the particles measured by the SMPS, together with the ratio between this concentration and the total P injected as H₃PO₄.

Table 1
Performed SMPS experiments

| Experiment | | SMPS results | | | |
|---|-----------------------------|-----------------------------|--|-------------------------------|----------------------|
| H ₃ PO ₄ added (ppmv) | P-added (g/m ³) | Particle mean diameter (nm) | Particle total concentration (#/m ³) | P-content (g/m ³) | P-inlet fraction (%) |
| 10 | 0.006 | 25.0 | 3.76E+14 | 0.003 | 50 |
| 20 | 0.012 | 31.8 | 4.63E+14 | 0.008 | 66 |
| 30 | 0.018 | 36.2 | 5.20E+14 | 0.013 | 72 |
| 40 | 0.024 | 39.7 | 5.42E+14 | 0.018 | 75 |
| 50 | 0.030 | 42.8 | 5.82E+14 | 0.024 | 80 |
| 70 | 0.042 | 46.9 | 6.30E+14 | 0.034 | 81 |
| 100 | 0.061 | 50.1 | 6.14E+14 | 0.041 | 67 |
| 200 | 0.121 | 59.4 | 7.13E+14 | 0.085 | 70 |
| 300 | 0.181 | 63.6 | 7.63E+14 | 0.103 | 57 |
| 400 | 0.243 | 66.9 | 8.14E+14 | 0.127 | 52 |

The P-content of the particles has been calculated by assuming the particles at the azeotropic mixture (P₂O₅ = 92.4 wt.%). *T* = 350 °C.

The P-content of the particles has been calculated by assuming the particles constituted by 92.4 wt.% P₂O₅. The reasons for this assumption will be clearer in Section 4.1. The particle density, ρ , has then been calculated as

$$\rho = (0.7102 + 0.01617 \text{ P}_2\text{O}_5 \text{ wt.}\%) - (11.7E - 4 - 6.00E - 6 \text{ P}_2\text{O}_5 \text{ wt.}\%)T$$

where *T* is the temperature in °C [15]. From the values reported in Table 1, it can be seen that 50–81% of the injected P reaches the catalyst in the particles. Apparently, the mass fraction of P that reaches the inlet of the SCR reactor goes through a soft maximum around 70 ppmv. The remaining may be in the gas-phase or is deposited on the walls of the setup before the catalyst.

3.2. Activity tests at the pilot-scale setup

The three catalyst elements P10, P100 and P1000 have been exposed for 819, 38 and 24 h, respectively. Prior to exposure,

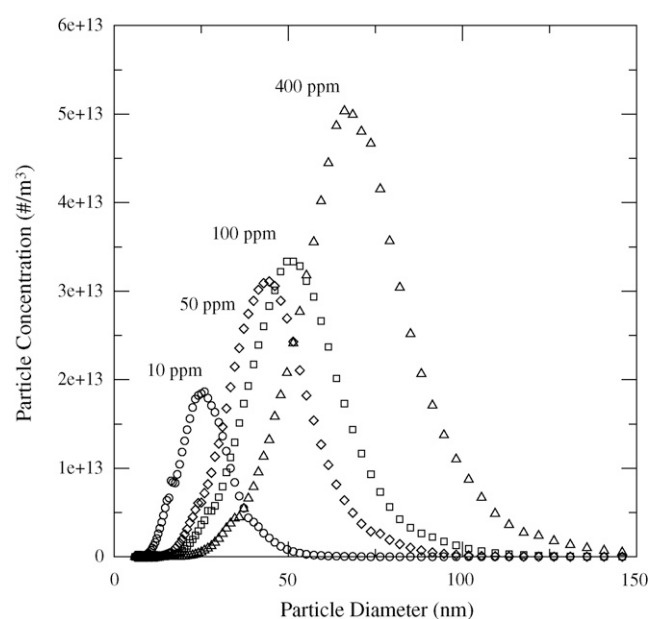


Fig. 2. Particle size distribution of polyphosphoric acids measured at the SCR reactor inlet at different H₃PO₄ addition by SMPS. *T* = 350 °C.

each element has been exposed to a “clean” flue gas for at least 1 week or until its activity had reached a stable value. The different values of activity for the fresh elements have then been used to calculate the relative activity of each catalyst element.

The results of the different deactivation tests are presented in a chronological order.

3.2.1. Exposure to 1000 ppmv H₃PO₄

The addition of 1000 ppmv H₃PO₄ was carried out for 24 h. During the first 2 h of exposure, the activity of the catalyst element was continuously measured. The results of the measurement are shown in Fig. 3. As it can be seen from this, the relative activity rapidly decreased as soon as the P-rich flue gas was flowing through the SCR reactor. After only 2 h the element lost already 33% of its original activity. At the end of the acid addition, the monolith showed no activity at all. The

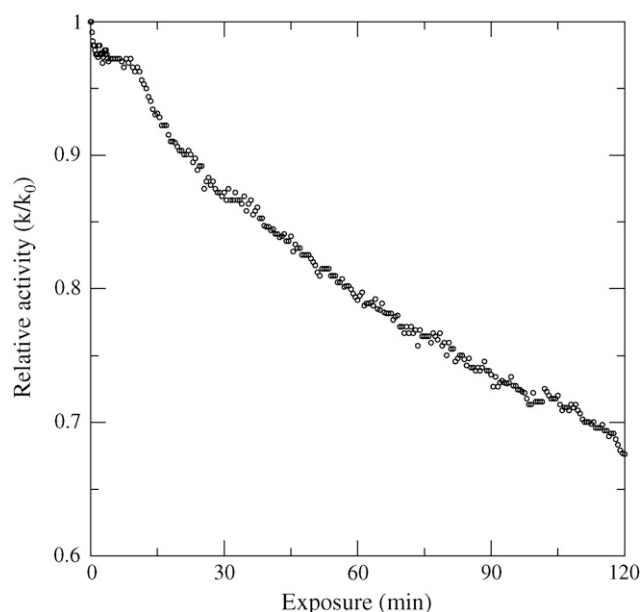


Fig. 3. Relative activity of the P1000 element during the first 2 h of exposure. *T* = 350 °C. Total flow 40 N m³/h. Gas composition on dry basis NO = 496 ppmv, NH₃ = 735 ppmv, O₂ = 10 vol.%, CO₂ = 6 vol.%, N₂ balance. 10 vol.% H₂O.

results show that high level of P in the flue gas may be very harmful to the catalyst.

This test had a tremendous impact on the whole setup. A lot of acid was found deposited on the setup pipe walls and therefore an extensive cleaning was carried out before starting the test at lower acid concentrations.

3.2.2. Exposure to 10 ppmv H_3PO_4

The addition of 10 ppmv H_3PO_4 corresponds to about 32 mg/Nm³ of P_4O_{10} in the flue gas, which is well below the expected P_4O_{10} concentration (3500 mg/Nm³) assuming a 4% co-firing thermal share of sewage sludge with a P-content of 7% and a solid–gas conversion equal to 50% [9]. Fig. 4 shows the decrease in relative activity of the exposed catalyst element. A fresh monolith was charged and exposed to a “clean” flue gas for about 430 h. This time was required in order to get a steady value for the NO conversion. However, the element had already lost about 28% of its original activity, probably due to deposit remaining in the setup even after the cleaning. The addition of 10 ppmv H_3PO_4 was then started. The exposure to the flue gas containing 10 ppmv H_3PO_4 further deactivated the catalyst. However this deactivation was found to be rather slow. Globally, the relative activity leveled off at around 65%, meaning that the element lost 7% of activity since the start of the exposure to 10 ppmv H_3PO_4 . The results indicate that low levels of P in the flue gas may not be very harmful to the catalyst.

During the activity measurements, a transient in the NO conversion was noted when NH_3 was added. This phenomenon was even more evident during the exposure to 100 ppmv H_3PO_4 , and will be therefore presented in the next section.

3.2.3. Exposure to 100 ppmv H_3PO_4

The addition of 100 ppmv H_3PO_4 was carried out for only 38 h. After this time, the element was exposed to a clean flue

Table 2

Results of the activity measurements performed with the P100 element

| Operating time (h) | H_3PO_4 addition (h) | X | | k/k_0 | |
|--------------------|------------------------|-------|--------------|---------|--------------|
| | | Max | Steady state | Max | Steady state |
| 0 | 0 | 0.585 | 0.585 | 1 | 1 |
| 20 | 20 | 0.569 | 0.390 | 0.957 | 0.562 |
| 134 | 38 | 0.549 | 0.312 | 0.905 | 0.425 |
| 158 | 38 | 0.531 | 0.366 | 0.861 | 0.518 |
| 180 | 38 | – | 0.369 | – | 0.523 |
| 471 | 38 | 0.535 | 0.388 | 0.871 | 0.558 |

gas for additional 433 h. Table 2 reports the activity measurements carried out. During all the measurements, the NO conversion was found to first go through a maximum and then reach a steady level at lower values as a function of time. In Table 2, both the maximum and steady state are reported. Fig. 5 shows the activity measurement carried out after 134 h of operating time. Here, the NO concentration in the flue gas is plotted against the time of the activity measurement. For times less than 0, no ammonia is present in the flue gas and about 514 and 484 ppmv NO are present at the reactor inlet and outlet, respectively. This difference was simply due to dilution of the flue gas with ambient air entering the setup from the pipe flanges. At time 0, around 600 ppmv of NH_3 are added to the flue gas and, as a result of the SCR reaction, the NO concentration starts decreasing until it reaches a concentration of 218 ppmv, corresponding to a NO conversion, X , of 55% and a relative activity, k/k_0 , of 0.91. However, right after reaching this value, the NO concentration in the flue gas starts increasing and reaches a steady-state value at 333 ppmv after about 1 h. In the meantime, the NO concentration at the inlet was measured twice in order to verify that the NO transient was not due to changes in the inlet values. In both cases, this was found equal to about 504 ppmv. This value was only 10 ppmv lower than the initial one and could have been caused by only few degrees change in the burner. At steady state, neglecting the small change in NO inlet concentration, the NO conversion, X , was equal to 0.31, corresponding to a relative activity, k/k_0 , equal to 42%. After having reached the steady state, the amount of NH_3 to the SCR reactor was doubled. Interestingly, the relative activity of the element increased to 50%. Since ammonia is introduced as a pure gas, it is excluded that the drop in NO concentration shown in Fig. 5 is due to dilution of the flue gas. This effect is more likely related to changes in the NH_3 adsorption properties of the P100 surface.

From the analysis of the activity measurements reported in Table 2, it is possible to see that at increasing time of H_3PO_4 exposure, both the maximum and the steady-state value of NO conversion are decreasing. However, when the element was exposed to a H_3PO_4 -free flue gas for some time, it slowly regained some activity. In fact, both the maximum and the steady-state values of NO conversion increased, indicating that part of the deposited acid causing the deactivation is slowly leaving the catalyst.

As it will be discussed later, it is believed that this element is clearly showing effects of chemical deactivation due to

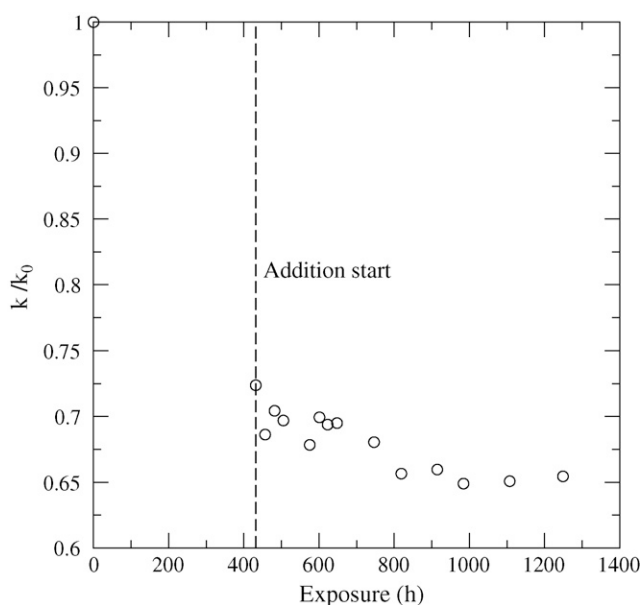


Fig. 4. Relative activity of P10 at 350 °C as a function of exposure time. Total flow 40 N m³/h. Average gas composition NO = 500 ppmv, NH_3 = 735 ppmv, O_2 = 10 vol.%, CO_2 = 6 vol.%, and 10 vol.% H_2O in N_2 .

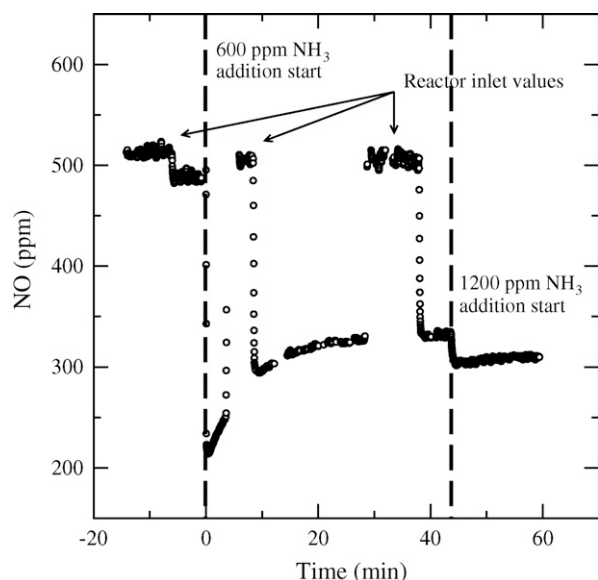


Fig. 5. Activity measurement for P100 at 350 °C and 50 N m³/h after 134 h of operating time. Gas composition on dry basis NO = 515 ppmv, NH₃ = 600–1200 ppmv, O₂ = 11 vol.%, CO₂ = 5.6 vol.%, N₂ balance. 10 vol.% H₂O.

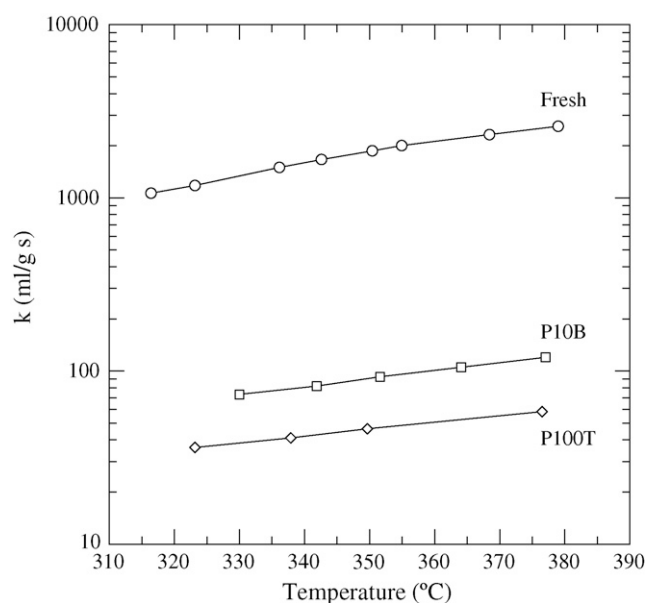


Fig. 6. Activity test on powdered samples. Total flow 2.8 N L/min. NO = 521 ppmv, NH₃ = 622 ppmv, O₂ = 5.2%, H₂O = 1.47%, N₂ balance. Catalyst mass W = 0.072 g.

polyphosphoric acids associated with the transient in NO conversion and due to the formation of V–P–O–NH₃ species, which are not or less active in the reduction of NO than the original sites. Finally, it is worth noting that the NO transient was fully reproducible provided that the NH₃ was shut off for about 1 h. If the element was exposed to an NH₃-free flue gas for shorter times before NH₃ was reintroduced in the flue gas, the NO transient was still present, but the measured maximum NO conversion was lower. This shows that it takes quite some time for the surface complexes to be consumed.

3.3. Lab-scale investigations

3.3.1. Activity tests on catalyst deactivated at the pilot-scale setup

The activity tests on powdered spent and fresh monoliths are shown in Fig. 6. The plot only reports the results in the

temperature range 320–380 °C, where external and internal mass transfer have been estimated not to limit the observed reaction rate. Therefore, the values reported in the plot represent the pseudo-first order intrinsic reaction rate constants. Both the powdered P10B and P100B showed an extreme deactivation: at 350 °C they retained only 5 and 2.6% of their original activity, respectively.

3.3.2. Activity tests on wet impregnated plates

The relative activities of the three different impregnated plates were found in the range 0.85–0.90. Even though the P/V ratios (i.e. 1.8, 2.9 and 4.7) for these plates were comparable to the ones measured on the monoliths P10 and P100 (Table 3), their deactivation was much lower, in agreement with other works [6,7] where both model and commercial catalysts have been doped by a wet impregnation method. The results indicate

Table 3
Results of the bulk and surface chemical analysis, and of the Hg-porosimetry for the fresh and spent monoliths.

| | Monolith | | | | | | Plate | |
|-------------------------------------|----------|-------|-------|-------|-------|--------|-------|-----------|
| | Fresh | P10T | P10B | P100T | P100B | P1000B | Fresh | P100plate |
| Bulk chemical analysis | | | | | | | | |
| V (% w/w) | 1.60 | 1.66 | 2.85 | 3.12 | 1.87 | 0.70 | 1.00 | 0.87 |
| P (% w/w) | 0.01 | 3.29 | 3.02 | 4.17 | 4.19 | 18.70 | 0.10 | 6.07 |
| P/V (mol/mol) | | 3.26 | 1.74 | 2.20 | 2.10 | 43.94 | | 11.48 |
| Surface chemical analysis | | | | | | | | |
| V (% w/w) | 2.1 | 3.1 | 3.3 | 3.9 | 2.7 | 1.1 | | |
| P (% w/w) | 0.0 | 5.4 | 4.4 | 7.9 | 6.3 | 21.8 | | |
| P/V (mol/mol) | 0.0 | 2.8 | 2.2 | 3.3 | 3.9 | | | |
| Hg-porosimetry | | | | | | | | |
| Total intrusion volume (mL/g) | 0.71 | 0.57 | 0.58 | 0.42 | 0.53 | 0.06 | 0.82 | 0.44 |
| Total pore area (m ² /g) | 36.84 | 31.16 | 22.77 | 19.60 | 30.67 | 5.42 | 73.05 | 17.19 |
| Catalyst bulk density (g/mL) | 0.96 | 1.15 | 1.14 | 1.38 | 1.17 | 2.11 | 0.89 | 1.20 |
| Porosity (%) | 68.60 | 65.27 | 66.47 | 57.73 | 61.96 | 11.83 | 73.02 | 53.02 |

that when P does not experience temperatures higher than the calcination temperature used during the doping process, it is not present on the catalyst surface as a polyphosphate. Its deactivating strength is therefore limited.

3.3.3. NH_3 chemisorption tests

Fig. 7 shows the results of the NH_3 chemisorption test performed at 350 °C with a sample cut from P100plate and a fresh plate of the same type. As it can be seen from the plot, the amount of NH_3 adsorbed on the P-deactivated sample was much higher than on the fresh sample. In fact, the P-deactivated sample is able to adsorb about five times more NH_3 than the fresh catalyst. This is in agreement with the increased acidity of the catalyst surface due to deposition of the polyphosphoric acids. However, the activity measurements show that the NH_3 adsorbed on the polyphosphates is much less active (or even non-active), which indicates that in the chemisorption test this NH_3 acts mainly as a reservoir.

3.4. In situ EPR spectroscopy

Fig. 8 shows the in situ EPR spectra of VO^{2+} present on the samples taken from exposure tests of the fresh, P10 and P100 elements measured at 350 °C. Vanadium in oxidation states +5 and +3 are both invisible in EPR at these temperatures. The oxidising mixture NO , O_2 , H_2O in N_2 is leaving the active oxovanadium species present on the catalyst surface mainly in their oxidation state +5. Under these conditions, the spectrum of the fresh catalyst exhibits a broad band from polymeric surface vanadium species. Superimposed on this, a spectrum exhibiting poorly resolved hyperfine structure is observed. The latter appears to be from dimeric V(IV) species, with only the most significant peaks clearly visible. No significant presence of monomeric V(IV) species at this temperature under oxidising

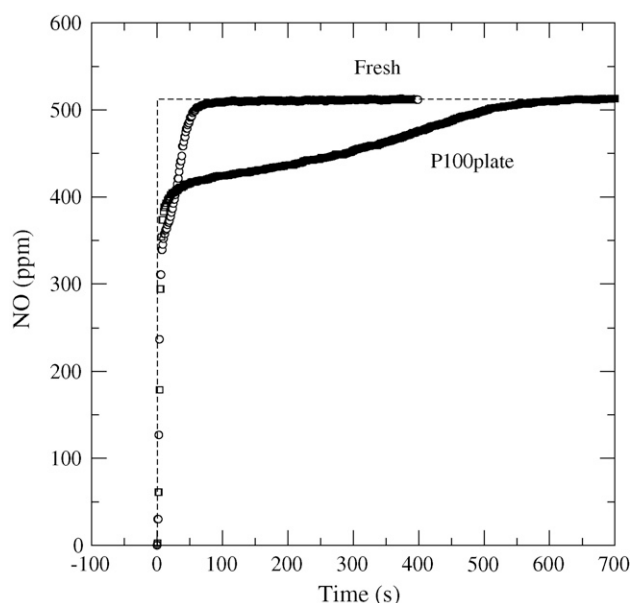


Fig. 7. NH_3 chemisorption test on fresh and P100 mini plate samples at 350 °C. Total flow 2.75 N L/min. NO = 501 ppmv, NH_3 = 601 ppmv, O_2 = 5%, N_2 balance. Catalyst mass W = 0.45 g.

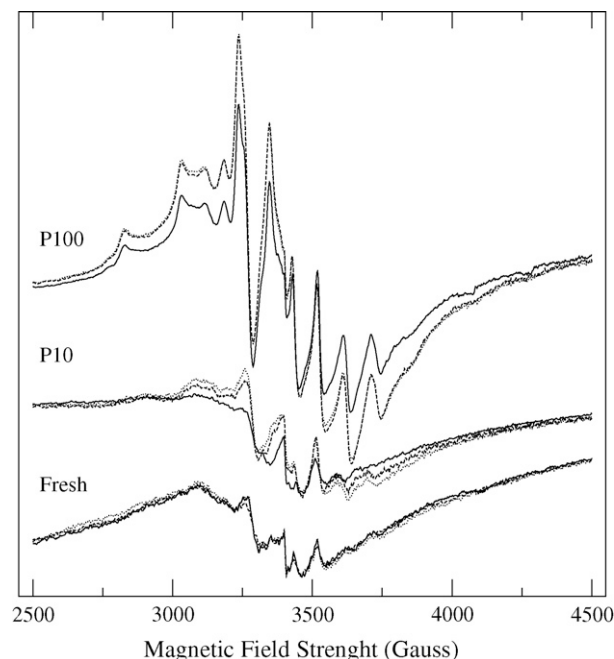


Fig. 8. In situ EPR spectra acquired at 350 °C of catalyst samples taken from pilot plant tests fresh, P10 and P100, exposed to various simulated flue gas compositions. Gas composition: 1000 ppmv NO (—), 1000 ppmv NO + 1000 ppmv NH_3 (···), 1000 ppmv NH_3 (- - -) and 3.5% O_2 , 3% H_2O in N_2 .

conditions is observed. During exposure to NH_3 -containing gases, the redox chemistry of the fresh catalyst surface is not altered at all, as shown by the identical spectra, which were recorded during exposure to the different gas mixtures.

The P10 sample essentially shows the same spectrum as the fresh catalyst after equilibration in the oxidising NO , O_2 , H_2O , N_2 atmosphere. However, unlike the uncontaminated sample, the exposure to an NH_3 -containing mixture caused an increase in VO^{2+} (or $(\text{VO}^{2+})_n$) content. In particular, the spectrum of the sample equilibrated in the SCR gas mixture exhibited the greatest difference from oxidising conditions.

Contrarily to the previous results, P100 showed a significantly increased broad band of polymeric $(\text{VO}^{2+})_n$ species even during exposure to the oxidising gas mixture. Superimposed on this signal, a new but recognisable contribution from monomeric VO^{2+} species is observed.

3.5. Catalyst characterization

The V- and P-content on both the surface and bulk of the fresh and doped catalyst are shown in Table 3. The results of the mercury porosimetry are also reported in Table 3. In all the tested cases, the P-levels in the bulk were found slightly higher at the inlet compared to the outlet of the catalyst element, according to both the higher particle concentration and the higher mass transfer due to the developing flow and higher level of turbulence.

The P-content of the P100 element was found slightly higher than the one measured for the P10 (i.e. about 4 wt.% against 3 wt.%). Considering the big difference in exposure time for the two experiments (819 h vs. only 38 h), and assuming a linear

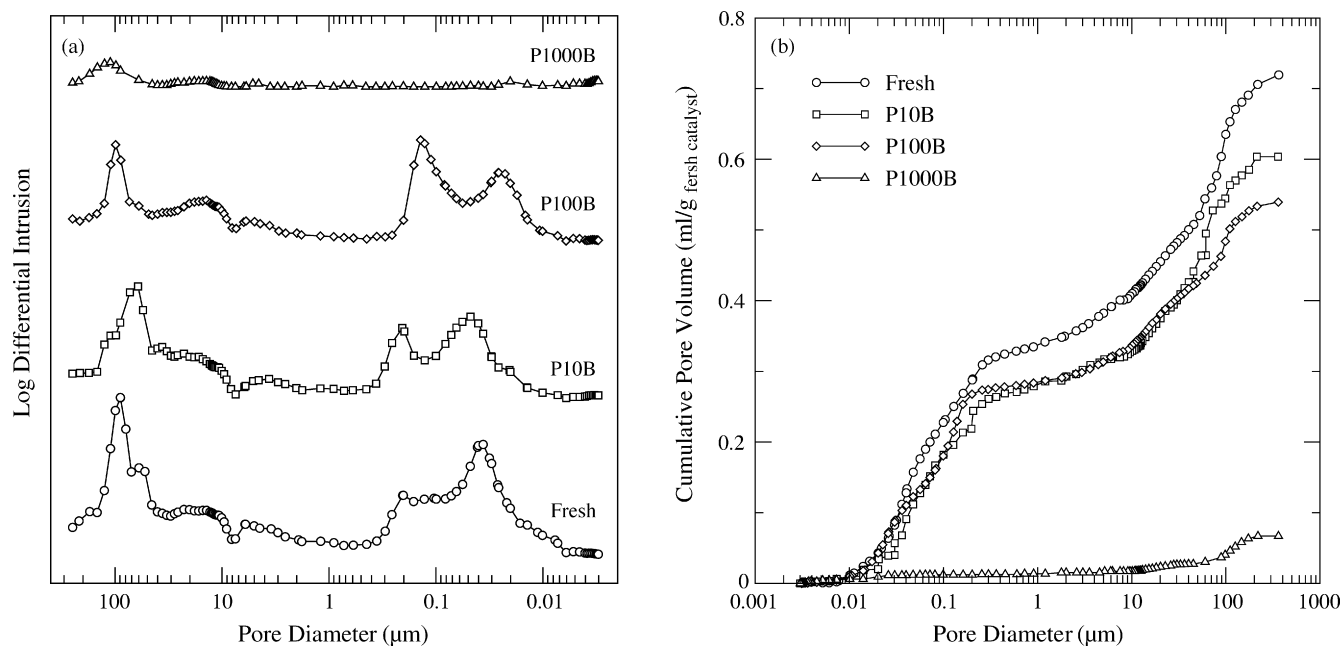


Fig. 9. Pore size distribution and cumulative intrusion volume measured by Hg-porosimetry with different monolithic samples.

and constant deposition of P vs. time, it can be calculated that the overall accumulation rates have been 0.09%/day and 2.6%/day for P10 and P100, respectively. Assuming a first order process for the particle deposition (i.e. the fraction of deposited particles not depending on the total particle concentration number) and making the conservative assumption that the particle formed during the addition of 10 ppmv H_3PO_4 have the same diffusivity of the bigger particles formed in the presence of 100 ppmv H_3PO_4 , the deposition rate for the 100 ppmv H_3PO_4 test should have been only 10 times higher than the one with 10 ppmv H_3PO_4 . As calculated before, the P-accumulation on P100 was instead found 29 times the P-accumulation on P10. This fact, as it will be discussed later, is considered as an indication that the overall P-accumulation is the result of a balance between particle deposition and deposit hydrolysis followed by P-vaporization from the sample.

According to the results obtained by Hg-porosimetry shown in Fig. 9, the deposition of polyphosphoric acid produced a shift toward smaller pore diameters in the pore size distribution for the different monoliths, pointing out the occurrence of physical deactivation due to pore blocking and condensation. In fact, it appears that the smaller pores at 40–50 nm of the bimodal mesoporous system are filled during P-addition, and a partial blocking of the interparticulate pore structure happened for P10 and P100. Furthermore, large crystalline formation has filled the void space in the macro-cracks above 100 μm. For the P10 a shift towards smaller macropores is observed due to this, whereas for the P100, a more dispersed destruction of the entire pore system is observed.

Overall, the total intrusion volume (TIV) was found to decrease at increasing P-content (Fig. 10).

The physical deactivation pointed out by the Hg-porosimetry measurements has also been confirmed by SEM analysis of the exposed catalysts (Fig. 11). From these it can be seen that

the surface of P100 looks uniformly covered by a glassy layer, whereas the porous structure of titania is more defined on the surface of P10. Instead, on this latter, some needle-shaped crystals are present. The analysis of these crystals by EDX showed enrichment in both P and V.

Fig. 12 shows the distribution of P into the walls of P10B and P100B as measured by EDX at the points shown in Fig. 11. P was found to penetrate the whole catalyst wall in both cases. In particular, the P-content in P100B was found constant around a value of 6.1 wt.%. Differently, the concentration profile measured on P10B showed a gradient in P-concentration in

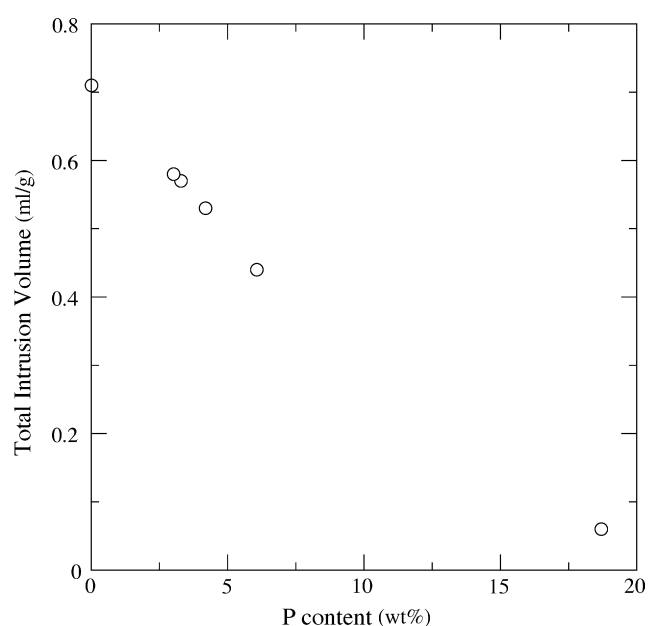


Fig. 10. Total intrusion volume measured by Hg-porosimetry as a function of P-content measured in the bulk of the different spent monoliths.

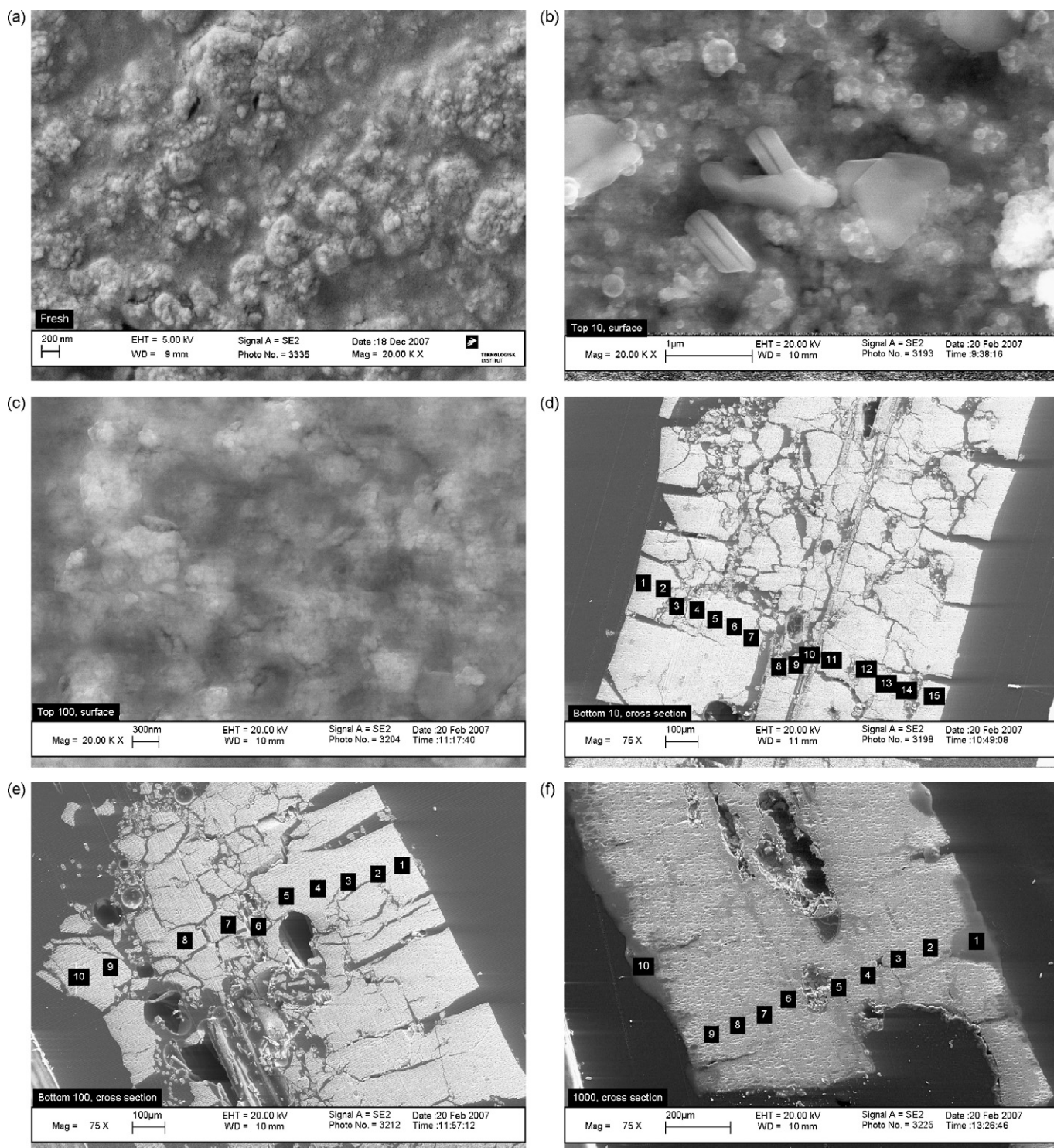


Fig. 11. SEM analysis of fresh and spent catalyst: (a) fresh surface; (b) P10T surface; (c) P100T surface; (d) P10B wall cross-section; (e) P100B wall cross-section and (f) P1000B wall cross-section.

the proximity of the surface, normally indicating a diffusion limited process in P-accumulation. However, in some points in the middle of the wall, especially in the proximity of a macropore, the P-concentration was found again higher. Overall, the average P-content in P10B wall was equal to 3.1 wt.%.

4. Discussion

A higher degree of deactivation was obtained by exposure to polyphosphoric acid aerosols at the pilot plant compared to the one obtained by wet impregnation of H_3PO_4 aqueous solutions. This indicates the importance in understanding the mechanism

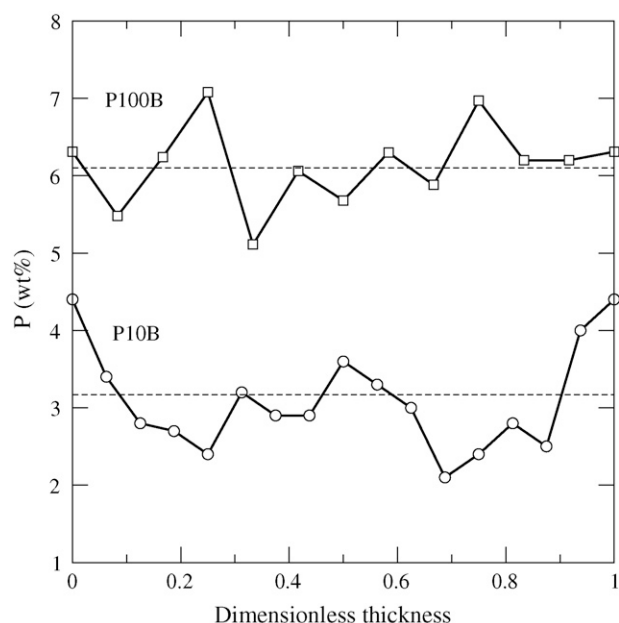


Fig. 12. P-content measured by EDX across some catalyst walls shown in Fig. 11.

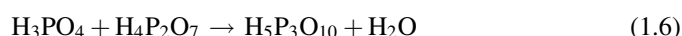
of formation of these particles and their influence on the activity of the vanadia-based catalysts. Apparently the real poisoning strength of P is not reproduced by the wet impregnation method normally used to dope both model and commercial catalysts.

4.1. Polyphosphoric acids formation and deposition

The measured particles had very small mean diameters and a total particle number concentration in the order of $1 \times 10^{14} \text{ \#}/\text{m}^3$ indicating their formation by homogeneous nucleation from the gas-phase. Condensation on particles already present (i.e. the ones measured during the blank measurement) cannot be completely excluded. However, this cannot be regarded as the main mechanism of particle formation since already at the lower acid concentrations (i.e. 10 ppmv), the particle number concentration was more than 10 times higher than the one found during the blank test. Furthermore, due to the very small size of the particles measured during the blank test, their mass fraction in the deposits can be neglected.

In order to explain the particle formation experienced, the formation of polyphosphoric acid will be here discussed based on Ref. [16]. The phosphoric acid molecule H_3PO_4 can be written as $1/2\text{P}_2\text{O}_5 \cdot 3\text{H}_2\text{O}$ and thus be considered as a 72.5% P_2O_5 solution having a boiling point temperature at 255 °C. When exposed to higher temperatures, water can evaporate until an azeotropic mixture consisting of 92.4% P_2O_5 is formed. This azeotropic mixture has a much higher boiling point at 864 °C. This water evaporation and the subsequent increase of P_2O_5 concentration is the result of condensation reactions taking place between the H_3PO_4 molecules in the gas-phase producing chains of poly-, pyro-, tri-, and *meta*-phosphoric acid, as

follows:



Due to their higher boiling point temperatures, the polyphosphoric acids may condense according to their vapor pressure when the gas cools down to the SCR reactor temperature.

Fig. 13 shows a plot of the partial pressure of different polyphosphoric acids as a function of P_2O_5 content [17]. Since particles have been found at the reactor inlet even at the lowest acid concentration of 10 ppmv, and considering the high temperatures (>850 °C) experienced in the spraying section of the setup, it is assumed that the composition of the deposited particles is equal to the azeotropic mixture. In this way, around 50–81% of the injected P-mass, was collected at the inlet of the SCR reactor. In the absence of a direct measurement of the P-content in the gas-phase, it is difficult to completely exclude and/or quantify the presence of gaseous P-species at the reactor inlet. Considering the equilibrium between the gas- and the liquid-phase as described by Fig. 13, no condensation with 10 ppmv H_3PO_4 is expected since this would have needed a supersaturated atmosphere in order to take place. However, this was not the case. Moreover, the fraction of P calculated from the particle number concentration measured by the SMPS was found in the range 50–81%. If it is assumed that at low acid concentrations the rest of the injected P is in the gas-phase, this should have been close to zero at increasing acid concentrations. However, as shown in Table 1, the collected P-fraction at 400 ppmv H_3PO_4 was almost the same as the one at 10 ppmv.

It is therefore assumed that: (i) the injected H_3PO_4 reacted in the gas-phase forming an azeotropic mixture of polyphosphoric

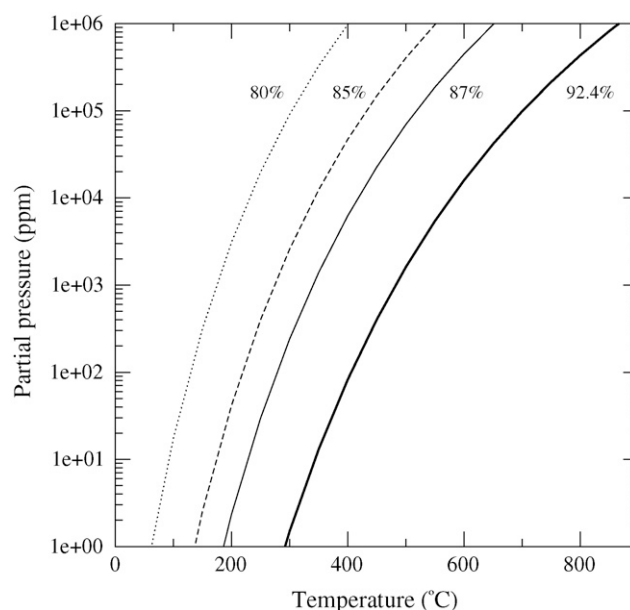


Fig. 13. Vapor pressure of polyphosphoric acids as a function of temperature at different P_2O_5 weight content. The lines are calculated by extrapolating at lower pressures the equation fitting the experimental data found at higher partial pressures [17].

acids; (ii) nucleation of polyphosphoric acid happened at temperatures $<500\text{ }^{\circ}\text{C}$; (iii) almost all the acid was present in the liquid-phase and (iv) the differences found between the total P-mass injected and the P-mass measured at the SCR reactor inlet was mainly due to particle deposition on the pipe walls leading to the SCR reactor.

Due to their submicron dimensions, the particles are very mobile and can diffuse towards the catalyst walls, deposit on the catalyst surface and even penetrate into the pore structure by capillary forces. Once deposited, however, some of the deposited polyphosphoric acid may be hydrolyzed in the presence of the flue gas moisture forming H_3PO_4 which evaporates from the catalyst. The resulting P-accumulation rate is therefore a balance between the particle deposition and evaporation of phosphoric acid. The hydrolysis of polyphosphoric acid in water is known to be a slow process and dependent on different factors, such temperature, chain length and pH [16]. Therefore the P-accumulation in the catalyst walls will be mainly controlled by the particle deposition rate at high total particle numbers, while deposit evaporation at low deposition rates and low total particle number concentrations becomes relatively more important.

Taking into account all these facts, together with the different P-concentration profiles measured by EDX on P10 and P100 (Fig. 12), it is possible to conclude that evaporation of phosphorus compounds effectively limited the P-accumulation in the P10 case and that the profile measured in the wall is the net result of deposition and evaporation. The deposition rate during the 100 ppmv H_3PO_4 addition was much faster than evaporation leading to a fast accumulation of P in the wall.

4.2. Deactivation mechanisms

The high P-concentration found in the bulk of the exposed catalysts, the even P-distribution measured along the catalyst walls, the decrease in TIV measured by Hg-porosimetry at increasing P-concentrations and the SEM analysis of the different catalyst surfaces, all point to the occurrence of physical deactivation due to surface masking, pore blocking and condensation, in agreement with previous investigations about P-deactivation. However, the transient in NO conversion observed during every activity measurements clearly points out the occurrence of a simultaneous chemical deactivation mechanism.

The in situ EPR measurements carried out with the fresh catalysts have shown that the different gas compositions are not able to change the redox properties of the surface. In particular, during the SCR reaction, the V(V) species are continuously reduced during formation of the reaction intermediates and then re-oxidised by O_2 [2,3]. The fact that this sample, when exposed to the complete SCR mixture, does not show an increased number of V(IV) species can be explained assuming that at $350\text{ }^{\circ}\text{C}$ the rate of re-oxidation of the active V(IV) species in the redox cycle of the mechanism is high enough to keep the vanadium as V(V). In other words, this behaviour confirms the literature consensus [1] that at this temperature, the order of reaction of oxygen is zero.

Under oxidising conditions, P10 practically exhibited the same spectrum as the fresh sample. However, when P10 was exposed to the complete SCR gas mixture, the number of $(\text{VO}^{2+})_n$ species slightly increased. This indicates that the SCR reaction is occurring, but that the re-oxidation step is significantly slower than for the fresh catalyst.

Contrarily to the previous results $(\text{VO}^{2+})_n$ species are present as a stable phase on the catalyst surface of the P100 sample already under oxidising conditions, suggesting that the VO^{2+} on P10 and P100 are exposed to two distinctly different phosphor species. Furthermore, the concentration of V(IV) is increased when NH_3 is added to the mixture and the SCR reaction takes place. The most likely explanation for this is that the intermediate V(IV) species, which are consistently formed during the SCR reaction [2,3], are being trapped by phosphate interactions, since it appears unlikely that phosphates alone should be able to reduce the V(V) compounds. This indicates that the deposited phosphates interact with parts of the active oxo-vanadium species, forming vanadyl-phosphate species which will not take part in the reaction anymore, thus inducing chemical deactivation by titration of the active species.

By considering this chemical deactivation, together with the effect of intra-particle diffusion limitations, the transient in NO conversion can be explained. As shown in Fig. 5, at the very beginning of the NH_3 addition, the monolith P100 still presents a relative good activity. As reported in Table 2, when the NO conversion goes through the maximum, the relative activity is equal to 0.91. The lost 9% of activity is mainly due to physical deactivation only. However, the V(IV) species which were initially formed during the SCR reaction, are then stabilized in complexes which are formed with the deposited polyphosphoric acids. NH_3 can then be considered as the responsible for this titration of active sites since it initiates their reduction due to the SCR reaction. This titration is assumed to happen first at the outer catalyst wall, since it is where the SCR reaction is first happening. The intrinsic rate of reaction then starts decreasing at the outer wall due to the formation of $\text{NH}_3\text{-P-V}$ species and the reagents have to diffuse further into the catalyst walls in order to find active sites where to react. The steady-state is finally reached when equilibrium between the formed P-V-complexes, the active V-species and NH_3 is reached along the catalyst wall. In the case shown in Fig. 5 and reported in Table 2, the additional 48% of activity which has been lost has to be considered due to chemical deactivation.

NH_3 is controlling the stability of the formed and inactive complexes. In fact, the NO transient during the activity measurement can only be reproduced if NH_3 has been taken off the flue gas for the time required by these complexes to completely disappear. Moreover, as shown in Fig. 5, further NO conversion can be obtained by increasing the NH_3 partial pressure, but again this will first show a maximum and then a steady-state level at lower values. This additional activity at higher NH_3 partial pressures can be related to the NH_3 adsorption constant of the catalyst surface, which is changed due to the presence of the polyphosphoric acids. As shown in Fig. 7, the amount of chemisorbed NH_3 is increased due to the polyphosphoric acid deposition. However this additional

adsorbed NH_3 can be assumed either *less active*, in agreement with Kamata et al. [7], or inactive, simply constituting an NH_3 storage on the surface. In the latter case, it has first to jump on an active site prior to react. Regarding the increased activity, which was measured when the NH_3 concentration was increased, it can then be argued that, due to the increased number of sites for the NH_3 chemisorption, the coverage of NH_3 appearing in Eq. (1.4) has become less than one at the typical condition of our activity measurements.

Finally, the reason for P100 for showing a more pronounced transient than P10 has to be found in: (i) a higher P-content in P100 and a consequent slower diffusivity due to the decreased pore sizes; (ii) a higher degree of polymerization of the deposits in P100 due to the faster deposition compared to the hydrolysis rate; (iii) a more uniform distribution of P in the P100 walls.

5. Conclusions

When exposed to the high temperatures of a combustion process, the H_3PO_4 molecules eventually released in the gas-phase start condensation reactions forming polyphosphoric acids. These species are characterized by higher melting point temperatures than the typical SCR reaction temperatures and are found in a liquid-phase at the SCR reactor inlet. Condensation of these species has been estimated to happen at temperatures lower than 500 °C. Therefore, there is a high probability that the formed aerosols will be characterized by high number concentrations of submicron liquid particles, due to the short time passing between the nucleation burst and the SCR reactor inlet. These particles therefore have high diffusivities and a high deposition rates on the monolith walls.

Deactivation by polyphosphoric acid has been found to follow both a physical and a chemical deactivation. Surface masking, fouling, pore blocking and condensation are definitely important contributions to catalyst deactivation. Once deposited on the catalyst outer surface, they are very mobile and can even be sucked into the walls by capillary forces. The P-accumulation, and consequently the implied deactivation, is however limited by the rate of hydrolysis of the deposits themselves. The H_2O present in the flue gas, at the SCR temperatures can break down the polyphosphoric acid chains and free some H_3PO_4 back in the gas-phase.

The physical deactivation, however is not the only effect responsible for the overall measured deactivation levels. Supported by the transient behaviour in NO reduction measured during activity tests with mass transfer-limited-catalysts, and in situ EPR analysis of the spent catalysts, it has been found that the deposited polyphosphoric acids tend to both increase and stabilize the number of *non-active* V(IV) species, which are formed as intermediate during the SCR reaction. Moreover, part of the NH_3 present in the gas-phase preferentially adsorbs

on the polyphosphoric acids and is only less active in the reduction of NO.

The results obtained in this work constitute the first reference about deactivation of vanadia-based catalysts explicitly due to polyphosphoric acid alone. It is believed they show the real deactivating potential of P, when this is present in the flue gas during post-treatment of combustion processes, which has been found much more poisonous than indicated by wet impregnated tests.

Acknowledgments

This work is part of the CHEC (Combustion and Harmful Emission Control) Research Center funded a.o. by the Technical University of Denmark, the Danish Technical Research Council, the European Union, the Nordic Energy Research, Dong Energy A/S, Vattenfall A.B., F L Smidth A/S, and Public Service Obligation funds from Energinet.dk and the Danish Energy Research program. In particular, it is supported by the PSO project “Deactivation of SCR Catalysts by Additives” (PSO Elkraft FU-4205). Supply of the catalyst samples by Haldor Topsøe A/S is gratefully acknowledged.

References

- [1] V.I. Parvulescu, P. Grange, B. Delmon, *Catal. Today* 46 (1998) 233–316.
- [2] N.-Y. Topsøe, H. Topsøe, J.A. Dumesic, *J. Catal.* 151 (1995) 226–240.
- [3] N.-Y. Topsøe, J.A. Dumesic, H. Topsøe, *J. Catal.* 151 (1995) 241–252.
- [4] Y. Zheng, A.D. Jensen, J.E. Johnsson, *Appl. Catal. B: Environ.* 60 (2005) 261–272.
- [5] Y. Zheng, A.D. Jensen, J.E. Johnsson, *Appl. Catal. B: Environ.* (2008), doi:10.1016/j.apcatb.2008.02.019.
- [6] J.P. Chen, M.A. Buzanowski, R.T. Yang, *J. Air Waste Manage. Assoc.* 40 (1990) 1403–1409.
- [7] H. Kamata, K. Takahashi, C.U.I. Odenbrand, *Catal. Lett.* 53 (1998) 65–71.
- [8] J. Blanco, P. Avila, C. Barthelemy, A. Bahamonde, J.A. Odriozola, J.F. Garcia de la Banda, H. Heinemann, *Appl. Catal.* 55 (1989) 151–164.
- [9] J. Beck, J. Brandenstein, S. Unterberger, K.R.G. Hein, *Appl. Catal. B: Environ.* 49 (2004) 15–25.
- [10] P.A. Jensen, L.H. Sørensen, G. Hu, J.K. Holm, F. Frandsen, U.B. Henriksen, Technical University of Denmark, KT-Report No. 0504, 2005.
- [11] L. Tobiasen, R. Skytte, L.S. Pedersen, S.T. Pedersen, M.A. Lindberg, *Fuel Process. Technol.* 88 (2007) 1108–1117.
- [12] J. Beck, R. Muller, J. Brandenstein, B. Matschenko, J. Matschke, S. Unterberger, K.R.G. Hein, *Fuel* 84 (2005) 1911–1919.
- [13] K.M. Eriksen, R. Fehrmann, N.J. Bjerrum, *J. Catal.* 132 (1991) 263–265.
- [14] M.Y. Kustova, S.B. Rasmussen, A.L. Kustov, C.H. Christensen, *Appl. Catal. B: Environ.* 67 (2006) 60.
- [15] T.D. Farr, *Phosphorus Properties of the Element and Some of Its Compounds*, Tennessee Valley Authority, Chemical Engineering Report No. 8, U.S. Government Printing Office, Washington, DC, 1950. From <http://www.innophos.com>.
- [16] J.R. Van Wazer, *Phosphorus and its Compounds*, Interscience Publisher, New York, 1958.
- [17] E.H. Brown, C.D. Whitt, *Ind. Eng. Chem.* 44 (1952) 615–618.

Appendix B



Influence of reaction products of K-getter fuel additives on commercial vanadia-based SCR catalysts Part I. Potassium phosphate

Francesco Castellino^a, Anker Degn Jensen^{a,*}, Jan Erik Johnsson^a, Rasmus Fehrmann^b

^a Department of Chemical and Biochemical Engineering, Technical University of Denmark, DK-2800 Kgs. Lyngby, Denmark

^b Centre for Sustainable and Green Chemistry, Department of Chemistry, Technical University of Denmark, Building 207, DK-2800 Kgs. Lyngby, Denmark

ARTICLE INFO

Article history:

Available online 14 November 2008

Keywords:

DeNO_x SCR catalysts
Catalyst deactivation
Vanadia
Biomass
Potassium poisoning
Polyphosphoric acids

ABSTRACT

Commercial vanadia-based full-length monoliths have been exposed to aerosols formed by injection of K₃PO₄ (dissolved in water) in a hot flue gas ($T > 850^\circ\text{C}$) from a natural gas burner. Such aerosols may form when burning fuels with high K- and P-content, or when P-compounds are mixed with biomass as a K-getter additive. The formed aerosols have been characterized by using both a SMPS system and a low pressure cascade impactor, showing a dual-mode volume-based size distribution with a first peak at around 30 nm and a second one at diameters $>1\ \mu\text{m}$. The different peaks have been associated with different species. In particular, the particles related to the 30 nm peak are associated to condensed phosphates, whereas the larger particles are associated to potassium phosphates. Two monoliths have been exposed during addition of 100 and 200 mg/Nm³ K₃PO₄ for 720 and 189 h, respectively. Overall, deactivation rates up to 3%/day have been measured. The spent catalysts have been characterized by bulk chemical analysis, Hg-porosimetry and SEM-EDX. NH₃-chemisorption tests on the spent elements and activity tests on catalyst powders obtained by crushing the monoliths have also been carried out. The catalyst characterization has shown that poisoning by K is the main deactivation mechanism. The results show that binding K in K–P salts will not reduce the rate of catalyst deactivation.

© 2008 Elsevier B.V. All rights reserved.

1. Introduction

1.1. The K-getters fuel additives

The release of K-salts during biomass combustion is known to cause several problems to the boiler equipment downstream the boiler, thus limiting the application of this CO₂-neutral process [1]. Among these problems, the fast deposition rate on the super-heater exchangers of highly corrosive ashes is by far the most undesired. When biomass (e.g. straw and wood) is fired, the potassium in the fuel, which is released in the gas phase during combustion, forms aerosols of pure KCl and K₂SO₄ [2,3]. Potassium chloride has a relatively low melting point (i.e. 776 °C) and is therefore found in a melted-phase at the temperatures of the super-heater exchangers, making the ashes sticky. Ash deposition on the exchanger surfaces is therefore enhanced, causing a decrease in steam production efficiency. A periodical removal of

these deposits, however, might not be sufficient in order to re-establish the original heat flux across the heat exchanger surfaces. In fact, since Cl is included in the formed deposits, these are very corrosive and a complete substitution of the tubing system might then be required in a shorter time than anticipated.

In order to limit these problems, Danish and Swedish power companies are currently evaluating the addition of different compounds to the biomass which are able to bind the potassium into particles with higher melting temperatures, while releasing the chlorine in the gas phase as HCl [4,5]. Sørensen et al. [6] developed a process where additives mainly constituted by P and Ca were mixed with the biomass in order to create the reaction conditions in the boiler at which the potassium gets captured in a phase consisting of K₂O–CaO–P₂O₅. As shown in Table 1, the compounds belonging to this system have melting points well above 1000 °C and will thereby not be found as melts at the super-heater section. Initial tests performed by feeding straw mixed with different additive compositions to an entrained flow reactor have shown a reduction of 74–98% of the level of Cl in the deposits when the molar ratios of P/(K + Na) and P/Ca in the resulting fuel mixture were in the ranges 1.9–3.2 and 0.8–0.9, respectively [7]. This seems

* Corresponding author. Tel.: +45 45 25 28 41; fax: +45 45 88 22 58.
E-mail address: aj@kt.dtu.dk (A.D. Jensen).

Table 1

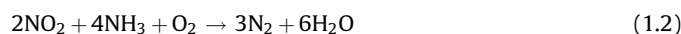
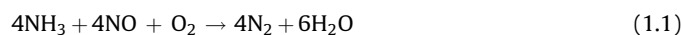
Possible products of biomass combustion and relative melting temperatures in the presence of K-getter fuel additives.

| | T_m (°C) |
|-----------------|------------|
| $K_4P_2O_7$ | 1105 |
| $K_2CaP_2O_7$ | 1143 |
| K_3PO_4 | 1340 |
| $KCaPO_4$ | 1560 |
| $K_4Ca(PO_4)_2$ | 1645 |
| $Ca_3(PO_4)_2$ | 1670 |

very promising from a deposition and corrosion point of view, but the addition process apparently requires an excess of both P and Ca with respect to the alkali fraction.

1.2. Additives influence on the SCR vanadia-based catalysts

Changes in fly ash composition due to the addition of P- and Ca-compounds might also have an effect on the equipment downstream the superheaters that must be addressed. Particularly sensitive to changes in both the fly ash content and composition is the selective catalytic reduction (SCR) process used for the abatement of the NO_x fraction of the flue gas [8]. This process relies on the ability of ammonia to selectively reduce the undesired NO_x present in the flue gas to molecular nitrogen according to the following global reactions:



The most active and selective catalysts are mainly constituted by vanadium pentoxide (V_2O_5 , total load varying between 1 and 5 wt% depending on the specific application), supported on a titania (TiO_2 , anatase form) carrier. These are normally shaped into monoliths with parallel channels with hydraulic diameters up to 9 mm, which allows operation even in the presence of fly ash loads ($>10 \text{ g/Nm}^3$) relevant for suspension firing before ESP with only low pressure drops over the reactor. A widely accepted mechanism of reaction for these catalysts at typical industrial operating conditions was proposed by Topsøe et al. [9,10]. This involves adsorption of NH_3 on Brønsted acid sites, activation of adsorbed ammonia by $V=O$ species and subsequently reaction with gaseous or weakly adsorbed NO . Deactivation of vanadia-based catalysts can be due to poisoning, fouling, surface masking, pore blocking and sintering according to the particular application. In most of these cases, however, the fly ash plays an important role since it may act both as physical deactivating agent, and as a carrier for different chemical deactivating species. For instance K, which according to different studies is a very strong poison for the vanadia-based SCR catalysts [3,11–17], is present as solid particles at the SCR reactor inlet. Therefore the observed rate of deactivation is directly related to the fluid dynamics controlling the rate of particle deposition. However, important as well is the rate of particle/poison penetration into the catalyst walls, and this is more likely related to the way the K-fraction is bound to the particle itself. For instance, up to 1%/day deactivation has been measured both at a biomass-fired combined heat and power plant [3] and in a pilot plant [17] where K was present as aerosols of pure KCl and K_2SO_4 . Contrary, accordingly to coal firing experience, when K is mainly bound to non-soluble silica-aluminates, the deactivation proceeds at much slower rates. In order to explain the influence of the particle composition on the different deactivation rates experienced, Zheng et al. [3] suggested that this is related to the K-mobility at the SCR temperatures. The reason for the good

mobility of KCl and K_2SO_4 was found in the Hüttig and Tamman temperatures of these compounds. These two temperatures are normally used to estimate the temperatures at which sintering starts [18] and are calculated with the following empirical expressions:

$$T_{\text{Hüttig}} = 0.3T_{\text{melting}}$$

$$T_{\text{Tamman}} = 0.5T_{\text{melting}}$$

When the Hüttig temperature is reached, atoms at vacancies start being mobile. When the Tamman temperature is eventually reached, the atoms in the bulk start showing mobility. According to their Hüttig and Tamman temperatures, the atoms forming the KCl and K_2SO_4 deposits may then be expected to be mobile at the SCR temperatures, and therefore react with the catalyst surface and further diffuse on it.

The discussion above indicates that binding K to ashes with higher melting temperatures by the addition process may reduce the rate of deactivation by decreasing the poison penetration in the catalyst walls. On the other hand, the increased P- and Ca-levels induced by the additive process could to some extent counter-balance this positive effect. P and Ca are known to be deactivating species for the vanadia-based SCR catalysts [11,12,19–22]. The excess levels of P with respect to the alkali fraction in the resulting fuel mixture required by the addition process might lead to an undesired formation of polyphosphoric acids. In a previous investigation [22] the formation and deactivating mechanisms of polyphosphoric acids have been reported. H_3PO_4 was found to form aerosols of viscous liquid polyphosphoric acids with diameters $<0.1 \mu\text{m}$ due to homogeneous nucleation occurring at temperatures $<500^\circ\text{C}$. These results were in agreement with the higher P-concentrations found in the submicron particles when coal was co-fired with P-rich secondary fuels at full-scale [23], or simply mixed with P-compounds and burned in an electrically heated plug flow reactor [24]. The polyphosphoric acid particles were characterized by very fast deposition rates due to both the high particle number and their high diffusivity due to their small size, and they caused a fast deactivation of the catalyst by both physical and chemical deactivation [22]. In particular, the chemical deactivation was related to the stabilization of $V(4+)$ species formed as intermediate during the SCR reaction by the polyphosphoric acids. However, no other species (apart from O_2 , CO_2 , H_2O and N_2) were present in the flue gas during the tests, leaving the question about the formation of polyphosphoric acids in a *non-clean* system still open.

1.3. Objectives

This work is part of a project, which aims at evaluating the effects of the addition of Ca-, P-based K-getter species on the vanadia-based SCR catalysts. This paper focuses on the potassium phosphate system, since in this system some of the potential reaction products of the K-getter fuel additives are found. The results of the investigations carried out by exposing full-length commercial SCR monoliths to a flue gas doped with K_3PO_4 in a pilot-scale SCR setup for up to 700 h are reported. The second part of the work will focus on the simultaneous addition of KCl, $Ca(OH)_2$, H_3PO_4 and H_2SO_4 in the flue gas, to simulate a more complete full-scale addition process.

Apart from estimating the potential effect of the addition process on the SCR catalysts, the tests shown in this paper offer the possibility: (i) to provide further input to the mechanism of K-deactivation by aerosols; (ii) to determine the possible formation of polyphosphoric acids and thereby provide additional information about the P-release during combustion.

2. Experimental

2.1. Catalysts

Commercial corrugated-type monoliths obtained from Haldor Topsøe A/S were used in this study. The catalysts were based on V_2O_5 (up to 5 wt%) and tungsten oxide (WO_3 , up to 9 wt%) dispersed on a fiber reinforced TiO_2 carrier. The monoliths had a size of 75 mm × 75 mm × 500 mm. The hydraulic diameter of the channels was 6.44 mm and the wall thickness was 1.0 mm. Pieces of both fresh and spent monoliths have been cut from both the inlet and the outlet in order to study their local properties under well defined reaction conditions in a laboratory fixed bed reactor. In order to run activity tests on powdered samples, they have been gently crushed in a mortar and the particle fraction in the range 105–125 μm has been collected by sieving.

2.2. SCR pilot plant

The SCR pilot plant setup used for this investigation is the same as described in [22]. Its main parts are a natural gas burner for flue gas production, a lance for injecting liquid solutions, a square duct hosting a full-length commercial monolith and a NH_3 supply system. NH_3 is injected both in the burner to produce the desired NO concentration at the reactor inlet, and in the flue gas duct leading to the reactor for the NO reduction. A soot blowing system running with compressed air is installed at the SCR reactor inlet to keep the monolith channels open.

2.3. K_3PO_4 addition

The addition of K_3PO_4 to the flue gas was performed by spraying water solutions through a two-fluid nozzle. The solutions were prepared by dissolving K_3PO_4 (reagent grade $\geq 98\%$, Sigma®) in distilled water. Two catalyst elements have been exposed to 100 and 200 mg/Nm^3 K_3PO_4 . In this work they will be identified by the labels “KP100” and “KP200”, respectively. The letters “T” and “B” added at the end of the labels will indicate a sample cut respectively from the top (first 10 cm) and the bottom (last 10 cm) of the element. In all tests, the salt concentration in the solutions was fixed at 21 g/L and the solution feed rate was then varied in order to get the desired concentration in the flue gas (i.e. 0.25 and 0.5 L/h to get 100 and 200 mg/Nm^3 , respectively).

2.4. Aerosol measurements

2.4.1. Scanning Mobility Particle Sizer

A Scanning Mobility Particle Sizer (SMPS, TSI Inc.), which included an Electrostatic Classifier (Model 3080) and a Condensation Particle Counter (Model 3775) was used to measure the particle concentration and size distribution during the exposure to K_3PO_4 . Particle sampling was carried out at the inlet of the SCR reactor by an ejector sampler running with dry, particle-free air. In this system the particle-containing flue gas was at the same time cooled and diluted thereby preventing: (i) water condensation; (ii) particle coagulation in the sample line by effectively decreasing its rate by several orders of magnitude; (iii) overloading of both the impactor and the SMPS. The dilution ratio, required to know the real particle concentration in the flue gas, was obtained by measuring the CO_2 concentration both in the flue gas and in the diluted sample.

2.4.2. Low pressure cascade impactor

A 10-stage Berner-type low pressure cascade impactor (LPI) with an aerodynamic diameter range of 0.03–12.7 μm connected

to a vacuum pump was used. The flow through the LPI was controlled by a critical orifice and was equal to 22.49 L/min at 25 °C and atmospheric pressure. The flue gas was sampled directly at the reactor inlet without any dilution. Therefore the sampling line and the LPI were heated to 90 °C in order to avoid any water condensation. Deposited particles were collected on aluminum foils coated with a thin film of Apiezon H grease. The grease served to limit bouncing of the particles and was added using a dilute toluene solution of the grease. The toluene was evaporated from the foils by drying these in an oven at 140 °C for 2 h. The sampling time was equal to 60 min, which allowed a suitable collection of particle mass. The weight gains from the deposited particles on each foil were determined by a Sartorius M5D-000V001 micro-balance. The foils were finally analyzed by electron dispersive X-ray analysis for chemical composition.

2.5. Activity measurements

The rate of the SCR reaction at typical industrial reaction conditions has been assumed to follow an Eley-Rideal mechanism of reaction with NH_3 adsorbed on the catalyst surface and NO reacting from the gas phase. The following expression for the rate of reaction, r_{NO} , can then be derived:

$$-r_{NO} \left[\frac{\text{mol}}{\text{m}^3_{\text{cat}} \text{s}} \right] = k c_{NO} \frac{K_{NH_3} c_{NH_3}}{1 + K_{NH_3} c_{NH_3}} \quad (1.3)$$

where k [1/s] is the rate constant, c_{NO} and c_{NH_3} [mol/m^3] are the concentrations of NO and NH_3 , respectively, and K_{NH_3} [m^3/mol] is the adsorption constant for NH_3 on the catalyst surface. The fraction term on the right-hand side of Eq. (1.3) is the NH_3 coverage of the catalytic surface, θ_{NH_3} .

At the pilot plant, the activities of the catalysts were measured at 350 °C in the presence of about 500 ppmv NO, 600 ppmv NH_3 , 10 vol% O_2 , 6 vol% CO_2 , and about 10 vol% H_2O . During activity measurements the flow through the SCR reactor was kept at 40 Nm^3/h . At this flow the gas velocity in the channels were about 6.5 m/s at 350 °C, similar to the velocities used at full scale applications. At this velocity, up to 50% external mass transfer limitations have been estimated.

Since ammonia in our measurements is added in excess with respect to NO (i.e. $NH_3/NO \approx 1.2$), the NH_3 coverage, θ_{NH_3} , can be assumed equal to 1 and the reaction rate can be regarded as pseudo-first order with respect to NO and zero order with respect to NH_3 . Therefore, directly from the fractional NO conversion, X , it is possible to calculate an observed catalyst activity constant, k' , that includes both the influence of external and internal mass transfer:

$$k' \left[\frac{\text{ml}}{\text{gs}} \right] = - \frac{F_{\text{gas}}}{m_{\text{cat}}} \ln(1 - X) \quad (1.4)$$

where F_{gas} is the gas flow rate (ml/s), m_{cat} is the weight of catalyst (g). The degree of deactivation can then be calculated as the ratio k/k_0 between the activity constant of the catalyst during exposure, k , and the one measured for the fresh element, k_0 , right before starting the poison addition.

In the laboratory, powdered samples have been tested for activity in a packed bed quartz micro-reactor with a diameter equal to 10 mm. Around 0.07 g of powder has been used during activity measurement. This has been mixed with sand of the same particle size in order to have a particle bed of about 10 mm, thus ensuring the applicability of the here assumed integral reactor model. In all experiments, the total flow was equal to 2.8 NL/min and was constituted by 500 ppmv NO, 600 ppmv NH_3 , 5 vol% O_2 and 1.4 vol% H_2O in N_2 . Activity measurements have been performed in the temperature range 250–400 °C. The catalyst

activity has been calculated according to Eq. (1.4) and the deactivation as the ratio between the activity constant of the spent catalyst and the one measured for the fresh one. At 350 °C, the observed activity constant, k' , for the fresh catalyst powder was found only 10% less than the one calculated in the total absence of mass transfer limitations. The latter value was calculated by extrapolating to higher temperatures a fit to the Arrhenius plot obtained in the kinetic regime in the range 250–330 °C.

During all activity measurements, the NO concentration in the flue gas has been measured with a conventional UV analyzer (Rosemount NGA 2000). Due to the presence of water in the gas composition during all activity measurements, no N_2O formation is expected [25].

2.6. Ammonia chemisorption

NH_3 -chemisorption is the first step of the reaction mechanism [9,10], and poisoning by K has been found to decrease the amount of chemisorbed NH_3 . Therefore, NH_3 -chemisorption tests have been periodically carried out at the pilot-scale setup during the K_3PO_4 addition. The measurements have been made at 350 °C and 40 Nm^3/h . Around 600 ppmv NH_3 have been added to the flue gas and flow through the SCR reactor for 30 min in order to saturate the catalyst sites. Previous investigations made with the same catalysts showed that this period of time is sufficient to saturate all the sites available for NH_3 -chemisorption on a fresh element. During this saturation period, only the NO produced by the natural gas combustion was present (i.e. ≈ 80 ppmv). After this time, the NH_3 was shut off and right after, around 500 ppm NO were produced by adding a stream of NH_3 to the burner. The amount of chemisorbed NH_3 can then be calculated by integrating over time the amount of reduced NO, due to the equimolar reaction between the gaseous NO and the chemisorbed NH_3 .

2.7. Catalyst characterization

Small pieces of catalyst were cut from the ends of both fresh and exposed monoliths and characterized without further treatment with respect to bulk chemical composition, mercury porosimetry and physical appearance by a Scanning Electron Microscope (SEM).

The chemical composition was obtained by ICP-OES at the laboratory of DONG Energy A/S. Prior to the measurements, the samples were cut to 1.5×1.7 cm² and dried at 105 °C for 2 h before analysis.

The total pore volume and the pore size distribution of the different catalyst samples were made by mercury intrusion in a Micromeritics Autopore II 9220 porosimeter. SEM-EDX analysis was performed at the Danish Technological Institute using a Zeiss Ultra55 and an Oxford ISIS with a PentaFet X-ray detector. In particular, for each sample the EDX analysis was performed on three different areas of about 200×200 μm^2 each. The numbers reported in this work are the averages of the different measurements. The standard deviations of the measurements have been found <0.5, 2 and 2.8 wt% for V, K and P, respectively.

3. Results

3.1. Aerosol measurements at the pilot-scale setup

3.1.1. SMPS measurements

Fig. 1 shows the number-based and volume-based particle size distributions measured during the addition of 100 mg/ Nm^3 K_3PO_4 . According to the number-based distribution, the aerosols were characterized by a peak at around 30 nm. However, when the volume-based distribution is plotted instead, a second peak at

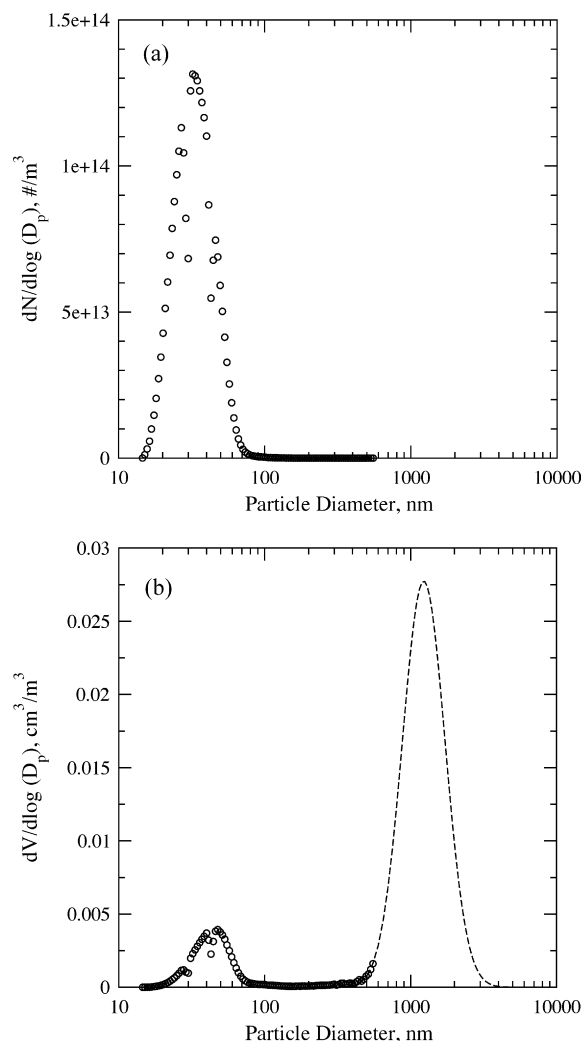


Fig. 1. Number-based (a) and volume-based (b) particle size distributions measured by SMPS at the reactor inlet during addition of 100 mg/ Nm^3 K_3PO_4 at $T = 350$ °C. The dashed line represents a lognormal distribution derived by fitting the data points in the particle diameter range 300–550 nm.

higher diameter appears. In particular, it can be seen in Fig. 1b that this second peak almost entirely extends outside the upper detection limit of the SMPS used. By assuming a density for these particles equal to the density of K_3PO_4 (i.e. 2.564 g/cm³), the total mass measured by the SMPS would be equal to around 8% of the injected one. This low value indicates that a great part of the injected mass is present at the larger diameters not detectable by the SMPS. By fitting the data obtained with a lognormal distribution, the curve showed in Fig. 1b can be obtained. The fitting has been made by minimization of

$$\sum_{d_p} [\psi_{V,SMPS}(d_p) - \psi_{V,logn}(d_p)]^2 \quad 300 \text{ nm} \leq d_p \leq 550 \text{ nm} \quad (1.5)$$

where $\psi_{V,SMPS}$ is the volume distribution $dV/d(\log dp)$ calculated from the SMPS measurement, $\psi_{V,logn}$ is the fitted distribution. The mean diameter of the lognormal distribution is equal to 1.25 μm . Overall, the total mass calculated is equal to around 40% of the injected K_3PO_4 . Both the mean diameter and the total mass at the reactor inlet would then be comparable to previous tests carried out at this setup [17]. As will be discussed later, the presence of this dual-mode particle distribution is related to the presence of mainly two different species, whose formation has followed different mechanisms.

Table 2

K- and P-content measured on different impactor stages by EDX. The particles were collected during addition of 100 mg/Nm³ K₃PO₄.

| Impactor stage number | Particle Diameter (nm) | K (at.%) | P (at.%) | K/P (molar) |
|-----------------------|------------------------|----------|----------|-------------|
| 4 | 1488 | 47.31 | 13.8 | 3.48 |
| 5 | 754 | 51.22 | 15.39 | 3.33 |
| 6 | 382 | 48.66 | 16.65 | 2.92 |
| 7 | 193 | 48.49 | 14.82 | 3.27 |
| 8 | 98 | 47.49 | 14.8 | 3.21 |
| 9 | 49 | 44.08 | 14.71 | 3.00 |

3.1.2. Cascade low pressure impactor measurements

Tests with the LPI have been performed during both the KP100 and KP200 experiments. In all cases, the particles collected at the different stages were very liquescent and were therefore melting as soon as they were exposed to ambient air. The determination of the weight of the different foils was therefore problematic. Not only the foils were increasing their weight due to water adsorption. Some of them were at some point even losing weight during their mass determination. This fact indicates that during exposure to ambient air at room temperature some gaseous species were released by the deposit. Due to these problems, the only partly useful indications obtained from the tests were those provided by the EDX analysis of the different foils reported in Table 2. Here, values of the K:P molar ratio in the range 3–3.5 were measured, which are slightly higher than the expected value of 3. Interestingly, the K:P values were increasing with the collected particle size (apart from the value measured on stage #6). These values may differ from the expected value of 3 simply because experimental uncertainty of the EDX measurements, but, recalling the particle size distribution measured by the SMPS, they may also indicate that part of the P was not collected on the lower impactor stages, probably because the remaining fraction was present in even smaller particles or in the gas phase.

3.2. Catalyst characterization

3.2.1. Bulk and surface chemical analysis

Table 3 reports the results of both the bulk and surface chemical analysis for the elements KP100 and KP200. The K-content in the

Table 3

Bulk, surface and Hg-porosimetry analysis for the fresh and spent monoliths.

| | Fresh | KP100T | KP100B | KP200T | KP200B |
|-------------------------------------|-------|--------|--------|------------------|------------------|
| Total exposure time (h) | | 720 | 720 | 189 ^a | 189 ^a |
| Bulk chemical analysis | | | | | |
| V (wt/wt%) | 1.60 | 2.46 | 1.61 | 1.76 | 2.70 |
| K (wt/wt%) | 0.0 | 2.45 | 1.44 | 0.80 | 0.90 |
| P (wt/wt%) | 0.01 | 0.77 | 0.46 | 0.75 | 0.40 |
| K/P (mol/mol) | | 2.52 | 2.46 | 0.85 | 1.79 |
| K/V (mol/mol) | | 1.30 | 1.17 | 0.59 | 0.44 |
| P/V (mol/mol) | | 0.31 | 0.47 | 0.70 | 0.24 |
| Surface chemical analysis | | | | | |
| V (wt/wt%) | 2.1 | 2.1 | 3.5 | 2.4 | 2.2 |
| K (wt/wt%) | 0.0 | 1.7 | 0.8 | 6.2 | 2.1 |
| P (wt/wt%) | 0.0 | 2.8 | 1.0 | 12.6 | 6.2 |
| K/P (mol/mol) | | 0.5 | 0.7 | 0.4 | 0.3 |
| K/V (mol/mol) | 0.0 | 1.1 | 0.3 | 2.7 | 1.2 |
| P/V (mol/mol) | 0.0 | 2.2 | 0.5 | 7.1 | 4.5 |
| Hg-porosimetry | | | | | |
| Total intrusion volume (ml/g) | 0.71 | 0.71 | 0.67 | 0.67 | 0.64 |
| Total pore area (m ² /g) | 36.84 | 37.04 | 37.65 | 48.66 | 39.46 |
| Catalyst bulk density (g/ml) | 0.96 | 0.94 | 1.01 | 1.03 | 1.11 |
| Porosity (%) | 68.60 | 66.92 | 67.66 | 69.64 | 70.78 |

^a This exposure time does not include the lance blocking.

bulk was varying in the range 0.8–2.5 wt%, whereas the P-content was varying in the range 0.4–0.8 wt%. Apart from the K-content in KP200, both the levels of K and P found in the bulk of the two elements were decreasing from the top to the bottom in agreement with both the higher particle concentration and the higher mass transfer due to the developing flow and higher level of turbulence at the top. About double levels of K were found on KP100 compared to KP200, whereas the levels of P were roughly the same. The calculated bulk K:P molar ratios were in the range 0.85–2.52 and therefore less than 3, which is the value introduced into the system by the K₃PO₄ molecule, indicating a different path for the accumulation of K and P in the catalyst walls.

Regarding the external surface composition measured by SEM-EDX shown in Table 3, very high concentrations of P have been found. In particular, the element KP200 reported P-concentrations up to 12.6 wt%. In the case of KP100, the P-content was ranging between 1.0 and 2.8 wt%. The cross sections of the samples KP100B and KP200T shown in Fig. 2 have also been analyzed by SEM-EDX in order to measure the distributions of K and P along the catalyst walls. The results of the EDX measurements are shown in Fig. 3a and c. As shown in the plots, both the K- and P-content decrease as a function of catalyst wall depth, indicating a diffusion limited process. Only in the case of KP100B, the K-content is almost constant around 0.7 wt% throughout the analyzed wall thickness. However, the major difference between the K- and P-distributions is that, in the case of K, the concentration in the walls always appears to level off at a finite K-level (i.e. 0.7 wt% in the cases shown in Fig. 3a), whereas the P-concentration decreases to zero.

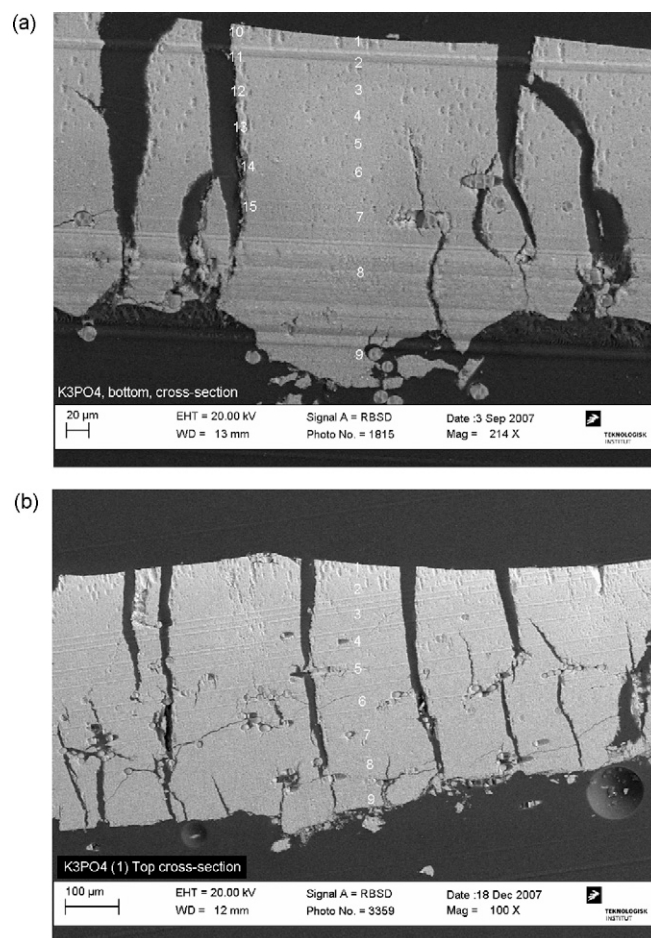


Fig. 2. SEM picture of the cross section of KP100B (a) and KP200T (b).

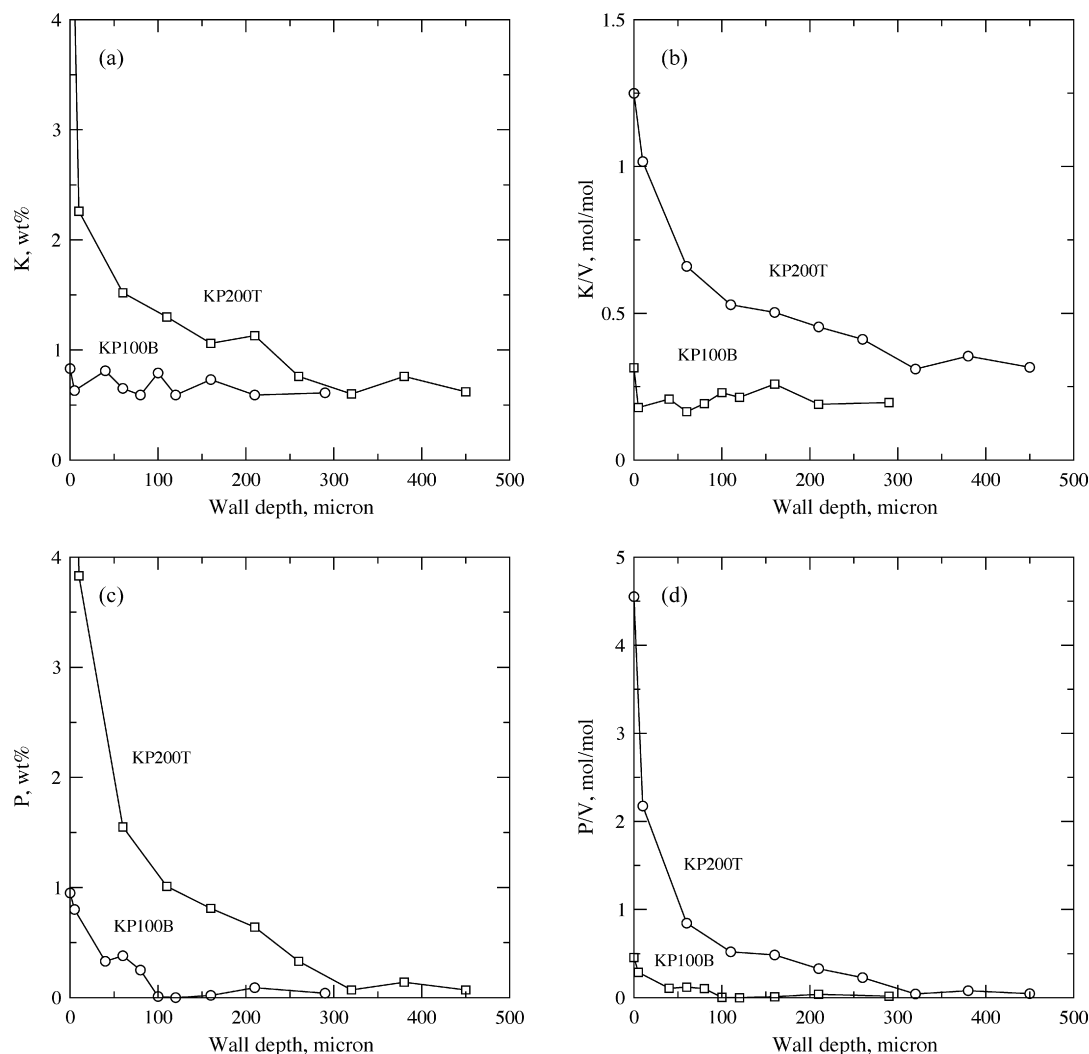


Fig. 3. K- and P-content and K:V and P:V molar ratios along the KP100B and KP200T walls as measured by SEM-EDX.

From these profiles, it appears that K tends to penetrate and remain in the catalyst wall, whereas P either is characterized by a slower mobility compared to K, or its penetration is counterbalanced by simultaneous evaporation of P as it was shown in our previous study [22]. As expected, in the presence of higher total K_3PO_4 concentrations in the flue gas, both K and P tend to accumulate on the outer catalyst surface.

Finally, Fig. 3b and d shows the calculated values for the K:V and P:V molar ratios, which can be used to estimate the local activities of the catalyst wall. According to values found in the literature [11,12], for K:V molar ratios equal to 0.2, up to 70% deactivation in the absence of mass transfer limitations can be expected.

3.2.2. Hg-porosimetry

The pore size distribution of the fresh and spent catalysts has been measured in order to clarify the presence of physical deactivation by pore blocking due to deposition of K–P particles. Fig. 4 reports the results of this investigation. The PSD of the fresh catalyst is clearly a dual-mode distribution, with the first peak found in the region 0.6–300 μm at 90 μm , and the second one in the region 0.003–0.6 μm at 0.03 μm . This dual-mode distribution is basically conserved in all spent catalyst samples. No major differences indicating pore blocking are found between the fresh and spent samples apart from the region 0.6–8 μm . Here, the spent samples consistently show almost no pores, whereas the fresh one

has a considerable amount of them. In particular, the porosity for the fresh sample in this diameter range has been calculated to be equal to 6.93%. This value dropped to 1.35 and 0.89% for KP100T and KP100B, respectively, and 1.32 and 1.19% for KP200T and KP200B, respectively. However, no major difference in the total intrusion volume of the spent catalysts compared to the fresh sample was found (Table 3). This fact may indicate that the sample outer wall layer, which is the first that gets in contact with Hg during the measurement, had no pores in that range due to deposit build-up and/or pore blocking, but kept the original structure of the inner wall.

3.3. Deactivation at the pilot-scale setup

3.3.1. Activity measurements

The results of the activity measurements carried out during exposure to 100 and 200 mg/Nm^3 K_3PO_4 are shown in Fig. 5. Overall the measured deactivation rate was increasing according to the K_3PO_4 concentrations in the flue gas. In both cases, the deactivation was very fast at the beginning of the exposure: The two elements lost respectively 26 and 31% of their original activity during the first 72 h. After this initial period, the deactivation proceeded at slower but still appreciable rates.

The addition of 100 mg/Nm^3 was carried out for 720 h. After this period of time, the element was exposed to clean flue gas for

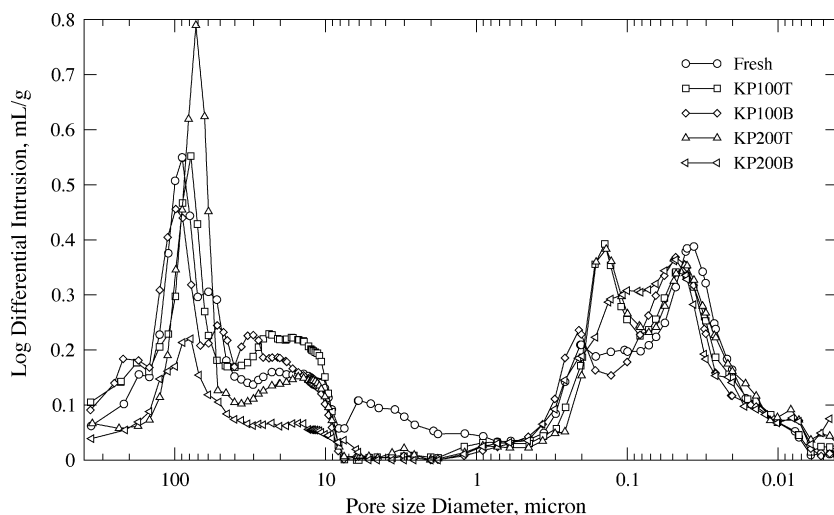


Fig. 4. Pore size distribution for fresh and spent samples measured by Hg-porosimetry.

additional 288 h, before it was taken out and characterized. The relative activity at the end of the addition time was 62%, corresponding to an overall deactivation rate of about 1.3%/day. During the subsequent exposure to the *clean* flue gas, the element regained 9% of relative activity. In particular, 7% was regained after the first 24 h after the addition was shut off. During these 24 h, the pressure drop over the monolith decreased by 11% indicating some cleaning of the channels due to soot blowing, which was continued after the addition stopped.

The addition of 200 mg/Nm³ was carried out for only 280 h and was more problematic than the previous test. Due to the higher K₃PO₄ load, the two-fluid nozzle used for atomizing the water solution tended to clog due to salt deposition. In particular, the compressed air line right at the meeting point with the liquid solution was the one that had the higher tendency in getting clogged. When this happened, the solution was not correctly atomized and was eventually introduced as a liquid jet. The jet was then simply hitting the hot pipe walls right after the lance and forming massive deposits of salt. Clogging of the nozzle mainly happened two times: After 89 and 284 h from the addition start. In

both cases, the activity measurement performed after the clogging showed an increased relative activity of the element compared to the previous test. These facts are in agreement with the result obtained with the element KP100, when this latter was exposed to a *clean* flue gas as discussed before. Overall, at the end of the experiment, the element KP200 had lost 22% of its original activity. However, the minimum relative activity was measured after 284 h during the last activity measurement before the nozzle clogged for the second time. Here the relative activity was equal to 73%, corresponding to a deactivation rate equal to about 2.3%/day.

3.3.2. NH₃-chemisorption tests

Fig. 6 shows the results of NH₃-chemisorption tests made with the element KP100 and KP200 during the addition of K₃PO₄. Since the amount of reduced NO is assumed equal to the amount of NH₃ chemisorbed on the catalyst surface, a longer time for the NO measured at the outlet to equalize to the value measured at the inlet indicates that more NH₃ is chemisorbed on the catalyst. From Fig. 6 it can be seen that the fresh element was able to chemisorb a higher amount of NH₃, and that this was decreasing as a function of the exposure to K₃PO₄. In particular, after 408 h of exposure the

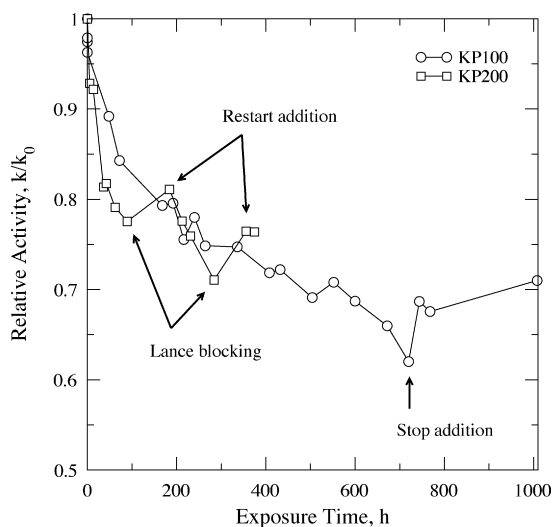


Fig. 5. Relative activity as a function of exposure time. Total flow: 40 Nm³/h. Gas composition: NO = 500 ppmv, NH₃ = 600 ppmv, O₂ = 10 vol%, CO₂ = 6 vol%, and 10 vol% H₂O in N₂. T = 350 °C.

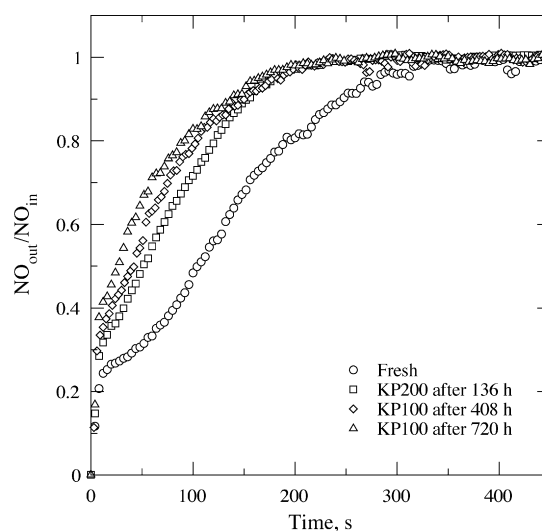


Fig. 6. NH₃-chemisorption test for the element exposed to 100 mg/Nm³ K₃PO₄ at different times during the exposure. T = 350 °C.

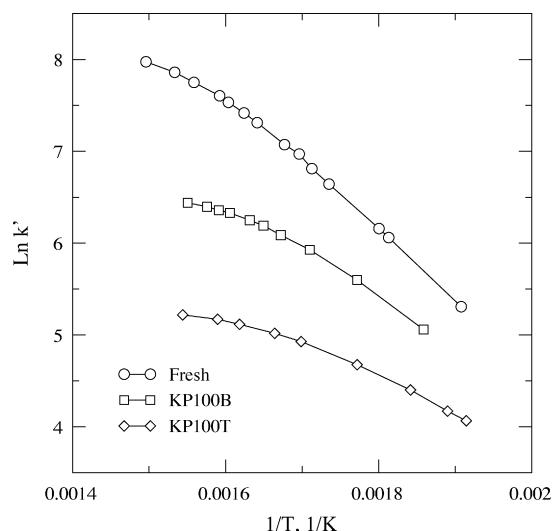


Fig. 7. Activity measurements on powdered samples. Total flow: 2.8 NL/min. NO = 521 ppmv; NH₃ = 622 ppmv; O₂ = 5.2%; H₂O = 1.47%; N₂ balance. Catalyst mass *W* = 0.072 g. Particle size: 105–125 μm.

amount of chemisorbed NH₃ on KP100 was about 54% of the fresh one. After 720 h, this further dropped to 47%. These results indicate that the deactivation was proceeding by deactivation of the sites for the NH₃-chemisorption.

3.4. Activity measurements in the laboratory

Fig. 7 shows an Arrhenius plot of the activities of powdered samples taken from the top and the bottom of the element KP100, together with a measurement made on a powdered fresh catalyst. The plot only reports the results in the temperature range 250–400 °C. In this range of temperatures, at the chosen experimental conditions, no external mass transfer limitations are present. Due to its very high activity, the fresh sample is subjected to some internal mass transfer limitations, as shown by the bending of the straight line at the higher temperatures in the Arrhenius plot (i.e. ≈ 10% at 350 °C). Due to the lower activity of the KP100T and KP100B samples, internal mass transport limitations are not responsible for the bending of the lines shown in the Arrhenius plot for these two doped samples. These may instead be the consequence of an increased activity in NH₃ oxidation at higher temperatures for the K-doped samples, as it was found in a previous work on K-poisoning [16].

As expected from the K- and P-content of the KP100 monolith, the top of the catalyst is more deactivated than the bottom. At 350 °C the relative activities for the top and the bottom of the element are equal to 9.1% and 30.0%, respectively.

4. Discussion

4.1. K- and P-accumulation and penetration mechanisms

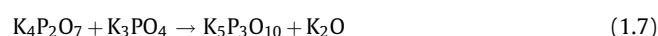
The bulk chemical analysis of the catalyst composition has shown a K:P molar ratio less than the theoretical value of 3, varying in the range 0.85–2.5. The same ratio was always lower than 1 on the outer surface. Assuming a reaction between the catalyst surface and the K₃PO₄ particles leading to accumulation of K in the wall and release of H₃PO₄ in the gas phase, in a similar way as the release of HCl from KCl on the catalyst surface [3], the resulting K:P molar ratio should have then been found higher than 3. This fact is clearly in contrast with the results of the bulk chemical analysis and indicates that the deposited particles are not only constituted by K₃PO₄.

Further confirming this fact is the dual-mode particle size distribution measured by the SMPS. As discussed above, both particles with a volume-based mean diameter around 30 nm and particles with diameters exceeding the upper limiting range of the SMPS were present in the gas. Simply based on their size, the following can be assumed for these two classes of particles:

1. Low particle diameters and high number concentrations indicate particle formation due to homogeneous nucleation in the gas phase. In other words, the particles with mean diameters of 30 nm are constituted by species which can be found in the gas phase at relatively high temperatures. Contrarily, particles with diameters up to 1 μm are more likely formed due to salt crystallization during water evaporation from the atomized aqueous solution according to their different solubilities.
2. The deposition rate of the smaller particles is higher due to the higher diffusion coefficients for these particles. In the presence of differences in the chemical composition as a function of particle size, the element characterizing the population with the higher number concentration and smaller particle diameters will accumulate faster on the catalyst surface.

In the absence of a detailed determination of the particle chemical composition due to the encountered experimental limitations, the scenario plotted in Fig. 8 is proposed.

1. *Condensate phosphates formation.* Potassium phosphate salts are reported to form condensate phosphates [26], here referred to as “KPO_x”



From these reactions K₂O is formed. According to equilibrium calculations performed in this work by using the commercial software FactSage 5.2, the formed K₂O will be converted to KOH by reacting with the flue gas moisture. At lower temperatures K₂CO₃ will be formed by reaction with CO₂.

2. *KH₂PO₄ formation.* Crystallization of salts which are not the thermodynamic stable phases under the conditions of crystallization is reported to be rather common for the potassium orthophosphate system [26]. This means that the salts formed during the fast water evaporation from every single K₃PO₄ solution drop sprayed into the flue gas may differ from the initial K₃PO₄. Table 4 shows the known P–K salts and their solubility in water. In this, the solubility for KOH is also reported. As it can be seen, KH₂PO₄ is the salt with the lowest solubility. This indicates that this compound is the first that precipitates when water evaporates from a drop in the hot flue gas. The remaining K, which is not bound to the formed KH₂PO₄ will later precipitate as KOH



Part of the P may also lead to some H₃PO₄. After water evaporation, the formed aerosols will be heated by the

Table 4
Solubility and melting temperature for different K-species.

| | Solubility (g/100 g H ₂ O) | Melting temperature (°C) |
|---------------------------------|---------------------------------------|--------------------------|
| K ₃ PO ₄ | 106 | 1340 |
| K ₂ HPO ₄ | 168 | dec. 465 |
| KH ₂ PO ₄ | 25 | 253 |
| KOH | 121 | 406 |
| K ₂ CO ₃ | 111 | 891 |

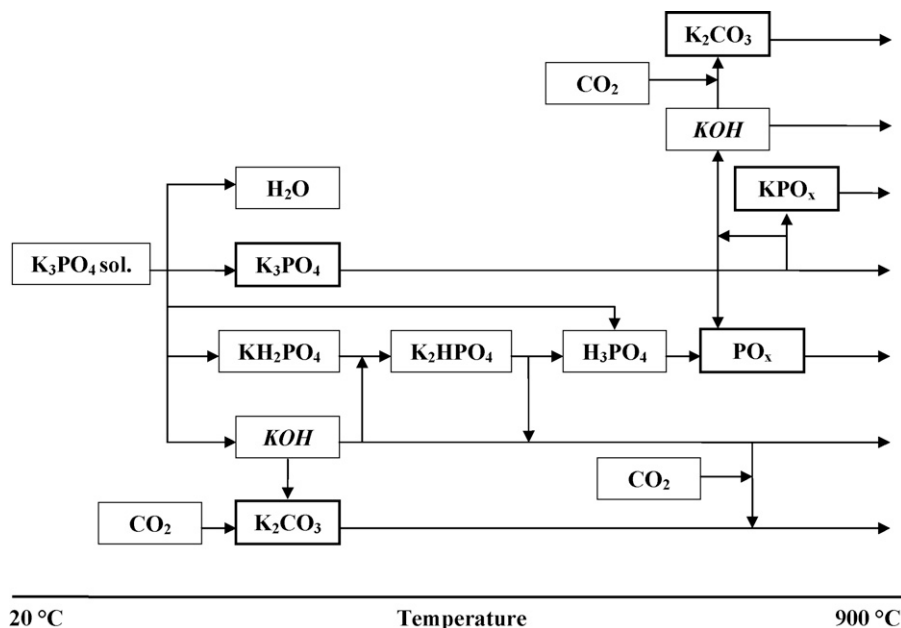
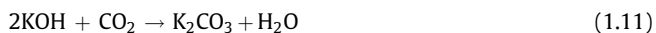


Fig. 8. Possible reactions during heating of K_3PO_4 solution droplets. The compounds in bold boxes are the ones most likely found at the SCR reactor inlet.

surrounding flue gas, and both the formed KH_2PO_4 and KOH are then converted to the more stable K_2HPO_4 :



At temperatures higher than 465 °C the K_2HPO_4 will finally decompose. This decomposition may lead to formation of gaseous H_3PO_4 . Moreover, the formed KOH will be converted to solid K_2CO_3 by reaction of KOH with CO_2 :



In both cases, the formation of H_3PO_4 , KPO_x , K–P-salts with K:P molar ratios lower than 3 and some K_2CO_3 , at the expenses of some of the original K_3PO_4 is foreseen. Among these species, H_3PO_4 can be regarded as responsible for the formation of the aerosols with mean diameter equal to 30 nm. Similar results have in fact been obtained during our previous investigation [22]. In this way, the high P-content on the outer catalyst surface measured by SEM-EDX would be explained, since it would be due to the higher deposition rates for these small particles compared to the bigger ones, where K is concentrated. Regarding the presence of K_2CO_3 , this cannot be proved by the tests carried out in this work. However, the relatively high K:P molar ratios measured on the impactor stages may be considered as an indication of the presence of P-free K-particles. Moreover, it can be argued that the gas released by the deposits collected with the impactor was CO_2 . Most of the compounds present in Fig. 8 are deliquescent, and therefore form a liquid solution when exposed to the ambient air, in agreement with the experience of the collected deposits. In this liquid solution then, release of CO_2 could be possible due to recombination of the species in the liquid phase, and could be favoured by the presence of acid compounds like the polyphosphoric acids.

The SEM-EDX of the catalyst wall cross sections indicate a faster net penetration for K compared to the one measured for P. Even though there still is an uncertainty about the real composition of the aerosols involved in the performed tests, and the presence of different species have been assumed, these different penetration rates are not likely associated to the presence of different species

with different particle sizes and mobilities in the solid state. These are instead more likely associated with the different affinities between the elements K and P towards the acidic surface of the catalyst. It is here assumed that *solid-state acid–base reactions* are the major driving force responsible for reaction between the K-atoms from the particles and the catalyst surface. Since particles are deposited at the outer layers of the catalyst walls, a K-surface-gradient in the wall is first formed. This gradient is then responsible for the further penetration/distribution of the K-atoms by *surface diffusion*. On the other hand, P is included in acidic compounds. Consequently, acid–base reactions between the P-containing particles and the catalyst surface are not expected. The penetration of P is then mainly controlled by capillary forces applied on the viscous liquid phase the polyphosphoric acids are made of, and possibly K–P solid particle diffusion in the external layers of the catalyst walls. Furthermore, considering that the PO_x are hydrolyzed by the flue gas moisture at the reactor temperature releasing gaseous H_3PO_4 [22], the P-concentration in the wall will approach zero as observed. This would in fact be the result of combined particle deposition and P-evaporation. The P which is included in K–P salts might also leave the particle as H_3PO_4 when the K reacts with the catalyst surface.

4.2. Deactivation mechanism

The exposure of the commercial monoliths used in this work to a flue gas containing aerosols of K- and P-species has rapidly lowered the activity of the tested elements. In the absence of particles, the deactivation did not continue any further. On the contrary, when the exposure was performed without any K_3PO_4 addition, some reactivation of the catalysts was observed (9%). These facts indicate that (i) the aerosols are necessary to get any deactivation; (ii) reversible physical deactivation by outer surface fouling is contributing to the measured deactivation. According to the K-content measured by SEM-EDX analysis and the activity measurements made on powders, an agreement with the poisoning data from the literature has been found. For instance, the SEM-EDX analysis for the sample KP100B showed a constant K:V value of 0.2 along the whole wall. For the same sample, the relative intrinsic activity measured on powder was equal to 30% at

300 °C (Fig. 7), in good agreement with previous studies of K-poisoning [11,12]. This fact and the results of the NH₃-chemisorption tests indicate that the deactivation measured is mainly due to poisoning by K via blocking of the active sites for NH₃-chemisorption as reported in previous works [3,11–15]. The influence of poisoning by polyphosphoric acid is in this work not significant due to: (i) the relative low levels of P found due to simultaneous hydrolysis of the deposited acids; (ii) their relative low poisoning strength compared to K; (iii) a possible lowering of the deactivation strength of the polyphosphates due to the presence of K.

Physical deactivation due to pore blocking or surface masking by particle deposition is not likely to be the main mechanism responsible for the deactivation measured, but it is clearly contributing to the overall deactivation as indicated by the partial reactivation obtained by exposing the spent monoliths to clean flue gas while soot blowing. In particular, the almost complete disappearance of the pores in the range 0.6–8 µm for all the spent catalysts, together with the small loss (i.e. 6%) of the total intrusion volume are indications of the formation of an outer fouling layer. With up to 12 wt% P found on the outer catalyst surface, and since the polyphosphoric acids are viscous liquids at the SCR temperature [22], it is believed that they are playing an important role in the formation of this fouling layer by gluing together the different deposited particles. In general, an efficient soot blowing system is required not only to keep the channels opened, but also to clean their external surface.

5. Conclusion

K₃PO₄ has been indicated as a potential product of combustion of biomass mixed with P- and Ca-based K-getter additives for reducing fouling and corrosion problems on superheater surfaces at power stations. In order to evaluate whether the formation of this compound might also have a positive effect on the vanadia-based SCR catalysts by limiting the fast rate of deactivation normally experienced with KCl or K₂SO₄, K₃PO₄ has been added in a hot flue gas at a SCR pilot-scale setup and the activity of two commercial vanadia-based monoliths has been followed as a function of exposure time.

During the performed tests, different K- and P-compounds have been formed from the originally injected K₃PO₄. A dual-mode volume-based particle distribution with peaks at around 30 nm and at diameters >1 µm has been measured at the SCR reactor inlet. The distribution of K and P in the different particles has thereby influenced the rate of deposition and accumulation of the species in the exposed catalysts. In order to explain the high P-concentrations and low K:P molar ratios found on the outer catalyst surface, the smaller particles have been associated with liquid phase phosphates (PO_x and KPO_x), whereas the larger ones have been associated to potassium phosphates formed during evaporation of water from the injected droplets.

Deactivation rates up to 3%/day have been measured. K has been found to penetrate the whole catalyst wall indicating that this is not strongly bound to the particles and relatively fast reacts with the catalyst surface and subsequently penetrates the catalyst wall by surface diffusion. The NH₃-chemisorption studies have shown that the deactivation has mainly proceeded via K-poisoning by blocking the sites for NH₃ adsorption. All these data recall the mechanism of deactivation previously reported during exposures to KCl and K₂SO₄ and therefore indicate that binding K to P by the

addition process does not seem to be an advantageous solution with respect to the vanadia-based SCR catalysts.

Poisoning by polyphosphoric acids is not clearly seen in this investigation due to both the relatively low P-content in the catalyst and the low poisoning strength compared to K. However, Hg-porosimetry has revealed the occurrence of fouling and pore mouth blocking at the outer catalyst surface. It is believed that the polyphosphoric acids play an important role in the formation of this layer by gluing together the deposited particles and should therefore be considered a fouling promoter.

Acknowledgments

This work is part of the CHEC (Combustion and Harmful Emission Control) Research Center funded a.o. by the Technical University of Denmark, the Danish Technical Research Council, the European Union, the Nordic Energy Research, Dong Energy A/S, Vattenfall A.B., F L Smidth A/S, and Public Service Obligation funds from Energinet.dk and the Danish Energy Research program. In particular, this work is supported by the PSO project "Deactivation of SCR Catalysts by Additives" (PSO Elkraft FU-4205). Supply of the catalyst samples by Haldor Topsøe A/S is gratefully acknowledged.

References

- [1] L.L. Baxter, T.R. Miles, T.R. Miles Jr., B.M. Jenkins, T. Milne, D. Dayton, R.W. Bryers, L.L. Oden, *Fuel Processing Technology* 54 (1998) 4778.
- [2] K.A. Christensen, H. Livbjerg, *Aerosol Science and Technology* 25 (1996) 185–199.
- [3] Y. Zheng, A.D. Jensen, J.E. Johnsson, *Applied Catalysis B: Environmental* 60 (2005) 261–272.
- [4] Å. Kling, C. Andersson, Å. Myringer, D. Eskilsson, S.G. Järås, *Applied Catalysis B: Environmental* 69 (2007) 240–251.
- [5] L. Tobiasen, R. Skytte, L.S. Pedersen, S.T. Pedersen, M.A. Lindberg, *Fuel Processing Technology* 88 (2007) 1108–1117.
- [6] L. Sørensen, J. Fjellerup, U. Henriksen, International Publication Number WO 01/05911 A2. (2001).
- [7] P.A. Jensen, L.H. Sørensen, G. Hu, J.K. Holm, F. Frandsen, U.B. Henriksen, Technical University of Denmark (2005) KT-Report No. 0504.
- [8] V.I. Parvulescu, P. Grange, B. Delmon, *Catalysis Today* 46 (1998) 233–316.
- [9] N.-Y. Topsøe, H. Topsøe, J.A. Dumesic, *Journal of Catalysis* 151 (1995) 226–240.
- [10] N.-Y. Topsøe, J.A. Dumesic, H. Topsøe, *Journal of Catalysis* 151 (1995) 241–252.
- [11] J.P. Chen, M.A. Buzanowski, R.T. Yang, *Journal of the Air and Waste Management Association* 40 (1990) 1403–1409.
- [12] J.P. Chen, R.T. Yang, *Journal of Catalysis* 125 (1990) 411–420.
- [13] L. Lietti, P. Forzatti, G. Ramis, G. Busca, F. Bregani, *Applied Catalysis B: Environmental* 3 (1993) 13–35.
- [14] H. Kamata, K. Takashi, C.U.I. Odenbrand, *Journal of Molecular Catalysis A: Chemical* 139 (1999) 189–198.
- [15] R. Khodayari, C. Andersson, C.U.I. Odenbrand, L.H. Andersson, *Proceeding of the Fifth European Conference on Industrial Furnace and Boilers*, vol. II, 11–14 April 2000, Espinho, Porto, Portugal, 2000.
- [16] Y. Zheng, A.D. Jensen, J.E. Johnsson, *Industrial and Engineering Chemistry Research* 43 (2004) 941–947.
- [17] Y. Zheng, A.D. Jensen, J.E. Johnsson, *Applied Catalysis B: Environmental* 83 (2008) 186–194.
- [18] J.A. Moulijn, A.E. van Diepen, F. Kapteijn, *Applied Catalysis A: General* 212 (2001) 3–16.
- [19] J. Blanco, P. Avila, C. Barthelemy, A. Bahamonde, J.A. Odriozola, J.F. Garcia de la Banda, H. Heinemann, *Applied Catalysis* 55 (1989) 151–164.
- [20] H. Kamata, K. Takahashi, C.U.I. Odenbrand, *Catalysis Letters* 53 (1998) 65–71.
- [21] J. Beck, J. Brandenstein, S. Unterberger, K.R.G. Hein, *Applied Catalysis B: Environmental* 49 (2004) 15–25.
- [22] F. Castellino, S.B. Rasmussen, A.D. Jensen, J.E. Johnsson, R. Fehrmann, *Applied Catalysis B: Environmental* 83 (2008) 110–122.
- [23] J. Beck, R. Müller, J. Brandenstein, B. Matschenko, J. Matschke, S. Unterberger, K.R.G. Hein, *Fuel* 84 (2005) 1911–1919.
- [24] J. Beck, S. Unterberger, *Fuel* 86 (2007) 632–640.
- [25] N.-Y. Topsøe, T. Slabicki, B.S. Clausen, T.Z. Srnak, J.A. Dumesic, *Journal of Catalysis* 134 (1992) 742–746.
- [26] J.R. Van Wazer, *Phosphorus and Its Compounds*, Interscience Publisher, New York, 1958.

Appendix C



Influence of reaction products of K-getter fuel additives on commercial vanadia-based SCR catalysts

Part II. Simultaneous addition of KCl, Ca(OH)₂, H₃PO₄ and H₂SO₄ in a hot flue gas at a SCR pilot-scale setup

Francesco Castellino^a, Anker Degn Jensen^{a,*}, Jan Erik Johnsson^a, Rasmus Fehrmann^b

^a Department of Chemical and Biochemical Engineering, Technical University of Denmark, Building 229, DK-2800 Kgs. Lyngby, Denmark

^b Centre for Sustainable and Green Chemistry, Department of Chemistry, Technical University of Denmark, Building 207, DK-2800 Kgs. Lyngby, Denmark

ARTICLE INFO

Article history:

Received 15 July 2008

Received in revised form 30 October 2008

Accepted 2 November 2008

Available online 14 November 2008

Keywords:

SCR

Deactivation

Vanadia

KCl

Polyphosphoric acid

Biomass

ABSTRACT

A commercial V₂O₅–WO₃–TiO₂ corrugated-type SCR monolith has been exposed for 1000 h in a pilot-scale setup to a flue gas doped with KCl, Ca(OH)₂, H₃PO₄ and H₂SO₄ by spraying a water solution of the components into the hot flue gas. The mixture composition has been adjusted in order to have P/K and P/Ca ratios equal to 2 and 0.8, respectively. At these conditions, it is suggested that all the K released during biomass combustion gets captured in P–K–Ca particles and the Cl is released in the gas phase as HCl, thus limiting deposition and corrosion problems at the superheater exchangers during biomass combustion. Aerosol measurements carried out by using a SMPS and a low pressure cascade impactor have shown two distinct particle populations with volume-based mean diameters equal to 12 and 300 nm, respectively. The small particles have been associated to polyphosphoric acids formed by condensation of H₃PO₄, whereas the larger particles are due to P–K–Ca salts formed during evaporation of the water solution. No Cl has been found in the collected particles. During the initial 240 h of exposure, the catalyst element lost about 20% of its original activity. The deactivation then proceeded at slower rates, and after 1000 h the relative activity loss had increased to 25%. Different samples of the spent catalyst have been characterized after 453 h and at the end of the experiment by bulk chemical analysis, Hg-porosimetry and SEM-EDX. NH₃-chemisorption tests on the spent elements and activity tests on catalyst powders obtained by crushing the monolith have also been carried out. From the characterization, it was found that neither K nor Ca were able to penetrate the catalyst walls, but only accumulated on the outer surface. Poisoning by K has then been limited to the most outer catalyst surface and did not proceed at the fast rates known for KCl. This fact indicates that binding K in P–K–Ca compounds is an effective way to reduce the negative influence of alkali metals on the lifetime of the vanadia-based SCR catalysts. On the other hand, P-deposition was favoured by the formation of the polyphosphoric acids, and up to 1.8 wt% P was accumulated in the catalyst walls. Deactivation by polyphosphoric acids proceeded at about 0.2% day^{−1}. About 6–7% of the initial activity was lost due to the accumulation of these species. However, the measured relative activity reached a steady-state level during the last 240 h of exposure indicating that the P-concentration in the bulk reached a steady-state level due to the simultaneous hydrolysis of the polyphosphoric acids.

© 2008 Elsevier B.V. All rights reserved.

1. Introduction

As described in Part I of this work [1], changes in the fly ash composition during biomass combustion are seen as a potential solution to both deposition and corrosion problems encountered

on the super-heaters at power plants. These problems are mainly due to the formation of KCl aerosols experienced during biomass combustion, which are formed during cooling of the flue gas. The above mentioned changes in the ash composition may involve the addition of P- and Ca-compounds in the boiler in order to create the reaction conditions at which (i) the K released by the biomass during combustion is captured in P–K–Ca compounds having higher melting temperatures than KCl; and (ii) the Cl is released in the gas phase as HCl thereby avoiding chlorine-induced corrosion.

* Corresponding author. Tel.: +45 45 25 28 41; fax: +45 45 88 22 58.
E-mail address: aj@kt.dtu.dk (A.D. Jensen).

Initial tests on P–Ca additives have shown up to 74–98% reduction in the Cl content of the deposits when the molar ratios of P/(K + Na) and P/Ca in the resulting fuel mixture were in the ranges 1.9–3.2 and 0.8–0.9, respectively [2]. For instance, similar values may be obtained by cofiring straw with about 13% meat and bone meal (MBM) on an energy basis.

The addition of these P- and Ca-compounds during biomass combustion and the corresponding changes in both ash load and composition may also have a beneficial effect on the fast SCR catalyst deactivation normally experienced during biomass combustion [3,4]. Here K, which is known as one of the strongest poisons for the vanadia-based catalysts normally used in the SCR process [5–11], once deposited as submicron particles of KCl and K_2SO_4 , is found to easily diffuse inside the catalyst wall and thereby deactivate the active sites. The transfer of K to the catalyst, as shown in Part I of this work, apart from being related to the submicron particles, is directly dependent on how strongly K is bound to the particle itself. In this sense, capturing K into P–K–Ca particles may decrease the amount of K that is released to the catalyst surface and deactivate it. These particles will in fact have higher melting temperatures and potentially a higher stability.

On the other hand, both Ca and P are known as deactivating compounds for the vanadia-based SCR catalysts [5,6,12–15]. Having a relatively weak poisoning strength, Ca is normally considered as a physically deactivating specie since during combustion it forms very stable compounds constituting the fly ash, which tend to block the pore structure of the catalyst wall. Furthermore, sulfation of the deposited Ca is often referred to form a fouling layer on the outer catalyst surface. On the other hand, P may act both as chemical and physical deactivating species according to the compounds it may form during combustion [15]. When polyphosphoric acids (PO_x) are formed, physical deactivation by pore blocking and surface masking is enhanced by the liquid viscous nature of these compounds. Furthermore, chemical deactivation at high concentrations (i.e. >100 ppmv) may be very fast and involves blocking of the catalytic cycle via formation of non-active V(4+) species [15]. Increasing the concentration in the flue gas of P and Ca by the addition process, which as stated above may require an excess of both species compared to K, may then lead to undesired deactivating effects. These may counterbalance the possible positive effects obtained by binding K into P–K–Ca particles.

The aim of this study is to evaluate the potential effects of the P, Ca addition process on the SCR catalysts by exposing a commercial vanadia-based SCR monolith to a flue gas doped with K, Ca and P for 1000 h and following its activity as a function of exposure time. The exposed catalysts are further characterized by a range of techniques.

2. Experimental

A water solution of KCl, $Ca(OH)_2$, H_3PO_4 and H_2SO_4 has been injected in a hot flue gas ($T > 900^\circ C$) from a natural gas burner. The resulting flue gas was then passed over a commercial SCR monolith, and the activity was periodically measured.

Both the setups and experimental procedures employed in the tests reported in this paper are the same as those described in Part I of this work, and are here only briefly introduced. For further details, see Ref. [1].

2.1. Catalysts

Commercial corrugate-type monoliths obtained from Haldor Topsøe A/S were used in this study. The catalysts were based on

V_2O_5 (up to 5 wt%) and tungsten oxide (WO_3 , up to 9 wt%) dispersed on a fibre reinforced TiO_2 carrier. The monoliths had a size of 75 mm × 75 mm × 500 mm. The hydraulic diameter of the channels was 6.44 mm. The wall thickness was about 1 mm. Pieces have been cut from both the fresh and spent monoliths in order to study their local properties under well defined reaction conditions in a laboratory fixed bed reactor. In order to run activity tests on powder samples, they have been gently crushed in a mortar and the particle fraction in the range 105–125 μm has been collected by sieving. The top and bottom 5 cm of the element were cut off after 453 h of exposure (indicated as “First cut” in this work), and the rest of the element was recharged in the reactor and the exposure restarted. In the following, the cut samples will be referred to as “ADD1T” and “ADD1B”, respectively. Two more samples were then cut off at the end of the test from the top and bottom 5 cm of the recharged element. They will be referred to as “ADD2T” and “ADD2B”, respectively.

2.2. SCR pilot plant

The SCR pilot plant setup used for this investigation is the same as described in [15]. It mainly consists of a natural gas burner for the flue gas production, a lance for spraying the aqueous solution, a square duct hosting a full length monolith and a NH_3 supply system. NH_3 is injected both in the burner to produce the desired NO concentration at the reactor inlet, and in the flue gas duct leading to the reactor for the NO reduction. Channel blocking is avoided by a soot blowing system installed at the reactor inlet.

2.3. K–P–Ca–S addition

In order to simulate the addition process, the molar P:K and P:Ca ratios in the flue gas have been fixed to 2 and 0.8, respectively. The KCl concentration has been fixed to 10 mg/Nm³. Accordingly, 13, 26 and 20 mg/Nm³ of $Ca(OH)_2$, H_3PO_4 and H_2SO_4 have been added. The addition has been carried out by preparing a water solution of the above listed compounds with the following concentrations: KCl = 6.7×10^{-3} mol/l, $Ca(OH)_2$ = 1.7×10^{-2} mol/l, H_3PO_4 = 1.3×10^{-2} mol/l, H_2SO_4 = 1.0×10^{-2} mol/l. In particular, H_2SO_4 was added in order to completely dissolve the different salts. Since the total flue gas flow at the injection point was equal to 50 Nm³/h, the solution feed has been fixed to 1 l/h. Only 40 Nm³/h were then let through the catalyst element during the whole exposure.

2.4. Aerosol measurements

Aerosol measurements were performed by using both a Scanning Mobility Particle Sizer (SMPS, TSI Inc.), which included an Electrostatic Classifier (Model 3080) and a Condensation Particle Counter (Model 3775), and a 10-stage Berner-type low pressure cascade impactor (LPI) with an aerodynamic diameter range of 0.03–12.7 μm connected to a vacuum pump. Sampling for the SMPS was made at the SCR reactor inlet by an ejector sampler running with dry, particle-free air. In the case of the LPI, the flue gas was sampled directly at the reactor inlet without any dilution. Both the sampling line and the LPI were therefore heated at 90 °C in order to avoid any water condensation.

2.5. Activity measurements

The rate of the SCR reaction at typical industrial reaction conditions has been assumed to follow an Eley–Rideal mechanism of reaction with NH_3 adsorbed on the catalyst surface and NO

reacting from the gas phase. The following expression for the rate of reaction, r_{NO} , can then be derived:

$$-r_{\text{NO}} (\text{mol/m}^3\text{s}) = k c_{\text{NO}} \frac{K_{\text{NH}_3} c_{\text{NH}_3}}{1 + K_{\text{NH}_3} c_{\text{NH}_3}} \quad (1.1)$$

where k [s^{-1}] is the rate constant, c_{NO} and c_{NH_3} [mol/m^3] are the concentrations of NO and NH_3 , respectively, and K_{NH_3} [m^3/mol] is the adsorption constant for NH_3 on the catalyst surface. The fraction term on the right-hand side of Eq. (1.1) is the NH_3 coverage of the catalytic surface, θ_{NH_3} .

At the pilot plant, the activities of the catalysts were measured at 350 °C in the presence of about 500 ppmv NO, 600 ppmv NH_3 , 10 vol.% O_2 , 6 vol.% CO_2 , and about 10 vol.% H_2O .

Since ammonia in our measurements is added in excess with respect to NO (i.e. $\text{NH}_3/\text{NO} \approx 1.2$), the NH_3 coverage, θ_{NH_3} , can be assumed equal to 1 and the reaction rate can be regarded as pseudo-first order with respect to NO and zero order with respect to NH_3 . Therefore, directly from the fractional NO conversion, X , it is possible to calculate an observed catalyst activity constant, k' , that includes both the influence of external and internal mass transfer:

$$k' (\text{ml/g s}) = -\frac{F_{\text{gas}}}{m_{\text{cat}}} \ln(1 - X) \quad (1.2)$$

where F_{gas} is the gas flow rate (ml/s), m_{cat} is the weight of catalyst (g). The degree of deactivation can then be calculated as the ratio k/k_0 between the rate constant of the catalyst during exposure, k , and the one measured for the fresh element, k_0 , right before starting the poison addition.

In the laboratory, powdered samples have been tested for activity in a packed bed quartz micro-reactor with a diameter equal to 10 mm. Around 0.07 g of powder has been used during activity measurements. This has been mixed with sand of the same particle size in order to have a particle bed of about 10 mm, thus ensuring the applicability of the here assumed integral reactor model. In all tests, the total flow was equal to 2.8 Nlitre/min constituted by 500 ppmv NO, 600 ppmv NH_3 , 5 vol.% O_2 and 1.4 vol.% H_2O in N_2 . Activity measurements have been performed in the temperature range 250–400 °C. The catalyst activity has been calculated according to Eq. (1.2) and the deactivation as the ratio between the activity constant of the spent catalyst and the one measured for the fresh one.

During all activity measurements, the NO concentration in the flue gas has been measured with a conventional UV analyzer (Rosemount NGA 2000). Due to the presence of water in the gas composition during all activity measurements, no N_2O formation is expected [16].

2.6. Ammonia chemisorption

NH_3 chemisorption tests have been periodically carried out at the pilot scale setup during exposure to the additive mixture. The measurements have been made at 350 °C and 40 Nm^3/h . Around 600 ppmv NH_3 has been added to the flue gas to the SCR reactor for 30 min in order to saturate the catalyst surface. During this saturation period, only the NO produced by the natural gas combustion was present (i.e. ≈ 80 ppmv). After this time, the NH_3 was shut off and right after, around 500 ppmv NO was produced by adding a different stream of NH_3 to the burner. The amount of chemisorbed NH_3 can then be calculated by integration over time the amount of reduced NO, due to the equimolar reaction between the gaseous NO and the chemisorbed NH_3 .

2.7. Catalyst characterization

Small pieces of the catalyst were cut from the ends of both fresh and exposed monoliths and characterized without further treatment with respect to bulk chemical composition, mercury porosimetry and physical appearance by a Scanning Electron Microscope (SEM).

The chemical composition was obtained by ICP-OES at the laboratory of DONG Energy A/S. Prior to the measurements, the samples were cut to $1.5 \times 1.7 \text{ cm}^2$ and dried at 105 °C for 2 h before analysis.

The total pore volume and the pore size distribution of the different catalyst samples were made by mercury intrusion in a Micromeritics Autopore II 9220 porosimeter. SEM-EDX analysis was performed at the Danish Technological Institute using a Zeiss Ultra55 and an Oxford ISIS with a Pentafet X-ray detector. In particular, the EDX analysis was performed on three different areas of about $200 \mu\text{m} \times 200 \mu\text{m}$ for each sample. The numbers reported in this work are the averages of the different measurements. The standard deviations of the measurements have been found <0.2, 0.2, 0.5, 0.6 and 0.2 wt% for V, K, P, Ca and S, respectively.

3. Results

3.1. Aerosol measurements at the pilot-scale setup

3.1.1. SMPS measurements

Fig. 1 shows the particle size distribution (PSD) measured by the SMPS. The number-based distribution (Fig. 1a) is characterized by a peak around 9 nm. Due to their small sizes, these particles are very mobile and are expected to have fast deposition rates on the catalyst surface. The volume-based distribution (Fig. 1b), which is proportional to the mass carried by the different particles, shows instead the presence of two distinct peaks. The first one has a mean diameter equal to 12 nm, whereas the second one has a peak around 300 nm. This second peak is clearly representing most of the volume/mass of the total PSD.

The dual-mode volume-based PSD measured by SMPS indicate the presence of mainly two classes of compounds:

1. The first one is constituted by small particles and high concentration numbers due to homogeneous nucleation of gaseous species. This class of particles accounts for about 6% of the total volume measured by the SMPS.
2. The second class is constituted by bigger particles with low total concentration numbers. Their formation is likely due to salt crystallization during water evaporation from the atomized solution droplets at the injection point. This class accounts for about 94% of the total volume measured by the SMPS.

Due to their different mobility and number concentrations, these two particle classes contribute differently to the species accumulation and penetration into the catalyst walls.

3.1.2. Low pressure cascade impactor test

The results of the tests made with the LPI are shown in Fig. 2 and reported in Table 1. Here a mass-based particle size distribution with a peak at around 200 nm can be seen. This value is lower than the one measured by the SMPS, and the difference is believed to be due to experimental uncertainties associated with the different sampling techniques and equipments. Particle deposition was found to happen at every single impactor stage as indicated by the non-zero particle concentration in the whole particle diameter range. The total mass concentration was about 10 mg/Nm^3 . The EDX chemical analysis of the collected deposits showed no Cl in

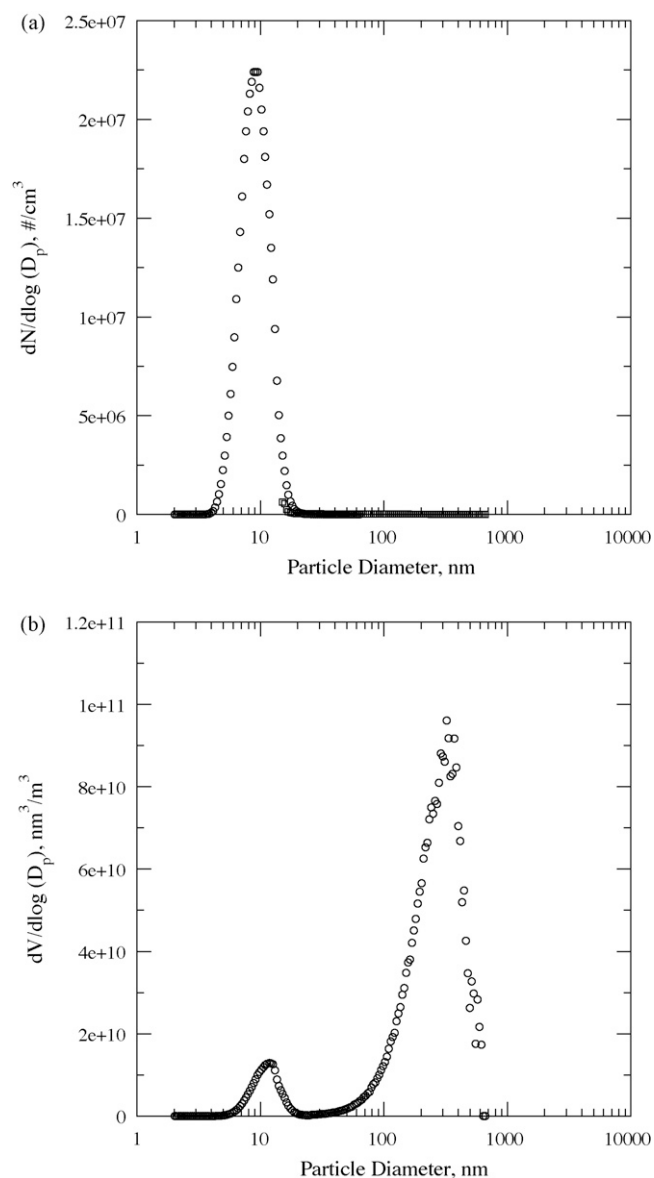


Fig. 1. Number-based (a) and volume-based (b) particle size distributions measured by a SMPS at the reactor inlet during simultaneous addition of KCl (10 mg/Nm³), Ca(OH)₂ (13 mg/Nm³), H₃PO₄ (26 mg/Nm³) and H₂SO₄ (20 mg/Nm³). *T* = 350 °C.

any of the impactor stages, indicating that Cl was effectively released to the gas phase prior to enter the SCR reactor. From the analysis of the element distribution shown in Fig. 2, it can be seen that both Ca and P are distributed in the particle diameter range

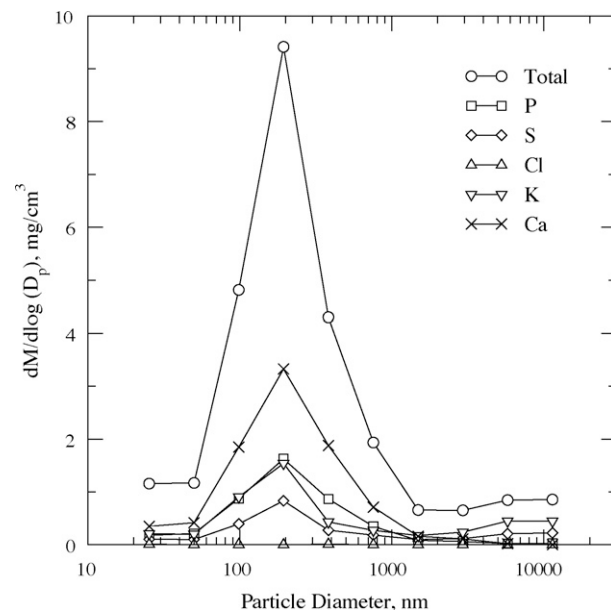


Fig. 2. Particle size distribution measured by a low pressure impactor at the reactor inlet during simultaneous addition of KCl (10 mg/Nm³), Ca(OH)₂ (13 mg/Nm³), H₃PO₄ (26 mg/Nm³) and H₂SO₄ (20 mg/Nm³). *T* = 90 °C. The curves for each single element have been obtained knowing their concentration on each single stage from EDX analysis.

25–3000 nm and are instead not found at higher diameters, where only K and S are found, probably due to the formation of some K₂SO₄. For each impactor stage, the different P:K, P:Ca, K:S and K:Ca molar ratios have been calculated and compared with the ones present in the injected solution. As it can be seen in Table 1, both P:Ca and K:S molar ratios have been found constant at around 0.65 and 1.55, respectively, throughout the whole particle size range, with only some exceptions for the P:Ca ratio at the first and second impactor stage. Simply based on these values it is not possible to identify the exact composition of the formed salts. However, by comparing the results with both the P:K and P:Ca injected, it is possible to conclude that some P is missing. This result might indicate the formation of gaseous P-compounds or the preferential formation of particles with diameters out of the impactor range, for instance those with volume-based mean diameter at 12 nm measured by the SMPS.

3.2. Catalyst characterization

3.2.1. Bulk and surface chemical analysis

Table 2 reports the results of both the bulk and surface analysis of samples taken from the exposed monolith at two different

Table 1
EDX analysis performed on the foils of the impactor stages.

| Stage (#) | Particle diameter (nm) | P/K (mol/mol) | P/Ca (mol/mol) | K/S (mol/mol) | K/Ca (mol/mol) |
|-----------|------------------------|---------------|----------------|---------------|----------------|
| 1 | 11,391 | 0.08 | 17.22 | 1.63 | 211.61 |
| 2 | 5,773 | 0.06 | 1.42 | 1.76 | 23.63 |
| 3 | 2,931 | 0.33 | 0.72 | 1.67 | 2.18 |
| 4 | 1,488 | 0.62 | 0.68 | 1.44 | 1.10 |
| 5 | 754 | 1.60 | 0.63 | 1.23 | 0.39 |
| 6 | 382 | 2.53 | 0.60 | 1.28 | 0.24 |
| 7 | 194 | 1.33 | 0.63 | 1.52 | 0.47 |
| 8 | 98 | 1.22 | 0.61 | 1.88 | 0.50 |
| 9 | 50 | 1.35 | 0.66 | 1.63 | 0.49 |
| 10 | 25 | 1.08 | 0.66 | 1.64 | 0.61 |
| Addition | | 2 | 0.8 | 0.67 | 0.4 |

Table 2

Bulk and surface chemical analysis for the fresh and spent monoliths.

| | Fresh | ADD1T | ADD2T | ADD2B | ADD1B |
|---------------------------|-------|-------|-------|-------|-------|
| Axial position (cm) | | 5 | 10 | 40 | 45 |
| Additive exposure (h) | | 453 | 1000 | 1000 | 453 |
| Bulk chemical analysis | | | | | |
| V% (wt/wt) | 1.6 | 2.4 | 1.9 | 1.8 | 1.7 |
| K% (wt/wt) | – | 0.1 | 0.2 | 0.1 | <0.1 |
| P% (wt/wt) | – | 0.7 | 1.8 | 1.3 | 0.5 |
| Ca% (wt/wt) | 1.7 | 2.1 | 1.9 | 1.7 | 1.8 |
| S% (wt/wt) | 0.3 | 0.4 | 0.4 | 0.3 | 0.3 |
| Cl% (wt/wt) | <0.1 | <0.1 | <0.1 | <0.1 | <0.1 |
| Surface chemical analysis | | | | | |
| V% (wt/wt) | 2.10 | 3.84 | 3.35 | 1.93 | 2.04 |
| K% (wt/wt) | – | 0.22 | 0.25 | 0.33 | 0.12 |
| P% (wt/wt) | – | 1.67 | 4.67 | 3.10 | 1.72 |
| Ca% (wt/wt) | – | 0.41 | 0.36 | 1.17 | 0.11 |
| S% (wt/wt) | 0.66 | 0.67 | 0.71 | 1.39 | 0.36 |
| Cl% (wt/wt) | – | – | – | – | – |

exposure times. According to the results obtained from the bulk elemental analysis, P is, among the different species, the element that has accumulated the most in the catalyst walls: on average, the P-accumulation rate is equal to 1.4×10^{-3} wt%/h, corresponding to about 4% of the incoming P mass. Regarding the Ca and S, the elemental bulk analysis did not show any important increase of these two species in the exposed samples. In fact, apart from ADD1T, the contents of Ca and S were similar to the ones measured for the fresh catalyst, indicating very low accumulation rates for these two elements. The same can be said for the Cl, where the levels were below the lower detection limits for all tested samples.

The results of the EDX surface chemical analysis showed the presence of all the added elements but Cl on the outer surface of the catalyst wall. P was again the most abundant element with a concentration in the range 1.7–4.7 wt%. These values are higher than the total P found in the bulk. As it will be seen later, the reason for the difference is in the decreasing P-concentrations measured along the cross-section of the catalyst wall. As stated before, Ca and S are normally found in the bulk of the fresh catalyst, but are not seen on the outer surface of the walls by EDX. This fact indicates that their presence might be due to the glass fibres, which are reinforcing the catalyst support. All the exposed samples showed instead some Ca and S also on the outer surface indicating that some deposition of these elements did happen during the exposure to the additive mixture. K was also found on the outer surface. The highest level was found on ADD2B, where this was equal to 0.3 wt%, corresponding to a K:V molar ratio equal to 0.2. Comparing the P:K and P:Ca ratios on the catalyst surface with the ratios in the injected solution indicates an enhanced accumulation of P in the catalyst walls.

3.2.2. SEM analysis

Aerosol deposition on the outer catalyst surface has been confirmed by the SEM pictures taken of the different samples, shown in Fig. 3. In the case of ADD1T shown in Fig. 3a, most of the characteristic macro-cracks were filled with particles. However, these particles which were deposited in the catalyst macro-cracks were able to penetrate the pores for only 20–30 μm , as shown in Fig. 3b for ADD1B, indicating that clogging of the macro-cracks did not necessarily require the complete filling of their pore volume. Fig. 3c shows a picture at higher magnifications of the deposits found in the macro-cracks.

At the end of the exposure, the appearance of the catalyst surface had changed. The SEM analysis made after 1000 h of exposure revealed the presence of layer on the outer catalyst surface. Fig. 4 shows the surface of the catalyst at different

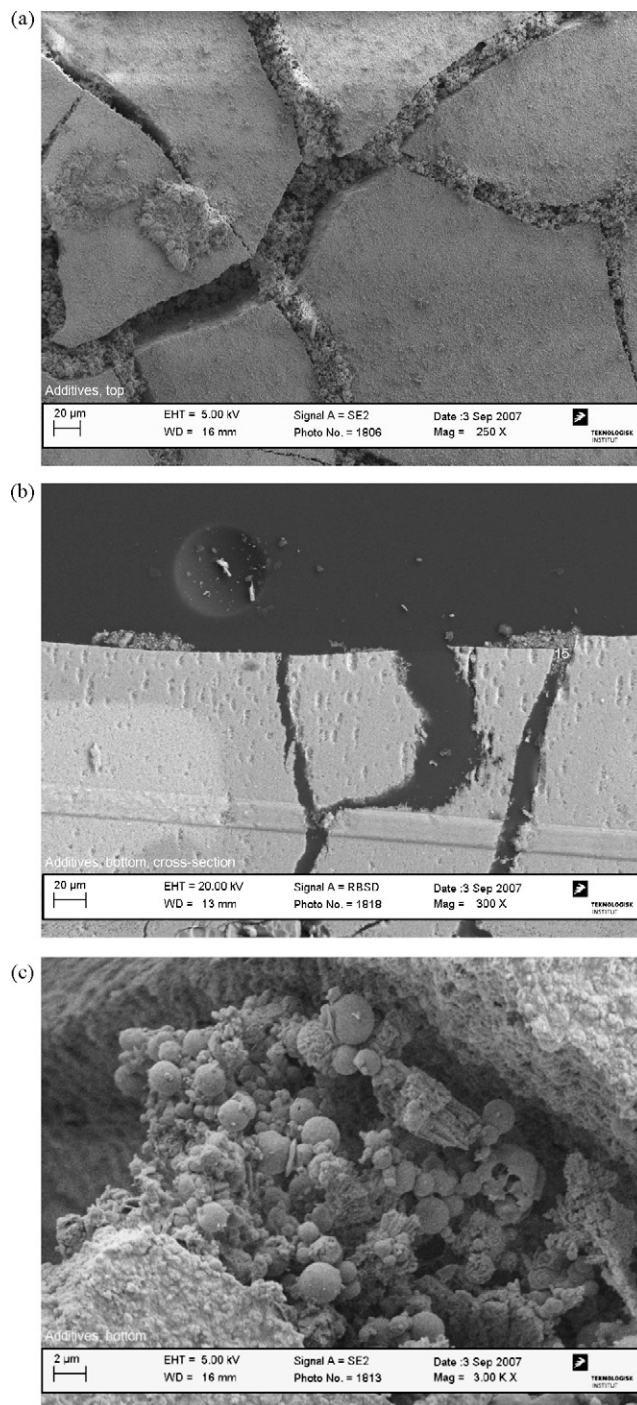


Fig. 3. SEM images of catalyst samples taken after 453 h of exposure: (a) ADD1T; (b) ADD1B; (c) ADD1B.

magnifications, together with pictures taken of a fresh sample at the same magnifications for comparison. This layer was revealed by the presence of unusual cracks on the surface as shown in Fig. 4a and b. As can be seen from these pictures, this layer appears as a compact phase about 2–3 μm thick. The comparison with the fresh sample surface clearly confirms the presence of this deposit covering the original catalyst surface. In fact, only the zones revealed by the deposit breakage somewhat recall the porous structure seen on the fresh sample. The EDX analysis of the zones underneath the formed layer, which were revealed by the outer layer cracks, had a reduced content of P compared to the top of the

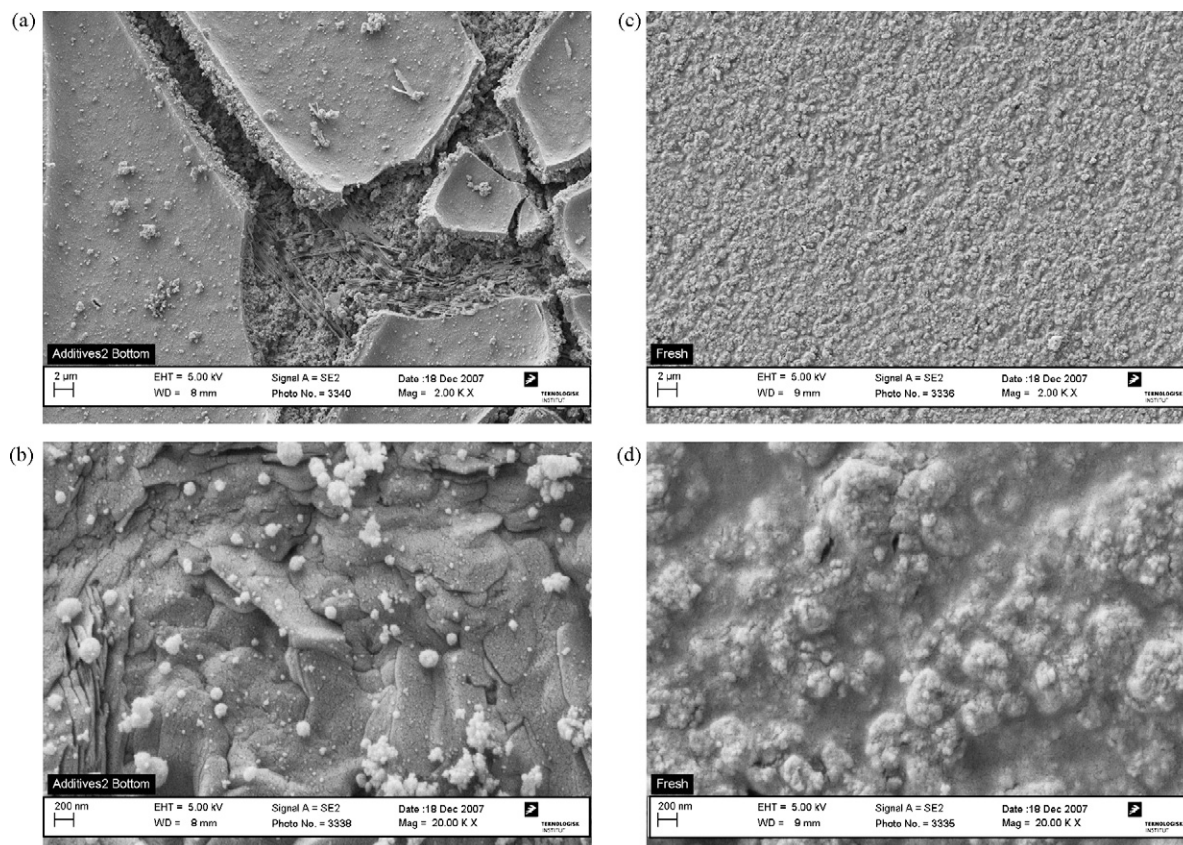


Fig. 4. SEM images of: (a and b) catalyst sample taken after 1000 h of exposure (ADD2B); (c and d) fresh sample. Magnification: (a and c) 2000 \times ; (b and d) 20,000 \times .

compact layer itself: in the zones opened to the original catalysts material, the P-content was found equal to around 1 wt%, whereas the average P-content of the surface was equal to 3 wt%.

Cross-sections of the catalyst sample have also been analyzed by SEM-EDX in order to measure the distribution of the different elements inside the catalyst walls. The P-distribution for the sample ADD1B and ADD2T are shown in Fig. 5. The measured

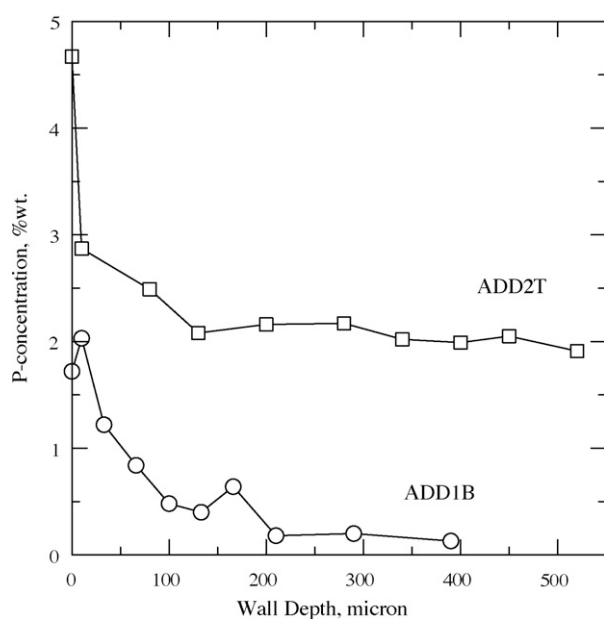


Fig. 5. P-concentration profile inside the spent catalyst walls.

profiles were those typical for diffusion limited processes, with the P-concentrations levelling off within the first 100 μm of the catalyst wall. In the figure, it can also be seen how the P-levels have increased according to the longer exposure in the sample ADD2T.

Regarding K and Ca, they were not found inside the catalyst walls indicating the inability of these elements in diffusing into the catalyst material. Sulphur was constantly ranging inside the walls between 0.4 and 0.5 wt%, identical to the values found for a fresh sample.

Overall, the results obtained from the analysis of the catalyst cross-sections clearly indicate (i) the ability of P in penetrating the whole catalyst wall; (ii) the inability of K and Ca, although deposited on the outer surface, to further diffuse inside the wall.

3.3. Deactivation at the pilot-scale setup

3.3.1. Activity measurements

Three activity measurements made after 0, 191 and 1000 h of exposure, respectively, are shown in Fig. 6. As it can be seen, apart from the different final conversions obtained, which are also dependent on different total catalyst mass due to the cut after 453 h, the conversion curve obtained at 1000 h differs from the other two curves because it first goes through a maximum value right after the NH_3 introduction, and then reaches a steady-state value after about 2 min of exposure to NH_3 . All the activity measurements made after around 300 h of exposure to the additive mixture have shown this behaviour. No NO conversion transient was instead measured at shorter exposure times, as shown by the activity tests made at 0 and 191 h of exposure. This NO transient was found in a previous investigation to be related to the accumulation of polyphosphoric acids in the catalyst wall and the subsequent titration of V(5+) active sites by formation of

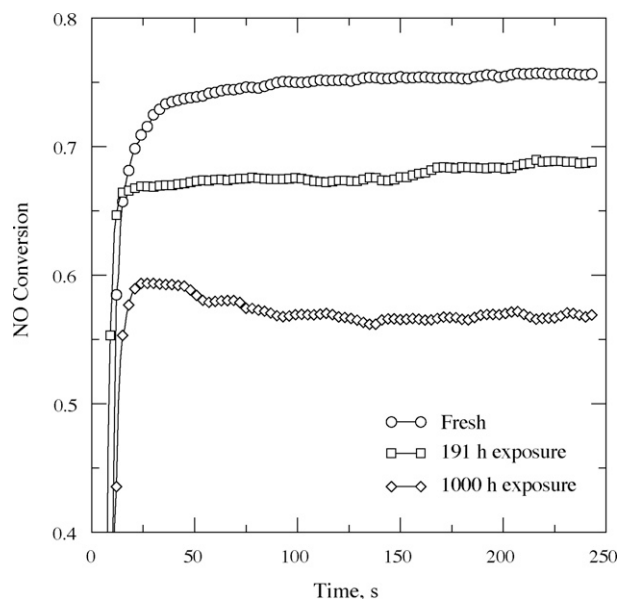


Fig. 6. Activity measurement made on fresh and spent monolith at 350 °C. Gas dry composition: NO = 500 ppmv, NH₃ = 600 ppmv, O₂ = 10 vol.%, CO₂ = 6 vol.%, H₂O = 10 vol.%. Flow: 40 Nm³/h.

P-V(4+) species during exposure to NH₃ [15]. From both the aerosol measurements and the catalyst characterization presented so far, it is clear that also in this case the transient can be associated to the PO_x. In order to isolate the PO_x effect on the overall degree of deactivation, for each activity measurement both a maximum and a steady-state relative activity have been calculated. The results of the calculation are shown in Fig. 7. As it can be seen, the two curves separate from each other after about 300 h of exposure. Fig. 8 shows a plot of the difference between the “Max X” and the “Steady-state” curve shown in Fig. 7. In the plot, the y-axis has

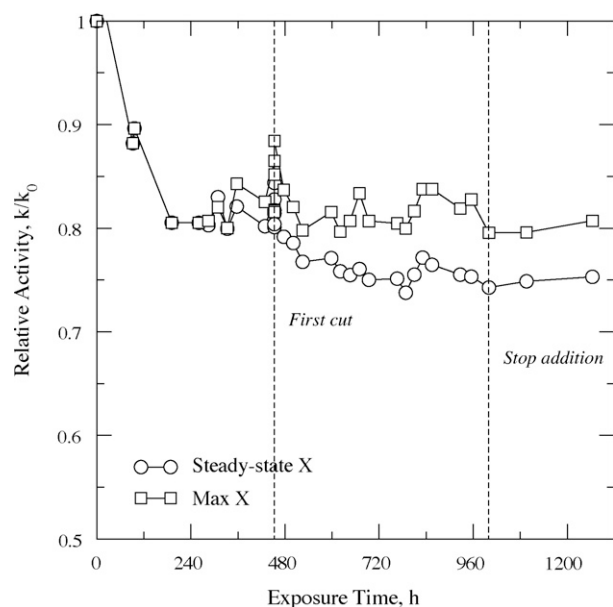


Fig. 7. Relative activity as a function of exposure time. The activity measurements were made at 350 °C. Gas dry composition: NO = 500 ppmv, NH₃ = 600 ppmv, O₂ = 10 vol.%, CO₂ = 6 vol.%, H₂O = 10 vol.%. Flow: 40 Nm³/h. The “Max X” data set represents the maximum NO conversion obtained during each single activity measurement, whereas the “Steady-state X” data set represents the final NO conversion obtained during the same measurements. The samples ADD1T and ADD1B were taken at the time indicated by “First cut”.

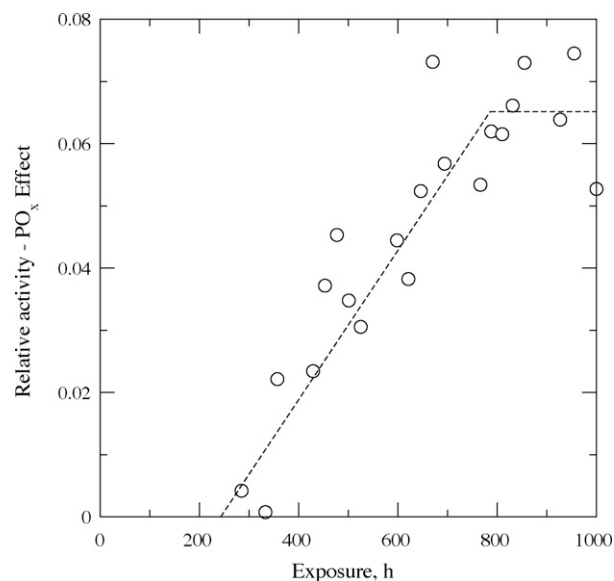


Fig. 8. PO_x deactivation effect as a function of exposure time. The data points represent the difference between “Max X” and “Steady-state X” curves in Fig. 6.

been labelled “Relative activity–PO_x effect” in order to underline that the curve represents the deactivation explicitly due to the polyphosphoric acids poisoning. As it can be seen, this mechanism caused a deactivation rate of 0.2% day^{−1} until about 750 h of exposure, after which the rate became nil, indicating a steady-state between P-deposition and loss by hydrolysis. At the end of the exposure, the percentage of total deactivation that could be associated to poisoning by PO_x was estimated equal to about 6–7%.

Apart from the quantification of the so-called “PO_x effect”, another important conclusion can be made from Fig. 7. Since the appearance of the NO conversion transient, the “Max X” relative activity has constantly remained around 81% throughout the whole exposure. In fact, 19% of the original activity was lost after the first 191 h of exposure, where no NO transient was measured. This result indicates that the components causing the fast drop of activity at the beginning of the exposure did not cause any further deactivation during the rest of exposure.

3.3.2. NH₃ chemisorption tests

The NH₃ chemisorption tests made before the first cut off of the top and bottom 5 cm are reported in Table 3, together with the observed steady-state relative activity for comparison, in order to understand the mechanism of deactivation that caused the steep initial decrease in relative activity. According to the NH₃ chemisorption tests, the 19% decrease of activity measured after 260 h of exposure was accompanied by a loss of only 16% in the total chemisorbed NH₃. A higher decrease in the relative amount of chemisorbed NH₃ compared to the decrease in relative activity would have been measured, if poisoning by K and/or Ca was the main responsible for the measured deactivation. This is because the monolith is operating under both external and internal mass

Table 3

Relative chemisorbed NH₃ and relative activity as a function of exposure time.

| Time (h) | NH ₃ (mol/kg) | NH ₃ /NH ₃₀ | k _{ss} /k ₀ |
|----------|--------------------------|-----------------------------------|---------------------------------|
| 0 | 0.033 | 1.00 | 1.00 |
| 260 | 0.028 | 0.84 | 0.81 |
| 333 | 0.028 | 0.84 | 0.80 |
| 357 | 0.029 | 0.86 | 0.82 |

transfer limitations, which are partially masking the effect of chemical deactivation on the intrinsic rate of reaction. Assuming (i) a square root dependency between intrinsic rate of reaction and the observed rate of reaction, valid for mass-transfer-limited reactions; and (ii) a linear relation between the chemisorbed NH_3 and the intrinsic activity, it can be calculated that poisoning only accounted for 8% of the lost activity. The remaining 11% was instead due to physical deactivation by pore blocking and surface masking.

After the first cut of material, a relative increase of chemisorbed NH_3 was measured. For instance, the element increased its capacity in chemisorbing NH_3 of about 39% in the last 600 h of exposure. This increase in chemisorbed NH_3 was found in our previous investigation to be related to the presence of polyphosphoric acids in the catalyst [15], which form P-sites where NH_3 can chemisorb. However, these sites are either *less active*, in agreement with Kamata et al. [13], or inactive, thus simply constituting an NH_3 -storage on the surface.

Similarly to our previous investigation [15], higher NO conversions could be obtained by increasing the NH_3 partial pressure in the flue gas, as shown in Fig. 9, where a standard activity measurement made after 1096 h of total exposure (i.e. after 1000 h exposure to the doped flue gas and 96 h exposure to a clean flue gas) followed by a test with the double amount of NH_3 introduced (i.e. 1200 ppmv) is reported. This additional activity at higher NH_3 partial pressures is related to changes in the NH_3 adsorption constant of the catalyst surface. It can then be argued that, due to the increased number of sites for the NH_3 chemisorption, the coverage of NH_3 appearing in Eq. (1.1) has become less than 1 at the typical condition of our activity measurements.

3.4. Activity measurements in the laboratory and Hg-porosimetry tests

Activity tests on powder samples have been carried out in the laboratory in order to more clearly identify the extent of deactivation measured on the monolith due to poisoning. Fig. 10 shows an Arrhenius plot of the activities of the fresh and spent

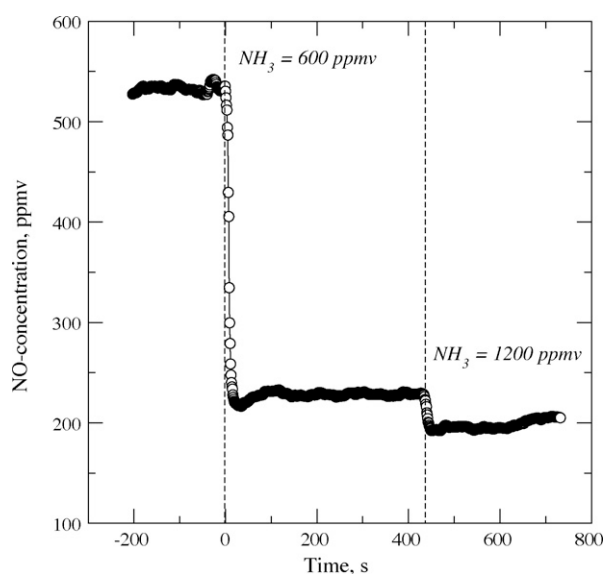


Fig. 9. Activity measurement on spent catalyst exposed for 1000 h to the doped flue gas and 96 additional hours to a clean flue gas. $T = 350^\circ\text{C}$. Gas dry composition: $\text{NO} = 500$ ppmv, $\text{NH}_3 = 600\text{--}1200$ ppmv, $\text{O}_2 = 10$ vol.%, $\text{CO}_2 = 6$ vol.%, $\text{H}_2\text{O} = 10$ vol.%. Flow: $40\text{ Nm}^3/\text{h}$.

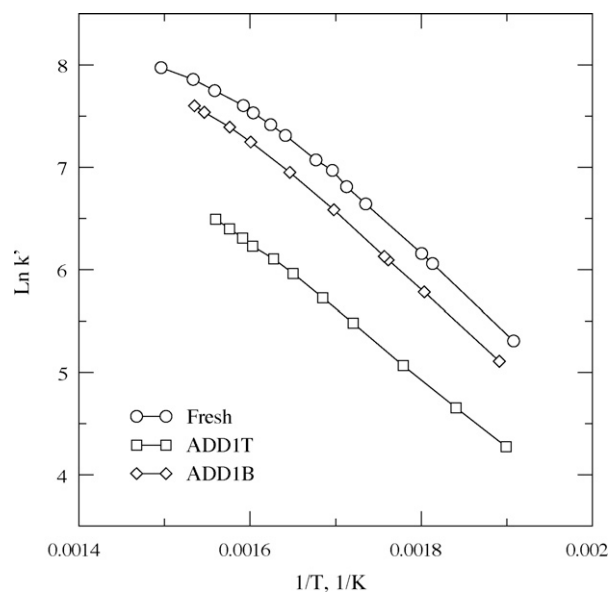


Fig. 10. Activity test on powder samples. Catalyst mass, $W = 0.07$ g. Total flow $F = 2.8$ Nlitre/min. Gas composition: $\text{NO} = 500$ ppmv, $\text{NH}_3 = 600$ ppmv, $\text{O}_2 = 5\%$, $\text{H}_2\text{O} = 1.4\%$ in N_2 .

catalyst samples exposed for 453 h (i.e. ADD1T and ADD1B). The plot only reports the results in the temperature range $250\text{--}400^\circ\text{C}$. In this range of temperatures, at the chosen experimental conditions, no external mass transfer limitations are present. Due to their high activities, both the fresh and ADD1B samples are subjected to some internal mass transfer limitations, as shown by the bending of the straight line at the higher temperatures in the Arrhenius plot. In particular, diffusion free conditions for the ADD1T and ADD1B samples are obtained at 326 and 337°C , respectively. The samples ADD1T and ADD1B had a relative activity of 27% and 75%, respectively. These values were constant in the whole temperature range as indicated by the same activation energy calculated from the Arrhenius plot (i.e. 63 kJ/mol).

Physical deactivation by formation of the external layer has been pointed out by the Hg-porosimetry analysis. Fig. 11 shows the pore size distribution for the fresh sample and ADD2B, which, as shown by the SEM pictures, presented a fouling layer on its external surface. As it can be seen in the figure, the ADD2B sample did not present any pores in the range $0.3\text{--}8\text{ }\mu\text{m}$. However the total intrusion volume did not differ between the two samples. This fact indicates that the outer surface of the ADD2B sample only presents pores smaller than $0.3\text{ }\mu\text{m}$ due to the formation of the fouling layer causing pore mouth closure.

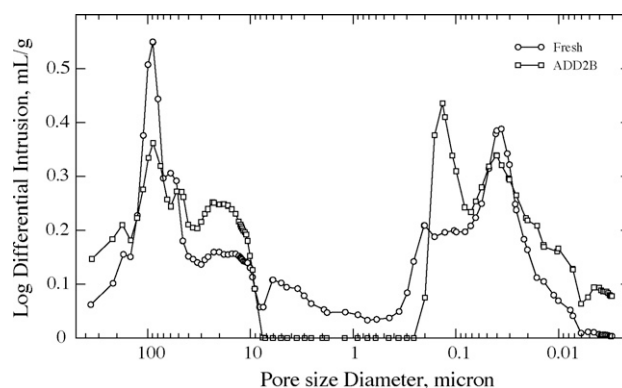


Fig. 11. Pore size distribution measured by Hg-porosimetry.

4. Discussion

4.1. Polyphosphoric acids formation

Based on the results obtained in a previous investigation about deactivation by polyphosphoric acids [15] and the results just described in this work (i.e. aerosol formation by homogeneous nucleation, NO conversion transient, increased amount of chemisorbed NH_3 , activity dependency on NH_3 partial pressures), there is no doubt about their formation during the exposure to the additive mixture in this work. The reasons for their formation during this particular test can be various, but they would all require the formation of gaseous H_3PO_4 and its exposure to temperatures higher than 600–700 °C. It is believed that some of the compounds which were formed during evaporation of the water from the atomized droplets went through decomposition at increasing temperatures and released some H_3PO_4 in the gas phase. This latter might also have been formed directly during the spraying process. At the end of the polyphosphoric acid investigation [15], it was not clear whether the formation would have been possible in a system including other different elements, or whether the formation was the result of the simplified flue gas composition used in those tests. The results obtained in this investigation have shown that the formation of polyphosphoric acids was possible in our system at the given P/K and P/Ca ratios. Depending on their concentration, polyphosphoric acids may constitute a high risk for a fast deactivation of the vanadia-based SCR catalysts, since for concentrations corresponding to 100 ppmv H_3PO_4 , their deposition might already be too fast compared to the rate of hydrolysis at SCR reaction conditions.

4.2. Particle deposition and penetration

The volume-based particle size distributions measured by the SMPS and the SEM pictures of the deposits have shown the presence of two distinct classes of particles. The first one with a volume-based mean diameter equal to 12 nm, and the second one with a volume-based mean diameter equal to 300 nm. Due to both a higher number concentration and a higher diffusion coefficient, the first class of particles is depositing faster than the other. By associating these particles to the polyphosphoric acids, which are liquid at the SCR temperatures, it can be assumed that the P found inside the catalyst walls is mainly due to their depositions and penetration due to capillary forces. On the other hand, the complete absence of Ca and K inside the walls is an indication that: (i) these elements are present in the bigger particles (i.e. $d_p > 0.1 \mu\text{m}$) which have lower deposition rates and practically no penetration ability; (ii) they are tightly bound to the particles themselves. This latter indication is particularly interesting since it further supports the mechanism of deactivation by K proposed in previous works [3,11]. It is now clear that the K present in the particles which are deposited on the outer surface of the catalyst needs to be released from the particles on atomic scale by interactions with the catalyst surface. It is only afterwards that K can diffuse inside the walls by surface concentration gradients. Particle diffusion is not likely to happen since the same mechanism would have also been active in this investigation, due to the similar particle sizes involved in the tests. K and Ca are instead accumulating on the outer surface. Due to the higher concentration of P found on the formed fouling layer, it is likely that the K–Ca–(P) crystals are glued together by deposited polyphosphoric acids forming the molten-looking layer. This fact would then indicate that the polyphosphoric acids can be regarded as fouling promoters. From the present data

it is not possible to know whether this outer layer would have continued growing or whether its thickness had reached a steady value. From the cracks found during the SEM analysis, it appears that some of it has fallen apart, but this could have happened during the cooling of the monolith and may not happen during normal operation.

Regarding the S-content, the SO_2 levels measured in the flue gas were approximately the same as those calculated by assuming the entire S added by the solution to be completely converted to SO_2 . Therefore it is believed that the additional S found on the outer surface of the catalyst is due to sulphation reactions between the deposits and the gaseous SO_2 . Moreover, since no additional S has been found inside the catalyst wall where only P had accumulated, it is assumed that the sulphation reaction preferentially takes place with K and Ca giving K_2SO_4 and CaSO_4 , respectively.

4.3. Deactivation mechanism

Based on the results presented, it can be concluded that the deactivation measured during this investigation followed different mechanisms, each of them acting in different periods of time. During the first 200 h of exposure, the steep decrease in observed deactivation (i.e. $2.4\% \text{ day}^{-1}$) was mainly due to physical deactivation surface fouling and blocking of the macro-cracks caused by particle deposition on the catalyst outer surface, with subsequent direct and indirect blocking of the active sites. Due to the pore blocking, the diffusion of both reactants and products is slowed down and, even though the inner layers of the wall are still very active since not attacked by the poison, they are less accessible. This mechanism of deactivation, however, is not expected to cause any further deactivation in the long term provided that the formed deposit layer will (i) keep some porosity, and (ii) not increase its thickness.

For exposure time >300 h, the observed deactivation was instead due to poisoning by polyphosphoric acids and initially proceeded at $0.2\% \text{ day}^{-1}$ and reached a steady-state level after about 750 h of exposure. Based on both the size and number concentration of the particles which have been assigned to the polyphosphoric acids (i.e. the peak around 9 nm) and the aerosols measurements made at different H_3PO_4 concentrations in a previous investigation [15], it can be estimated that these were counting for about 3–4 ppmv P during the test reported in this work, i.e. half of the total P injected in the flue gas. At these low concentrations, P-accumulation in the catalyst walls is limited by the hydrolysis of the polyphosphoric acids at the SCR temperature by the gas moisture [15]. Therefore, it is believed that the relative activity levelled off due to a steady-state PO_x -level in the catalyst wall obtained due to simultaneous deposition and hydrolysis.

Based on these considerations, it is not expected that further deactivation due to the just discussed mechanisms would have been measured if the exposure was continued.

5. Conclusion

Simultaneous addition of KCl, H_3PO_4 , $\text{Ca}(\text{OH})_2$ and H_2SO_4 in a hot flue gas has been carried out for 1000 h and a commercial SCR catalyst has been exposed to the resulting flue gas while the activity was followed as a function of exposure time. The test has been used to estimate the effects of the potential products of the K-getter additives during biomass combustion. In the test carried out, the P/K and P/Ca molar ratios have been fixed to values of 2 and 0.8, respectively, suggested in the literature.

Either K or Ca did penetrate the catalyst walls but only accumulated on the external catalyst surface. Poisoning by K and

Ca was therefore limited to the most outer wall layers. It has been estimated that 8% of initial relative activity (i.e. about 1/3 of the overall deactivation measured at the end of the test) was lost due to this mechanism, whereas 11% was lost due to physical deactivation by fouling and pore blocking.

At the chosen experimental conditions, formation of polyphosphoric acids has been favoured and about half of the total P has been estimated to be present in these compounds, which formed aerosols with volume-based mean diameter equal to 12 nm. The known deactivating effects of the polyphosphoric acids (i.e. NO transient, activity dependency on NH_3 partial pressures) have been identified: after the initial loss of activity, they controlled the overall deactivation rate, which was about $0.2\% \text{ day}^{-1}$. However, due to their relatively low concentration and the simultaneous occurrence of hydrolysis at the SCR reaction condition, the catalyst activity reached a steady-state after about 750 h of exposure. No additional deactivation was then measured in the following 250 h of addition.

Based on the results obtained in this work, it can be concluded that binding K into P–K–Ca compounds is an effective way of reducing the deactivation rates normally experienced during biomass combustion. Reactions between K and the V active sites are in fact prevented, and so is the penetration of K in the catalyst walls by surface diffusion. However, in real applications, the formation of polyphosphoric acids needs to be controlled, since this may counterbalance the just mentioned positive effects by promoting fouling and by poisoning the active sites. In particular, regarding the poisoning, PO_x levels in the range 1–10 ppmv may still be acceptable since their accumulation will be limited by their simultaneous hydrolysis, and a steady-state level in the catalyst wall will be reached. This situation could however be different in the presence of higher K-concentrations in the flue gas. If the fraction of P forming the PO_x is mainly controlled by the P/K and P/Ca ratios, at higher K-contents the amount of formed PO_x could be higher and thereby lead to faster deactivation rates. More tests at different P/K and P/Ca ratios would be necessary to understand the formation of PO_x , and suggest the conditions to limit it.

Acknowledgments

This work is part of the CHEC (Combustion and Harmful Emission Control) Research Center funded a.o. by the Technical University of Denmark, the Danish Technical Research Council, the European Union, the Nordic Energy Research, Dong Energy A/S, Vattenfall A.B., F L Smidth A/S, and Public Service Obligation funds from Energinet.dk and the Danish Energy Research program. In particular, this work is supported by the PSO project “Deactivation of SCR Catalysts by Additives” (PSO Elkraft FU-4205). Supply of the catalyst samples by Haldor Topsøe A/S is gratefully acknowledged.

References

- [1] F. Castellino, A.D. Jensen, J.E. Johnsson, *Applied Catalysis B: Environmental* 86 (2009) 166–175.
- [2] P.A. Jensen, L.H. Sørensen, G. Hu, J.K. Holm, F. Frandsen, U.B. Henriksen, Technical University of Denmark (2005) KT-Report No. 0504.
- [3] Y. Zheng, A.D. Jensen, J.E. Johnsson, *Applied Catalysis B: Environmental* 60 (2005) 261–272.
- [4] Å. Kling, C. Andersson, Å. Myringer, D. Eskilsson, S.G. Järås, *Applied Catalysis B: Environmental* 69 (2007) 240–251.
- [5] J.P. Chen, M.A. Buzanowski, R.T. Yang, *Journal of the Air and Waste Management Association* 40 (1990) 1403–1409.
- [6] J.P. Chen, R.T. Yang, *Journal of Catalysis* 125 (1990) 411–420.
- [7] L. Lietti, P. Forzatti, G. Ramis, G. Busca, F. Bregani, *Applied Catalysis B: Environmental* 3 (1993) 13–35.
- [8] H. Kamata, K. Takashi, C.U.I. Odenbrand, *Journal of Molecular Catalysis A: Chemical* 139 (1999) 189–198.
- [9] R. Khodayari, C. Andersson, C.U.I. Odenbrand, L.H. Andersson, *Proceeding of the Fifth European Conference on Industrial Furnace and Boilers*, Vol. II, Espinho, Porto, Portugal, 11–14 April, 2000.
- [10] Y. Zheng, A.D. Jensen, J.E. Johnsson, *Industrial and Engineering Chemistry Research* 43 (2004) 941–947.
- [11] Y. Zheng, A.D. Jensen, J.E. Johnsson, *Applied Catalysis B: Environmental* 83 (2008) 186–194.
- [12] J. Blanco, P. Avila, C. Barthelemy, A. Bahamonde, J.A. Odriozola, J.F. Garcia de la Banda, H. Heinemann, *Applied Catalysis* 55 (1989) 151–164.
- [13] H. Kamata, K. Takahashi, C.U.I. Odenbrand, *Catalysis Letters* 53 (1998) 65–71.
- [14] J. Beck, J. Brandenstein, S. Unterberger, K.R.G. Hein, *Applied Catalysis B: Environmental* 49 (2004) 15–25.
- [15] F. Castellino, S.B. Rasmussen, A.D. Jensen, J.E. Johnsson, R. Fehrmann, *Applied Catalysis B: Environmental* 83 (2008) 110–122.
- [16] N.-Y. Topsøe, T. Slabæk, B.S. Clausen, T.Z. Sørensen, J.A. Dumesic, *Journal of Catalysis* 134 (1992) 742–746.